Correlation between atmospheric stability, dynamics, and cloud properties in observations, re-analyses, and models

by

Christophe Corbel

"Ingénieur diplômé de l'École Polytechnique"
M.Eng. (equivalent to), École Polytechnique, 2009

A THESIS SUBMITTED IN PARTIAL FULFILLMENT OF
THE REQUIREMENTS FOR THE DEGREE OF

MASTER OF SCIENCE

in

THE FACULTY OF GRADUATE STUDIES
(Atmospheric Sciences)

THE UNIVERSITY OF BRITISH COLUMBIA
(Vancouver)

March 2012

Abstract

Clouds, especially low clouds, are key to our ability to understand and predict climate. They are an important component of the physical climate system and contribute significantly to the difference in climate projections by General Circulation Models (GCMs). Cloud predictors, such as atmospheric stability and large-scale circulation, are often used in model parametrizations.

This thesis evaluates the performance of the latest Canadian atmospheric GCM (CanAM-4.1), in particular with respect to its cloud simulation. Its output is compared to observations, re-analyses, and its predecessor (AGCM-3). The analysis focuses on low clouds in the 30°S–30°N tropical band over the ocean.

Results show that CanAM-4.1 systematically performs better than AGCM-3 (when compared to observations). Variability between observational datasets is also shown to be much smaller than variability between observations and models (or re-analyses).

A model-to-satellite approach is used — i.e. the CFMIP Observation Simulator Package (COSP) — and reduces observations-CanAM-4.1 differences in low cloud fractions. Results are not as unambiguous for high clouds.

Three cloud regimes (stratiform, convectiform, and storm track) are well reproduced by all datasets — i.e. CanAM-4.1, AGCM-3, the ECMWF Interim Re-Analysis (ERA-Interim), and the ECMWF 40 years Re-Analysis (ERA-40).

Conditional sampling of low cloud fractions as a function of the Lower Tropospheric Stability (LTS), Estimated Inversion Strength (EIS), and vertical velocity at the 500 hPa level (ω_{500}) show good agreement with observations. Overall, conclusions are not sensitive to using EIS rather than LTS, except for the storm track regime.

In comparison to observations from the International Satellite Cloud Climatology Project (ISCCP), CanAM-4.1, AGCM-3, and ERA-40 underestimate the low cloud fraction in stratiform regimes. ERA-Interim is shown to reproduce particularly well low cloud regimes and the relationship between large-scale circulation and stability

Résumé

Les nuages, et plus particulièrement les nuages bas, jouent un rôle clé dans notre capacité à comprendre et prédire le climat. Ils sont un élément important du système climatique physique et contribuent significativement aux différences entre projections climatiques par les modèles de circulation générale ("GCM"). Des prédicteurs de nuages, telles que la stabilité atmosphérique ou la circulation à grande échelle, sont souvent utilisés dans les paramétrisations de modèles.

Cette thèse évalue les performances du dernier modèle atmosphérique Canadien (CanAM-4.1), en particulier par rapport à sa simulation des nuages. Les données qu'il a produites sont comparées à des observations, à des re-analyses et à son prédécesseur (AGCM-3). L'analyse se concentre sur les nuages bas dans la bande tropicale (30°Sud–30°Nord) au-dessus des océans.

Les résultats montrent que CanAM-4.1 est systématiquement meilleur que AGCM-3 (comparativement aux observations). Il est aussi démontré que la variabilité entre observations est bien plus faible que la variabilité entre observations et modèles (ou re-analyses).

Une approche "modèle-à-satellite" est employée — utilisant le paquet de simulateurs pour observations de CFMIP ("COSP") — et réduit les différences entre observations et CanAM-4.1 pour les nuages bas. Les résultats ne sont pas aussi clairs pour les nuages de hautes altitudes.

Trois régimes de nuages (strati-forme, convecti-forme, et frontal) sont bien reproduits par l'ensemble des données — c'est-à-dire CanAM-4.1, AGCM-3, la re-analyse 'interim' de ECMWF ("ERA-Interim"), et la re-analyse sur 40 ans de ECMWF ("ERA-40").

L'échantillonnage conditionnel des nuages bas en fonction de la stabilité de la troposphère basse ("LTS"), de l'estimation de l'intensité de l'inversion ("EIS") et de la vitesse verticale à 500 hPa ("ω_{500} ") démontre une bonne concordance avec les observations.

Dans l'ensemble, les conclusions ne sont pas sensibles au choix d'utiliser EIS plutôt que LTS, sauf pour le régime frontal.

Comparativement aux observations du projet international de climatologie des nuages ("ISCCP"), CanAM-4.1, AGCM-3 et ERA-Interim sous-estiment les nuages bas dans les régimes strati-formes. ERA-Interim reproduit particulièrement bien les divers régimes de nuages bas et les relations entre circulation à grande échelle et stabilité.

Table of Contents

List of Tables

List of Figures

List of Acronyms

AGCM	Atmospheric General Circulation Model
AGCM-3	Atmospheric General Circulation Model - 3rd generation. CCCma third generation atmospheric GCM
ALPEX	ALPine EXperiment
AMIP	Atmospheric Model Intercomparison Project
ASTEX	Atlantic Stratocumulus Transition EXperiment
ATOVS	Advanced TIROS Operational Vertical Sounder
BOMEX	Barbados Oceanographic and Meteorological EXperiment
CAFC	Cloud Aerosol Feedback and Climate
CALIPSO	Cloud-Aerosol Lidar and Infrared Pathfinder Satellite Observations
CanAM-4.0	CANadian Atmospheric Model - 4th generation. CCCma fourth generation AGCM
CanAM-4.1	CANadian Atmospheric Model - 4th generation, updated version. CCCma updated fourth generation and current AGCM
CAPE	Convective Available Potential Energy
CC	Cloud Cover
CCCma	Canadian Centre for Climate Modelling and Analysis
CCNs	Cloud Condensation Nuclei
CEBAF	CERES Energy Balanced And Filled
CERES	Clouds and the Earth's Radiant Energy System
CF	Cloud Fraction
CFCAS	Canadian Foundation for Climate and Atmospheric Sciences
CFMIP	Cloud Feedback Model Intercomparison Project
CGLMSE	Corrected Gap of Low-level Moist Static Energy
CIP	Cloud Ice Profile

CLAUS	CLoud Archive User Service
CMAP	CPC Merged Analysis of Precipitation
CMIP	Climate Model Intercomparison Project
COADS	Comprehensive Ocean-Atmosphere Data Set
COSP	CFMIP Observation Simulator Package
CPC	Climate Prediction Center
CRE	Cloud Radiative Effect
CRF	Cloud Radiative Forcing
CRM	Cloud Resolving Model
CT	Cloud Thickness
CTH	Cloud Top Height
CTP	Cloud Top Pressure
CTT	Cloud Top Temperature
CWP	Cloud Water Profile
DL	Decoupled Layer
DMSP	Defense Meteorological Satellite Program
EBAF	Energy Balanced And Filled
ECMWF	European Centre for Medium-range Weather Forecasts
EIS	Estimated Inversion Strength
ENSO	El Niño-Southern Oscillation
EOS	Earth Observing System
ERA-40	ECMWF 40 years Re-Analysis
ERA-Interim	ECMWF Interim Re-Analysis
ERBE	Earth Radiation Budget Experiment
ERS	European Remote-sensing Satellite
ESA	European Space Agency
EUMETSAT	EUropean organisation for the exploitation of METeorological SATellites
FGGE	First GARP Global Experiment
FIRE	First ISCCP Regional Experiment
FT	Free Troposphere
GARP	Global Atmospheric Research Program
GATE	GARP Atlantic Tropical Experiment
GCM	General Circulation Model

GCSS	GEWEX Cloud System Study
GEWEX	Global Energy and Water Cycle Experiment
GHG	GreenHouse Gas
GMS	Geosynchronous Meteorological Satellite
GOES	Geostationary Operational Environmental Satellite
GOME	Global Ozone Monitoring Experiment
GPCP	Global Precipitation Climatology Project
GPI	GOES Precipitation Index
IFS	Integrated Forecasting System
IPCC	Inter-governmental Panel on Climate Change
IR	InfraRed
ISCCP	International Satellite Cloud Climatology Project
ISCCP-FD	ISCCP Flux Data
ITCZ	Inter-Tropical Convergence Zone
JRA-25	Japanese 25 year Re-Analysis
LCL	Lifting Condensation Level
LES	Large Eddy Simulation
lhs	left hand side
LTS	Lower Tropospheric Stability
LW	LongWave
LWP	Liquid Water Path
MBL	Marine Boundary Layer
MERRA	Modern Era Retrospective-analysis for Research and Applications
METEOSAT	METEOrological SATellite (exploited by EUMETSAT)
MISR	Multi-angle Imaging SpectroRadiometer
MODIS	MODerate resolution Imaging Spectroradiometer
MSU	Microwave Sounding Unit
NASA	National Aeronautics and Space Administration
NCAR	National Center for Atmospheric Research
NCEP	National Centers for Environmental Prediction
NCEP/NCAR	NCEP / NCAR Re-Analysis
NCL	NCAR Command Language

NCRE	Net Cloud Radiative Effect
netCDF	NETwork Common Data Form
NOAA	National Oceanic and Atmospheric Administration
NSERC	Natural Sciences and Engineering Research Council of Canada
OD	Optical Depth
OLR	Outgoing Longwave Radiation
OPI	Outgoing Longwave Radiation (OLR)-based Precipitation Index
PARASOL	Polarization and Anisotropy of Reflectances for Atmospheric Sciences coupled with Observations from a Lidar
PBL	Planetary Boundary Layer
PDF	Probability Distribution Function
RMS	Root-Mean-Square
RMSD	Root-Mean-Square Difference
SCM	Single Column Model
SGE	Super Greenhouse Effect
SML	Surface Mixed Layer
SRES	Special Report on Emission Scenarios
SSM/I	Special Sensor Microwave/Imager
SST	Sea Surface Temperature
SW	ShortWave
TIROS	Television and InfraRed Observation Satellite
TOA	Top Of the Atmosphere
TOGA-COARE	Tropical Oceans Global Atmosphere / Coupled Ocean-Atmosphere Response Experiment
TOVS	TIROS Operational Vertical Sounder
TRMM	Tropical Rainfall Measuring Mission
VIS	VISible
VTPR	Vertical Temperature Profile Radiometer
WG	Working Group

List of Symbols

CO_2	Carbon dioxide
R	Correlation coefficient
E'	Centered root-mean-square (RMS) difference

r_{eff}	Droplet effective radius. The cloud drop effective radius (alternatively cloud effective radius or effective radius) is a weighted mean of the size distribution of cloud droplets. Physically, it is an area weighted radius of the cloud drop particles. $r_{eff} = \frac{\int_{r_1}^{r_2} \pi \cdot r^3 \cdot n(r)\, dr}{\int_{r_1}^{r_2} \pi \cdot r^2 \cdot n(r)\, dr}$
θ_e	Equivalent potential temperature. The temperature a parcel of air would reach if all the water vapor in the parcel were to condense, releasing its latent heat, and the parcel was brought adiabatically to a standard reference pressure, usually 1000 hPa.
$\Delta\theta$	Inversion strength. The jump in potential temperature (θ) at the inversion that typically caps the planetary (or marine) boundary layer. Or, in other words, the difference in θ between the top of the surface mixed layer and the bottom of the decoupled layer.
ω_{500}	Vertical (pressure) velocity at the 500 hPa level
ω_{700}	Vertical (pressure) velocity at the 700 hPa level
ω_{850}	Vertical (pressure) velocity at the 850 hPa level

θ Potential temperature.
The temperature that a parcel at pressure P and temperature T would acquire if adiabatically brought to a standard reference pressure P_0, usually 1000 hPa.
$\theta = T\left(\frac{P_0}{P}\right)^{R/c_p}$

σ Standard deviation

σ_{observ} Standard deviation of a particular dataset (e.g. "observation") or variable (e.g. temperature)

τ Optical depth (also called optical thickness).
A measure of transparency defined as the negative logarithm of the fraction of radiation (e.g. light) that is not scattered or absorbed on a path. It expresses the quantity of light removed from a beam during its path through a medium. Given I_0, the intensity of radiation at the source, and I, the observed intensity after a given path, then τ is defined as:
$\tau = -\ln\left(\frac{I}{I_0}\right)$ or $I = I_0 \cdot e^{-\tau}$

Acknowledgments

I would like to thank my advisor Philip H. AUSTIN as well as my committee members Douw STEYN and Andreas CHRISTEN for their guidance and support during my Master's research.

I would like to acknowledge Jason COLE and Knut Von SALZEN from the Canadian Centre for Climate Modelling and Analysis (CCCma) for their help and collaboration to this project.

I would also like to show my appreciation to my officemate Jordan T. DAWE, especially for his help with python and the pleasant discussions we had.

Finally, I would like to deeply thank my friends Kathrin, Marianne, and Drew, whose support as well as struggles in their own graduate programs helped me put mine into perspective.

All figures *created* for this project were generated using the Matplotlib library in the Python programming language.

This thesis has been written and compile using LaTeX(version 3.1415926-1.40.11, TeX Live 2010). The source code, as well as the bibliography and scripts, used to generate this PDF file are attached to it.

Financial support for this work was provided by the Natural Sciences and Engineering Research Council of Canada (NSERC) and the Canadian Foundation for Climate and Atmospheric Sciences (CFCAS) through the Cloud Aerosol Feedback and Climate (CAFC) network.

I gratefully acknowledge the international groups for providing their data for analysis:

- The International Satellite Cloud Climatology Project (ISCCP) data were obtained from the ISCCP web site (`http://isccp.giss.nasa.gov`) maintained by the ISCCP research group at the National Aeronautics and Space Administration (NASA)

Goddard Institute for Space Studies, New York, NY or from the ISCCP data archives at NOAA/NESDIS/NCDC Satellite Services Group (ncdc.satorder@noaa.gov).

- The MODerate resolution Imaging Spectroradiometer (MODIS) data were obtained through the online Data Pool at the NASA Land Processes Distributed Active Archive Center (LP DAAC), USGS/Earth Resources Observation and Science (EROS) Center, Sioux Falls, South Dakota (http://lpdaac.usgs.gov/get_data).
- The Global Precipitation Climatology Project (GPCP) combined precipitation data were developed and computed by the NASA/Goddard Space Flight Center's Laboratory for Atmospheres as a contribution to the Global Energy and Water Cycle Experiment (GEWEX) Global Precipitation Climatology Project, and available through anonymous ftp from the National Oceanic and Atmospheric Administration (NOAA) (ftp.ncdc.noaa.gov/pub/data/gpcp).
- The Climate Prediction Center (CPC) Merged Analysis of Precipitation (CMAP) precipitation data were provided by the NOAA/OAR/ESRL Physical Sciences Division (PSD), Boulder, Colorado, USA, from their web site at http://www.esrl.noaa.gov/psd/.
- The three Clouds and the Earth's Radiant Energy System (CERES) datasets were obtained from the NASA Langley Research Center Atmospheric Science Data Center.
- The European Centre for Medium-range Weather Forecasts (ECMWF) ERA-40 and ERA-Interim data used in this study have been provided by ECMWF and obtained from its Data Server.
- The output from the Canadian models were retrieved from the Data Center of the Canadian Centre for Climate Modelling and Analysis (CCCma), Climate Research Branch, Meteorological Service of Canada, Environment Canada (http://www.cccma.bc.ec.gc.ca/) (CCCma third generation atmospheric GCM (AGCM-3) and CCCma updated fourth generation atmospheric GCM (CanAM-4.1)).

Introduction

This introduction is a quick overview of this thesis' chapters, whose main goals are to evaluate how the latest Canadian General Circulation Model (GCM) performs when simulating low clouds?

Chapter 1 (*"Clouds and climate"*) addresses the question: "Why focus on clouds?" It demonstrates their relevance and importance for climate and its study, especially from an energy balance viewpoint (see Figure 1.1). It also emphasizes the need for universal proxies for clouds that have explanatory and predictability values.

Chapter 2 (*"Stability, dynamics, and clouds"*) addresses the question: "Why choose stability and dynamics as cloud dependencies?" It explains the need for better tools to compare observational data and model output. It also justifies the particular choices of the Lower Tropospheric Stability (LTS) for the stability component and the vertical velocity at the 500 hPa level (ω_{500}) for the dynamics component.

Chapter 3 (*"Data and methods"*) details the datasets (observations, re-analyses, and simulations), processes (regridding and computation), and tools (2D-histogram and Taylor diagram) used while conducting this research.

Chapter 4 (*"Variability between datasets"*) addresses the question: "How many sets of observations does a meaningful analysis require?" It shows that the variability between observational datasets is smaller than between observations and simulations (or re-analyses). It therefore justifies following choices of references when comparing (low) cloud fields.

Chapter 5 (*"Two generations"*) addresses the question: "Does the latest Canadian GCM — CanAM-4.1 — perform better than its predecessor — AGCM-3 — when simulating (low) clouds?" It also focuses on other dataset comparisons (e.g. re-analyses) as well as other variable comparisons (e.g. model-to-satellite simulations).

Chapter 6 (*"Qualitative analysis"*) addresses the question: "How do CanAM-4.1 cloud fields compare to AGCM-3 or observations from a dynamic-thermodynamic perspective?" It provides new information with regards to chapter 2 (literature review).

Conclusion summarizes why and how this research was conducted, as well as its context. Using the results, it answers the research questions posed in chapters 1 and 2. It compares the conclusions with the literature and suggests possible further developments.

Chapter 1

Clouds and climate

Les nuages sont comme le sucre dans le lait chaud.
Ils sont partout et nul part à la fois,
et plus on les cherche, moins on les trouve.

(Clouds are like sugar in hot milk.
They are both everywhere and nowhere,
and the more one seeks them the less one finds them.)

after Coluche (1944–1986 ; French comedian and actor Michel Colucci)

1.1 The climate system

1.1.1 How and why we study climate

The ultimate goals of meteorology and climatology are fundamentally to understand and predict the Earth's System (Figure 1.2).

That means understanding every single one of its components (atmosphere, biosphere, ocean...), processes (dynamics, thermodynamics, chemistry...), and how they interact with each other (coupling, feedbacks...) to produce the weather and climate Earth (and Humans) have experienced, experiences, and will experience.

Although the Earth's System (including the atmosphere) is, *at any time*, regulated by the same physical laws, its study provides very different information depending on the *time scale and focus*. Shorter time scale studies (typically from hours to few days) are considered to be part of the weather realm, whereas longer time scale studies (typically from month to years or centuries) are considered to be part of the climate realm. Also, while weather projections focus on knowing the precise state of the atmosphere (or Earth's System) at a precise time and place, climate projections focus on knowing its average (or typical) state through time and space.

The traditional approach that people, including scientists, take in order to study past, present, and future climate (or weather) has four steps: first observing and measuring; second understanding and explaining; third predicting, contradicting, and reproducing; and fourth going back to step one for new observations guided by new hypotheses developed in steps two and three.

In addition to this intellectual challenge, very strong incentives exist nowadays for producing accurate and reliable weather or climate projections. Those incentives, to cite only a few, can be economic, such as weather insurance for weddings or extreme events insurance for real estate; policy related, such as GreenHouse Gas (GHG) emission regulations or climate-sensitive urban planning; or even political, such as defining an international climate-refugee status or allocating North Pole mining resources between the eight Arctic states.

One common way of *conceptually* breaking down the study of future climate into

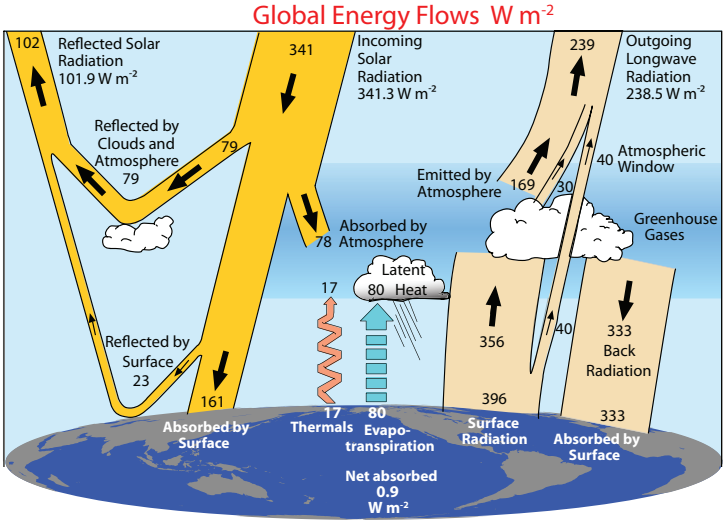

Figure 1.1: The global annual mean Earth's energy flux budget for the March 2000 to May 2004 period (W/m^2). The broad arrows indicate the schematic flow of energy in proportion to their importance. Clouds are shown to be involved in several, if not all, significant fluxes. From Trenberth et al. (2009), by permission.

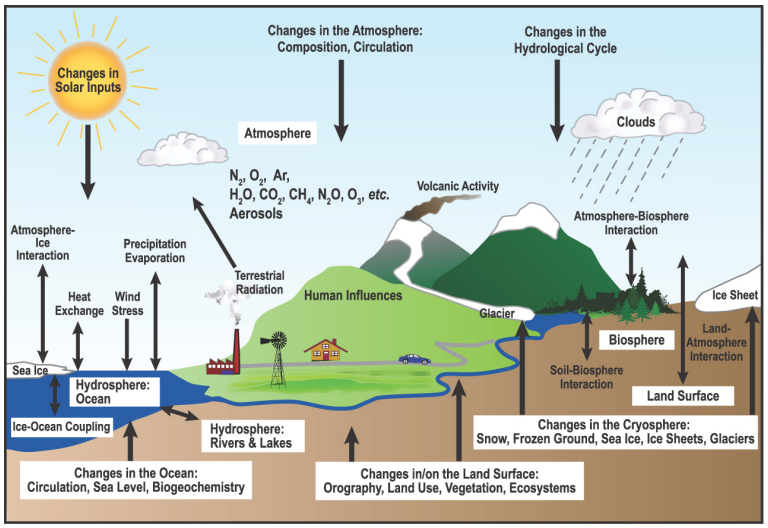

Figure 1.2: Schematic view of the components of the Earth's System, their processes and interactions. From Solomon et al. (2007), by permission.

smaller, easier-to-tackle, problems, is to write:

$$\text{climate change} = \text{climate sensitivity} \times \text{climate perturbation} \tag{1.1}$$

where "climate change" would be the change in one proxy for climate (traditionally global and annual mean temperature, expressed in Kelvin), "climate perturbation" would be the perturbation that the Earth's System encounters (traditionally an increase in GHG atmospheric concentration, expressed in Carbon dioxide (CO_2) doubling or W/m^2), and "climate sensitivity" would be the change in climate per unit of perturbation (traditionally in $K/(CO_2 \text{ doubling})$ or $K/(W/m^2)$).

Following this simple, conceptual definition, the *formal* definition of climate sensitivity is (see glossary of Solomon et al. (2007)): the equilibrium change in the annual mean global surface temperature following a doubling of the atmospheric equivalent carbon dioxide concentration. Roe (2009) demonstrates how climate forcing ("perturbation"), sensitivity, and response ("change") have exact mathematical definitions that arise from a linearized energy balance for an idealized Earth's System (with an average temperature, a mass, and a heat capacity) at the equilibrium. Whether ignoring the non-linear terms significantly compromises these definitions or not is still actively debated (Roe and Baker 2011)

Therefore, climate change study is the product of both climate sensitivity study (focusing on some climate processes, while other processes are held fixed) and climate perturbation study (focusing on some forcings, while all processes are active). Although a lot has still yet to be discovered about climate perturbation(s), most of the *scientific* uncertainty about climate change comes from uncertainty in climate sensitivity estimates (as most perturbation uncertainties come from human and political affairs, for example in determining future GHG emission scenari, see Figure 1.3). In other words, scientists' inability to narrow down the predicted climate change range comes from their inability to narrow down the current and future climate sensitivity range. Indeed, despite spanning more than a decade, the Intergovernmental Panel on Climate Change (IPCC) Working Group (WG) I Second (Houghton et al. 1996), Third (Houghton et al. 2001), and Fourth (Solomon et al. 2007) assessment reports have almost identical climate sensitivity estimates (1.5–4.5°C, 1.5–4.5°C, and 2.0–4.5°C per CO_2 doubling respectively).

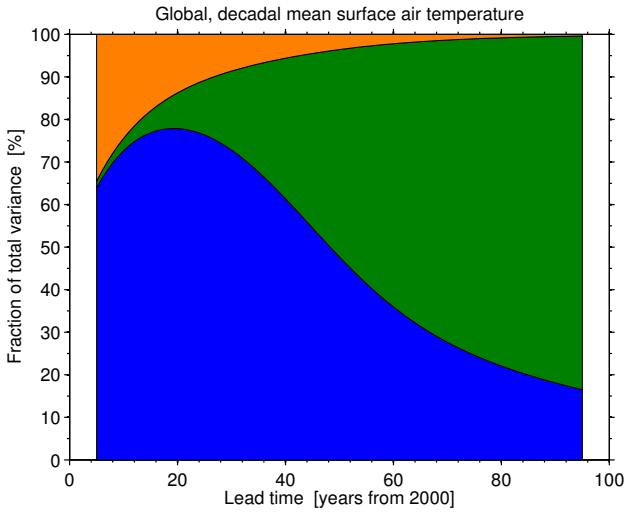

Figure 1.3: The fraction of total variance in decadal global mean surface air temperature predictions explained by the three components of total uncertainty. **Blue** regions (bottom) represent General Circulation Models (GCMs) uncertainty, **green** regions (middle) represent (emission) scenario uncertainty, and **orange** regions (top) represent the internal variability component. From Hawkins and Sutton (2009), by permission.

Following Bony et al. (2004), thus also ignoring any chemical changes (e.g. in concentration of Cloud Condensation Nuclei (CCNs)), variable anomalies (e.g. the change of cloud fraction with time relative to its time average) are broken down into three components:

- *dynamic*: originating from changes in the large-scale atmospheric circulation (an increase in vertical velocity for example)
- *thermodynamic*: originating from changes under fixed dynamical conditions, or in other words, all non-dynamic effects
- *co-variation*: originating from interactions, or correlation, between the two previous effects.

This study aims at contributing to our understanding of one component of the Earth's System: clouds. It considers dynamical and thermodynamical processes as well as their interactions, in order to improve climate sensitivity estimates.

1.1.2 Types and uses of models

To help better understand how weather and climate work, models are built based on current theory and knowledge.

Although a variety of models exists, they all fall within three categories: physical (e.g. tank experiments), analytical (e.g. mathematical formulations), and numerical (e.g. computer simulations). The goal is that they will both (i) reproduce correctly what they are intended to simulate and (ii) allow hypothesis testing with customized experiments. Indeed, since there is, to our knowledge, only one Earth, no alternative climate experiment is possible in the real world. (Although history — or paleoclimatology — makes it possible, through sampling, to infer past states of the Earth atmosphere or climate; which might be considered as a form of "alternative" or "experiment".)

Large numerical models, in particular General Circulation Models (GCMs), are the only way to produce *usable* climate projections. World policy makers, above all, need robust information about what climate will be in the near and far future (ten to hundred years) and in regions ranging from local (a city) to global (worldwide). This diversity of needs arises from tasks as different as managing air quality in a city or planning the energy mix (i.e. total and relative contributions of various sources to the energy production and consumption) of a country in fifty years. In this thesis, unless otherwise stated, GCM refer indifferently to atmospheric, oceanic, coupled, or Earth's System GCM.

Models were initially created to improve our understanding of the Earth's System. Nowadays their main use, in the scientific community, is still to help studying climate by, for example, focusing on specific processes (e.g. latest Atmospheric Model Intercomparison Project (AMIP) (Gates et al. 1999), Climate Model Intercomparison Project (CMIP) (Covey et al. 2003), and Cloud Feedback Model Intercomparison Project (CFMIP) (McAvaney and Le Treut 2003) phases). But being aware of the important, and sometimes urgent, needs for "good" (e.g. reliable or accurate) climate projections on the one hand, and knowing that GCMs are currently the favourite tools for actually making these on the other hand, makes evaluating how well GCMs perform become an obvious absolute necessity.

This study focuses on one simulation of the present climate, involving a full atmospheric GCM.

1.1.3 Validation and evaluation of models

Validation and evaluation of models is a field in itself, and is only a part of the more general quest for knowledge, as illustrated in Figure 1.4[1]. This section will only present a glimpse of it, mostly relevant to this research and its use of "Taylor diagram" (in section 3.2).

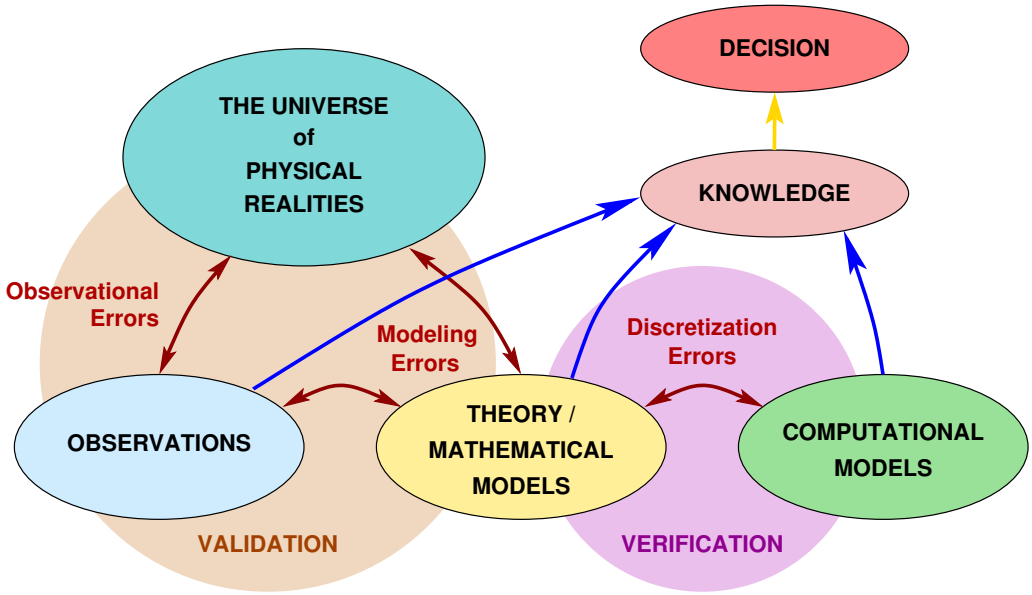

Figure 1.4: The Imperfect Paths to Knowledge, from Moser (2010). Note how, in this conceptual representation, computational models are only a part of the global search for knowledge. From Oden and Prudhomme (2011), by permission.

Observation as reference

The traditional, and still most used, way of evaluating a GCM (or model more generally speaking) is to compare its output to observational data. Although it implies an "observation is truth" paradigm, scientists usually moderate it to "observation is our best approximate for truth". This subtlety especially matters when one considers climate, which requires good long-term data, or past-climate, which needs reconstructed data. This is indeed a

[1] from the talk *"Calibration, Validation and Uncertainty Quantification for Atmospheric Reentry Vehicles"* by Robert D. Moser on February 9, 2010 at the Institute for Computational Engineering and Sciences, The University of Texas, Austin, accessible online: `https://asc.llnl.gov/ascpihome/RMoser.pdf`

problem, since, if a validation criterion requires that GCM uncertainty lies within observational uncertainty, then a model could be validated (or invalidated) on the sole basis that observations are of poor quality.

Previous studies account for observational uncertainties (Williams et al. 2003; Gleckler et al. 2008; Pincus et al. 2008), and either assume or demonstrate that observation errors are small *for the intended purpose*. Williams et al. (2003) states that cloud satellite observation errors are likely to be small relative to inter-GCM differences, especially for clouds that are radiatively the most active. Gleckler et al. (2008) systematically compare two observational datasets to simulations and conclude that "for the metrics considered [...], the impacts of uncertainties associated with a limited observational record are small when compared to the magnitude of current model errors". Pincus et al. (2008) also use two independent sets of observations (different instruments and sometimes epochs). They conclude that "that model simulations disagree with the observational record so much that observational uncertainty does not limit the ability to gauge model performance". Direct comparison of models and observations is hardly possible, by their very nature (partial versus total data availability, irregular versus regular space-time distribution, etc).

One way to cope with this particular difficulty is to use re-analysis. This is when a model is forced by and relaxed to observations, or in other words, it is a model-based time-space interpolation with enforcement of physical consistency between thermodynamics and dynamics. It stands in between observations (because forced by) and models (because ruled by).

The model-to-satellite approach (Klein and Jakob 1999; Webb et al. 2001) makes for more meaningful comparisons (between model outputs and satellite observations). This method consist in taking the vertical or 3D profile given by the GCM, and (forward) computing what would be measured by a satellite. Among others, the CFMIP Observation Simulator Package (COSP) (Bodas-Salcedo et al. 2011) is a "multi-instrument simulator that enables quantitative evaluation of clouds, humidity and precipitation processes in numerical models with observational satellite products by making consistent assumptions". One example would be to use COSP to calculate the low cloud fraction that the CloudSat satellite would measure if observing this model location (e.g. considering how high clouds would hide low clouds, or how conservative CloudSat is in its scene attribution algorithms).

This study uses all three "data" types: observations, re-analyses, and simulations. More details about the data are given in section 3.1.

How we evaluate climate projections

Now, coming back to climate projection, one of the big challenges is to validate models against something that does not exist yet. Or, in other words, how to know that a GCM correctly simulating past or present climates will *also* correctly simulate future climates. Nowadays, most selections of model schemes are based on the skill with which they represent current climate (Williams et al. 2003). Unfortunately, as shown by Williams and Webb (2009) and others, the climate change (cloud) response strongly depends on present climate (cloud) simulation.

A last, but not least, way of evaluating one specific GCM is to compare it with other GCMs. Although this implies a "consensus is truth" paradigm that is intensely debated, this is out of the scope of this study. However, even while measuring GCMs against each other, one must still ask what to compare and why.

The first question asks what tools to use. A lower (surface), upper (tropopause), or integrated (Top Of the Atmosphere (TOA)) perspective? What variables (temperature, moisture, radiation, fluxes...) to consider? One metric, or a combination of metrics (Murphy et al. 2004; Reichler and Kim 2008; Gleckler et al. 2008; Pincus et al. 2008)?

The second question asks why breaking down the problem this way is relevant. Is a geographical (pixel-per-pixel) or dynamical (large-scale circulation) approach more appropriate? Is a step-function uniform $\pm$2K Sea Surface Temperature (SST) perturbation more pertinent than a steady GHG atmospheric concentration increase? (see Table 1.1)

Indeed, a key question, with respect to GCM evaluation, is how sensitive the simulated climate response is to the type of perturbation. Unfortunately there is no short answer, as this depends on the system considered or simulated (only atmosphere or whole Earth, clouds or glaciers, etc).

This study confronts its three data types for fields of different natures: surface (e.g. precipitation rates from the Climate Prediction Center (CPC) Merged Analysis of Precipitation (CMAP)), level (e.g. cloud fraction from the International Satellite Cloud Climatology

Forcing type	Example of advantage	Project or Reference
SST increase:		
±2 K uniform	Easy to analyze, 2K is a conventional threshold	CMIP 1
±4 K uniform	Easy to analyze, 4K make changes more detectable	CMIP 5
El Niño patterned	More realistic, easier comparisons with analogues	AMIP 1
GHG concentration:		
sudden doubling	Faster to reach equilibrium, make changes more detectable	AMIP 2
steady increase	More realistic, easier to compare former runs with new data	CMIP 3
"realistic" increase	Even more realistic, related to GHG emissions scenarios	CMIP 5

Table 1.1: Examples of climate forcings used in simulations. For full names (expanded acronyms) see the glossary page xi. Numbers refer to the project's phase.

Project (ISCCP)), or integrated (e.g. TOA net radiative fluxes from the ISCCP Flux Data (ISCCP-FD)). Both geographical and dynamical analysis are done using Taylor diagrams In order to compute the Taylor diagram (see section 3.2) and 2D-histogram (see section 3.3) respectively. More details about the data and analysis are given in section 3.2 and section 3.3.

Parametrization and tuning

Ideally, one would want to create and run a climate model solely based on fundamental physical laws (gravity, energy conservation, phase changes to cite a few). However this cannot be the case for two reasons. First, some processes are not (well) understood, such as entrainment. Second, some processes occur at time and space scales that cannot be resolved by the model (the "sub-grid scale" problem).

Therefore, one must adjust ("tune") a model parametrization in order to match data (e.g. field campaign observations) or outputs from higher resolutions simulations (e.g. Large Eddy Simulation (LES) or Cloud Resolving Model (CRM)). Progressively improving both physical understanding and model resolution should gradually lead to no tuning (see Figure 1.5).

Parametrization also has to be evaluated. Usually this involve four steps: choose a feature that happens in the physical world (El Niño-Southern Oscillation (ENSO), north-south seasonal migrations of the Inter-Tropical Convergence Zone (ITCZ)); develop a parametrization whose goal is to reproduce it as closely as possible; run the GCM and compare its outputs to expected results; iterate this process as many times as necessary to reach a predefined agreement threshold.

This study strives to participate in this general, collaborative effort toward model and parametrization validation. It concentrates on qualitatively comparing, in a relevant manner, cloud properties from one GCM simulation to observations or re-analyses, and quantitatively evaluating their respective performances. Therefore, it fits mainly in the aforementioned third step.

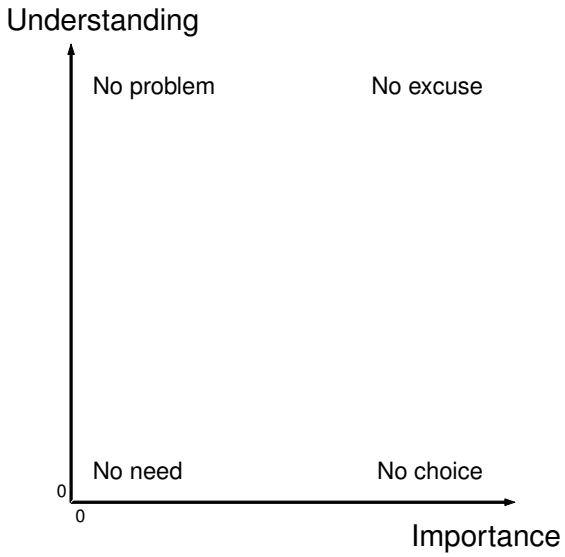

Figure 1.5: A diagram illustrating the role of tuning in a model, according to the importance of the process and the degree to which it is understood. From Randall and Wielicki (1997), adapted by permission.

1.2 Cloud-climate interactions

1.2.1 Complex but crucial

Clouds are only one of the many components involved in the atmosphere, itself only one of the many components involved in the Earth's System. They encompass many processes (formation, rain, radiative cooling, etc.) and inter-components interactions (aerosols through micro-physics, ocean through moisture, snow/ice through albedo, land through orography). Although cloud basic properties, effects, or interactions have been known for many decades, a lot more still has to be discovered to fully understand their role(s) in regulating the current and future climate.

Clouds are difficult to study for several reasons. To cite only a few:

- Water exists in three phases with very different optical and thermodynamic properties. Moreover, the transition between visually transparent vapor and visually opaque cloud occurs nearly instantaneously and is of crucial importance.

- GCM grid-cell size is unsuitable for cloud study: too big to represent clouds as resolved plumes and too small to contain a statistically large number of deep convective clouds (David Randall, personal communication).
- Cloud processes are non-linear in many aspects. Cloud convection, for instance, is a metastable process (due to feedbacks such as the positive and mutual reinforcement of condensation and buoyancy).
- Clouds are strongly coupled with their immediate and far environment (depend on it and modify it, for example through the moist adiabatic lapse rate).

Many efforts, usually international collaborations, exist to further explain behaviour of clouds. They have been observed from space (see the Earth Radiation Budget Experiment (ERBE), the MODerate resolution Imaging Spectroradiometer (MODIS) on Terra and Aqua satellites, the CloudSat satellite, or the International Satellite Cloud Climatology Project (ISCCP)). Clouds have also been observed from the surface, by land or ship measurements (see the First ISCCP Regional Experiment (FIRE), the Atlantic Stratocumulus Transition EXperiment (ASTEX), or the Barbados Oceanographic and Meteorological EXperiment (BOMEX)). Atlases were dedicated to them (see the Comprehensive Ocean-Atmosphere Data Set (COADS) or Warren et al. (1986a) and Warren et al. (1986b)). Clouds have been numerically modelled in: "0"-dimension (Lilly 1968), 1-dimension (Anthes 1977), 2-dimensions (Moeng 1986), or 3-dimensions (Khairoutdinov and Randall 2003).

They are often studied according to some categories (Randall et al. 2003): boundary layer clouds (GEWEX Cloud System Study (GCSS) Working Group (WG) 1) (includes stratocumulus and shallow cumulus), cirrus clouds (GCSS WG 2), extra-tropical layer cloud systems (GCSS WG 3), precipitating deep convective cloud systems (GCSS WG 4), or polar clouds (GCSS WG 5).

Despite all these efforts, clouds are still among the least well understood and simulated components of the Earth's System climate (e.g. Figure 1.6 shows the uncertainty in climate forcing due to the cloud-aerosol interactions). Indeed, in order to correctly simulate them, clouds must be both (i) well understood (properties/processes) and (ii) well represented (parametrization) in numerical models.

However, clouds were early on established as one of the key driver of climate due to their important contribution to the Earth radiation budget (Houghton et al. 1990). Among five

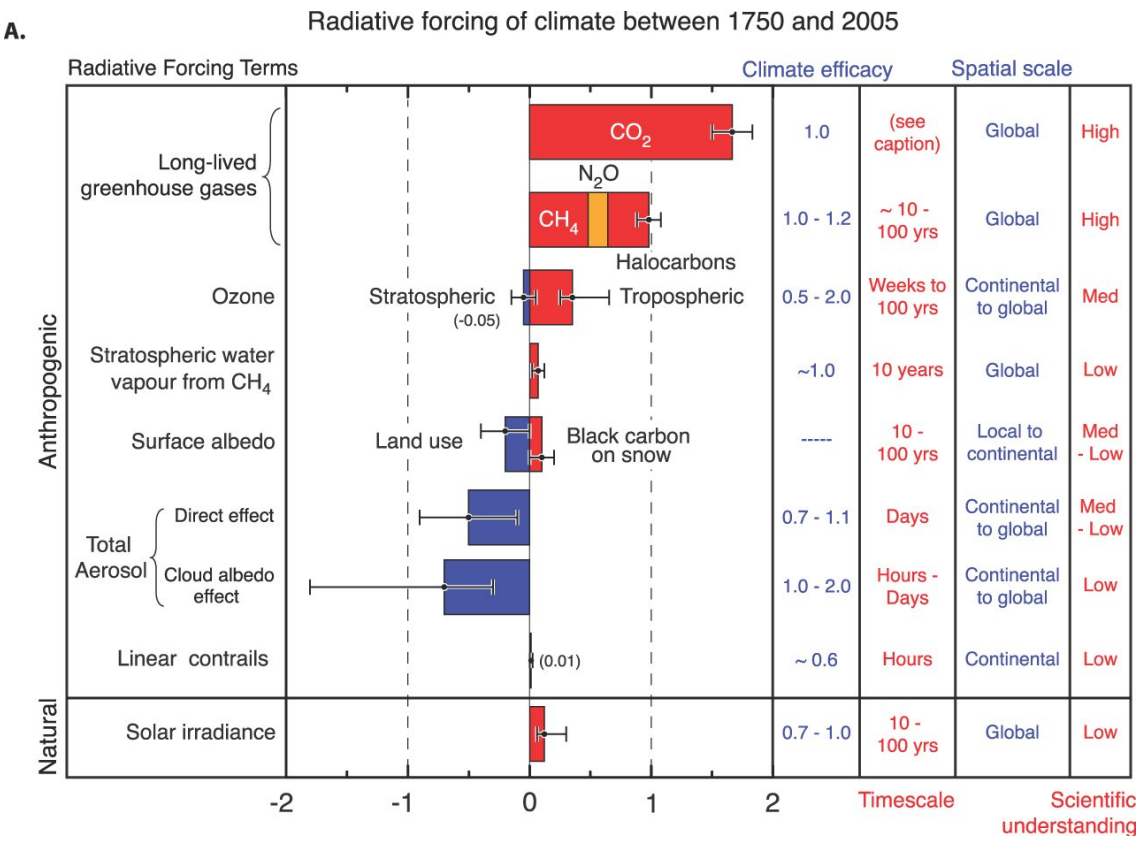

Figure 1.6: Anthropogenic forcings ranked by scientific understanding. Some of the numerous cloud effects are embedded in aerosol indirect effect. This shows that clouds (at least one of their interactions) are among the least understood components. From (Solomon et al. 2007), by permission.

GCSS classifications, low clouds are the main Cloud Radiative Effect (CRE) contributors (Randall et al. 1984; Slingo 1990). This is actually why, in average, cloud net effect is to cool (Harrison et al. 1990; Ramanathan et al. 1989): because the warming net effect of high clouds is over compensated by the cooling net effect of low ones.

Clouds are also among the main sources of spread in climate sensitivity estimates, i.e. of uncertainty in climate projections. Low clouds, in particular, have been shown to have a significant responsibility in this regard (Bony and Dufresne 2005).

As for climate, scientists break down clouds into as many basic components and dependencies as possible, looking for decomposition that are as orthonormal as possible (to use mathematical vocabulary). Throughout the scientific literature, cloud studies made noticeable choices of focus. Here are the most noticeable:

1. *Location*. The majority of these studies focus on the tropics for mostly three different reasons. It can be because the 30°S–30°N tropical band represent half of the globe (tropical oceans account for 37% and tropical land for 13% of the Earth surface, Williams et al. (2003)). Since the incoming solar energy is higher at lower latitudes, this band represent more than half of the total Earth radiative energy input. Another reason is the slow and small variations in SST over time and space in the tropics, in contrast with mid- or high-latitudes (higher gradients, more complex SST-induced large-scale circulation). This also makes the dependency of clouds on the large scale environment simpler, with most variation coming from one variable (e.g. SST). Finally, the tropics are seen as a boundary condition for the extra-tropics, relative stationary over the past thousand years, therefore making it a priority.

2. *Surface*. Many cloud studies focus on the ocean, rather than land or both for simplicity, relevancy, and accuracy. Indeed, lack of orography and an unlimited supply of moisture make it easier to specify the cloud environment. Oceans cover approximately 71% of the globe surface and low clouds, subject to particular attention, occur mainly over them (Klein and Hartmann 1993). Moreover, better retrieval of cloud properties are possible thanks to the very strong albedo contrast — "dark" (i.e. non-ice covered) ocean $\approx$ 5% and "bright" (i.e. high visible reflectivity) clouds from 30% to 90%, Kondratyev (1973)). Finally oceans are a priority also because of the albedo contrast,

which makes clouds a more powerful climate driver (unlike, for example, ice, which has about the same reflectivity if it is covered by clouds or not).

3. *Remote dependency*. The sensitivity of clouds to distant or perturbation sources or to large-scale influences is usually answered in focusing on the vertical velocity at the 500 hPa level (ω_{500}). Indeed, ω_{500} can be a proxy for vertical motion, often correlated with (vertical) advection of moisture (for instance). Thus subsiding (e.g. cold, dry) air ($\omega_{500} > 0$) is easily distinguished from uplifting (e.g. warm, moist) air ($\omega_{500} < 0$). This is traditionally called the dynamical cloud response.

4. *Local dependencies*. The sensitivity of clouds to local perturbation sources or to atmospheric structure changes is usually called the thermodynamical cloud response (consistently with Bony et al. (2004)). This dependency, unlike the remote one, has been explained with many different variables: SST (Bony et al. 1997), SST anomalies (Norris and Leovy 1994), (Williams et al. 2003), dry static stability (or Lower Tropospheric Stability (LTS) (Klein and Hartmann 1993)), moist static stability (Weaver and Ramanathan 1997), Estimated Inversion Strength (EIS) (Wood and Bretherton 2006), Corrected Gap of Low-level Moist Static Energy (CGLMSE) (Kawai and Teixeira 2010), etc.

5. *Type of clouds*. Cloud studies generally isolate a few types of clouds: high (convective) clouds, especially at the ITCZ; low (stratiform and cumuliform) clouds, especially in subsidence areas.

6. *Properties*. CRE (longwave (LW) or shortwave (SW)) is a traditional choice, because it is (i) a good proxy for cloudiness, (ii) what matters for the energy budget, and (iii) observations (or retrievals) are more straightforward. (See also section 1.2.2.)

The bottom line is that (low) clouds matter, from a physical and energetic viewpoint, but are hard to study exhaustively at once (if possible at all).

This study looks at cloud fractions and CRE; with two local and one remote dependencies; separately over land, ocean, and both; independently for all low clouds and all high clouds.

1.2.2 Simulation and evaluation of clouds

Cloud radiation variables

Because the Cloud Radiative Effect (CRE) is a very frequently used variable while studying clouds, it is necessary to clarify some literature vocabulary.

CRE is defined as the Top Of the Atmosphere (TOA) radiative impact of clouds on the Earth radiative budget (in $\mathrm{W/m^2}$) (Charlock and Ramanathan 1985; Ramanathan et al. 1989).It is traditionally expressed as the difference between the radiative flux for all sky and clear sky conditions (the remainder being thus the cloudy conditions contribution) or, in mathematical form:

$$CRE_{cloudy} = CRE_{all} - CRE_{clear} \tag{1.2}$$

When CRE was initially defined, more than twenty years ago, it was called Cloud Radiative Forcing (CRF), and its goal was to measure the radiative impact of a *change of cloud cover*. Since then, and in order to avoid confusion between cloud *forcing* and cloud *feedback* (which would both be shortened "CRF"), the denomination "Cloud Radiative Forcing" has been (mostly) abandoned. Now, and in this study, CRE represents the radiative impact due to a change in cloud cover (while CRF would represent the radiative impact due to cloud forcing, e.g. due to aerosol-cloud interactions).

Another important notation is commonly used in cloud studies: the Net Cloud Radiative Effect (NCRE) (Williams and Webb 2009). In general, CRE represents the radiative impact due to one particular type of cloud, cloud regime, wavelength band (LW or SW), or any combination of them. On the other hand, NCRE usually represent the CRE of all clouds over the whole radiation spectrum or, in mathematical form:

$$\begin{aligned} NCRE &= CRE_{LW} + CRE_{SW} \\ &= CRE_{low\ clouds} + CRE_{middle\ clouds} + CRE_{high\ clouds} \end{aligned} \tag{1.3}$$

Therefore, in this study, comparisons of present climate between observations and simulations use the variables (and notations): NCRE and CRE. A final word on forcing and feedback, people usually call an impact:

- a "feedback" when, *within the time span considered*, the impact produced by the change in clouds following the initial perturbation *does* affect the perturbation itself;
- a "forcing" when, *within the time span considered*, the impact produced by the change in clouds following the initial perturbation *does not* affect the perturbation itself.

For example, changes in surface temperature, at the decadal time scale, are considered as a (cloud) feedback, whereas changes in CCNs, at the daily time scale, are considered as a (cloud) forcing.

Cloud properties and predictors

One does not study clouds but cloud *properties*. To do so, the first step is to pick one property, either intrinsic such as the amount ("cloudiness") or the droplet effective radius (r_{eff}), or environment dependent such as radiative fluxes (CRE) (see Table 1.2) The second step is to pick one physical quantity (e.g. SST, LTS, Liquid Water Path (LWP)), estimate and characterize how the chosen cloud property depends upon this variable (or predictor). The third step is to explain on a physics level, why the dependency, if any, behaves this way (e.g. linear, cubic, exponential; one or more regimes; weak or robust correlation).

Cloud Properties		
Optical Depth (OD)	Cloud Thickness (CT)	Cloud Top Temperature (CTT)
Cloud Cover (CC)	Cloud Water Profile (CWP)	Cloud Top Height (CTH)
Cloud Ice Profile (CIP)	Cloud Fraction (CF)	Cloud Top Pressure (CTP)

Table 1.2: Non-exhaustive list of cloud properties commonly used in cloud studies and satellite retrievals.

In many studies, clouds are reduced to their cloud properties. For example, Bony et al. (1997) explains that many observational studies (such as Graham and Barnett (1987) or Waliser et al. (1993)) uses Outgoing Longwave Radiation (OLR) as proxy for convective cloudiness, and Weaver and Ramanathan (1997) explain that the cloud shortwave (SW) radiative effect (CRE_{SW}) is a measure of cloudiness. Some studies justify their choices of

cloud properties and variables (Cess et al. 1990; Pincus et al. 2008; Gleckler et al. 2008), while others simply pick them.

A predictor would be ideal for good reasons, or in other words, for understood physical reasons. Ultimately, that is why scientists want to characterize dependency between cloud properties and some physical quantity: to understand cloud behavior and physics. The ideal predictor (or proxy) for clouds would be "one size fits all", that means:

- for all cloud properties — presence (yes/no), amount (0–100%), etc.
- independent of the time scale (hourly to centennial)
- independent of the space scale and location (local to global on the one hand, tropics to pole on the other hand)
- independent of the cloud type (low to high, stratiform to convective, liquid to ice, clean to polluted)
- constrained by physics — not merely a statistical fit.

One reason to look for a predictor independent of the space scale could be that regional definitions are somewhat arbitrary and depend highly on study location. Klein and Hartmann (1993) use tropical, subtropical, mid-latitude, and polar regions, while Williams and Webb (2009) use tropical, ice-free extra-tropical, and ice-snow covered regions. Williams and Tselioudis (2007) define tropics as the 20°S–20°N band, while Williams et al. (2003) defines tropics as the 30°S–30°N band. Finally almost all studies focus on clouds over the ocean, very few on clouds over land.

In GCMs, clouds (actually cloud properties) are simulated based on their relationships with selected predictors. Having a proxy independent of cloud type would mean faster/easier computation, and a more fair treatment of the different cloud types. This is, unfortunately, not yet the case, as Williams and Webb (2009) show that, according to their metrics, no reviewed model simulates correctly and consistently all cloud regimes.

In this study, and in particular in chapter 6 ("Qualitative analysis"), I focus on one cloud *property* (cloud fraction or amount) that is assumed a good proxy for clouds in a more general sense. I use two *predictors* (atmospheric stability and large-scale circulation), where two *proxies* (LTS and EIS) represent the former, and one *proxy* (ω_{500}) represents the latter. Details about how location, time scale, and cloud type affect the cloud properties-predictors relationships is further discussed in chapter 6.

Known problems in clouds simulation

As previously demonstrated, clouds, and in particular low ones, are crucial in climate projections and their uncertainties. Not only do they matter from a (radiative) energy perspective, but they are also known to be difficult to represent in models (see Figure 1.7). Some of the most known and problematic features of cloud simulation by GCMs are:

1. a lack of stratocumulus, relative to observations (Williams et al. 2003)

2. the stratocumulus regime and the transition regime (between stratus and stratocumulus) are too reflective in models, probably because of an excessive optical depth (τ) according to Williams and Webb (2009)

3. clouds are the main cause of climate projection spread between GCMs. In other words, the discrepancy in simulated global annual mean temperature responses to a change in external forcing is mostly due to the radiative response from clouds (Senior and Mitchell 1993; Webb et al. 2006; Soden and Held 2006; Ringer et al. 2006; Cash et al. 2007)

4. low clouds are the main contributors to the spread of climate sensitivity between GCMs (Bony and Dufresne 2005)

5. the magnitude, and even the sign, of the cloud radiative feedback changes, for uniform 2 K SST perturbation (Cess et al. 1989, 1990). This result is robust regardless of the type of perturbation, and may come from physical processes affecting the cloud radiative feedback (Williams et al. 2001; Senior 1999)

6. low clouds are a major source of CRF spread between models. Comparing GCMs outputs (between models as well as between equilibrium and 2 times CO_2 runs), Williams and Webb (2009) show that 65% of CRF variance comes from low cloud regimes (47% from the stratocumulus regime and 18% from the transition regime). However, their results are dominated or led by mostly one model.

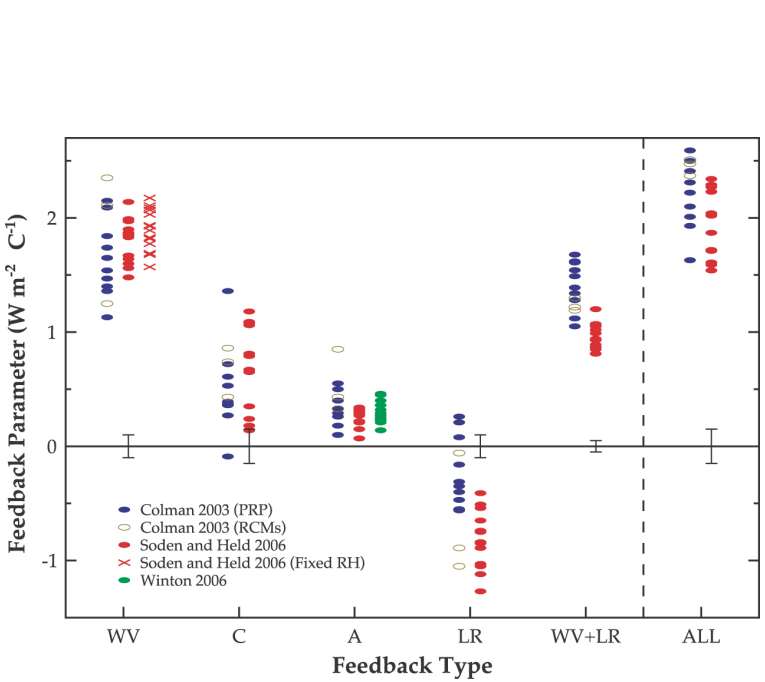

(a) Radiative feedback estimates. The bars are the uncertainties. Labels are: "WV": water vapor, "C": cloud, "A": aerosol, "LR": lapse rate, "WV+LR": both water vapor and lapse rate, "All": all feedbacks together. (Solomon et al. (2007), by permission)

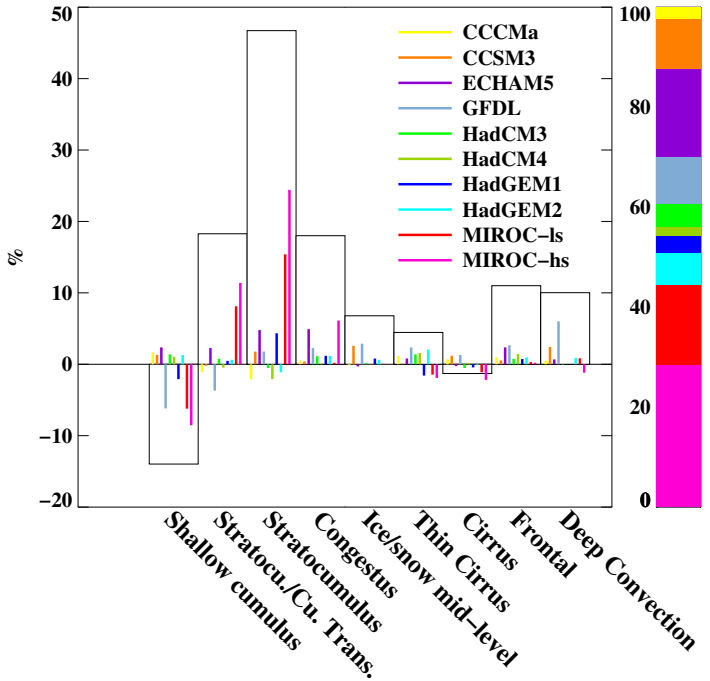

(b) Contribution to the total global variance in change of "NCRF" (actually NCRE in this thesis notation) from each cloud regime. (Williams and Webb (2009), © British Crown Copyright 2012, the Met Office, UK; by permission)

Figure 1.7: These two figures show that (a) the cloud ("C") feedback uncertainty is the largest and (b) the low clouds are the main contributors to the total global mean variance in the change of Net Cloud Radiative Effect (NCRE). This shows how clouds and especially low clouds are important to narrow down climate sensitivity estimates.

The Canadian GCM has both successes and difficulties when simulating (low) clouds. Indeed, on the one hand, it performs well according to some metrics (Williams and Webb 2009) and gets correct TOA radiation fluxes, while, on the other hand, it gets some cloud properties incorrect, e.g. smaller cloud fraction and thicker clouds than observed (Cole et al. 2011). Finally, its sensitivity in shallow cumulus regime is an outlier relative to other climate centers' models (Philip Austin personal communication). Although this disagreement does not prove a problem, it incites to be even more careful when considering this GCM output.

Two special notes should be made concerning relative importance: the first one about low clouds within clouds and the second one about clouds within the climate system. Low clouds are the main NCRE contributor, due partly to their geographical extent and their strong cooling effect (estimated to approximately 15 W/m^2 by Hartmann et al. (1992)). Consequently, the NCRE is a cooling of the atmosphere that is significant in the Earth radiation total balance (Manabe and Strickler 1964; Manabe and Wetherald 1967). Therefore, in addition to the scientific interest — key contributor to the Earth radiation budget, itself a key driver of the climate — clouds, with even a small change in the Earth cloud cover (just few percents), might completely offset a climatic perturbation as significant as a doubling of CO_2 (or several W/m^2) (Ramanathan 1995), whether "naturally" occurring or geo-engineered.

This study, by comparing the output of the latest Canadian climate model to re-analyses and observations (using a model-to-satellite approach) will further assess known problems (1) and (2) for one particular GCM. It will also suggest a way to contribute to the next generation of the CFMIP, i.e. (3), (4), (5), and (6) (if its methods were used to look at $\pm$4K uniform SST perturbation).

Techniques recently used in cloud studies

Over the past decade, two techniques have increasingly been used to study specific cloud types in more detail. Permanent increase in computational power and storage capacities is likely to explain, to some extent, this trend. 'Breaking down' clouds has recently been done in two ways:

1. compositing: manually define regimes after some criteria (location, temperature, large-scale dynamics...), then treat (e.g. average) all data associated with one regime (Bony et al. 1997; Tselioudis et al. 2000; Norris and Weaver 2001; Ringer and Allan 2004; Bony et al. 2004; Williams et al. 2006). Two arguments against this technique are: (i) the subjectivity of the (arbitrary) choice, and (ii) the risk of mis-allocation because of indistinguishable features for the criteria.

2. clustering: objectively define regimes using (iterative) algorithms, then either study the transitions between them (Khouider et al. 2010), or perform conventional compositing based on these regimes (Jakob and Tselioudis 2003; Gordon et al. 2005; Williams and Tselioudis 2007). This technique has the advantage that it produces regimes that are, in some way, (statistically) optimal and objective. However these regime definitions are traditionally still specific to one dataset, and not (physically) optimal. That is why Williams and Webb (2009) suggest to use (i) a more objective methodology by using one "reference" dataset (in their case ISCCP) to define cloud regimes that will be used by all the other datasets, and (ii) a more tolerant assignment system, to make allocation more physical (by adding some "distance" between regimes in the program).

A major advantage of compositing (after clustering or not) is to study both cloud regime properties and occurrences. Note that, although cloud regimes aim at unequivocally identifying cloud types, they are not perfect and mismatches happen. Hopefully this happens, most of the time, only in an insignificant or irrelevant manner .

Compositing, sometimes called conditional sampling, allows a deeper understanding of individual cloud regimes (for example by looking at average vertical profiles). This is especially useful because the cloud response, *as a whole*, to a change in environmental conditions is very sensitive to the type of perturbation (uniform increase in SST, ENSO-patterned increase in SST, steady increase in GHG concentration, sudden doubling in CO_2 ...). However, one cloud type could be very sensitive to one type of perturbation and not to others. For example, Williams et al. (2003) shows that low cloud response is mostly dependent on the local SST anomalies if over tropical oceans, and should be mostly dependent on the regional SST gradients if over mid- or high-latitude oceans.

Lindzen and Nigam (1987) and Bony et al. (1997) also demonstrated that one cloud property (cloudiness) and one predictor (large-scale circulation) are influenced by the spatial distribution of SST. These results emphasized the cloud response dependency on the type of (climate) perturbation, which usually means a lower or biased sensitivity to uniform SST perturbation experiments.

This study uses a visualization tool (2D-histogram, section 3.3) to subjectively identify cloud regimes. Then compositing is realized to further study and confirm the nature of the defined regimes (vertical profile and back-mapping).

1.3 Research objectives

I present here the research questions that this thesis elaborates (in this chapter) and addresses (in chapters 4, 5, and 6). Other research questions are developed in the next chapter (2, "Stability, dynamics, and clouds") and summarized at its end (section 2.5).

The goal is to improve climate projections by models as well as our understanding of the climate system. Considering the previous section, it appears, in particular, that:

- GCM uncertainty is a significant contributor to climate projection uncertainty;
- model (low) cloud representations are significant contributors to GCMs spread in climate projections (and climate sensitivity estimates);
- clouds are one of the key (physical) components driving the climate; and
- GCMs need to be evaluated (or validated) in face of observations.

That is why, this study compares (low) cloud parametrizations from a GCM — the CCCma updated fourth generation atmospheric GCM (CanAM-4.1) — and its predecessor — the CCCma third generation atmospheric GCM (AGCM-3) — relative to observations (and re-analyses).

It uses two methods: a geographical (or local) point-by-point comparison ("Taylor diagram") and a conditional (or dynamical) regime-by-regime analysis ("2D-histogram"). Analysis evaluates: (i) several datasets respective performances at simulating (low) clouds, and (ii) several variables respective performances at predicting (low) clouds properties.

Research objective 1:

How meaningful is a comparison between AGCM-3 and CanAM-4.1, relative to observations (or re-analyses)? (i.e. relevance of analysis.)

Research objective 2:

How well does CanAM-4.1's simulated (low) cloud field agree with observational data? (i.e. model evaluation relative to the "reference".)

Research objective 3:

How well CanAM-4.1 reproduces (low) cloud regimes? (i.e. realism of simulated clouds.)

Research objective 4:

Does CanAM-4.1 perform better than AGCM-3 when simulating (low) clouds? (i.e. model and parametrization improvements.)

Research objective 5:

How much does CanAM-4.1's *ISCCP-simulated* (low) cloud field improve relative to its raw output? (i.e. model-to-satellite approach benefits.)

Chapter 2

Stability, dynamics, and clouds

In theory there is no difference between theory and practice.
But in practice, there is.

Johannes Lambertus Adriana van de Snepscheut
(1953–1994 ; Computer scientist and educator)

Le travail n'épouvante que les âmes faibles.
(Work terrifies only the weak.)

Louis XIV (1638–1715 ; King of France and Navarre,
longest-reigning king in European history)

2.1 From dependency to compositing

This section aims at putting into perspective the compositing technique by looking at its rationale. It provides the background information necessary to understand how a 2D-histograms (section 3.3) are computed and why they are relevant visualization tools.

2.1.1 Using statistical fits

"Influenced by", "correlated with", "controlled by", "dependent on", "affected by", or "impacted by" are phrases frequently used in order to express a particular relationship, ideally physically meaningful, between two quantities.

It is important to note that dependency is first of all a fact, usually an observed one. It is neither an explanation, nor a cause, nor a consequence in itself (as noted by Klein and Hartmann (1993) and Weaver and Ramanathan (1997)). Only people can make logical or physical sense out of this fact by fitting it into a story called theory. (In modelling, such factual relationships or statistical fits are frequently used and called parametrizations). Nowadays the limits are less and less about finding the dependency — as computers, machine learning, and data mining makes the search increasingly easier — and more and more about the capability of scientists to ask good questions, and then formulate good explanations.

Dependency is used, for example, by Weaver and Ramanathan (1997) to *explain* a particular cloud behavior while looking at plots of longwave (LW) Cloud Radiative Forcing (CRF) as a function of vertical velocity at the 500 hPa level (ω_{500}) ("A plausible interpretation of Fig. 9 in the most general sense is [...]"). It is also used, for example, by Miller (1997) to *predict* a particular cloud behavior — a warmer world would have a higher Lower Tropospheric Stability (LTS), thus would have more low clouds (because of the noticeable impact of LTS on low cloud amount), thus damping the initial warming.

2.1.2 Using more than one variable

More and more variables have progressively been used when looking at correlations (or co-relations). For low cloud fractions, only one variable (e.g. Sea Surface Temperature

(SST) in Hanson (1991)) was used to explain the observations, then two variables (e.g. SST and ω_{500} in Bony et al. (1997) or Norris and Weaver (2001)) were used to explain more completely the observations. The need for more than one variable was felt decades ago (at least as early as Ramanathan and Collins (1991)). An example is that, for a given large-scale vertical circulation, the *type* of cloud formed is significantly determined by the static stability, a proxy used for (low) clouds (Cotton and Anthes 1997; Klein and Hartmann 1993; Wallace and Hobbs 2006). Another example comes from Hallberg and Inamdar (1993) and Weaver et al. (1994), who showed that their Super Greenhouse Effect (SGE) (i.e. when the increase in clear-sky atmospheric greenhouse effect with tropical SST is greater than the corresponding increase in surface emission, featuring a local runaway situation) could not be understood solely with thermodynamical feedbacks (they suspected large-scale dynamical processes to be involved). And again, but more recently, once two variables were discovered to be insufficient, then three variables were used. For instance Williams et al. (2003) broke down the variation in cloudiness (ΔCLD) into three main components (SST, SST anomaly, and large-scale circulation) : $\Delta CLD = \Delta CLD_{SST} + \Delta CLD_{SST\ anom} + \Delta CLD_{\omega_{500}} + others$.

However, doubling the number of dependencies that one looks at does not necessarily double the quality or explanatory value of the answer. Ideally, two (or more) quantities can be largely independent (orthogonal input). Indeed, many ω_{500} values are possible for a given SST (Bony et al. 1997). Nevertheless, more often than not, these variables are *not* independent:

- local SST and large-scale circulation — a warmer ocean surface creates deeper convection (Ramanathan and Collins 1991),
- (remote) SST gradient and large-scale circulation — a strong temperature difference can create a circulation, like a sea breeze (Lindzen and Nigam 1987; Lau et al. 1994),
- local SST and (remote) SST gradient — an increase in SST can lead to an increase in the SST gradient (Ramanathan et al. 1994).

2.1.3 Choosing for compositing

Compositing (also sometimes called "conditional sampling") is the technique of grouping together or ordering data based on one (or more) variables in order to study it with a

new perspective. For clouds, compositing can be used (with classification) in order to compute mean properties of a cloud type (e.g. stratocumulus or stratus). To give a more concrete example, if one has a model output of both daily temperature and precipitation rates over a 2.5° by 2.5° grid, then computing the Probability Distribution Functions (PDFs) of temperature from pixels whose precipitation rates lie in given intervals would be compositing.

Figure 2.1 gives an example of compositing CRE_{LW} in different large-scale circulation regimes defined by ω_{500} — using data from the CCCma updated fourth generation atmospheric GCM (CanAM-4.1) (in 2.1a) and comparing to Bony et al. (2004) data (in 2.1b).

As we saw, many variables were reported to influence clouds and their properties (a list is given in Table 2.1). Therefore, with the profusion of available data and the ever increasing power of data analysis tools, the major difficulty is now more to decide what to study and less how to study it. The next two sections — "First dimension : stability" (2.2) and "Second dimension: dynamics" (2.3) — justify the predictor choices of this study and give more details about the designated proxies.

Meteorological factors	Correlations
Sensible heat flux	Low
Latent heat flux	Low
10-m wind speed	Low
Relative humidity at 1000 hPa	Low
Relative humidity at 850 hPa	High
2-m temperature	High
Lower Tropospheric Stability (LTS)	High
Estimated Inversion Strength (EIS)	High

Table 2.1: Non-exhaustive list of variables and their correlations to cloud properties (cloud amount, homogeneity, skewness, and kurtosis of Liquid Water Path (LWP) Probability Distribution Functions (PDFs)), as reviewed by Kawai and Teixeira (2010) ("low correlations": correlations of 0.31 or less; "high correlations": correlations of more than 0.31).

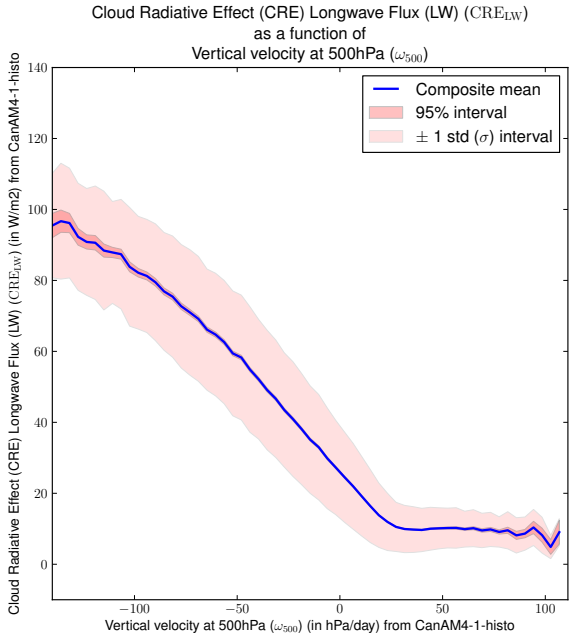

(a) CanAM-4.1

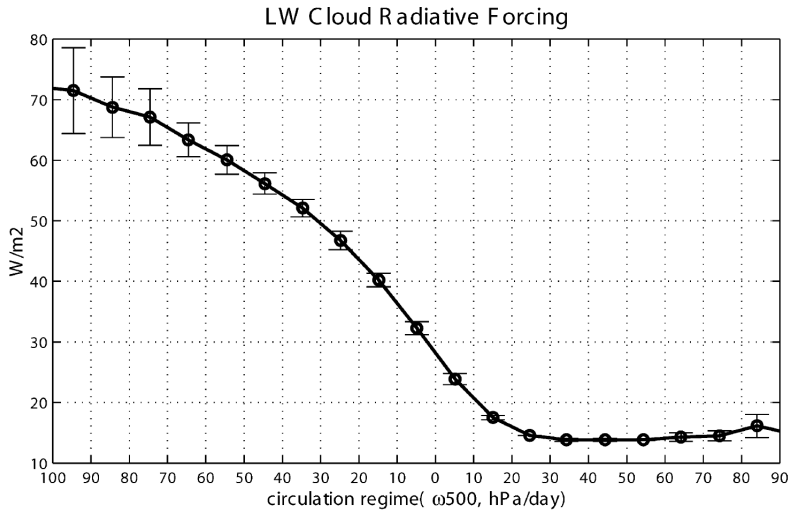

(b) Bony et al. (2004)

Figure 2.1: A compositing example from (a) the CCCma updated fourth generation atmospheric GCM (CanAM-4.1) and (b) Bony et al. (2004) (by permission). Conditional (a) CanAM-4.1 and (b) Earth Radiation Budget Experiment (ERBE)-derived longwave (LW) Cloud Radiative Effect (CRE) (called "Cloud Radiative Forcing (CRF)" in Bony et al. (2004)) as functions of the vertical velocity at the 500 hPa level (ω_{500}) (i.e. large-scale circulation). Average (thick lines) and standard deviation (lighter red in (a), vertical bars in (b)) show the ω_{500} -CRE_{LW} relationship. Results are similar when data are from the ECMWF Interim Re-Analysis (ERA-Interim) or the CERES Energy Balanced And Filled (CEBAF). Note that the negative sign ("$-$") is missing on the lhs of the x-axis in (b).

2.2 First dimension : stability

2.2.1 Overview

This section focuses on the thermodynamic dependence of clouds. The variables described here are related (more or less closely) to the stability of the atmospheric column. Here I review in details only two proxies, LTS and EIS, thus leaving many others unexplored, such as the Convective Available Potential Energy (CAPE) or the Corrected Gap of Low-level Moist Static Energy (CGLMSE) (developed in Kawai and Teixeira (2010)).

Clouds are suspensions of liquid water or ice particles in air. Therefore it is natural that people who first tried to understand them started by looking at temperature (which controls cloud buoyancy and condensation of water vapor). However, both because it is much easier to measure temperature at the ground level than in clouds (a pragmatic reason), and because the surface is a boundary condition for the whole overlying air column (a physical reason), (sea) surface temperature is used. In addition, because (low) clouds predominate found over the ocean, the convention is to use the Sea Surface Temperature (SST) as a proxy for the stability dependency.

Many cloud studies base their analysis on SST. For instance, Bony et al. (1997) explains that SST is good choice even on a monthly basis because local variations, within the tropics, are small at this time scale. Which is a good thing since many data products are available as monthly values, i.e. monthly means of daily means, such data from ERBE or the International Satellite Cloud Climatology Project (ISCCP). But this is also a limitation since SST-based analyses are therefore of limited quality outside the tropics.

Vertical profiles of temperature interpolated on to models grid were then available, first thanks to case studies, often based on field campaigns, then from model or re-analysis of global observations. This gave researchers the opportunity to study the relationship between clouds and the vertical (temperature) structure, rather than with merely its lower boundary value. For example, Weaver and Ramanathan (1997) use the difference of equivalent potential temperature (θ_e) as a measure of moist static stability: $\Delta\theta_e = \Delta\theta_e^{500-1000} = \theta_e^{500\text{ hPa}} - \theta_e^{1000\text{ hPa}}$. Although they acknowledge its value is somewhat dominated by the temperature inversion, which frequently exists in Marine Boundary Layers (MBLs), they

show that (i) $\Delta\theta_e$ is correlated with shortwave (SW) CRF but not with LW CRF, and that (ii) it is anti-correlated with cumulus amount while correlated with stratus amount (no value given by the authors but a visual estimate would be approximately 3% per K in $\Delta\theta_e$).

Finally, SST is not always the main driver of clouds and cloud properties. Williams et al. (2003) shows that a greater part of the variance in cloud amounts is explained by SST anomalies rather than SST alone. Despite the limits of this particular result, which arise from one study over the tropics based on only one model, this clearly demonstrates that a better proxy for the stability predictor is needed. The next two sections detail each one.

2.2.2 Lower tropospheric stability (LTS)

Definition

The Lower Tropospheric Stability (LTS) is one way of measuring how stable the lower part of the atmosphere is. It was invented and used from a MBL perspective. LTS is formally defined by Klein and Hartmann (1993) as:

$$LTS = \theta_{700} - \theta_{surface} \tag{2.1}$$

with θ_{700} and $\theta_{surface}$ the potential temperatures of the air at the 700 hPa level and at the surface respectively.

Depending on the studies, the last term ($\theta_{surface}$) is sometimes replaced by the SST (only over ocean), the surface air temperature ($T_{surface}$), the 2-metre air temperature ($T_{2\ metre}$), or the air temperature at the 1000 hPa level ($T_{1000\ \mathrm{hPa}}$) (in particular over land for the last three). Since this choice is usually not explicitly justified, I can only guess that this is driven by data (un)availability. In my computations, I used primarily $\theta_{surface}$. Where $\theta_{surface}$ was unavailable or impossible to compute, I used $\theta_{2\ metre}$, or $\theta_{1000\ \mathrm{hPa}}$ if necessary.

Justifications

Klein and Hartmann (1993) justify the choice of the 700 hPa level because the inversion (or "trade-inversion"), which typically caps MBLs, usually lies under the 750 hPa level (Neiburger et al. 1961; Riehl et al. 1951; von Ficker 1936a,b).

They expect LTS to be richer (in terms of information) than one surface temperature or one upper level temperature because: (i) T_{700} (and thus θ_{700}) has a wider range than $T_{surface}$ (and thus $\theta_{surface}$), and (ii) T_{700} anomalies are not correlated with $T_{surface}$ anomalies (see Figure 2.2).

The authors focus on one specific type of low cloud, namely stratus, that they define as cloud with a top below the 680 hPa level and an Optical Depth (OD) greater than 3.55 (corresponding to an albedo approximately greater than 30%) because stratus cloud amount is, in the subtropical regions, the main driver of Net Cloud Radiative Effect (NCRE) (-1 W/m^2/ per % of stratus cloud fraction). This finding is consistent with (Hartmann et al. 1992) who found a -0.63 W/m^2/% relationship for all low cloud types.

Findings and limits

The key finding of Klein and Hartmann (1993) is a striking correlation between LTS and stratus cloud amount, across large space and time scales (as shown in Figure 2.3). They found that an increase of one degree in LTS leads to an increase in stratus cloud amount of 4% to 6% by (respectively) comparing two decades of data or by comparing ten stratus-prone areas. In addition to these two estimates, two others, inferred from other studies (though lacking upper air temperature records), confirmed a slope of +5% ($\pm$1%) in stratus amount per degree in LTS.

Klein and Hartmann (1993) are well aware that the sudden and significant increase ("jump") in potential temperature (θ) at the inversion is one of the two main contributors of LTS and has a role in cloud formation (for a detailed discussion of how the inversion participate in cloud formation, see Klein and Hartmann (1993) or Stull (1988)). Despite these and the robust correlation between LTS and stratus cloud amount, they warn against any unjustified conclusion of causality between the inversion strength and the amount (or fraction) of stratus (*association is not causation*). In other words, they know the importance of the inversion on both cloud existence and LTS; they demonstrate a correlation between cloud quantity and LTS; but they cannot unambiguously infer a causal relation between inversion strength and cloud quantity.

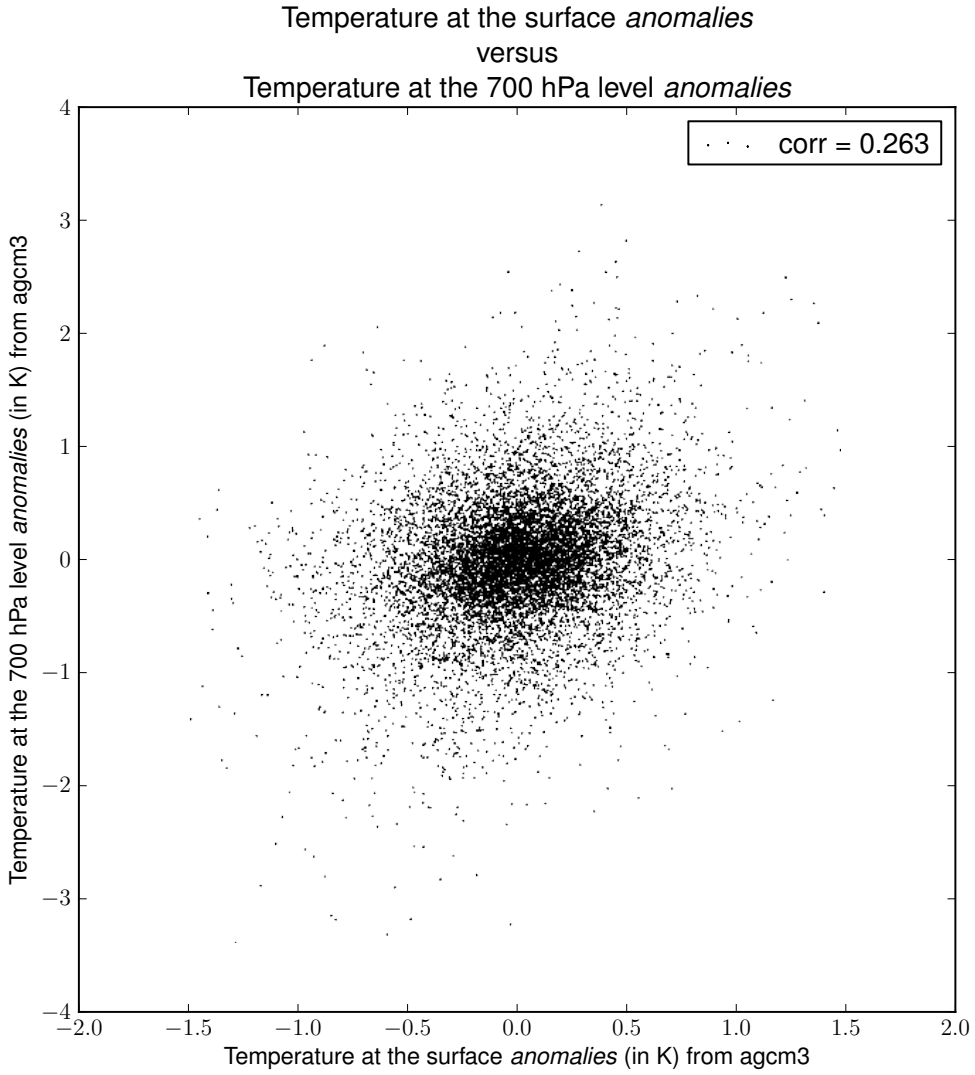

Figure 2.2: Comparison and correlation between the anomalies (relative to the climatological monthly mean) of $T_{surface}$ and T_{700}. Visibly, $T_{surface}$ and T_{700} anomalies are not correlated (i.e. very poorly, here $R < 30\%$). Data are (10,000 randomly selected points) from the CCCma third generation atmospheric GCM (AGCM-3), for January 1990 to January 2000, over the ocean, from the tropics (30°S–30°N). Figures with data from the ECMWF 40 years Re-Analysis (ERA-40), the ECMWF Interim Re-Analysis (ERA-Interim), or the CCCma updated fourth generation atmospheric GCM (CanAM-4.1) are all similar (not shown).

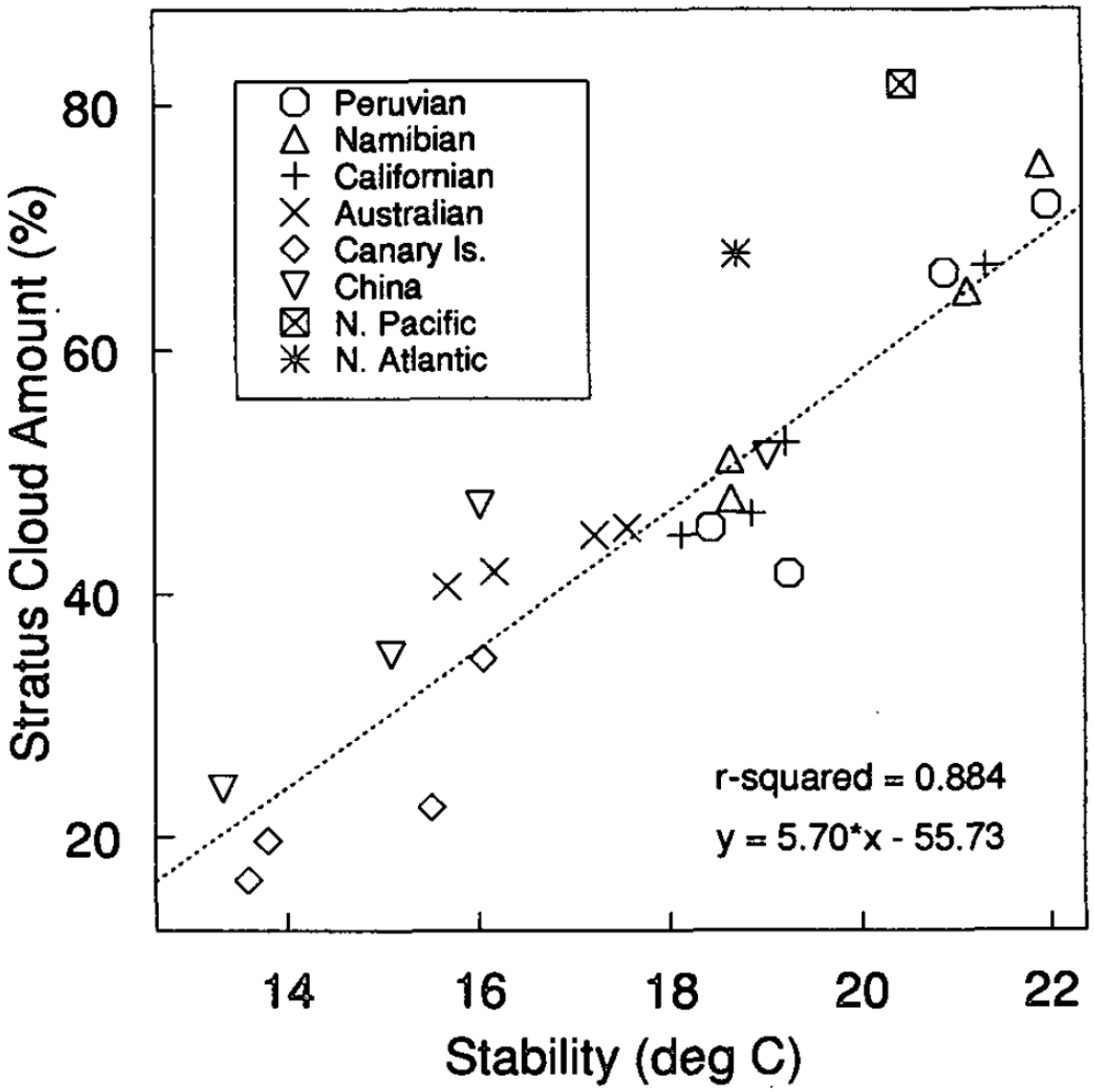

Figure 2.3: Stratus cloud amount vs. stability: Scatter-plot of seasonally averaged stratocumulus cloud amount with seasonally averaged Lower Tropospheric Stability (LTS) for several oceanic low cloud regions. Labels are the regions described in Figure 2.4. From Klein and Hartmann (1993), by permission.

This direct LTS-low cloud relationship was used (as a parametrization) in General Circulation Models (GCMs), GCMs studies (Slingo 1987; Rasch and Kristjansson 1998; Miller 1997; Larson et al. 1999), climate sensitivity studies (Larson et al. 1999), and Miller's thermostat hypothesis (Miller 1997). However, the implementation of this relationship yielded a (too) strong negative feedback of NCRE on surface temperatures (Klein and Hartmann 1993; Wood and Bretherton 2006). Although out of the scope of this study, a crucial question would be: "will this relationship hold in a (different) future climate?".

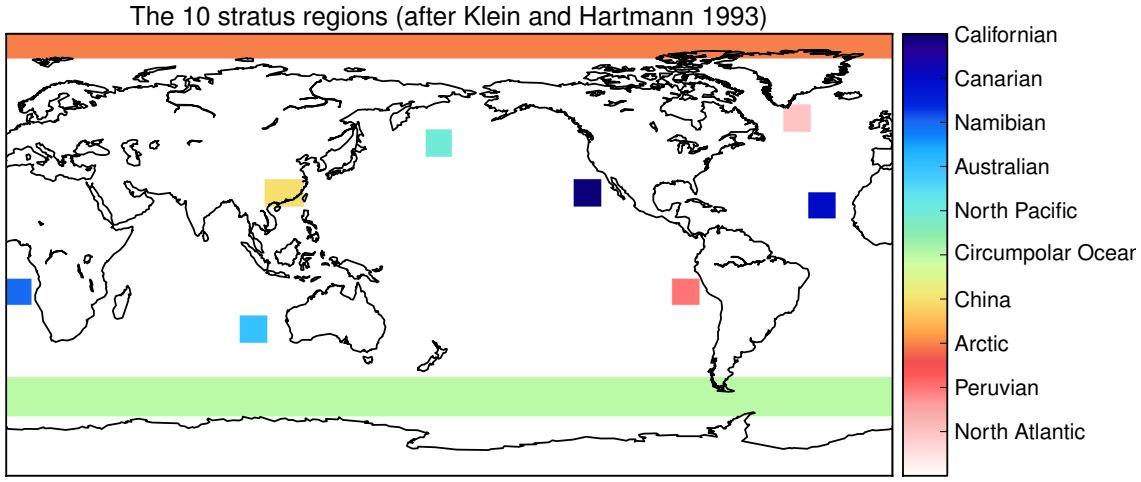

Figure 2.4: The "10 stratus regions", as first described and studied by Klein and Hartmann (1993). These are the regions named in Figure 2.3. The region "China" is the only one over land. Note that (at least) the region "Arctic" is mostly over ice (and not open water). All regions but "China", "Australian", and "Circumpolar Ocean" are northern summer (maximum) stratus regions (i.e. "North Atlantic", "North Pacific", "Peruvian", "Namibian", "Canarian", "Californian", and "Arctic").

2.2.3 Estimated inversion strength (EIS)

Idealization, approximations and justifications

The Estimated Inversion Strength (EIS), like LTS, is one way of measuring how stable the lower part of the atmosphere is. But unlike LTS, it focuses on the inversion and its associated jump in potential temperature (θ). EIS was also invented and used from a Marine Boundary Layer (MBL) perspective.

Wood and Bretherton (2006), following Albrecht et al. (1979), Betts and Ridgway (1988), and Park et al. (2004), modelled the troposphere using three layers (or four levels), from surface (land or ocean) to top (700 hPa level): Surface Mixed Layer (SML), Decoupled Layer (DL), and Free Troposphere (FT), separated by the Lifting Condensation Level (LCL) and the (temperature) inversion (see Figure 2.5). This idealized troposphere is then used to define the inversion strength ($\Delta\theta$) as the potential temperature difference between the DL top and the FT bottom (i.e. the inversion level). Note that only the SML and DL belong to the Planetary Boundary Layer (PBL) (i.e. MBL when over the ocean).

In this section (and thesis), $\Delta\theta$ refers to the actual (or observed) jump in potential temperature (θ) at the inversion, while EIS refers to its estimate (or approximation) when using Wood and Bretherton (2006) model and equation.

Assuming a constant lapse rate (or linear profile) for the potential temperature in each of the three layers, Wood and Bretherton (2006) estimate the inversion strength ($\Delta\theta$) as:

$$\Delta\theta = (\theta_{700} - \theta_{surface}) - \Gamma^{FT} \cdot (z_{700} - z_{inversion}) - \Gamma^{DL} \cdot (z_{inversion} - z_{LCL}) \tag{2.2}$$

with Γ^{FT} and Γ^{DL} the lapse rates of DL and FT respectively (in $\mathrm{K/m}$); z_{LCL}, $z_{inversion}$, and z_{700} the altitude (in metre) of the LCL, the inversion, and the 700 hPa level respectively. Recognizing that (i) the first two terms on the right hand side are LTS, and (ii) the other terms are not constant, one can see that $\Delta\theta$ will differ from LTS.

Wood and Bretherton (2006) argue that the FT lapse rate is very close to a moist adiabat in the tropics (Sobel et al. 2001; Stone and Carlson 1979), in the subtropics, and in the mid-latitudes (Schneider and Sobel 2007). That is why they approximate Γ^{FT} by Γ^{FT}_{moist}, and more precisely by the moist adiabatic lapse rate at the 700 hPa level (Γ^{700}_{moist}).

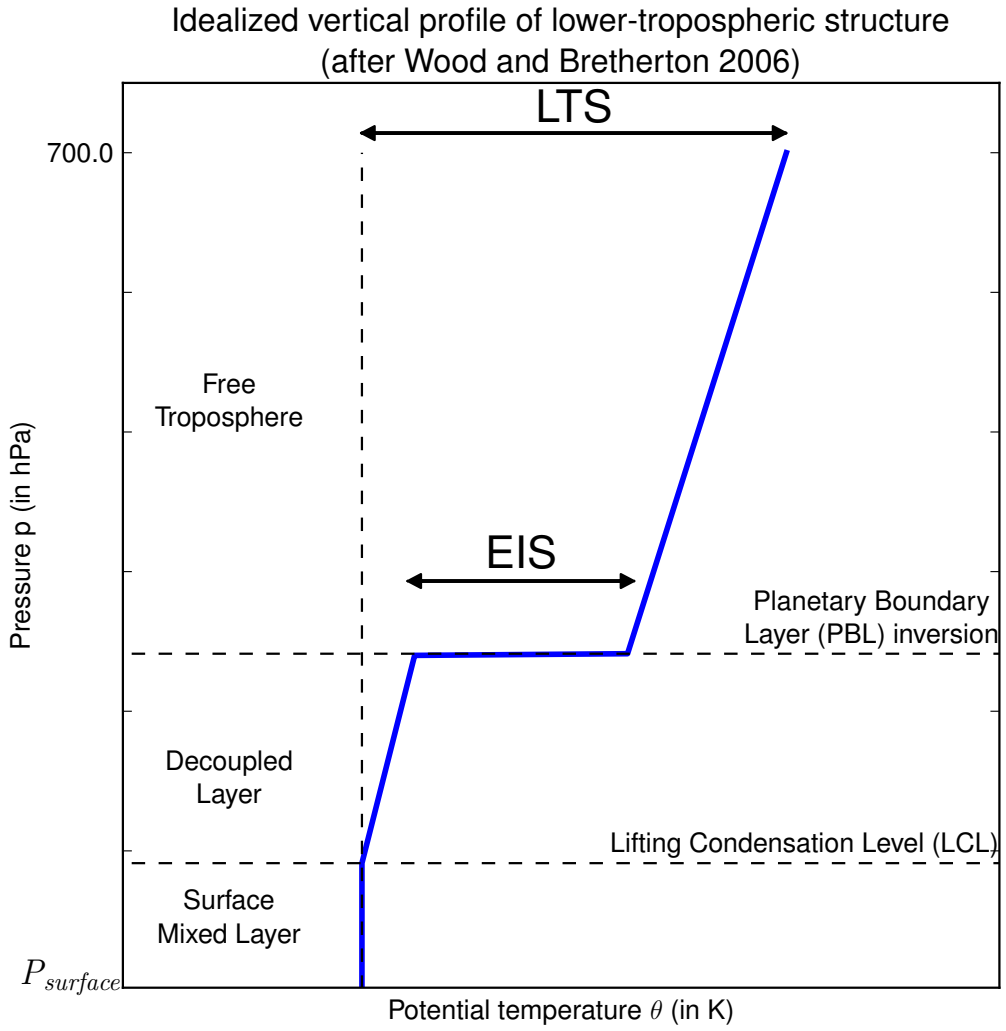

Figure 2.5: Idealized potential temperature (θ) vertical profile of lower-tropospheric structure during periods of undisturbed flow — for instance a moderate tropospheric subsidence typically conducive to the formation of extensive low clouds. From Wood and Bretherton (2006), adapted by permission.

In addition, they argue that the DL lapse rate ranges from zero for a shallow PBL to moist adiabatic for a deeper PBL (Albrecht et al. 1995; Park et al. 2004; Wood and Bretherton 2004). From Equation 2.2, the shallower the PBL, the smaller $(z_{inversion} - z_{LCL})$, thus the smaller the error due to the approximation of Γ^{DL} would be (and conversely). Hence, approximating Γ^{DL} by Γ^{DL}_{moist} is sound, both physically (it happens) and analytically (it is the limiting behaviour). Also, since the DL is both colder and shallower than the FT, its contribution in estimating $\Delta\theta$ will be smaller. That is why the authors approximate Γ^{DL} by Γ^{DL}_{moist}, and more precisely by the moist adiabatic lapse rate at the LCL (Γ^{LCL}_{moist}).

After two other approximations — exponential (or single scale) atmosphere and $\Gamma^{850}_{moist} \approx \Gamma^{700}_{moist} \approx \Gamma^{DL}_{moist}$ — EIS is formally defined by Wood and Bretherton (2006) as:

$$EIS = LTS - \Gamma^{850\text{ hPa}}_{moist} \cdot (z_{700} - z_{LCL}) \tag{2.3}$$

with *LTS* the Lower Tropospheric Stability (LTS) and $\Gamma^{850\text{ hPa}}_{moist}$ the moist adiabatic lapse rate at the 850 hPa level.

Validation, findings and limits

In order to evaluate (or validate) that EIS is actually a good estimate of the inversion strength ($\Delta\theta$), Wood and Bretherton (2006) test these two quantities in periods or regions dominated by low cloud conditions using observational data from Albrecht et al. (1995), Bretherton et al. (2004), Klein (1997), and Norris (1998) — see Figure 2.6.

The key finding of this study is a strong and robust correlation between EIS and low cloud fraction (all types, not just stratus like LTS from Klein and Hartmann (1993)). They found that an increase of one degree in EIS leads to an increase in low cloud fraction of 6% ($\pm$1%). EIS by itself explains over 80% of the regional and seasonal variance in low cloud amount.

This result challenges Miller's thermostat hypothesis, which is based on the LTS-cloud amount relation and which predicts a strong climate-low cloud negative feedback. Indeed, if the troposphere warms, LTS will increase (even more because of the wider range of T_{700}), then low cloud amount will increase, which will dampen (or reduce) the initial warming. However, a new Miller's thermostat hypothesis, based on the EIS-cloud amount relation,

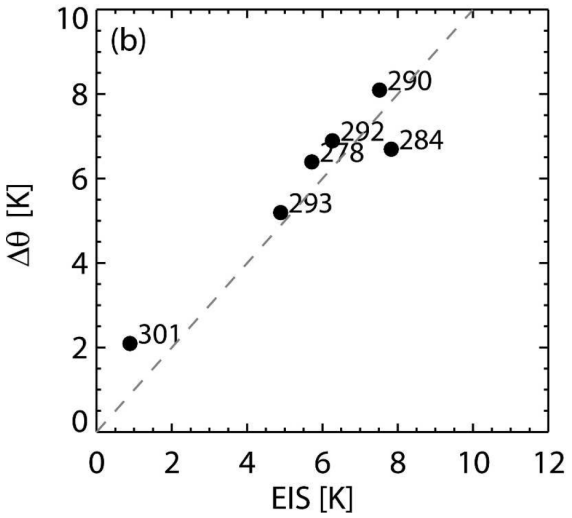

Figure 2.6: Relationship between the mean Estimated Inversion Strength (EIS) and the mean inversion strength ($\Delta\theta$). Data are from several field studies and show a very good agreement, demonstrating that EIS is a good estimate for the actual $\Delta\theta$. Next to the data points are shown mean surface air temperatures ($T_{surface}$, in K). From Wood and Bretherton (2006), by permission.

would predict a much weaker (negative) feedback. In this case, as the troposphere warms, EIS would not increase as much as LTS, thus low cloud amount would not increase as much either, and the initial warming would not be dampened (or reduced) so much.

2.2.4 Conclusions about both LTS and EIS

Unlike LTS, which is a bulk measure of the stability of the lower part of the atmosphere, *as a whole*, EIS is a *local* measure of the stability and stratification of the lower part of the atmosphere.

Thirteen years after Klein and Hartmann (1993), the role of the inversion that caps the planetary (or marine) boundary layer in cloud formation is better known (in particular as a moisture trap) but far from completely understood. Wood and Bretherton (2006) assumed that, among LTS contributors, the inversion strength would be the only or most important with respect to cloud formation (presence) *and* amount (quantity).

LTS and EIS are significantly correlated (as shown in Equation 2.3, Wood and Bretherton (2006), or Figure 2.7). However, the correlation seems to depend to a great extent on the region. Two important points while comparing LTS and EIS are:

1. the two main contributors to LTS are the inversion strength ($\Delta\theta$) and the Free Troposphere (FT) part ($\Gamma^{FT} \cdot (z_{700} - z_{inversion})$); and

2. the FT part is strongly temperature dependent (since the moist adiabat that it typically follows is temperature dependent).

Therefore LTS and EIS are related, but not identical. In particular, for a constant LTS, the colder the troposphere, the larger EIS. Conversely for a constant EIS, the warmer the troposphere, the larger LTS. Or, in other words, the larger the temperature, the smaller the relative contribution of the inversion to LTS (see Figure 2.8). That is why, if one assumes that $\Delta\theta$ is a better predictor of low cloud amount (ideally for physically good and understood reasons), one would expect EIS to be a better proxy.

According to Wood and Bretherton (2006), although LTS and stratus cloud amount are strongly correlated across time and space scales, the relationship (slightly) changes between the tropics, subtropics, and mid-latitudes. On the other hand, the correlation between EIS and low cloud amount is independent of the time and place of study.

Although it can be quite surprising, it is nevertheless very convenient that a metric using only two temperatures (at the surface and the 700 hPa level), such as LTS, can predict so well the presence and amount of stratus cloud. This seems to make *LTS a robust (hence privileged) stratus cloud amount proxy*.

On the other hand, EIS, unlike LTS, requires more than just temperatures at two levels. It also requires a measure of the moisture content (dew point temperature, mixing ratio, relative or specific humidity). Although EIS was shown to be a much better predictor for low cloud amount, it also has higher requirements in terms of data input availability and quality. This seems to make *EIS a better but less robust low cloud fraction proxy*.

This study looks both at LTS and EIS, but focuses more on LTS than on EIS. As the results show, qualitative conclusions mostly either do not change depending on the variable (section 6.1) or are in favor of EIS (subsection 6.5.3).

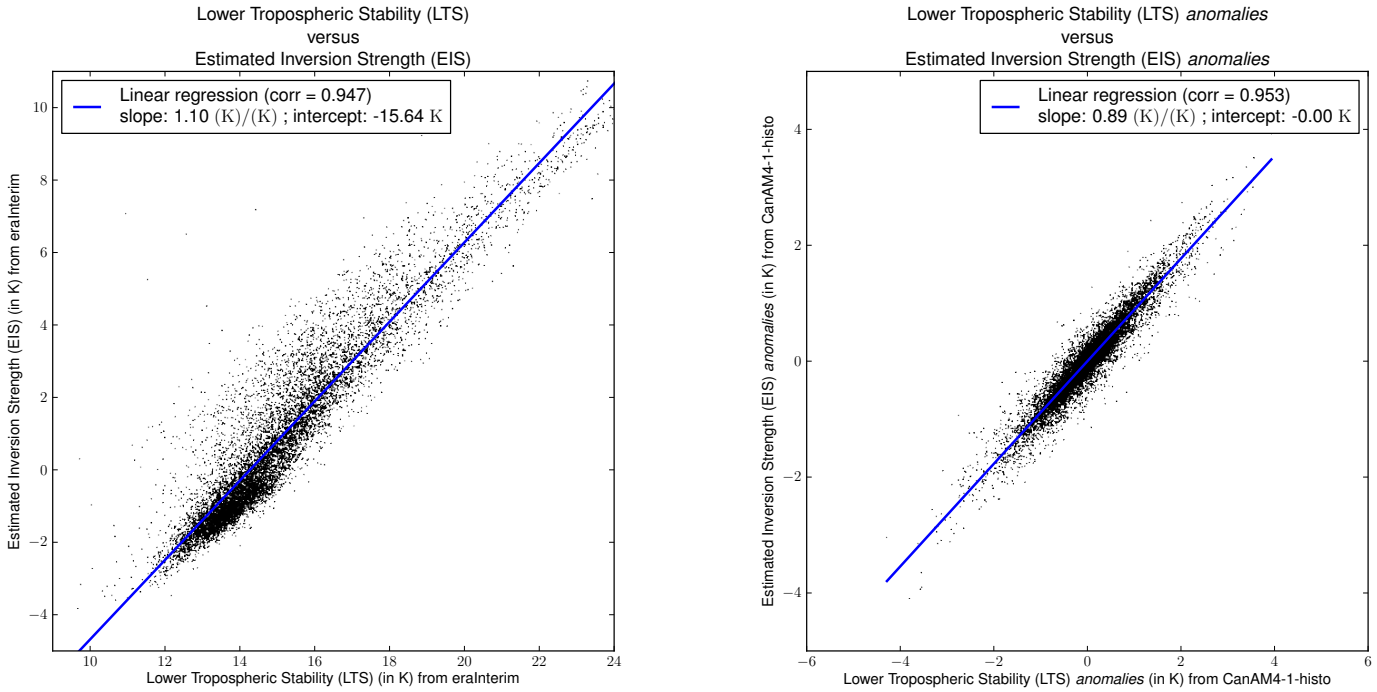

(a) LTS-EIS scatter plot

(b) LTS anomaly-EIS anomaly scatter plot

Figure 2.7: Comparison and correlation between the Lower Tropospheric Stability (LTS) and the Estimated Inversion Strength (EIS). Visibly, LTS and EIS are well correlated, as well as their anomalies (relative to the climatological monthly mean). Data are (10,000 randomly selected points) from (a) the ECMWF Interim Re-Analysis (ERA-Interim) and (b) the CCCma updated fourth generation atmospheric GCM (CanAM-4.1), for January 1990 to January 2000, over the ocean, from the tropics (30°S–30°N). Figures with data from the ECMWF 40 years Re-Analysis (ERA-40) or the CCCma third generation atmospheric GCM (AGCM-3) are all similar (not shown).

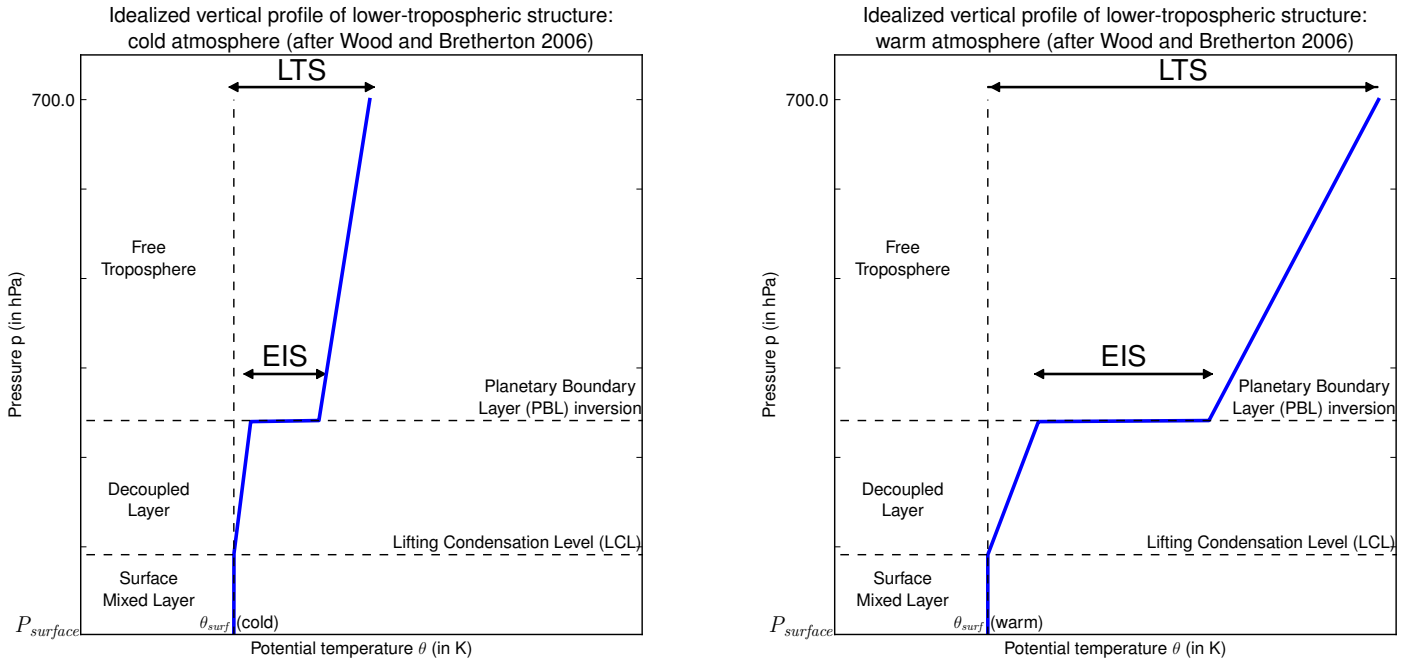

(a) Cold

(b) Warm

Figure 2.8: Idealized potential temperature (θ) vertical profile of lower-tropospheric structure during periods of undisturbed flow for (a) colder and (b) warmer atmospheres. This illustrates that the larger the temperature, the smaller the relative contribution of the Estimated Inversion Strength (EIS) to the Lower Tropospheric Stability (LTS). After Wood and Bretherton (2006).

2.3 Second dimension: dynamics

2.3.1 Overview

This section focuses on the dynamical dependency of clouds. The variable described here is closely related to the dynamics of the atmospheric column. Interestingly, and unlike stability, dynamics is almost exclusively represented by only one variable (ω_{500}, see next section).

Clouds "float" in the air, at various altitudes, and can sometimes rise and deepen before your eyes within minutes or hours. It is thus by a simple logical association that one could think of the coupling between the air vertical motion and the presence of clouds.

Many studies have tried to correlate large-scale (vertical) circulation with clouds and their properties, either as a self-sufficient explanation or as a complement for another predictor, such as SST (Ramanathan and Collins 1991; Fu et al. 1992; Hallberg and Inamdar 1993; Hartmann and Michelsen 1993; Weaver et al. 1994). One example of a variable used as a proxy for vertical motion (of water vapor) is given by Prabhakara et al. (1979) and Stephens (1990), who used $\frac{W-\overline{W}}{\overline{W}}$ (with W the monthly precipitable water and $\overline{W}$ its value expected according to the SST).

2.3.2 Vertical velocity at the 500 hPa level (ω_{500})

As already said, the vertical velocity at the 500 hPa level (ω_{500}) is by far the most used proxy for the dynamics predictor in cloud studies. This section both justifies the choice of this quantity and reviews some insights about its correlation with clouds.

The reader must note that ω_{500} is a *pressure velocity*, therefore rising means ω_{500} negative ("uplift", "ascending") and sinking means ω_{500} positive (" subsidence", "descending"). It is usually expressed in either hPa/day or Pa/s.

Examples of ω_{500} distributions are given in Figure 2.9 (page 48) and in Figure 6.2b (page 125). As visible in these figures, and considering that an ω_{500} value of 50 hPa/day is of the order of 1 cm/s, note how the vast majority of the data points (or pixels) belongs to vertical motion at low or moderate speed. Also, note that subsidence ($\omega_{500} > 0$) tend be typically slower (i.e. smaller $|\omega_{500}|$) than uplift ($\omega_{500} < 0$) (i.e. larger $|\omega_{500}|$).

Bony et al. (1997), among the first, explains, before using it, that ω_{500} is a good proxy for the large-scale circulation in the tropics. They look at ω_{500} more as a complement variable when SST is not enough, probably because ω_{500} is not an entirely new, separate dimension, but rather a function of SST.

A key finding is that, at least in *re-analysis* data, ω_{500} is demonstrated to be good enough on both a daily and monthly bases (for the study purposes). This last point is important since it directly relates to the type of data used in this thesis (re-analysis and monthly).

By conducting their analysis with both ω_{500} and the vertical velocity at the 850 hPa level (ω_{850}), Weaver and Ramanathan (1997) report that they are both very strongly correlated, and that results are not sensitive to this choice. This study's datasets also have very well correlated ω_{500} and ω_{850} (or ω_{700}), as shown in Figure 2.10, and results do not depend on using ω_{850} or ω_{700} rather than ω_{500} (not shown).

In addition to this, they show that ω_{500} is a good proxy for rising motion both on a daily and monthly basis, even more particularly through the Free Troposphere (FT). Furthermore, two distinct ω_{500} regimes are identified for LW CRF and SW CRF (upward motion for convective clouds, downward motion for stratiform clouds) The authors point out extremely important facts about ω_{500} :

1. strong uplift and subsidence often occur in geographically close places, at least on a short time scale, therefore space and time averaging (if any) matters a lot.

2. because cloud-ω_{500} coupling may not be linear — and in fact has been shown to be non-linear for some variables and time scales — (extreme) variations do not necessarily average out. In other words, for an ω_{500} with a constant mean value, a change in its standard deviation $\sigma_{\omega_{500}}$ can lead to a change in the cloud property.

3. relevant to this thesis, monthly mean ω_{500} magnitude is demonstrated to be much smaller than daily mean ω_{500} magnitude, precisely because, in the average process, the extremes get averaged out.

Following the warning of Weaver and Ramanathan (1997), Williams et al. (2003) assume, as I do, a linear response of low cloud to ω_{500} (so that extremes average out and their net

effects cancel out too) on the ground that they ignore how well monthly mean ω_{500} values represent daily mean ω_{500} values. Williams et al. (2003) compute two composites: one based on values (SST and ω_{500}) and one based on climatological anomalies ($SST_{anomalies}$ and $\omega_{500anomalies}$). Not knowing if a positive ω_{500} anomaly means an increased descent or a reduced ascent is a noticeable analysis drawback. Nonetheless, some useful information comes from this anomaly analysis (see next section).

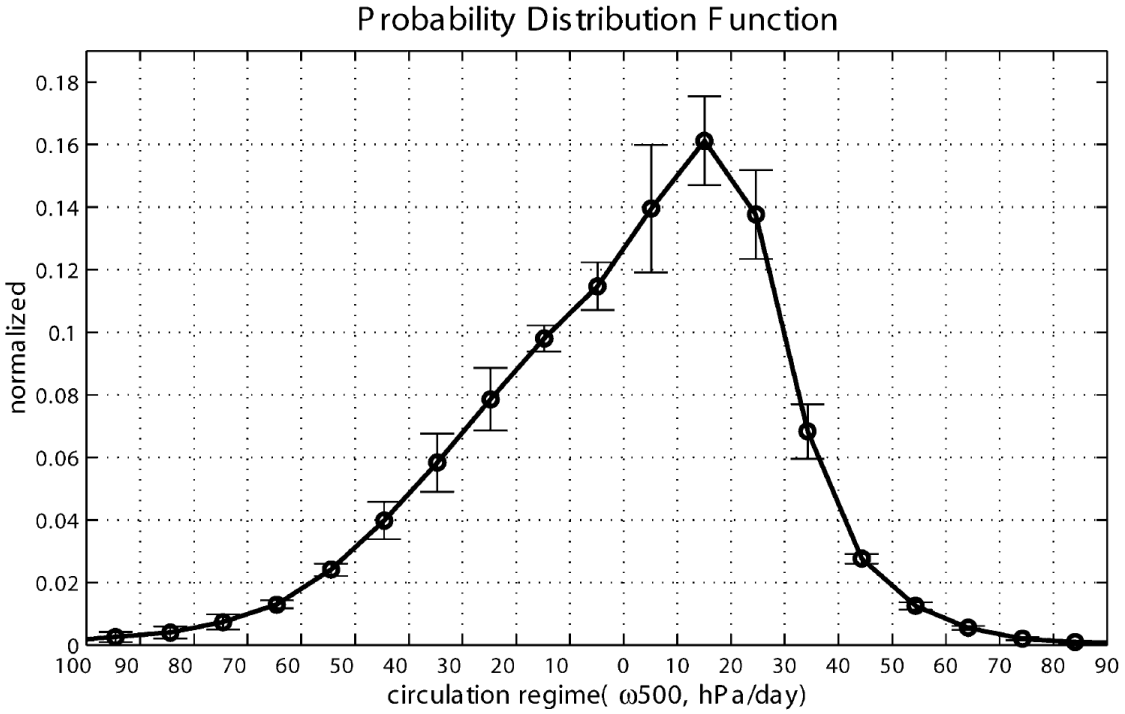

Figure 2.9: The Probability Distribution Function (PDF) of vertical velocity at the 500 hPa level (ω_{500}) in the tropics (30°S–30°N) derived from meteorological reanalyses. Remark that the negative sign ("−") is missing on the left hand side (lhs) of the x-axis. To compare with other ω_{500} distributions, see Figure 6.2b (page 125). From Bony et al. (2004), by permission.

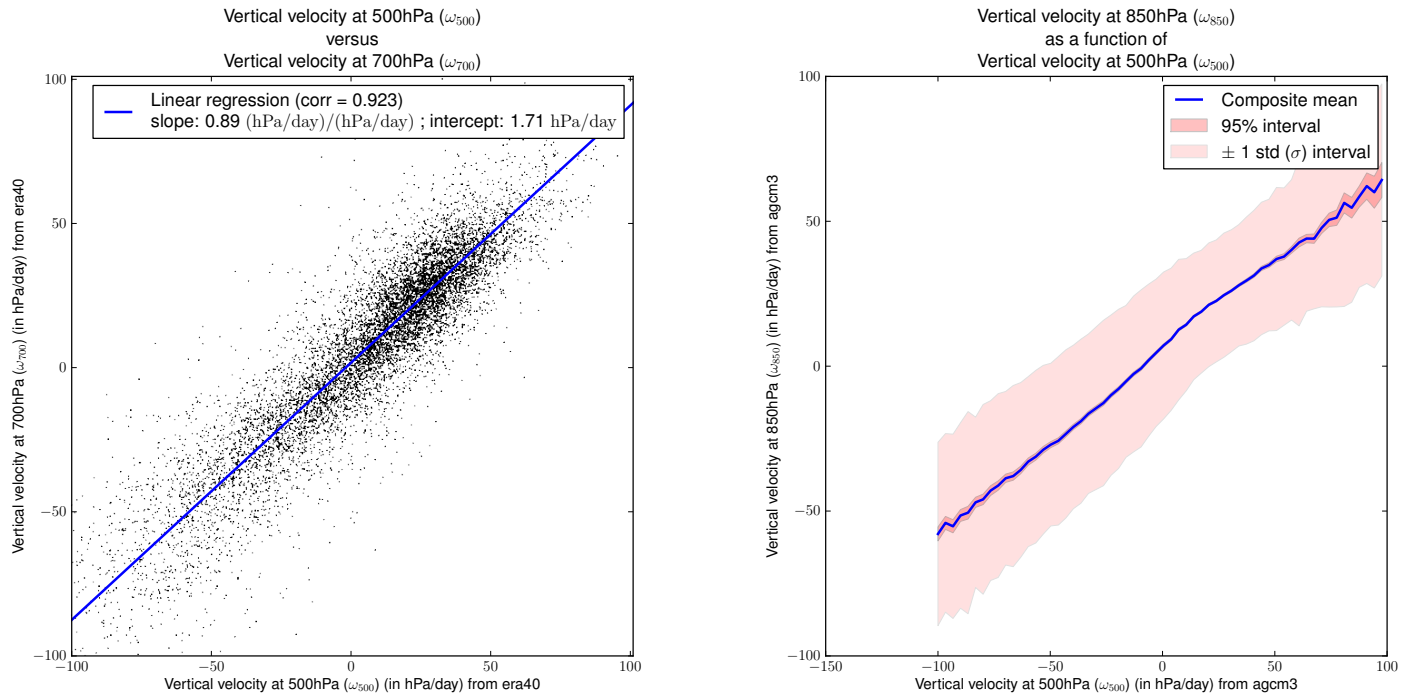

(a) ω_{500}-ω_{700} scatter plot

(b) ω_{500}-ω_{850} composite histogram

Figure 2.10: Comparison and correlation between the vertical velocity at the 500 hPa level (ω_{500}), ω_{700} , and ω_{850} . Visibly, ω_{500} is very well correlated with ω_{700} (as well as with ω_{850}), thus making the choice of ω_{500} over ω_{700} or ω_{850} impact-less on the conclusions. Data are from (a) the ECMWF 40 years Re-Analysis (ERA-40) and (b) the CCCma third generation atmospheric GCM (AGCM-3), for January 1990 to January 2000, over the ocean, from the tropics (30°S–30°N). Figures with data from the ECMWF Interim Re-Analysis (ERA-Interim) or the CCCma updated fourth generation atmospheric GCM (CanAM-4.1) are all similar (not shown).

2.4 A stability-dynamics basis for cloud regimes

Borrowing from the mathematical vocabulary, and as said earlier in this thesis, being able to break down the study of cloud using predictors, or dimensions, as orthogonal as possible maximizes the information gained while analyzing, i.e. increases the explanatory value of an experiment.

I chose the two predictors: stability and dynamics because: (i) both are strongly related to clouds and cloud properties, (ii) both are commonly used, thus making comparisons with other studies easier, and (iii) they are the two with the best trade-off between independence and explanatory value. This last point is of crucial importance to a simple, straightforward analysis. That is why, in this section, I give a quick overview of how independent the proxies I chose are (LTS and EIS for stability; ω_{500} for dynamics).

Bony et al. (1997) illustrate the relation between SST and large-scale vertical motion (in the tropics), and in particular how Super Greenhouse Effect (SGE) episodes need both variables to meet specific conditions to arise. They also investigate the tropical SST-CRF relation, and show that it has three distinct regimes, directly related to the three regimes of the relation SST-ω_{500} .

Using anomaly analysis, Weaver and Ramanathan (1997) show that when their two dimensions ($\Delta\theta_e$ and ω_{500}) vary in opposite directions, the correlation with cloudiness (CRF) is greatly reduced, if not canceled or negative. This result was part of a more general reflection about the relative importance of each variable and how they interact.

While focusing on the great dependency of clouds on SST anomalies, Williams et al. (2003) affirm that SST anomalies and patterns create, or at least contribute to, the large-scale circulation, for example through surface temperature gradients. They explain that the cloudiness dependency is affected by the location: its main driver is the SST anomaly in the tropics but the SST in the mid-latitudes. However, their unusual and changing definition of SST anomaly complicates comparisons of their results with other studies. Consistent with Bony et al. (1997), their results show that high clouds are more correlated with ω_{500} whereas low clouds are more correlated with SST anomalies (both results mainly true for thicker clouds).

The point of this section was simply to warn the reader of the apparent simplicity and

linearity of the analysis. It does not mean there is no benefit to it. It simply means that caution must be taken while visualizing the 2D-histograms (see section 3.3) as a basis decomposition.

2.5 Research objectives

I present here the research questions that this thesis elaborates (in this chapter) and addresses (in chapters 4, 5, and 6). Other research questions have been developed in the previous chapter (1, "Clouds and climate") and summarized at its end (section 1.3).

The goal is to improve climate simulation by models. Considering the previous section, it appears, in particular, that:

- factual (or statistical) relationships between multiple physical quantities exists and are not always proof of causality;
- in some cases, such links are conveniently used in models (as parametrization);
- compositing (or conditioning) helps to find and identify such co-relations;
- stability and large-scale circulation are well known predictors for (low) clouds;
- LTS and EIS (stability) as well as ω_{500} (large-scale circulation) have already been shown to be effective proxies; and
- unless proven to be (analytically) exact, a simple linear approximation, however convenient, is never sufficient.

That is why, this study compares 2D-histograms (as described in section 3.3) for cloud related variables, based on LTS, EIS, and ω_{500} — between GCMs and observations (or re-analyses).

Research objective 6:

How meaningful is a stability and large-scale circulation compositing comparison between observations and simulations (or re-analyses)? (i.e. relevance of analysis.)

Research objective 7:

How predictable are (low) clouds with respect to LTS, EIS, and ω_{500} ? (i.e. observed global validity of statistical fits.)

Research objective 8:

How well do GCMs (or re-analyses) reproduce the predictability of (low) clouds by LTS, EIS, and ω_{500} ? (i.e. realism of simulated clouds.)

Chapter 3

Data and methods

Luck is what happens when opportunity meets preparation.

Seneca (5 BC – 65 AD ; Roman dramatist, philosopher, and politician)

La chance ne sourit qu'aux esprits bien préparés.
(Luck smiles only on well prepared minds.)

after Louis Pasteur (1822–1895 ; Biologiste et chimiste français)

3.1 Data sets

This section presents the data used in this study, with its origins, characteristics, and post-processings (such as interpolation on a new grid or file conversion). It also explains what my intentions were when I chose each of these data sets (comparison, validation, etc.)

3.1.1 Characteristics overview

As stated in this thesis title, my goal was to look at correlations between the atmospheric stability, dynamics, and cloud properties in observations, re-analyses, and models. Therefore, I needed each of these fields (stability, dynamics, clouds) for each of these source types (observations, re-analyses, models). Moreover, to increase the results' robustness and significance, and also because it was an exploratory process, I tried as much as possible to use data from at least two sources. They were not always independent, but they would always bring additional information (e.g. a comparison between an older and a newer version of a model shows how model changes impact performances).

Table 3.1 summarizes while Table C.1 (in Appendix C, page 159) lists and details all datasets that are used plus some that could be (to complete or extend this research). Additional information (i.e. not in Table C.1) for each of these datasets is given in the next sections. The datasets are classified in three main types:

1. observational data (ISCCP and MODIS for clouds, GPCP for precipitation, CEBAF for radiation)
2. re-analysis output (ERA-40 and ERA-Interim)
3. model output (AGCM-3 and CanAM-4.1)

Note that there is an incomplete (time) overlap, thus some comparisons and plots in this thesis do not involve all the datasets but only some at a time. As Figure 3.1 illustrates it, AGCM-3 and CanAM-4.1 can be compared (i.e. simulations' epochs overlap) only when one observational dataset is available for clouds or radiative fluxes (i.e. ISCCP). This may be problem since an estimate of the variability between simulation and observation would not have any meaning without an estimate of the variability between observations.

That is why, chapter 4 first demonstrates the relevance of the "reference" choice in comparing several observational datasets with re-analyses and model outputs (time overlap shown in Figure A.2). Then CanAM-4.1 is actually (quantitatively) compared to multiple observations in chapter 4 and to AGCM-3 in chapter 5 (time overlap shown in Figure A.1). Finally, possible reasons for discrepancies are (qualitatively) examined in chapter 6, such as differences in stability, dynamics, precipitations, or cloud regimes.

All data used in this thesis are monthly data, i.e. monthly means of daily means, that were downloaded in or converted to the NETwork Common Data Form (netCDF) format[1].

Nature		Data sets		
		Clouds	*Precipitation*	*Radiation*
Observation	Used	ISCCP MODIS	GPCP CMAP	CERES ISCCP-FD
	Available	MISR CloudSat CERES ISCCP-like PARASOL	TRMM	ERBE
Re-analysis	Used	ERA-40 ERA-Interim		
	Available	NCEP/NCAR JRA-25 NASA's MERRA		
Models	Used	CCCma AGCM-3 CCCma CanAM-4.1		
	Available	Any model or center that submitted simulation outputs for AMIP or CFMIP		

Table 3.1: Summary of datasets used or available. Available sets are given as examples and are *not* an exhaustive list of alternatives or complements. For full names (expanded acronyms) see the glossary page xi.

[1]More information on this file format can be found here `http://en.wikipedia.org/wiki/NetCDF` or here `http://www.unidata.ucar.edu/software/netcdf/`.

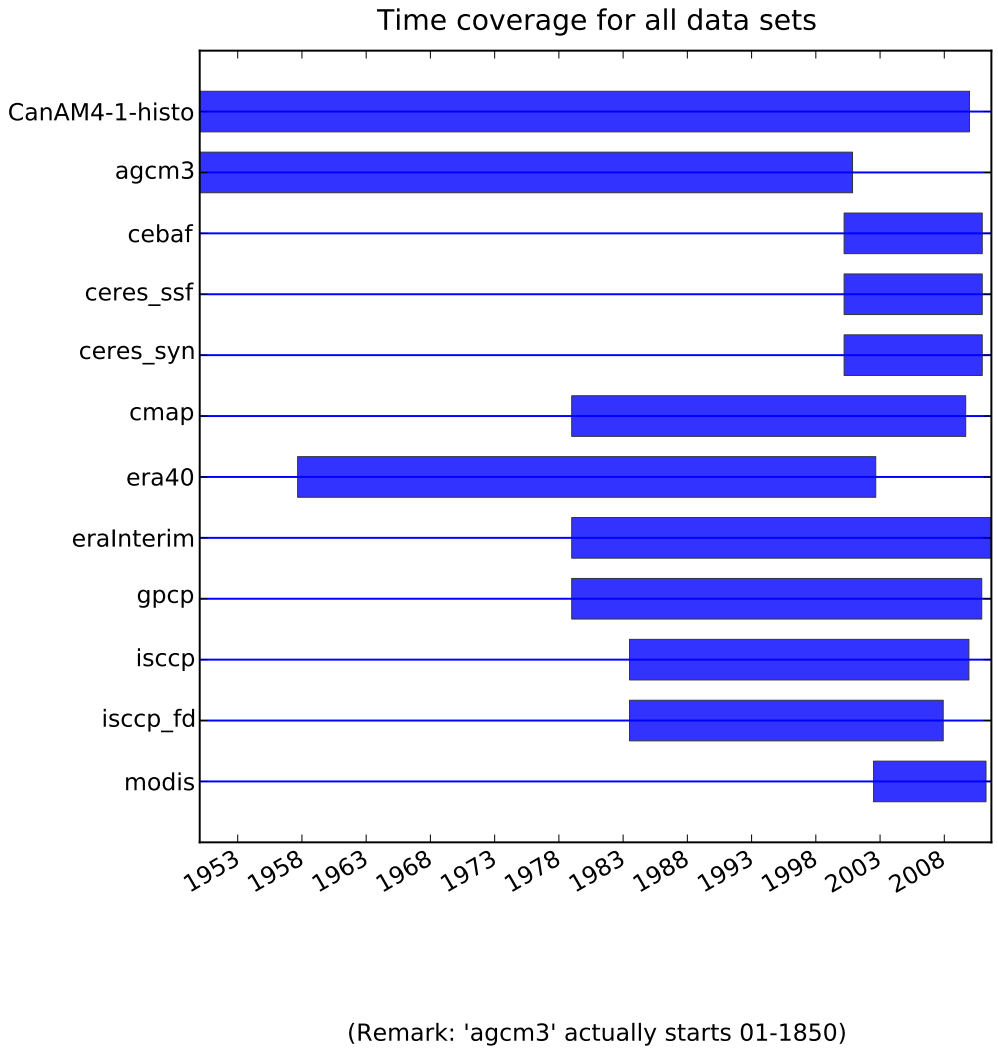

Figure 3.1: Time coverage for all datasets used in this study. One can see that two periods are particularly interesting: in the 2000's when many datasets are available on one hand, in the 1980's and 1990's when both the CCCma third generation atmospheric GCM (AGCM-3) and the CCCma updated fourth generation atmospheric GCM (CanAM-4.1) are available on the other hand. See Figures A.1 and A.2 for detailed overlaps (pages 153 and 154).

3.1.2 Regridding process

In order to compute the Taylor diagram (see section 3.2) and 2D-histogram (see section 3.3) of several datasets, the chosen variable must be recorded on the same grid (or array). However, as Table C.1 shows, my datasets were initially saved on various grids ($2.5^\circ \times 2.5^\circ$, $1.5^\circ \times 1.5^\circ$, $1.0^\circ \times 1.0^\circ$, with different center reference, etc.)

Therefore, it was necessary to regrid them all to one "reference" grid. For practical purpose, the Canadian Centre for Climate Modelling and Analysis (CCCma) grid used in AGCM-3 and CanAM-4.1 simulations was chosen to be the reference.

My regridding process is a simple (statistical) bilinear interpolation from one rectilinear grid to another (with also a nearest-neighbor interpolation in order not to mask neighbors of missing data)[2]. This particular regridding process sufficiently preserves the mean, the standard deviation (σ), and even the shape of the Probability Distribution Function (PDF), as shown in Figure 3.2 for precipitation from Global Precipitation Climatology Project (GPCP). Preservation of the distribution and main statistical moments is of similar quality for other regridded fields (not shown).

All necessary datasets (International Satellite Cloud Climatology Project (ISCCP), GPCP, ECMWF 40 years Re-Analysis (ERA-40)...) have also been interpolated by CCCma to their own grid with their own method, which was the practical reason aforementioned to focus on this particular grid.

These two different regridding processes were tested and compared. Table 3.2 reveals that fields are not sensitive to the use of one interpolation scheme over the other. Thus, results shown in this thesis are based indifferently on the datasets regridded using either my bilinear interpolation or the CCCma mean-conservative interpolation scheme.

To summarize, neither the interpolation scheme (Table 3.2) nor the "reference" grid choice (Figure 3.2) matter to the distribution and main statistical moments of the fields used in this study.

[2]Library and method used, see: `http://matplotlib.sourceforge.net/basemap/doc/html/api/basemap_api.html#mpl_toolkits.basemap.interp`

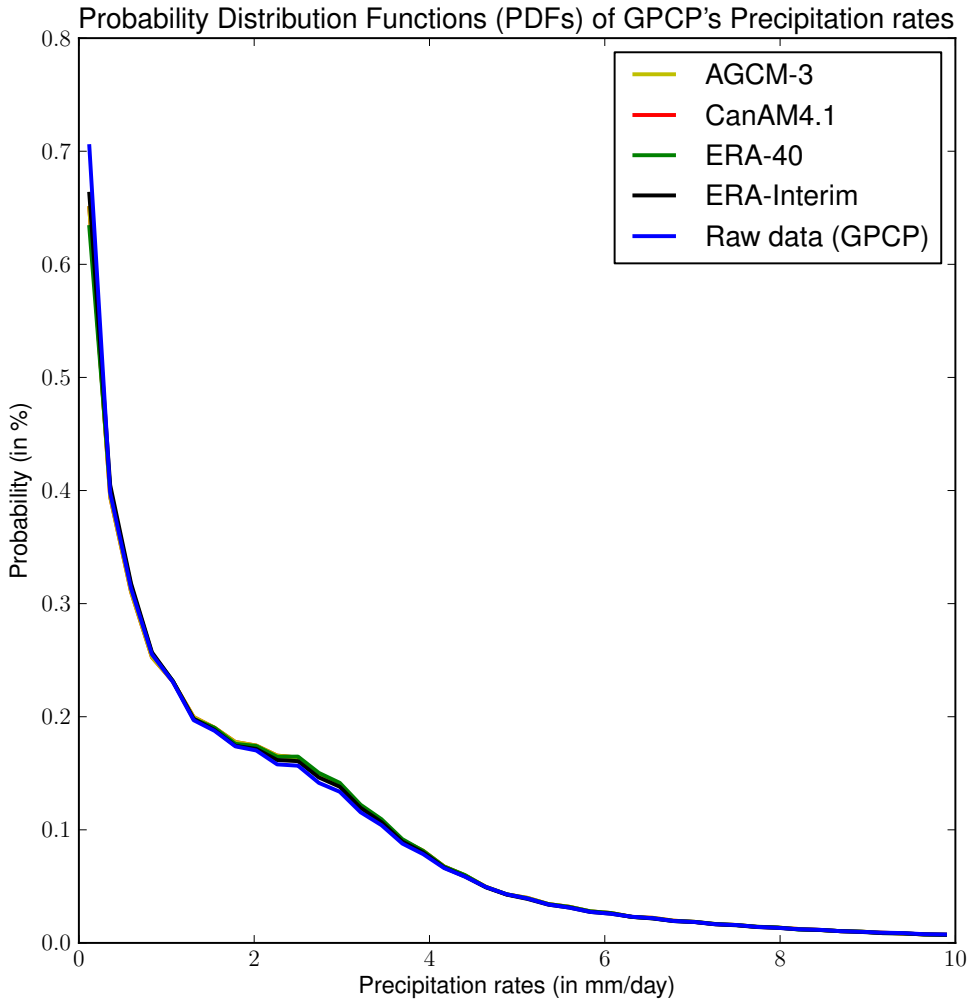

Figure 3.2: Sensitivity of the Probability Distribution Function (PDF) to the interpolation (i.e. regridding). This example is for precipitation rate from the Global Precipitation Climatology Project (GPCP) when interpolated to several grids, including the "reference" grid (Canadian Centre for Climate Modelling and Analysis (CCCma) grid used in CanAM-4.1 simulation). The blue line ("Raw data (GPCP)") is the observational, non interpolated, data. Distributions (and their statistical moments such as means and standard deviations) are very similar. Averages are identical within less than 3% of relative difference.

Variable	Interpolation	Mean	Rel. diff.	Std σ	Rel. diff.
Low cloud (%)	Bilinear	25.83	0.04 %	14.21	0.14 %
	CCCma	25.84		14.19	
High cloud (%)	Bilinear	22.88	0.09 %	15.05	0.33 %
	CCCma	22.90		15.10	
Precipitation (mm/day)	Bilinear	2.89	0.34 %	2.81	0.00 %
	CCCma	2.90		2.81	

Table 3.2: Sensitivity of the mean and standard deviation to the interpolation scheme. High and low cloud fractions are from the International Satellite Cloud Climatology Project (ISCCP). Precipitation rates are from the Global Precipitation Climatology Project (GPCP). The same datasets are interpolated to the same grid — CanAM-4.1 from the Canadian Centre for Climate Modelling and Analysis (CCCma) — using either a simple bilinear scheme, or the CCCma scheme. Values are taken for the 60°S–60°N band, from July 1983 to December 2007, for both land and ocean. "Std" stands for standard deviation and "Rel. diff." stands for relative difference, computed as $\frac{100 \cdot |a-b|}{\frac{a+b}{2}}$ and expressed in percent.

3.1.3 Cloud fields

ISCCP and MODIS

are two independent satellite datasets for clouds and cloud properties. Using both gives a feel (at worst) or an estimate (at best) of observational uncertainty for the satellite cloud property dataset.

Both instruments share similarities: they are passive nadir-viewing, have 1 km^2 pixel sizes at nadir, and have difficulties detecting thin clouds. However, post-processing of measurements are handled in varying ways, in particular for these hard-to-see thin clouds (Williams et al. 2003). ISCCP has a more liberal approach and categorizes as "thin cirrus" any detected clouds with an optical depth (τ) lower than its detection limit, believed to be between 0.1 over ocean and 0.3 over land (Rossow and Schiffer 1999). On the other hand, MODerate resolution Imaging Spectroradiometer (MODIS) has a more conservative approach and discards any detected clouds with an indeterminable τ .

That is why many studies, and in particular this one, ignore clouds with $\tau < 0.3$ when computing cloud fractions. This allows a better comparison between studies as well as between MODIS and ISCCP.

"Daytime only" data

or "sun-lit-only" data were used in this study, for three reasons. First, using two spectral domains — VISible (VIS) and InfraRed (IR)— ensures a greater accuracy or quality. Second, much of the spread in Cloud Radiative Effect (CRE) and Cloud Radiative Forcing (CRF) among General Circulation Models (GCMs) is in the shortwave (SW) (Bony and Dufresne 2005; Williams et al. 2006). Third, the simulator that computes ISCCP-like values for CCCma CanAM-4.1 — the CFMIP Observation Simulator Package (COSP) — assumes daytime, i.e. the post-COSP value is what the satellites (here ISCCP) would have seen given the simulated atmospheric column *and* given an observation during daytime (VIS + IR).

Comparisons

are most relevant between: observations and CanAM-4.1 (“modis”, “modis_mask”, “isccp”, “isccp_IR”, and “CanAM4-1-histo (cloud-isccp)”), on one hand; and re-analyses and models (“era40”, “eraInterim”, “agcm3”, and “CanAM4-1-histo”), on the other hand.

Cloud reference

was chosen to be observations from ISCCP both because of CanAM-4.1’s *ISCCP-simulated* field, and because it is the only dataset covering the two periods (1980’s-1990’s versus 2000’s).

Naming conventions (in figures):

- low cloud observational data from MODIS, i.e. when clouds are detected *and* their properties can be retrieved (’Retrieval’, **“modis”**) or cannot be retrieved (’Mask’, **“modis_mask”**);
- low cloud observational data from ISCCP, i.e. when clouds are detected only during day time using both visible and IR channels (’VIS’, **“isccp”**) or during both day and night time using only IR channels (’IR’, **“isccp_IR”**);
- low cloud simulated outputs from CanAM-4.1’s *historical* run, as it would be ’observed’ by a model (**“CanAM4-1-histo”**) or by ISCCP’s satellites (**“CanAM4-1-histo (low_cloud-isccp)”** or **“CanAM4-1-histo (high_cloud-isccp)”**).

3.1.4 Radiation fields

Clouds and the Earth’s Radiant Energy System (CERES) products include both solar-reflected and Earth-emitted radiation from the top of the atmosphere to the Earth’s surface. However, CERES product Top Of the Atmosphere (TOA) fluxes are known for having a positive net imbalance, due mostly to CERES instrument absolute calibration.

That is why, radiations observed by the CERES can be then processed (adjusted) so that it is consistent with other data:

- no post-processing other than temporal interpolation (**“ceres_ssf”**)

- GEO-enhancement, temporal interpolation, and post-processing for flux profiles consistent with cloud properties (**"ceres_syn"**)
- GEO-enhancement, temporal interpolation, clear-sky filling, and post-processing for flux profiles consistent with energy balance (**"cebaf"**)

For "cebaf", an algorithm is used to adjust SW and longwave (LW) TOA CERES fluxes within their range of uncertainty to remove the inconsistency between average global net TOA flux and heat storage in the Earth-atmosphere system. This (new) dataset is called "CERES Energy Balanced And Filled (CEBAF)" and is designed for climate modelers that need a net imbalance constrained to the ocean heat storage, which is the case in this study.

CEBAF (or "cebaf" in figures) is chosen as the *radiation reference* for the most recent period (2000's) because this dataset is tuned to the same standard than models (the energy balance, especially considering the ocean heat transfers), as Figures 4.9–4.10–4.11 clearly shows (pages 86–87–88).

ISCCP Flux Data ("isccp_fd") is chosen as the *radiation reference* for the least recent period (1980's-1990's) since it is the only observational dataset readily available covering this period. ECMWF Interim Re-Analysis (ERA-Interim) output was not (readily) available (therefore are missing in the figures).

3.1.5 Precipitation fields

Data from the Global Precipitation Climatology Project (GPCP) was (arbitrarily) chosen as the *precipitation reference* for both periods (over data from the Climate Prediction Center (CPC) Merged Analysis of Precipitation (CMAP)).

ERA-Interim outputs were not (readily) available (therefore are missing in the figures of chapters 4, 5, and 6).

Purely (satellite) observations (**"cmap"**) were completed with National Centers for Environmental Prediction (NCEP) / National Center for Atmospheric Research (NCAR) Re-Analysis (NCEP/NCAR) outputs in order to fill in missing data (**"cmap_enh"**).

Here precipitation rate (**"gene_precip"**) is the sum of all precipitation (in particular, both stratiform and convectiform).

3.2 Taylor diagram

3.2.1 Purpose and application

Taylor diagrams (Taylor 2001) provide a way to graphically summarize how closely a pattern (or model results) matches a reference model or, most commonly, observations[3]. An illustration is given in Figure 3.5 (page 68). The diagram provides a way of plotting three statistics on a 2-D graph, because of the relationship that ties them together. The similarity between two patterns is quantified in terms of:

1. their correlation (R),
2. their centered root-mean-square difference (E') (also called the "skill score"), and
3. the amplitude of their variations (represented by their standard deviations σ).

The plotted values are generally derived from monthly or seasonal climatological means of one or more variables. These diagrams are therefore especially useful in evaluating multiple aspects of complex models or in gauging the relative skill of many different models, potentially relative to observations. Other information can be readily available from a Taylor diagram:

- another skill measure (instead of the Root-Mean-Square Difference (RMSD), isolines of the skill measure are substituted)
- observational uncertainty (with several *independent* sets of observations)
- a model's internal variability (with several runs of the same model)
- a model's improvements between two versions (if runs from each version are compared to a third set, reference model or observations)
- comparison of different variables, such as precipitation and cloud amount (if the diagram is initially normalized)

Symbol	Meaning
C_{observ}	A variable (e.g. cloud fraction) from an observational dataset. It will be used as the "reference" field
C_{model}	A variable (e.g. cloud fraction) from a model simulation. It will be used as the "test" field and compared to C_{observ}
R	The correlation coefficient between the test (C_{model}) and the reference (C_{observ}) fields
E'	The centered RMSD between the test (C_{model}) and the reference (C_{observ}) fields
σ_{observ}	The standard deviation (*std*) of the reference field (C_{observ})
σ_{model}	The standard deviation (*std*) of the test field (C_{model})
σ^2_{observ}	The variance of the reference field (C_{observ})
σ^2_{model}	The variance of the test field (C_{model})

Table 3.3: Symbols used in order to explain and illustrate the Taylor diagram construction.

3.2.2 Equation and graphic construction

The three statistics considered (correlation, standard deviation, and Root-Mean-Square (RMS) difference) are defined by:

$$R = \frac{\frac{1}{N}\sum_{n=1}^{N}\left(C_{observ} - \overline{C_{observ}}\right)\left(C_{model} - \overline{C_{model}}\right)}{\sigma_{observ} \cdot \sigma_{model}} \tag{3.1}$$

$$\sigma^2_{observ} = \frac{1}{N}\sum_{n=1}^{N}\left(C_{observ} - \overline{C_{observ}}\right)^2 \tag{3.2}$$

$$E'^2 = \frac{1}{N}\sum_{n=1}^{N}\left[\left(C_{observ} - \overline{C_{observ}}\right) - \left(C_{model} - \overline{C_{model}}\right)\right]^2 \tag{3.3}$$

with $\bar{x}$ the mean value of x.

Taking an example using the notation given in Table 3.3, linear algebra shows that the

[3] A four-page pdf document, "Taylor Diagram Primer", by Karl Taylor, is available here: `http://www-pcmdi.llnl.gov/about/staff/Taylor/CV/Taylor_diagram_primer.pdf`

relation between these three statistics is:

$$E'^2 = \sigma_{observ}^2 + \sigma_{model}^2 - 2 \cdot \sigma_{observ} \cdot \sigma_{model} \cdot R \tag{3.4}$$

which looks extremely similar to the Law of Cosines for a triangle :

$$c^2 = a^2 + b^2 - 2ab\cos(\phi) \tag{3.5}$$

where a, b, and c are the lengths of the sides of a triangle and ϕ is the angle opposite side c (as illustrated in Figure 3.3).

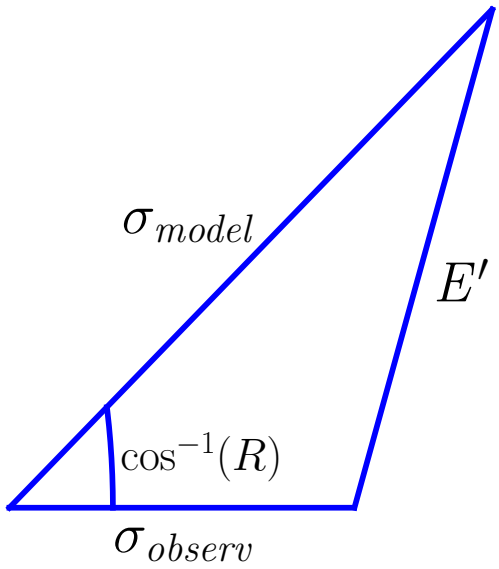

Figure 3.3: Geometric relationship between the correlation coefficient R, the centered pattern Root-Mean-Square (RMS) difference E', and the standard deviations σ_{observ} and σ_{model} of the reference and test fields, respectively. It illustrates how the three statistics involved in a Taylor diagram are related. See Table 3.3 for more information on the notations. After Taylor (2001).

3.2.3 Example

First of all, a field is chosen as the "reference". In this section, I use an arbitrary temperature field made of a latitude gradient (from 243 K to 303 K) plus some white noise (from -2.5 k to +2.5 k), as shown in Figure 3.4.

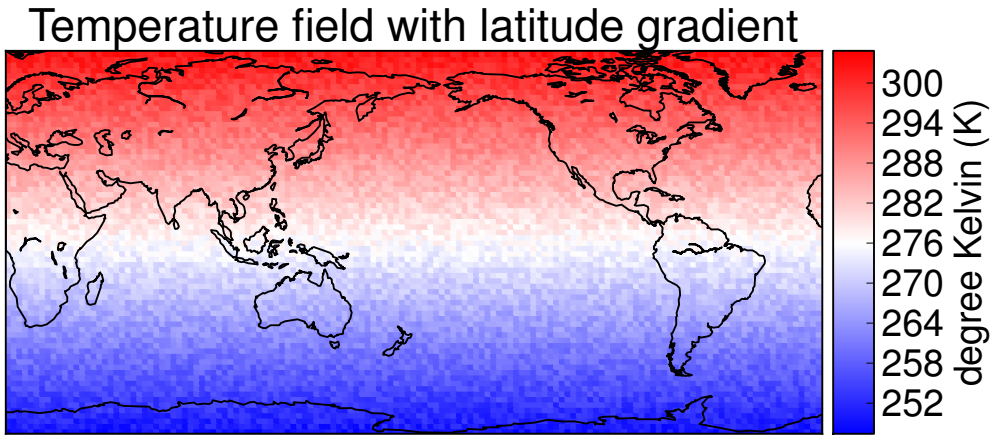

Figure 3.4: An example of an arbitrary and noisy temperature field with a latitude gradient.

Then — for the sake of the example — I create seven other fields:

- *"lat_shift"* : the original field but shifted in latitude (11°northward), so it has the same standard deviation but is a bit colder (same main trend) and its noise is off relative to the original one (different local variations). (Remark: South-pole data is the continuation of the latitude gradient.)
- *"weak_noise"* : the original field with an additional weak white noise (from -2.5 k to +2.5 k) (i.e. as strong as the one used in the original field), therefore increasing a bit the standard deviation and reducing a bit the (local) correlations.
- *"strong_noise"* : the original field with an additional strong white noise (from -5.0 k to +5.0 k) (i.e. twice stronger than the one used in the original field), therefore increasing a lot the standard deviation and reducing a lot the (local) correlations.

- *"uniform"* : a uniform field whose value is the mean of the original one (273 K), plus a white noise as strong as the original one (i.e. from -2.5 k to +2.5 k), so it is uncorrelated and has almost the same standard deviation (slightly smaller because it lacks the component due to the gradient).
- *"mix_unif_33"* : a mix field $1/3$ original + $2/3$ uniform, therefore being a bit closer to the original.
- *"mix_unif_67"* : a mix field $2/3$ original + $1/3$ uniform, therefore being closer to the original.
- *"mix_unif_91"* : a mix field $10/11$ original + $1/11$ uniform, therefore being much closer to the original.

Before adding a new dataset (or field) to a Taylor diagram, it is necessary to check that Equation 3.4 is verified to a certain degree, i.e. the following equation must be true:

$$\left| E'^2 - \left(\sigma^2_{observ} + \sigma^2_{model} - 2 \cdot \sigma_{observ} \cdot \sigma_{model} \cdot R \right) \right| < threshold \tag{3.6}$$

with *threshold* a pre-defined limit of agreement that the user can tolerate (typically 1%, 5%, or 10%).

The "reference" and seven additional fields are all shown on the Taylor diagram in Figure 3.5. It is particularly interesting to note that, despite being built in completely different ways, and having different meanings, the following three pairs have very similar RMS errors (E'): [*"mix_unif_91"* and *"lat_shift"*], [*"mix_unif_67"* and *"weak_noise"*], as well as [*"mix_unif_33"* and *"strong_noise"*]. This "third" axis, or skill score axis, allows the user to literally *see* how much a change in performance is attributable to the standard deviation component or to the correlation component.

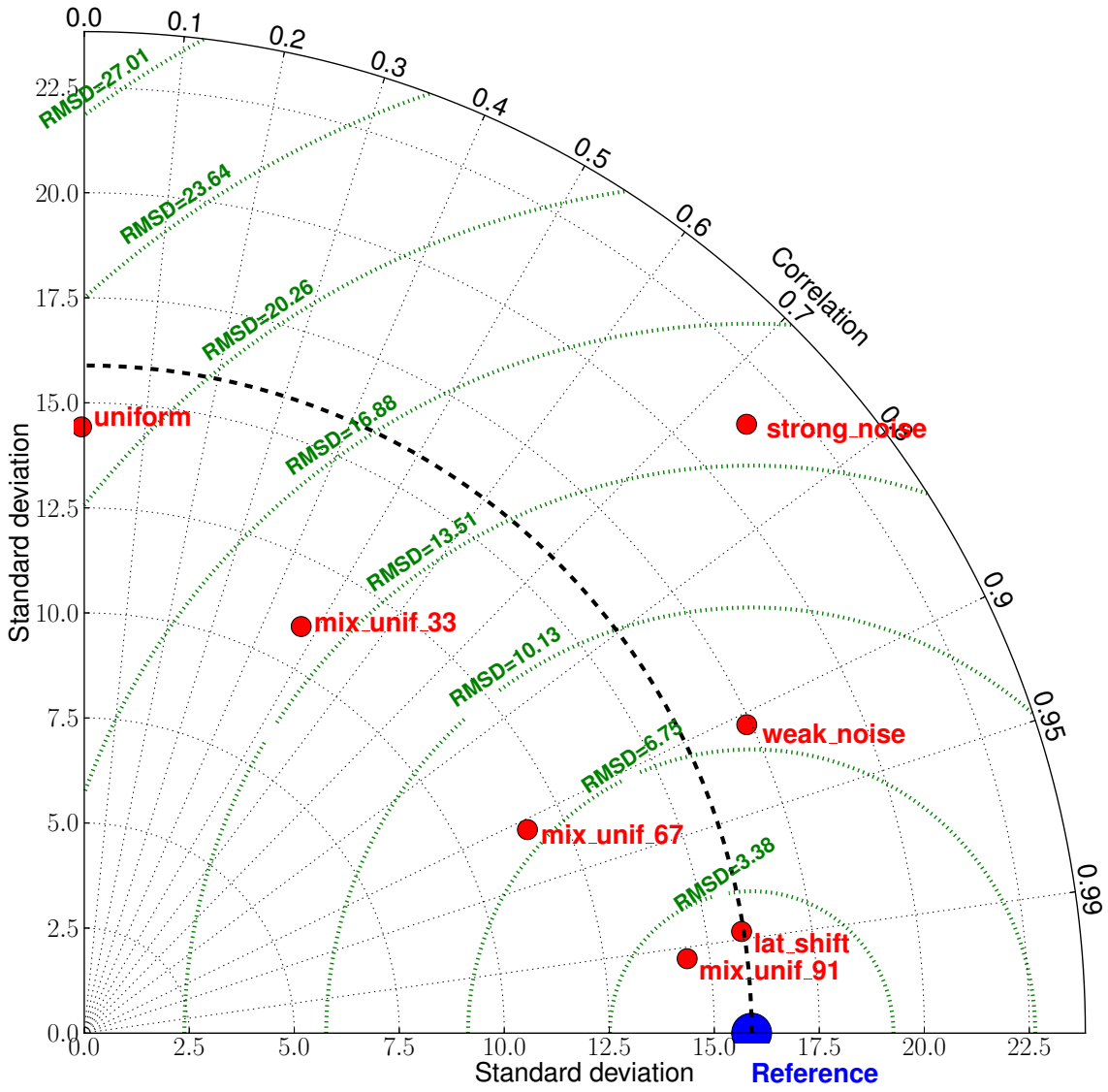

Figure 3.5: An example of a Taylor diagram. See subsection 3.2.3 and Figure 3.3 for more details on the computation and meaning of the reference and seven additional datasets. The black dashed line represents the standard deviation (σ_{observ}) isoline. The green dotted lines represent the Root-Mean-Square (RMS) difference isolines. Note that the correlation axis (R) is, by construction, non linear (ticks marked only for regular increment from 0.10 to 0.90, plus 0.95 and 0.99). Note that a second quadrant, on the left, can be used if negative correlations are found.

3.3 2D-histogram

3.3.1 Purpose

A 2D-histogram is a flattened and discrete representation of a three variable scatter plot or, almost equivalently, a two axis (hence "2D") *composite* histogram (hence "Histogram"). Although low resolution versions (less than 5x5 or 10x10 bins) have already been used in many studies, Medeiros and Stevens (2011) are among the first ones to use much higher binning (50×50 or 100×100).

Scatter plots are strongly intuitive way of representing pairs of variables, and allow users to readily see correlations, in particular if easy to see (such as linear). For instance, Figure 2.7 (page 44) shows a case where a linear fit, with relative strong correlation, performs well, whereas Figure 2.2 (page 36) shows a case where no linear fit appears to perform well (very poor correlation).

However, convenient representation are usually limited to one relation, or two variables. That is why, when two relations, or three variables, need to be simultaneously plotted against each other, another method is required.

Moreover, basic scatter plots are not suitable for data that are not uniformly weighted or masked, as it is the case in this study (because of the nature of the grid). Therefore, a specific way is needed to "collapse" the distribution along one of the 3D scatter plot to produce a 2D figure that accounts for weights. While collapsing the data, any special value of the distribution can be chosen (e.g. median, mean, variance, etc.)

The approach chosen in this study is a 2D-histogram, which helps us to visually answer the questions (for variables X, Y, and Z): "for given values of X and Y, what is such statistical moment of Z?" or "how influenced by Y is the relationship between X and Z?" 2D-histograms are similar to Taylor diagram in the sense that they both allow users to literally "see" how much to attribute to each variable for the variability in relationship.

3.3.2 Construction and examples

See illustration examples in Figure 3.6 and construction process in Figure 3.7 and Figure 3.8. For three variables (X, Y, and Z), if Z is the one whose data would be represented in the third dimension, then:

1. Z is binned relative to X, as would be done for a (composite) histogram
2. Z is binned relative to Y, as would be done for a (composite) histogram
3. for each pair bin (X_i, Y_i), one statistical moment (e.g. mean) is computed out of all Z values that belongs to this (X_i, Y_i) bin.
4. a pseudo color plot is built with the X bins on the x-axis, the Y bins on the y-axis, and the Z computed value on the color- or z-axis.
5. optionally, contours of the population density can be super-imposed (so that spurious relationship due to a low number of data points can be easily spotted).

Note that the variables (two, X-Y, for a heatmap or three, X-Y-Z, for a full version) must be expressed on the same grid, in order to accommodate the binning process. However, they do not need to all come from the same data source (e.g. ERA-40, CanAM-4.1, or ISCCP). Although this might seem an inconsistent analysis, it simply is a necessity as, for example, ISCCP knows only about clouds and not temperature or vertical velocity.

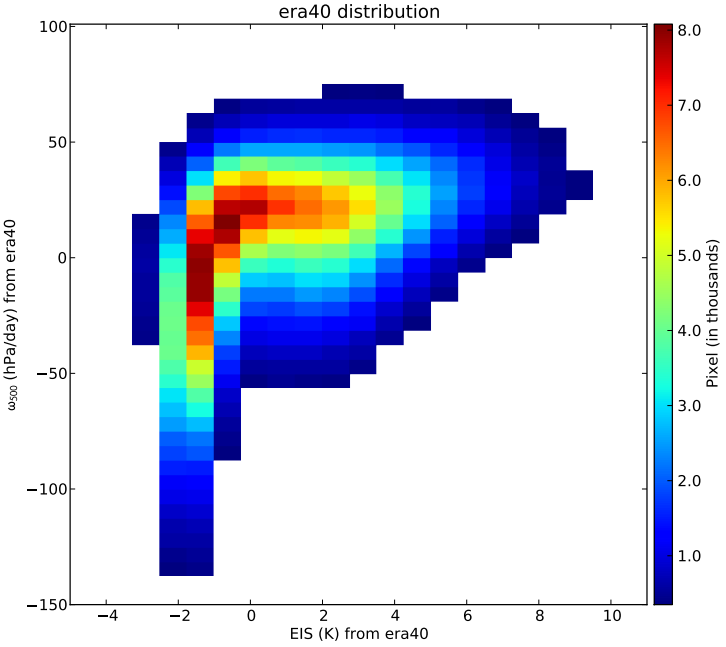

(a) Population density (“distribution”)

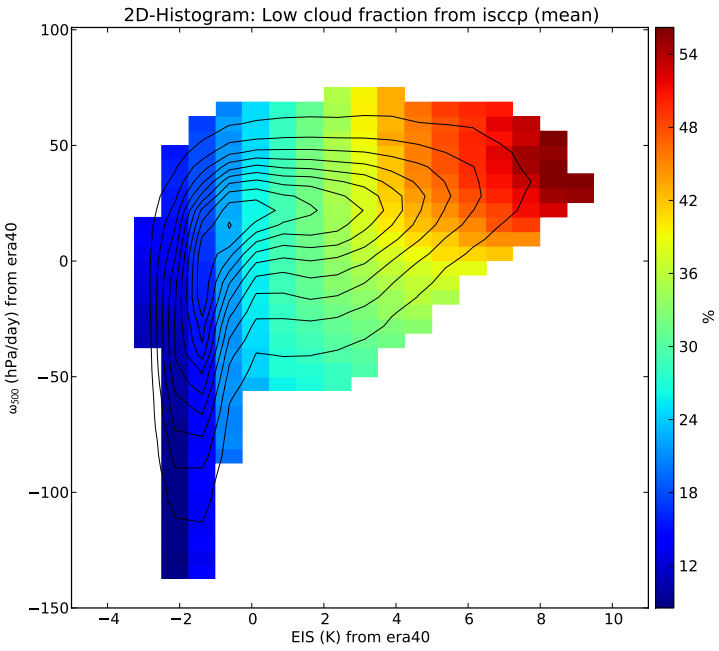

(b) Average (“mean”)

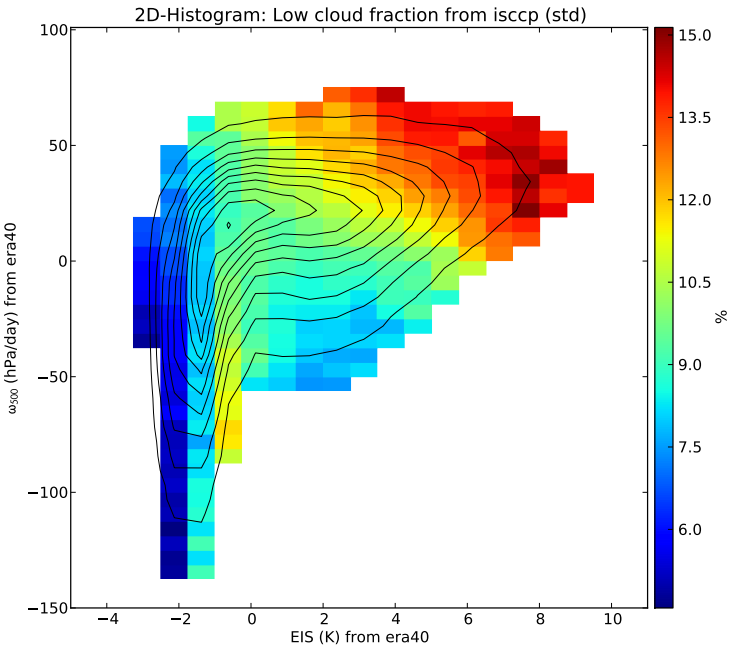

(c) Standard deviation (“std”)

Figure 3.6: Examples of 2D-histograms. X = Estimated Inversion Strength (EIS) and Y = vertical velocity at the 500 hPa level (ω_{500}) data come from the ECMWF 40 years Re-Analysis (ERA-40) and are binned on a 40x40 bins grid. Z = low cloud fraction data come from the International Satellite Cloud Climatology Project (ISCCP). Data points are for the 40°S–40°N band, over the ocean, from January 1985 to December 2001. The colored values are (a) the number, (b) the mean value, or (c) the standard deviation *of pixels falling into the 2D-bins.* Note that (a) is very similar to a “heatmap”, and that the contour lines in (b) or (c) are the population density lines. Bins with no or too few data points are not colored (i.e. , in this case and thereafter, the lower 5% of all 2D-bins cumulative population).

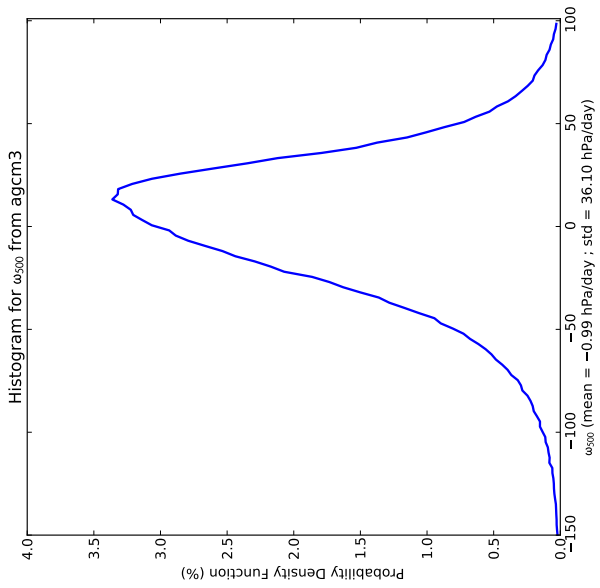

(a) ω_{500} distribution histogram

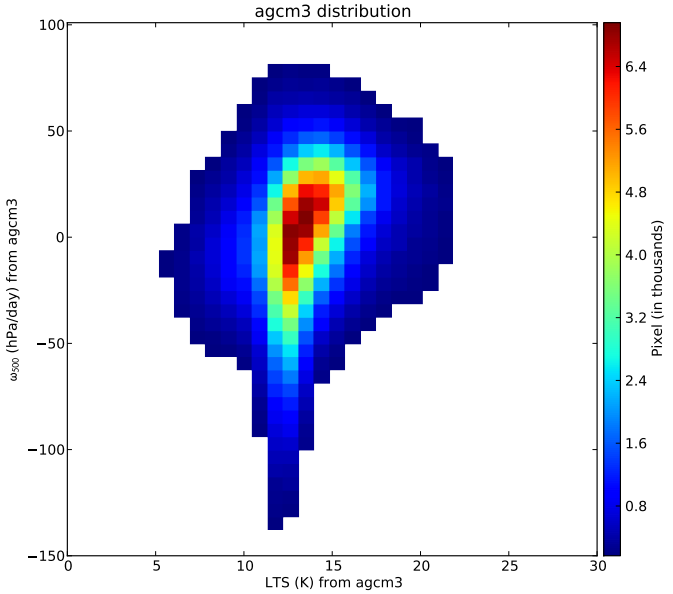

(b) LTS - ω_{500} distribution 2D-Histogram

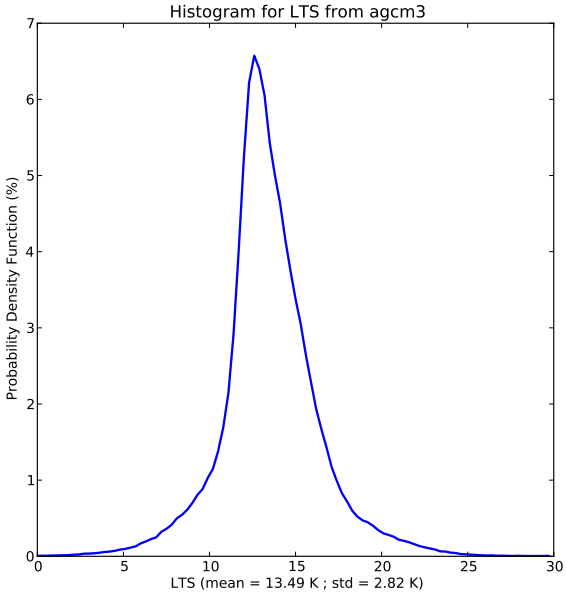

(c) LTS distribution histogram

Figure 3.7: Schematic of how a 2D-histogram is conceptually built. X = Lower Tropospheric Stability (LTS) and Y = vertical velocity at the 500 hPa level (ω_{500}) data come from the Canadian Centre for Climate Modelling and Analysis (CCCma) CCCma third generation atmospheric GCM (AGCM-3) and are binned on a 40x40 bins grid. Data points are for the 60°S–60°N band, over the ocean, from January 1990 to January 2000. (a) and (c) can be imagined as input for the 2D-histogram (b). Or, conversely, collapsing (b) data along X onto Y would give (a), while collapsing (b) data along Y onto X would give (c).

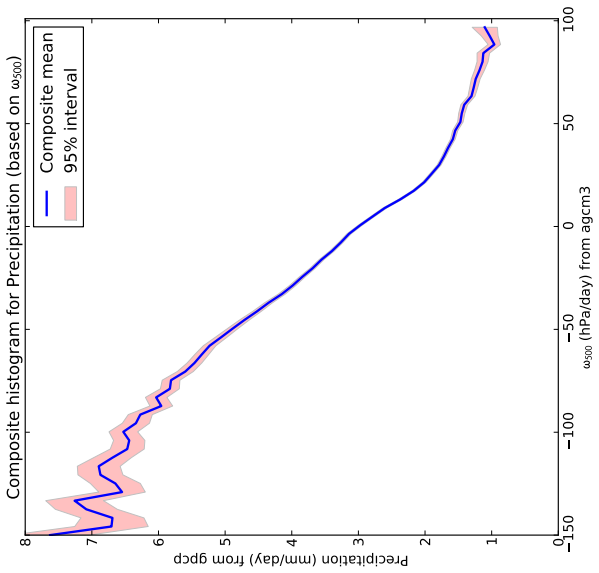

(a) Precipitation - ω_{500} composite histogram

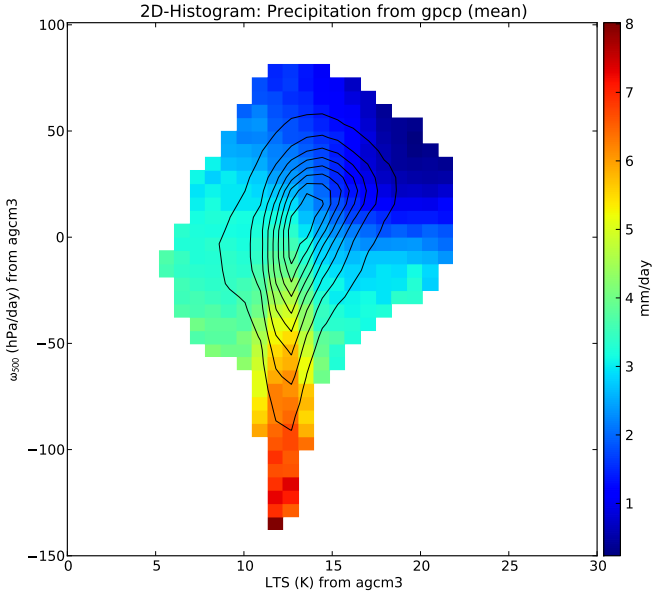

(b) LTS - ω_{500} mean precipitation 2D-Histogram

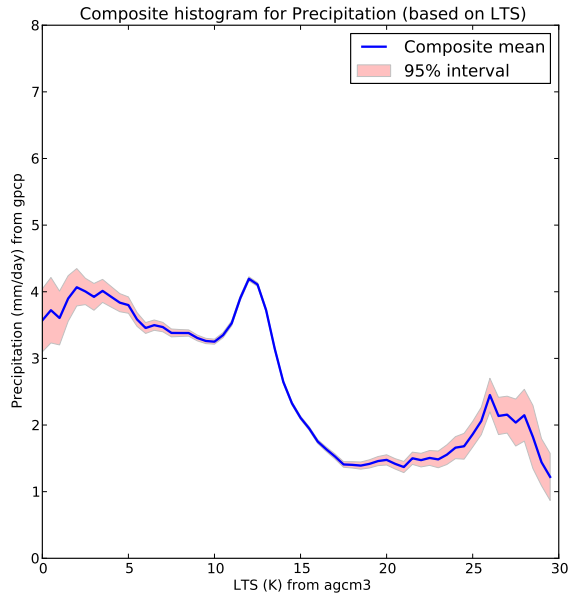

(c) Precipitation - LTS composite histogram

Figure 3.8: Schematic of how a 2D-histogram is conceptually built. X = Lower Tropospheric Stability (LTS) and Y = vertical velocity at the 500 hPa level (ω_{500}) data come from the CCCma CCCma third generation atmospheric GCM (AGCM-3) and are binned on a 40x40 bins grid. Z = precipitation data come from the Global Precipitation Climatology Project (GPCP). Data points are for the 60°S–60°N band, over the ocean, from January 1990 to January 2000. (a) and (c) can be imagined as input for the 2D-histogram (b). Or, conversely, collapsing (b) data along X onto Y would give (a), while collapsing (b) data along Y onto X would give (c).

Chapter 4

Variability between datasets

Een juist gevoel voor het grootte der dingen is van onschatbare waarde.
(A reasonable feeling for the sizes of things is of inestimable value.)

Marcel Minnaert (1893–1970 ; Belgian astronomer, biologist and physicist)

We must take change by the hand or rest assuredly,
change will take us by the throat.

Sir Winston Leonard Spencer-Churchill (1874–1965 ;
Former British prime minister, army officer, historian,
artist, and winner of the Nobel Prize in Literature)

Unless stated otherwise, all figures in this chapter are based on data (i) over the oceans (not over land), (ii) for the 30°S–30°N 'tropical' band, and (iii) from July 2002 to December 2007 (Figure A.2).

Each section compares the Probability Distribution Functions (PDFs), time series, Taylor diagrams, or a statistics table relative to its fields, plus, if necessary, some additional explanation for the comparisons.

4.1 Cloud fractions

4.1.1 Low clouds

Generally for low clouds (see Figures 4.1 and 4.2), data from the MODerate resolution Imaging Spectroradiometer (MODIS) detects low clouds the most ("modis_mask" highest value) but screens out potentially cloudy pixels the most (with his conservative retrieval algorithms) ("modis" lowest value).

In between, data from the International Satellite Cloud Climatology Project (ISCCP) have less low clouds ("isccp_IR" second highest value) especially while using only day time data (but is more liberal with its attribution algorithms) ("isccp" second lowest value).

According to Figure 4.1, output from the CCCma updated fourth generation atmospheric GCM (CanAM-4.1) and its *ISCCP-simulated* field ("low_cloud-isccp") are very similar and in between data from MODIS and ISCCP.

The processes of screening out unidentifiable low clouds are usually very visible when looking at PDFs (in Figure 4.2). Also, the *ISCCP-simulated* low cloud field from the CanAM-4.1 seem closer to more conservative observations than its direct output.

Following Figure 4.3 "ranking", CanAM-4.1's *ISCCP-simulated* field ("low_cloud-isccp") performs better that CanAM-4.1 raw output; but the ECMWF Interim Re-Analysis (ERA-Interim) performs even better; and observations are (still) closer to the reference ISCCP (e.g. MODIS).

Estimates of statistics are given in Table 4.1 and quantify the datasets proximity to ISCCP. Improvement depends to some extent on the scale used (e.g. mean, standard deviation, correlation) and progression is therefore not linear (e.g. see Figure 4.4).

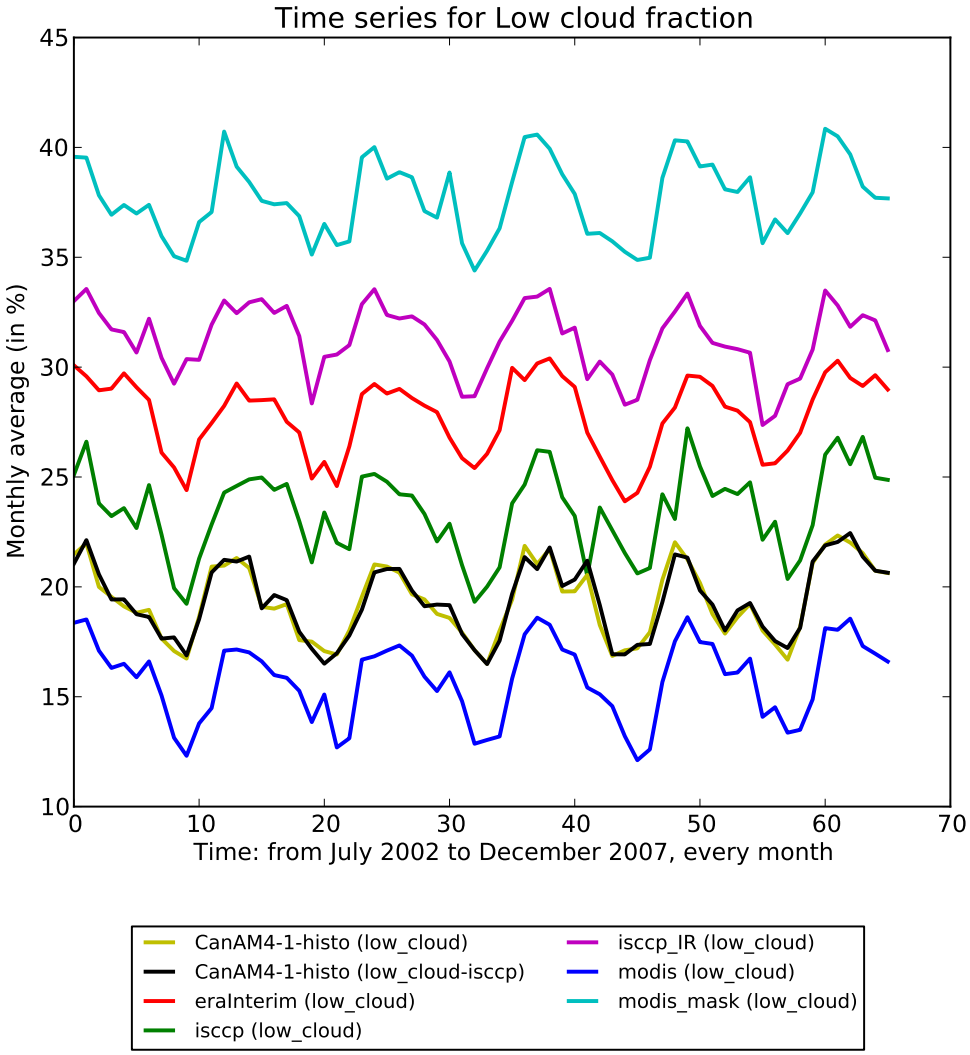

Figure 4.1: Low cloud time series by datasets. One can see some sort of ranking among observations, from most conservative (lowest cloud fraction) to most liberal (higher cloud fraction): (1) "modis", (2) "isccp", (3) "isccp_IR", and (4) "modis_mask". Data from ERA-Interim is ranked in the middle of these four observations. Data from CanAM-4.1 and its *ISCCP-simulated* field ("low_cloud-isccp") are very close to each other and are both in between data from MODIS and ISCCP

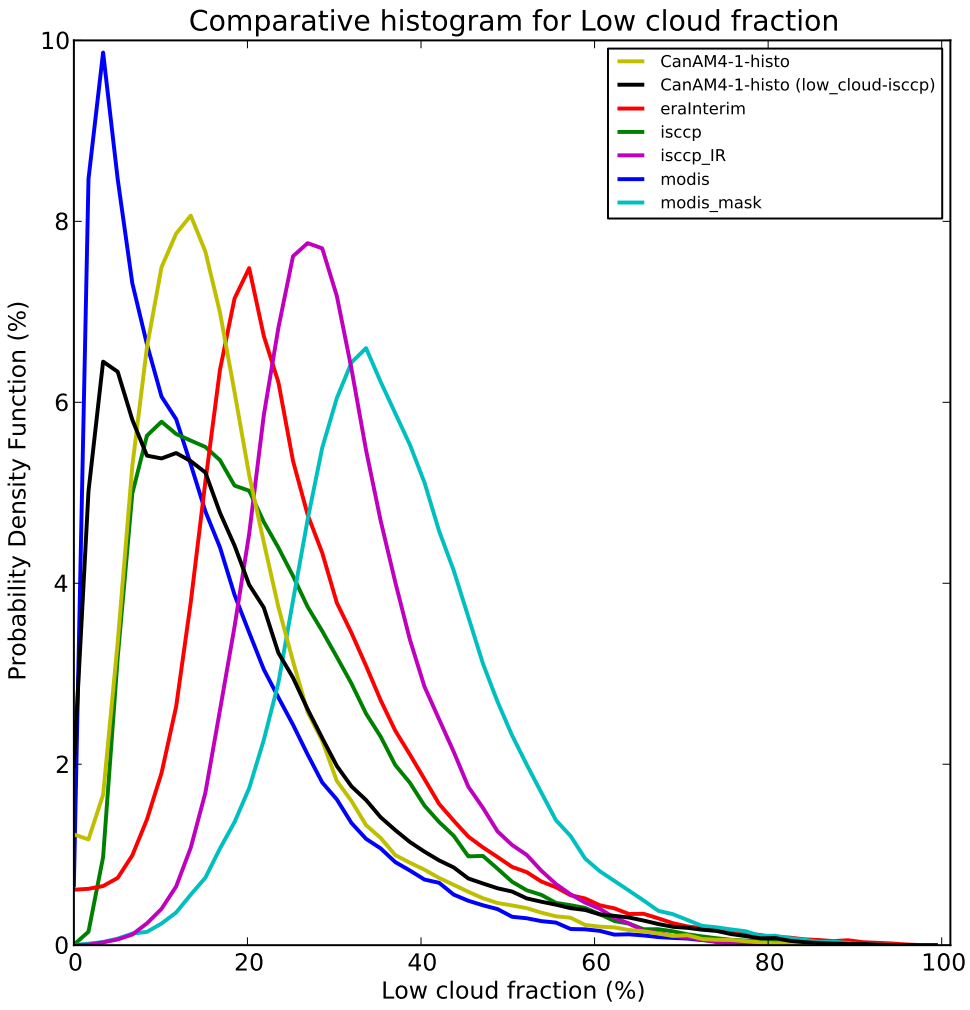

Figure 4.2: Low cloud distributions by datasets. One can clearly see the reduction in small low cloud fractions between "modis" and "modis_mask" due to the screening out of unidentifiable (thin) low clouds. Interestingly, CanAM-4.1 output is closer to ERA-Interim and the more liberal observations, while its *ISCCP-simulated* field ("low_cloud-isccp") is significantly closer to more conservative observations (MODIS and even more particularly ISCCP).

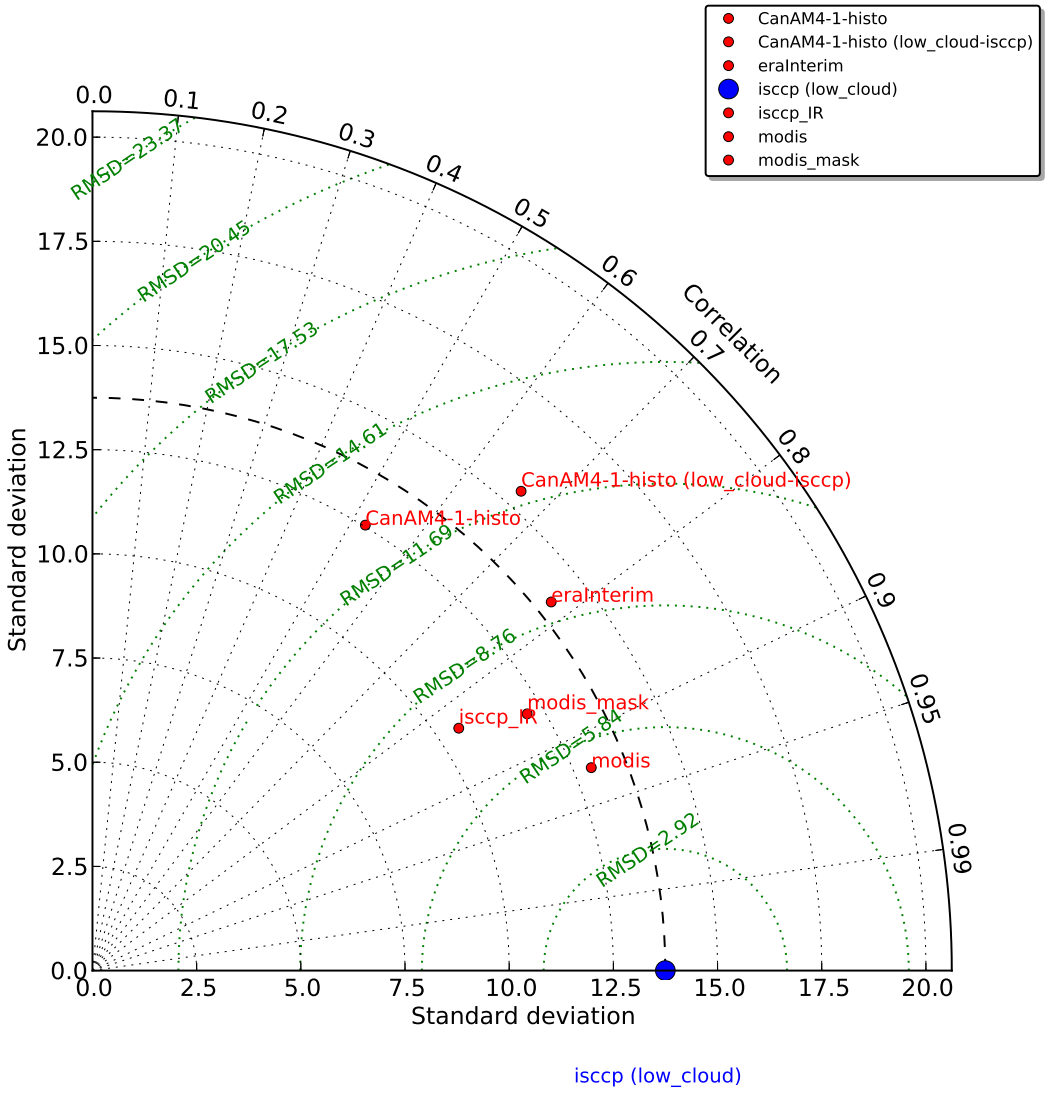

Figure 4.3: Taylor diagram for low clouds. Standard deviations (σ) are given in percent. Correlations are unit-less (dimensionless). All coordinates values are given in Table 4.1: Std (σ), Correlation (Corr), and Root-Mean-Square Difference (RMSD). One can see that, relative to ISCCP data, the closest are: first, MODIS, "modis_mask", and "isccp_IR"; then, second, ERA-Interim; finally, third, CanAM-4.1's *ISCCP-simulated* field ("low_cloud-isccp") and CanAM-4.1'raw' output. Although it could be surprising that CanAM-4.1 "low_cloud-isccp" has a higher standard deviation, Figure 4.2 shows that its PDF is flatter than CanAM-4.1 "raw" output (hence its higher standard deviation). Finally, it is worth noting that, in this case, the COSP simulator ("low_cloud-isccp") does provide some improvement.

Source (Ref. first)	Min	Median	Mean (μ)	Max	Std (σ)	Corr (%)	RMSD	RMSD/μ
isccp	0.2	20.3	22.8	91.4	13.7	100.00	0.00	0.00
CanAM4-1-histo	0.0	15.9	18.9	99.4	12.5	52.23	12.89	0.68
— (low_cloud-isccp)	0.0	15.4	19.0	95.5	15.4	66.66	12.01	0.63
eraInterim	0.0	23.9	26.9	98.4	14.1	77.95	9.26	0.34
isccp_IR	1.4	29.4	30.9	83.2	10.5	83.39	7.64	0.25
modis	0.0	11.8	15.2	93.2	12.9	92.63	5.18	0.34
modis_mask	0.7	36.0	37.3	94.8	12.1	86.11	7.00	0.19

Table 4.1: Comparison for low clouds. Minimum (Min), Median, Average (Mean, μ), Maximum (Max), Standard deviation (Std, σ), and Root-Mean-Square Difference (RMSD) are expressed in percent (cloud fraction units). Correlation (Corr) is also expressed in percent. RMSD/μ is expressed without units. Min, Median, Mean, and Max can be visualized in Figure 4.2. Std, Corr, and RMSD can be visualized in Figure 4.3. Corr, RMSD, and RMSD/μ are computed relative to the reference (here ISCCP). relative to ISCCP, the ranking from closest to farthest is identical, whether one looks at correlation or at RMSD (first, MODIS, "modis_mask", and "isccp_IR"; then, second, ERA-Interim; finally, third, CanAM-4.1's *ISCCP-simulated* field ("low_cloud-isccp") and CanAM-4.1'raw' output). But the relative improvements, although monotonic, are not linear (as shown in Figure 4.4). For example, "low_cloud-isccp" slightly improves its RMSD but significantly improves its correlation.

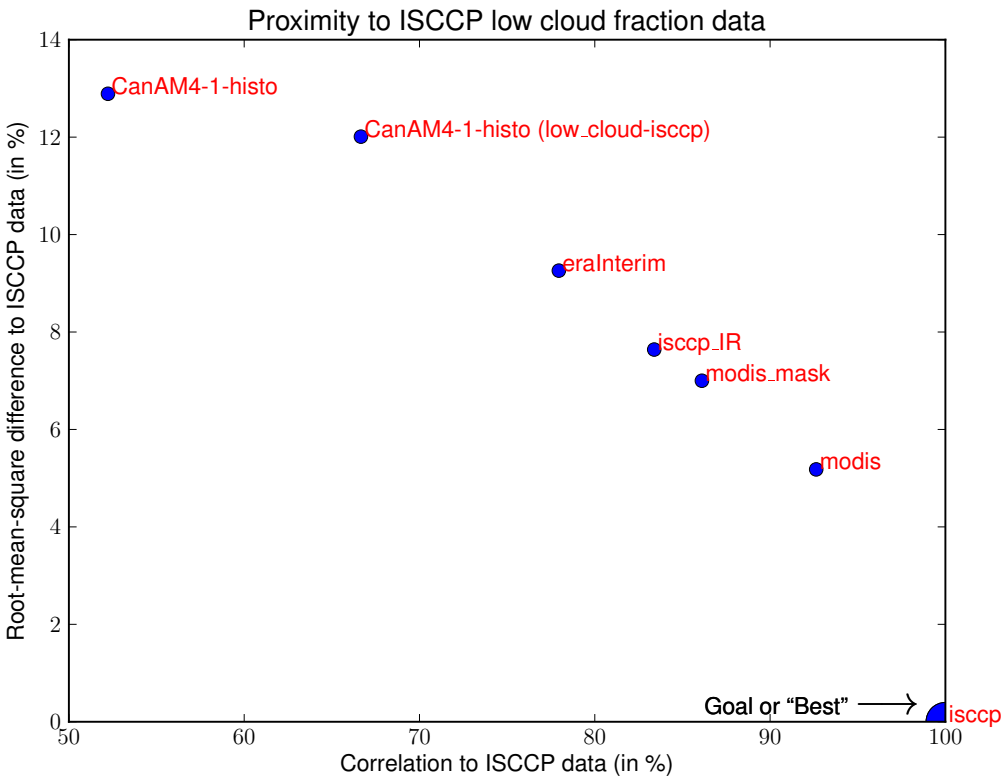

Figure 4.4: Proximity to the low cloud reference (ISCCP) as estimated using two distinct measures: Standard deviation and Correlation. Evolution, although monotonic, is not linear. Like the Taylor diagram, this figure takes into account standard deviations (see relationship in Figure 3.3), but, unlike the Taylor diagram, it does not explicitly display standard deviation differences. Another difference: the correlation axis is linear.

4.1.2 High clouds

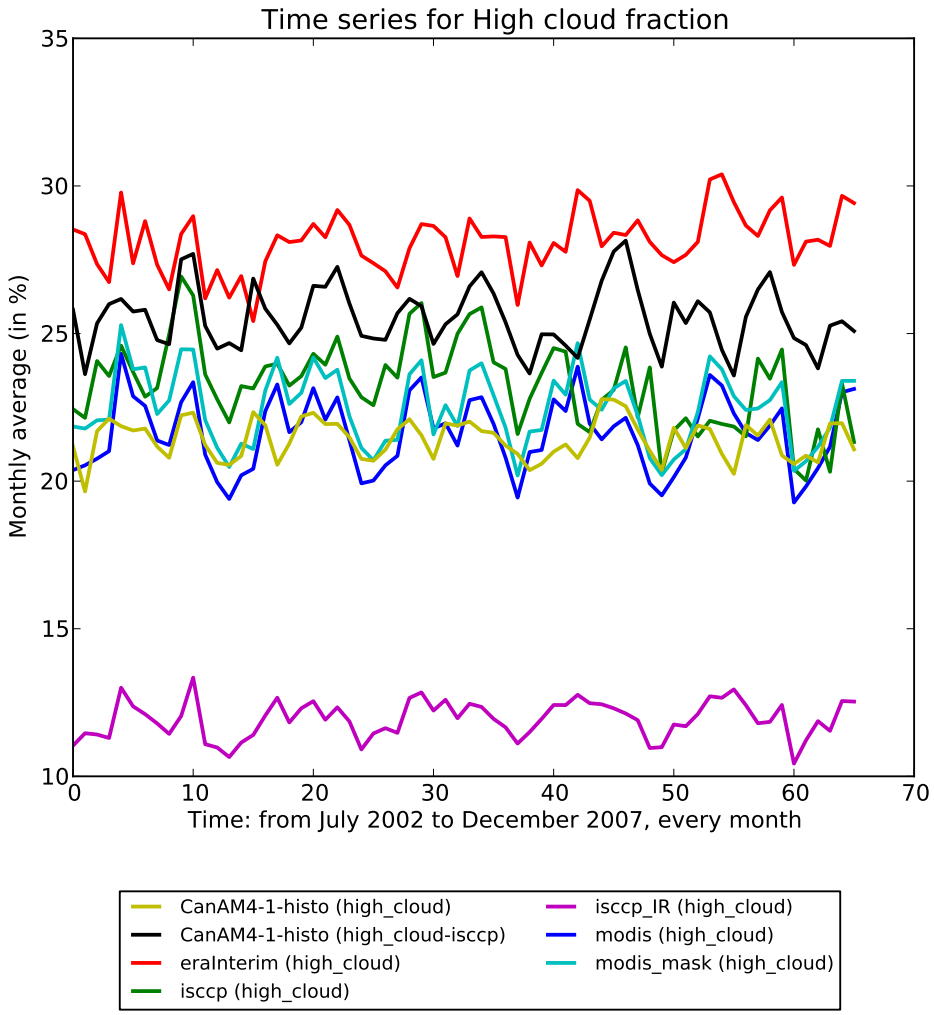

Figure 4.5: High cloud time series by datasets. (Same as Figure 4.1 but for high clouds). Most notable features here are (i) the fairly low "isccp_IR", (ii) "isccp" in between CanAM-4.1 and its *ISCCP-simulated* field, (iii) a possible decreasing trend in ISCCP data.

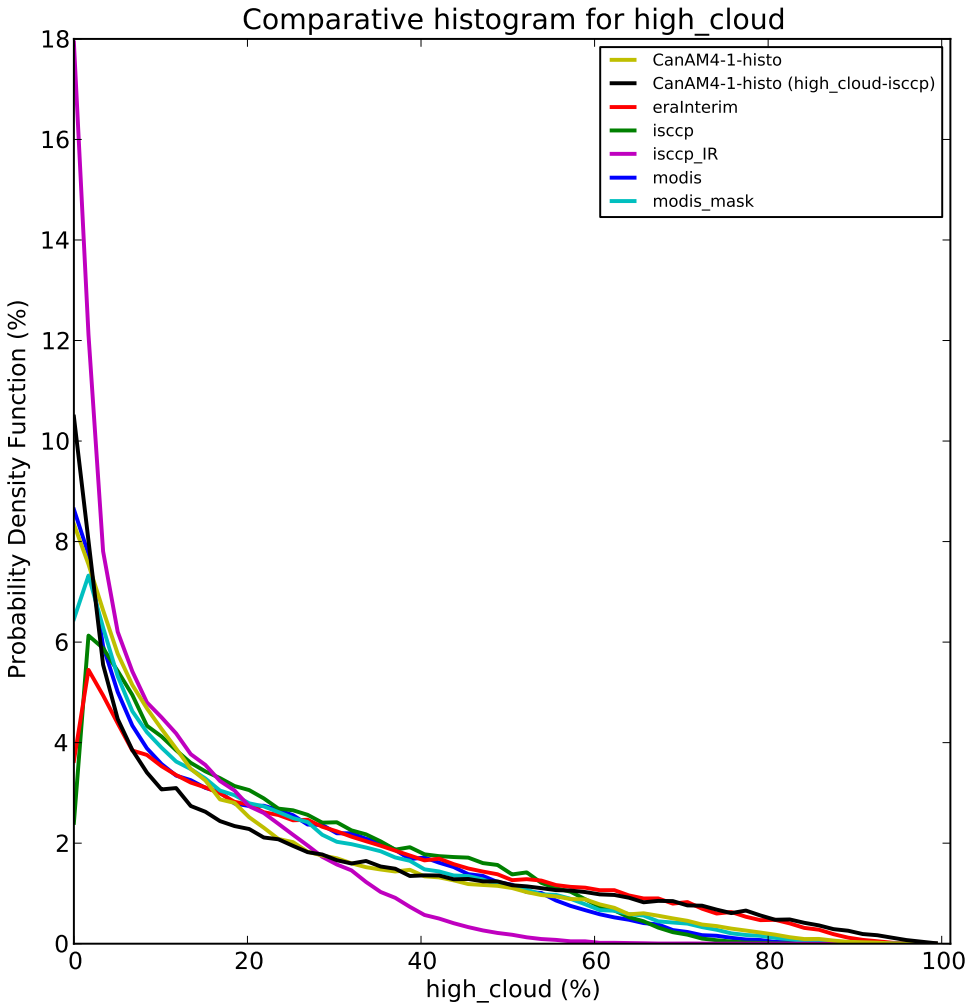

Figure 4.6: High cloud distributions by datasets. (Same as Figure 4.2 but for high clouds). Most notable feature here is the very high detection rate of small high cloud fractions for "isccp_IR", as well as its very low detection rate of large high cloud fractions, both consistent with its focus on InfraRed (IR) channels.

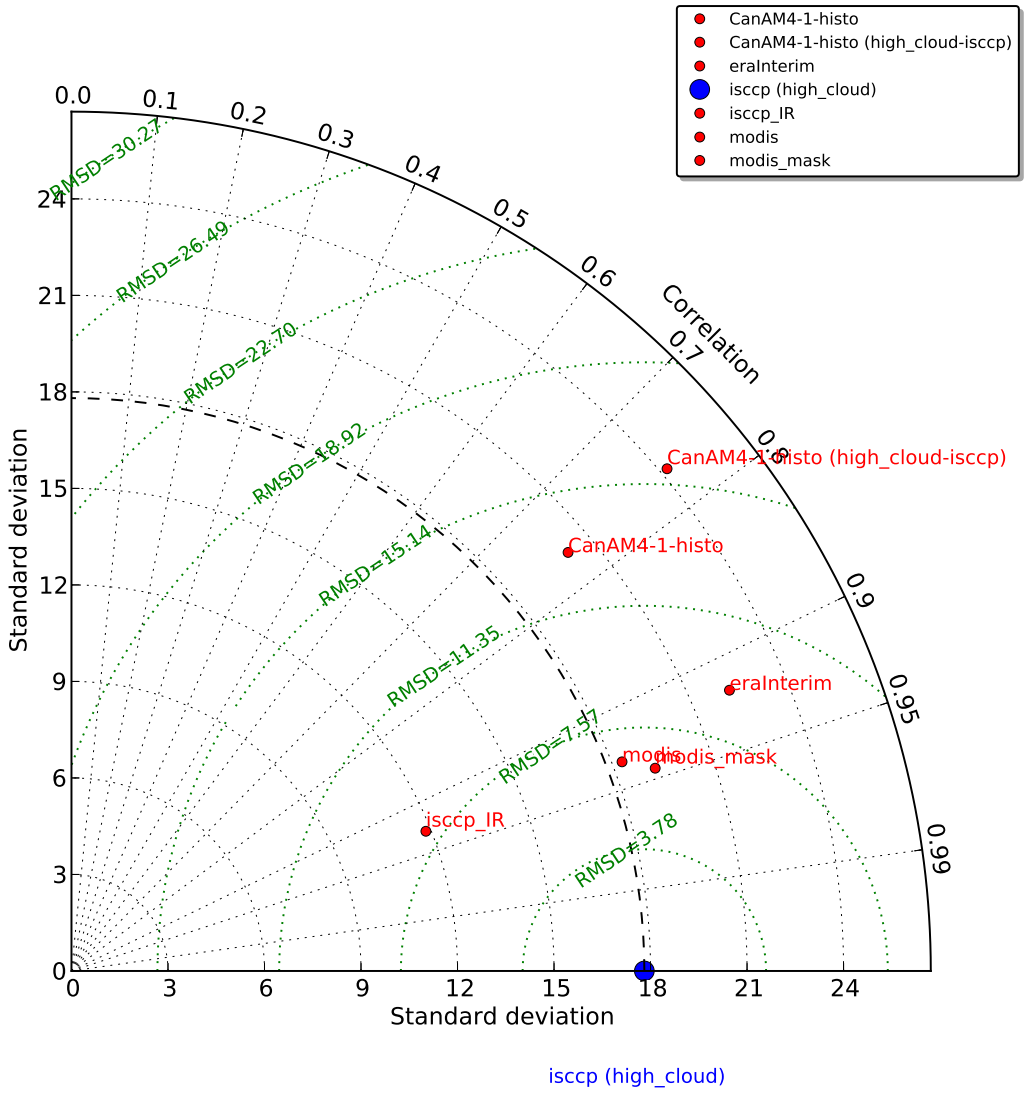

Figure 4.7: Taylor diagram for high clouds. (Same as Figure 4.3 but for high clouds). One can see that all datasets but "isccp_IR" have higher standard deviations than the reference. Remarkably, CanAM-4.1's *ISCCP-simulated* field ("high_cloud-isccp") does not do better than the original output.

Source (Ref. first)	Min	Median	Mean (μ)	Max	Std (σ)	Corr (%)	RMSD	RMSD/μ
isccp	0.0	18.9	23.1	85.1	17.8	100.00	0.00	0.00
CanAM4-1-histo	0.0	14.2	21.4	97.5	20.2	76.46	13.22	0.62
— (high_cloud-isccp)	0.0	17.7	25.5	99.6	24.2	76.45	15.63	0.61
eraInterim	0.0	22.2	27.7	97.1	22.2	91.98	9.12	0.33
isccp_IR	0.0	7.7	11.6	79.3	11.8	93.03	8.06	0.69
modis	0.0	16.5	21.1	95.6	18.3	93.48	6.54	0.31
modis_mask	0.0	16.7	22.0	94.6	19.2	94.46	6.31	0.29

Table 4.2: Comparison for high clouds. (Same as Table 4.1). Main point is that "low_cloud-isccp" does not improve its correlation and does degrade its RMSD.

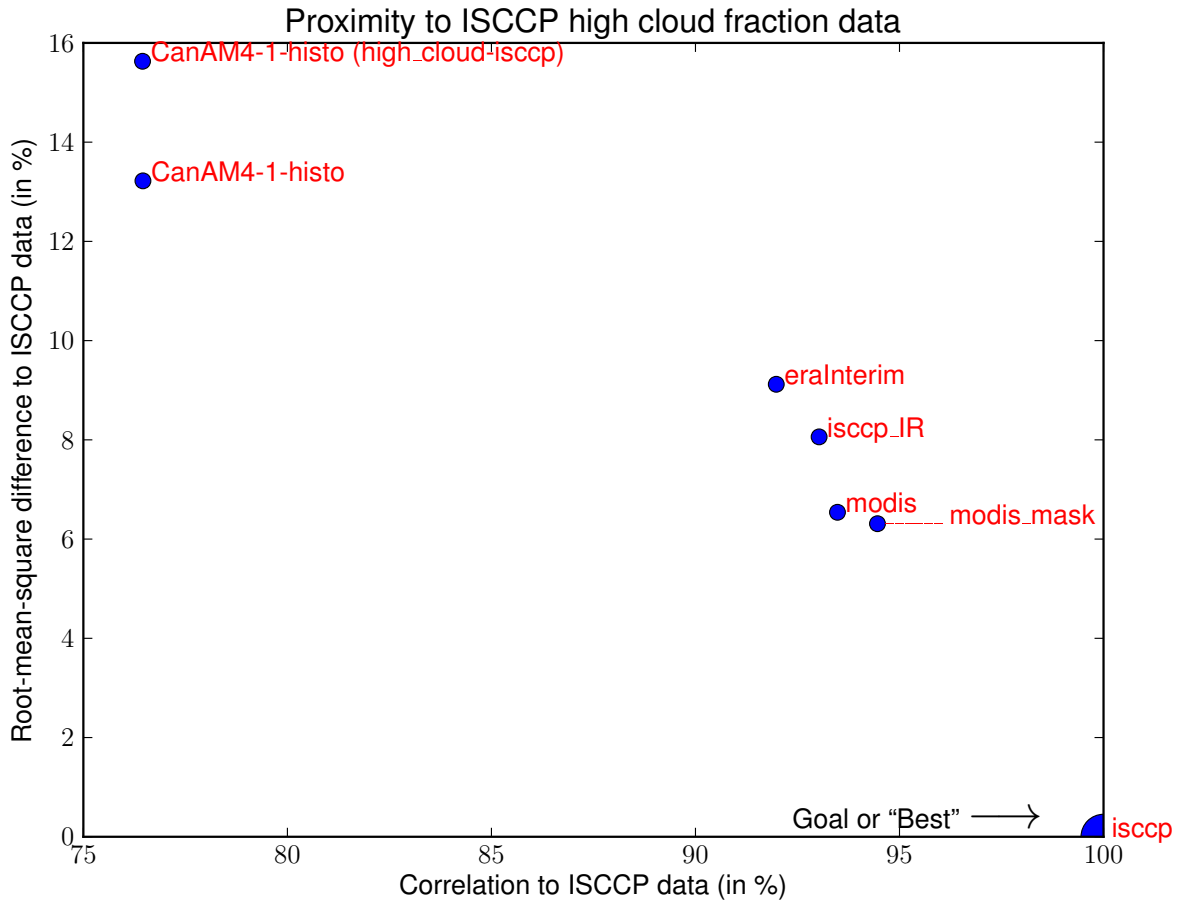

Figure 4.8: Proximity to the high cloud reference (ISCCP) as estimated using two distinct measures: Standard deviation and Correlation. Progression, although monotonic, is not linear.

4.2 Radiation fields

Radiation fields are important from an energy standpoint (as already discussed). It is interesting to do the comparisons for clouds and radiation side-by-side, in particular because of the strong relations (at least in models) between radiation fields and cloudiness (through clouds' thickness and reflectivity).

Results in the following sections are also very similar for Cloud Radiative Effect (CRE), both shortwave (SW) and longwave (LW), as well as for Top Of the Atmosphere (TOA) Clear-sky conditions (Clr) fluxes.

The TOA SW for all-sky conditions ("ALL") (Figure 4.9 and Table 4.3) shows clearly that the post-processing does not change the results, i.e. "ceres_ssf", "ceres_syn", and "cebaf" are the closest. It also shows that CanAM-4.1 output is much further from the reference than all other observational datasets. The TOA LW for all-sky conditions (Figure 4.10 and Table 4.4) shows the same.

On the other hand, the TOA net radiative fluxes for all-sky conditions (Figure 4.11 and Table 4.5) shows a much better performance of CanAM-4.1. This illustrates well the tuning of General Circulation Models (GCMs), as already explained in subsection 3.1.4.

4.2.1 Top of the atmosphere (TOA) shortwave flux (SW), all-sky conditions (ALL)

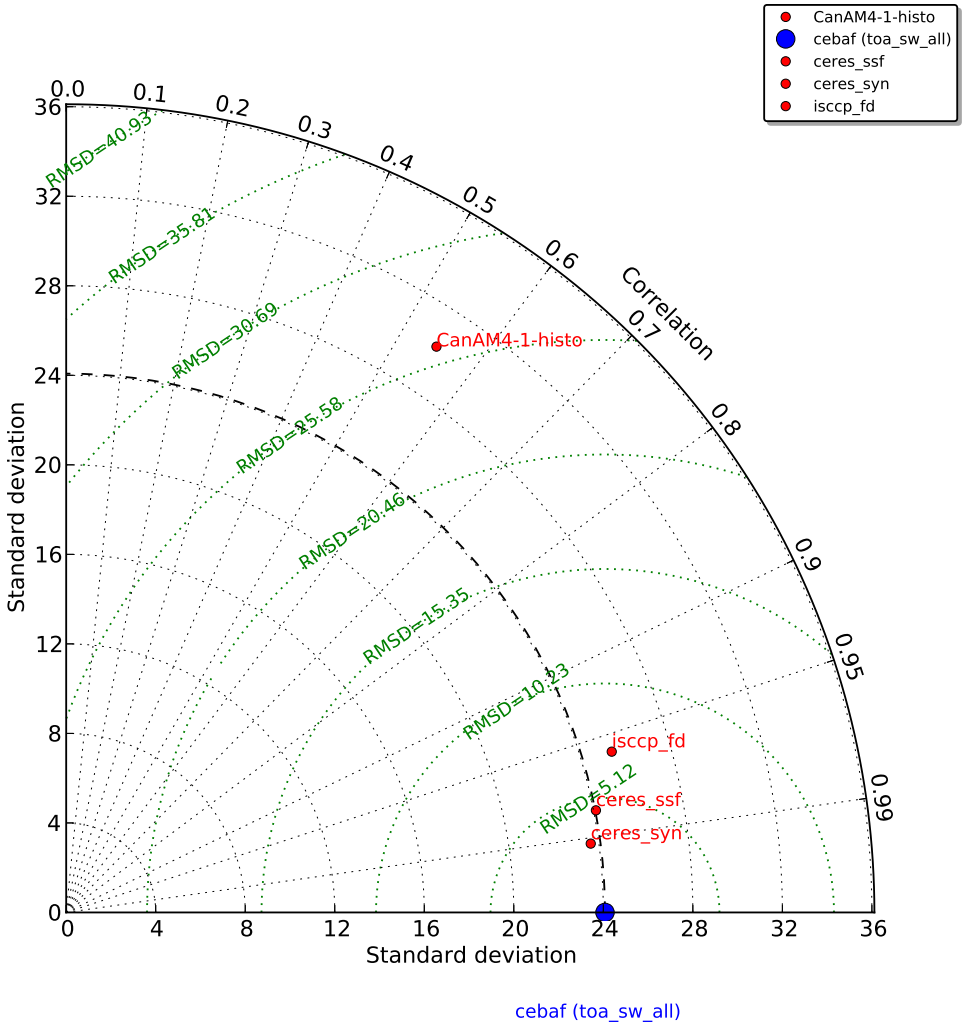

Figure 4.9: Taylor diagram for TOA SW fluxes (All skies). (Same as Figure 4.3 but for TOA SW fluxes (All skies)). Standard deviations (σ) are given in W/m^2.

Source (Ref. first)	Min	Median	Mean (μ)	Max	Std (σ)	Corr (%)	RMSD	RMSD/μ
cebaf	33.6	80.9	85.3	226.4	24.1	100.00	0.00	0.00
CanAM4-1-histo	30.9	81.3	87.6	260.5	30.2	54.76	26.38	0.30
ceres_ssf	31.6	76.9	81.5	217.6	24.1	98.19	4.58	0.06
ceres_syn	32.3	78.5	82.7	217.1	23.6	99.15	3.14	0.04
isccp_fd	39.0	90.5	94.5	235.2	25.4	95.92	7.19	0.08

Table 4.3: Comparison for TOA SW fluxes (All skies). (Same as Table 4.1). Minimum (Min), Median, Average (Mean, μ), Maximum (Max), Standard deviation (Std, σ), and RMSD are all expressed in W/m^2 (TOA SW fluxes units).

4.2.2 Top of the atmosphere (TOA) longwave flux (LW), all-sky conditions (ALL)

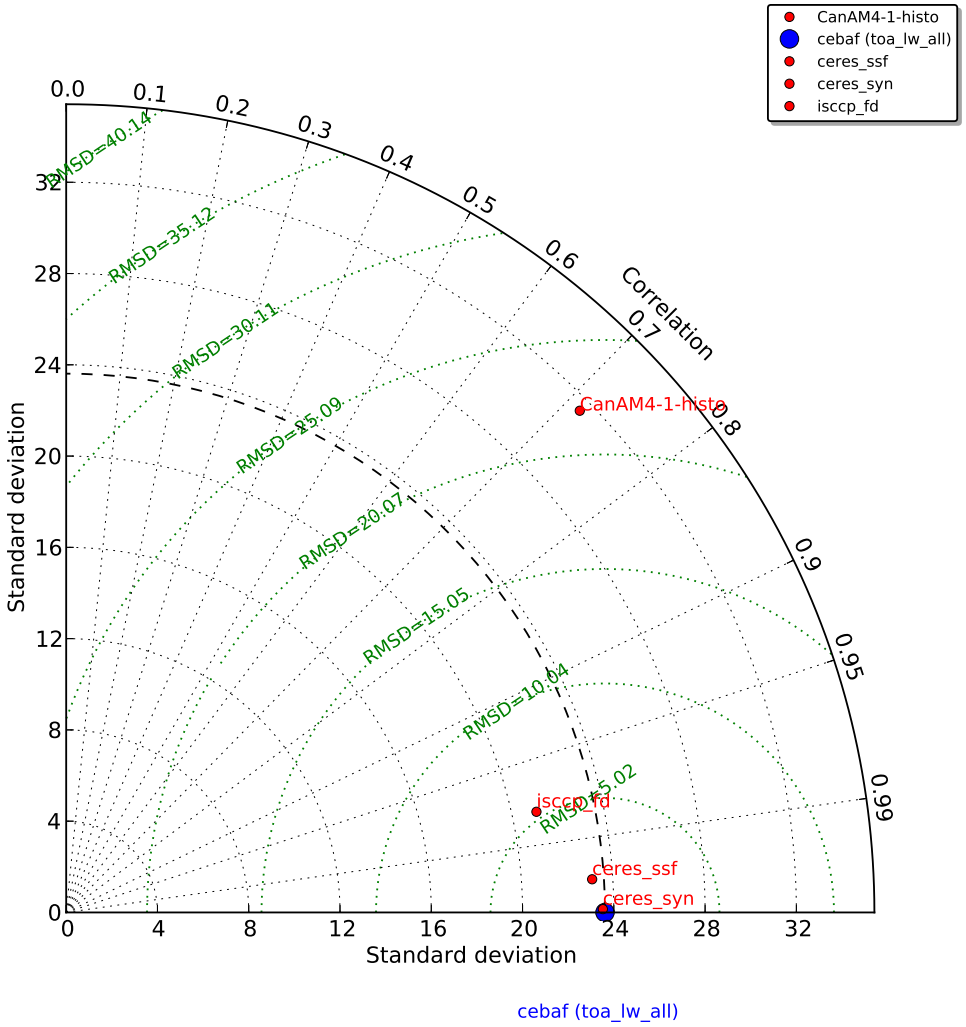

Figure 4.10: Taylor diagram for TOA LW fluxes (All skies). (Same as Figure 4.3 but for TOA LW fluxes (All skies)). Standard deviations (σ) are given in W/m^2.

Source (Ref. first)	Min	Median	Mean (μ)	Max	Std (σ)	Corr (%)	RMSD	RMSD/μ
cebaf	156.6	266.2	262.1	327.2	23.6	100.00	0.00	0.00
CanAM4-1-histo	137.4	265.5	258.2	328.1	31.5	71.53	22.02	0.09
ceres_ssf	158.1	265.7	261.6	326.9	23.1	99.80	1.56	0.01
ceres_syn	155.9	265.1	260.9	326.0	23.5	100.00	0.09	0.00
isccp_fd	168.0	261.6	257.9	317.6	21.1	97.78	5.34	0.02

Table 4.4: Comparison for TOA LW fluxes (All skies). (Same as Table 4.1). Minimum (Min), Median, Average (Mean, μ), Maximum (Max), Standard deviation (Std, σ), and RMSD are all expressed in W/m^2 (TOA LW fluxes units).

4.2.3 Top of the atmosphere (TOA) net flux (NET), all-sky conditions (ALL)

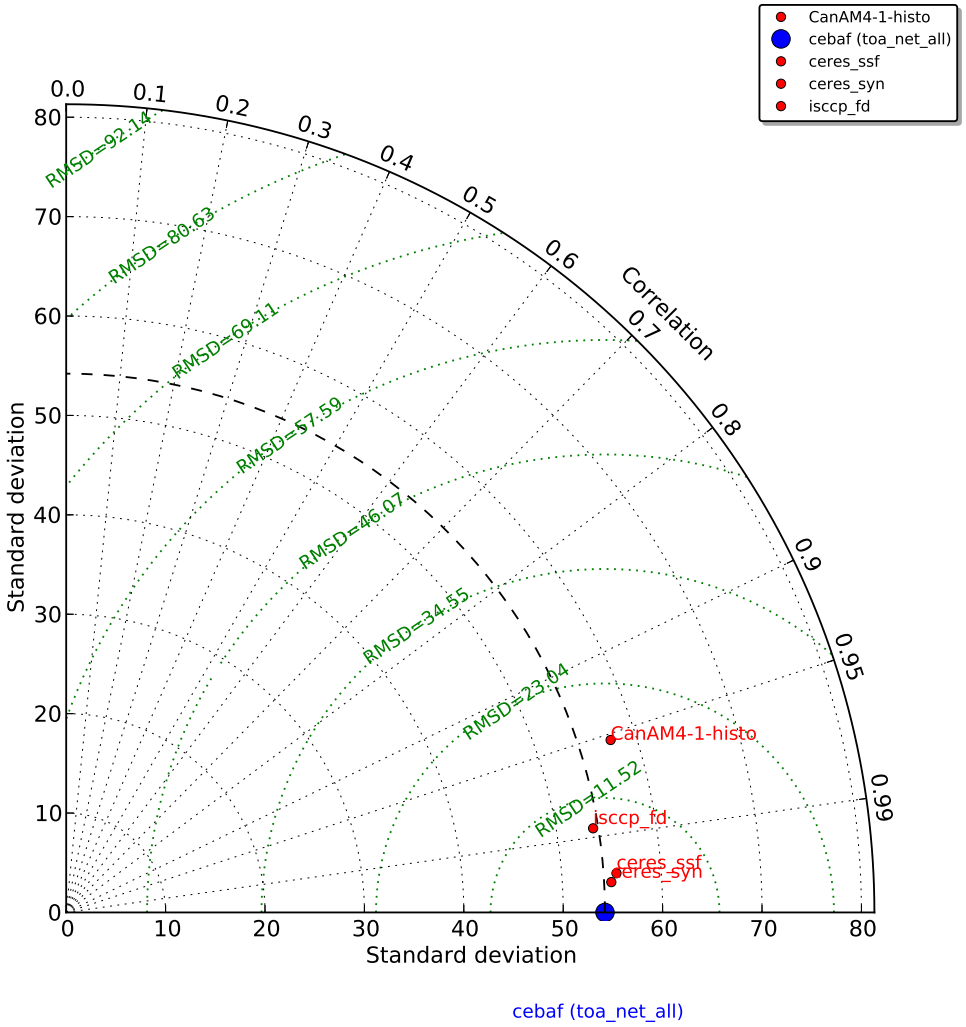

Figure 4.11: Taylor diagram for TOA NET fluxes (All skies). (Same as Figure 4.3 but for TOA NET fluxes (All skies)). Standard deviations (σ) are given in W/m^2.

Source (Ref. first)	Min	Median	Mean (μ)	Max	Std (σ)	Corr (%)	RMSD	RMSD/μ
cebaf	-122.2	67.7	52.4	165.5	54.2	100.00	0.00	0.00
CanAM4-1-histo	-125.2	68.3	55.3	170.5	57.5	95.33	17.36	0.31
ceres_ssf	-120.3	71.5	56.6	173.9	55.5	99.75	4.11	0.07
ceres_syn	-119.6	71.6	56.0	170.3	54.9	99.85	3.13	0.06
isccp_fd	-123.1	63.4	49.0	167.5	53.7	98.75	8.55	0.17

Table 4.5: Comparison for TOA NET fluxes (All skies). (Same as Table 4.1). Minimum (Min), Median, Average (Mean, μ), Maximum (Max), Standard deviation (Std, σ), and RMSD are all expressed in W/m^2 (TOA NET fluxes units).

4.2.4 Net Cloud Radiative Effect (NCRE)

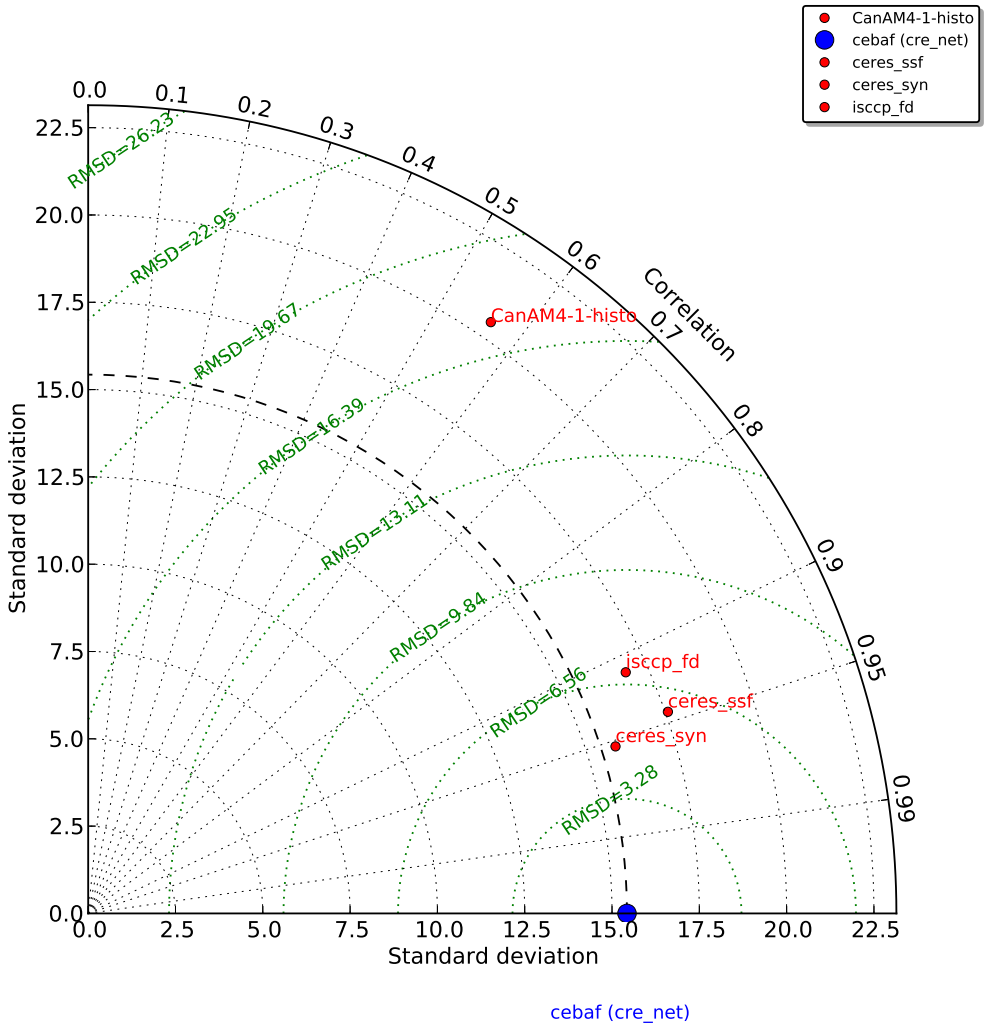

Figure 4.12: Taylor diagram for net CRE. (Same as Figure 4.3 but for net CRE). Standard deviations (σ) are given in W/m^2.

Source (Ref. first)	Min	Median	Mean (μ)	Max	Std (σ)	Corr (%)	RMSD	RMSD/μ
cebaf	-125.9	-17.1	-20.2	58.6	15.4	100.00	0.00	0.00
CanAM4-1-histo	-166.9	-17.0	-20.7	35.0	20.5	56.29	17.37	-0.84
ceres_ssf	-157.4	-12.7	-16.4	225.5	17.6	94.45	5.89	-0.36
ceres_syn	-132.7	-13.8	-16.9	178.7	15.8	95.33	4.79	-0.28
isccp_fd	-133.9	-19.4	-22.9	15.3	16.9	91.24	6.91	-0.30

Table 4.6: Comparison for net CRE. (Same as Table 4.1). Minimum (Min), Median, Average (Mean, μ), Maximum (Max), Standard deviation (Std, σ), and RMSD are all expressed in W/m^2 (TOA NET fluxes units).

4.3 Precipitation rates

As in the previous section, it is interesting to do the comparisons for clouds and precipitation side-by-side, in particular because of the strong relations (at least in models) between precipitation and cloudiness.

Monthly variations from the Global Precipitation Climatology Project (GPCP) and the Climate Prediction Center (CPC) Merged Analysis of Precipitation (CMAP) appear very similar (Figure 4.13), despite their average discrepancy (3.0 versus 3.4 mm/day, or 12.5% relative difference). Also, CanAM-4.1 seems to have difficulties reproducing the larger variations, but is consistently overestimating.

In Figure 4.14 CanAM-4.1 seems to overestimate both very low and very high precipitation rates, while underestimating medium ones.

Figure 4.15 and Table 4.7 show, again, how much simulations are significantly further from one observational dataset than are the other observations.

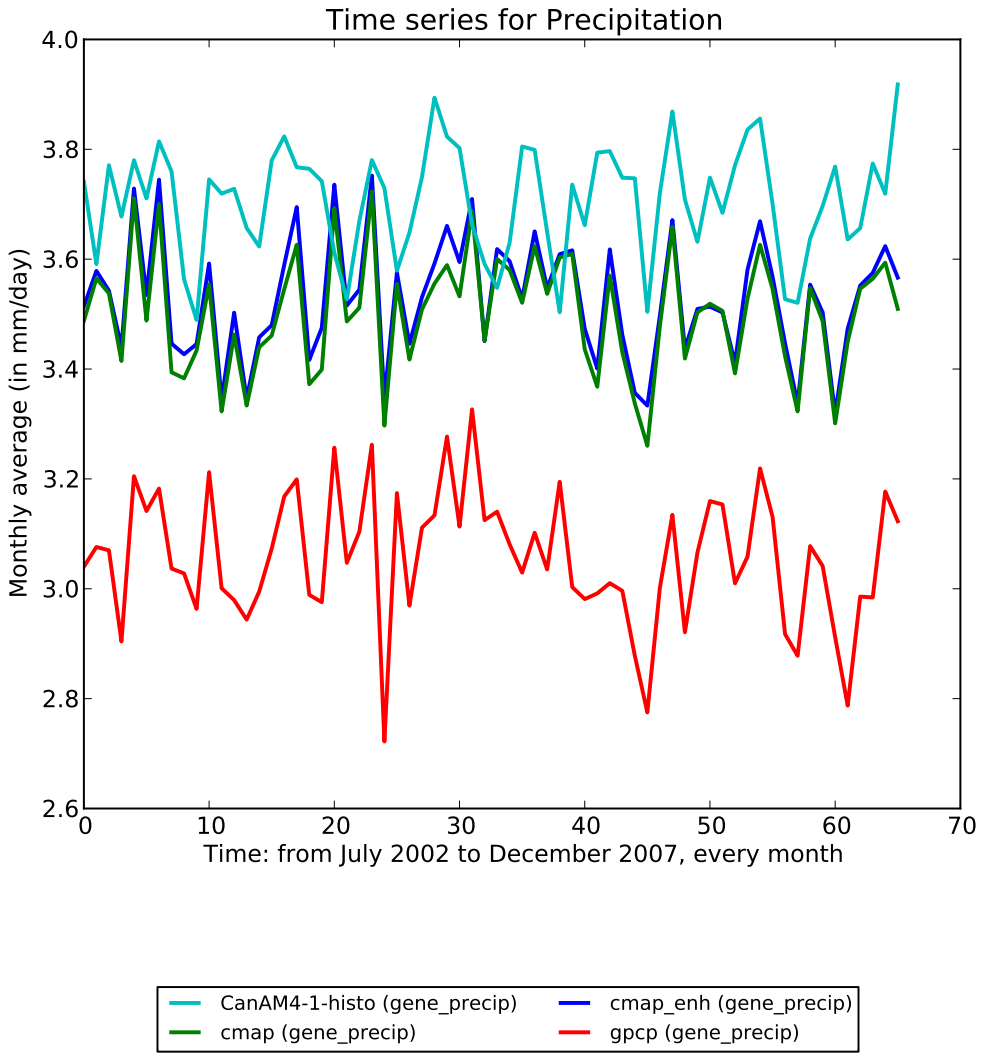

Figure 4.13: Precipitation time series by datasets. (Same as Figure 4.1 but for precipitation rates).

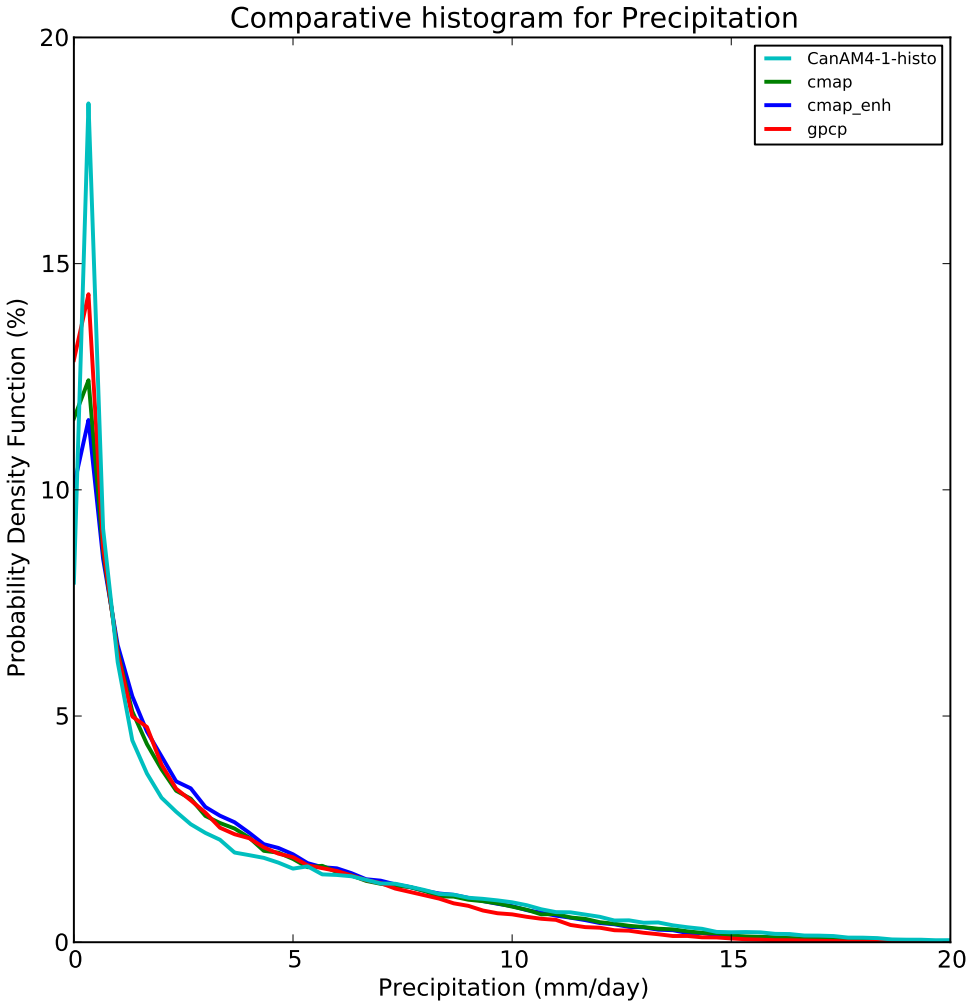

Figure 4.14: Precipitation distributions by datasets. (Same as Figure 4.2 but for precipitation rates).

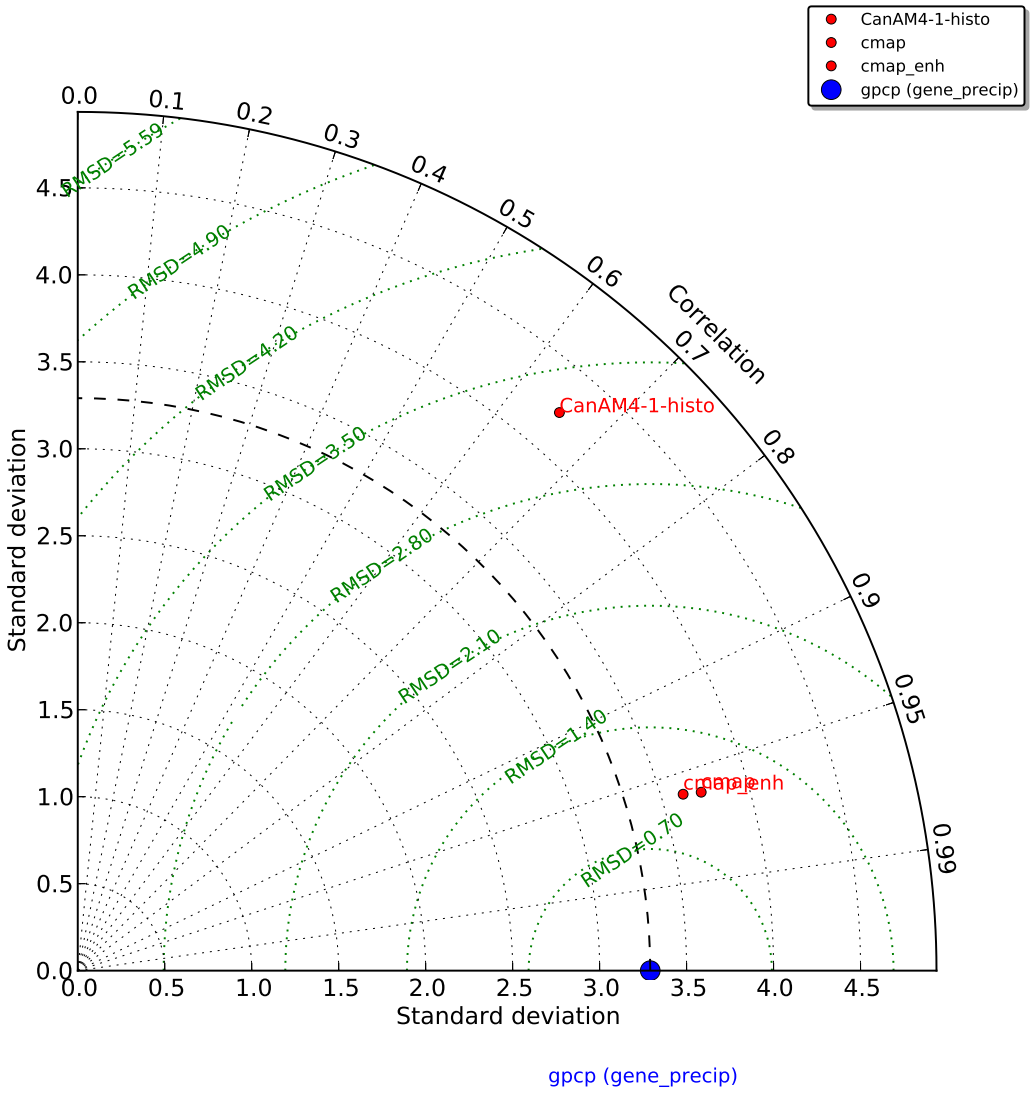

Figure 4.15: Taylor diagram for precipitation rates. (Same as Figure 4.3 but for precipitation). Standard deviations (σ) are given in mm/day.

Source (Ref. first)	Min	Median	Mean (μ)	Max	Std (σ)	Corr (%)	RMSD	RMSD/μ
gpcp	0.0	1.7	3.0	28.8	3.3	100.00	0.00	0.00
CanAM4-1-histo	0.0	1.8	3.7	46.5	4.2	65.34	3.25	0.89
cmap	0.0	1.9	3.4	33.8	3.7	96.14	1.07	0.31
cmap_enh	0.0	2.1	3.4	32.1	3.6	96.01	1.03	0.30

Table 4.7: Comparison for precipitation rates. (Same as Table 4.1). Minimum (Min), Median, Average (Mean, μ), Maximum (Max), Standard deviation (Std, σ), and RMSD are all expressed in mm/day (precipitation rates units).

4.4 Model simulations

CanAM-4.1's historical simulation was run four times for this experiment of the Climate Model Intercomparison Project (CMIP) (fifth phase).

All runs ("r1", "r2", "r3", and "r4") started with slightly different initial conditions (but with a one year spin off before the actual recording).

As the differences between these runs were systematically much smaller (by at least an order of magnitude) for any variable (than the differences with the other datasets), I (arbitrarily) chose one run ("r1") and always used the same one throughout all comparisons.

For completeness purposes, a few illustrations are given in Figures 4.16, 4.17, 4.18, and 4.19. Extreme similarities are shown, as examples for:

- monthly averages of low cloud fractions (Figure 4.16);
- correlation and RMSD of low cloud fractions (Figure 4.17);
- standard deviation, correlation and RMSD of precipitation rates (Figure 4.18); and
- monthly averages of TOA SW for clear-sky conditions ("CLR") (Figure 4.19).

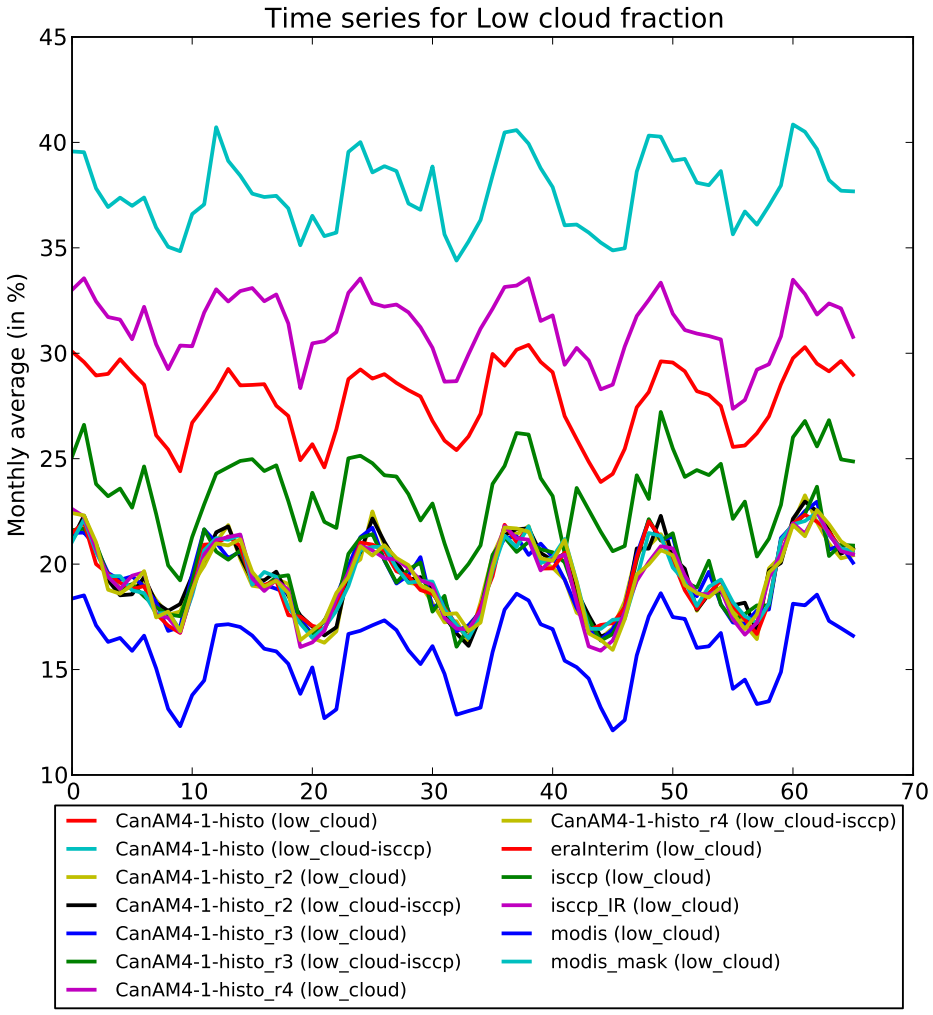

Figure 4.16: Low cloud time series by datasets. (Exactly like Figure 4.1).

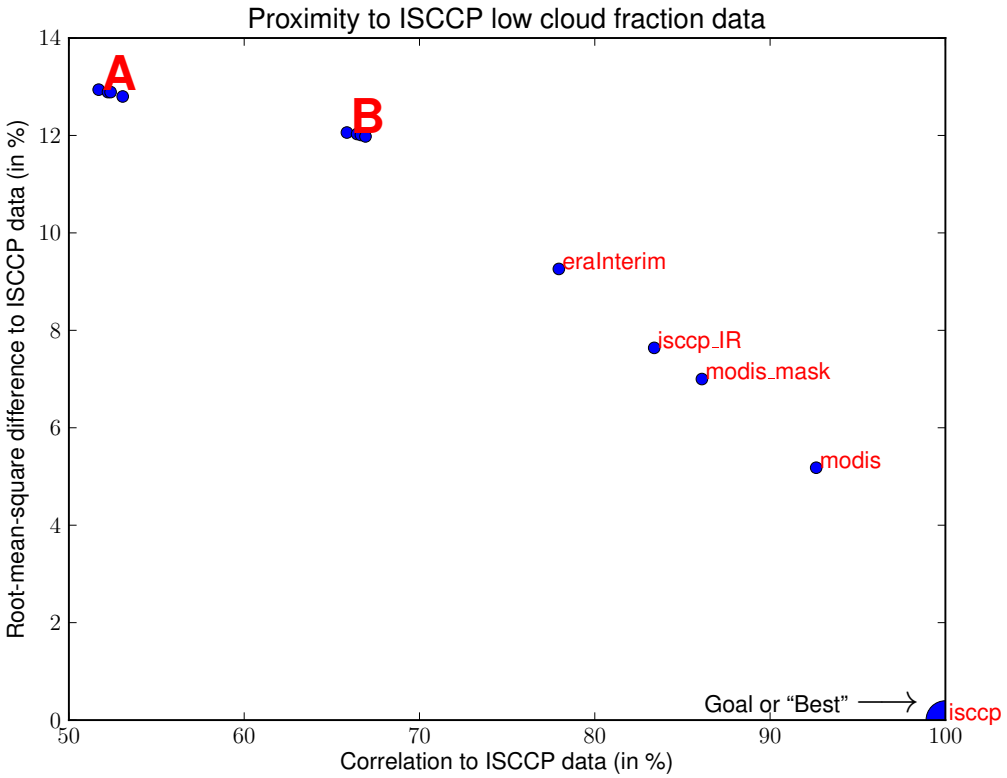

Figure 4.17: Proximity to the high cloud reference (ISCCP) as estimated using two distinct measures: Standard deviation and Correlation. "**A**" represents the raw (low cloud) output for the four runs of CanAM-4.1, while "**B**" represents the COSP-*ISCCP-simulated* low cloud field ("low_cloud-isccp") for the four runs of CanAM-4.1. Progression, although monotonic, is not linear. (Exactly like Figure 4.4).

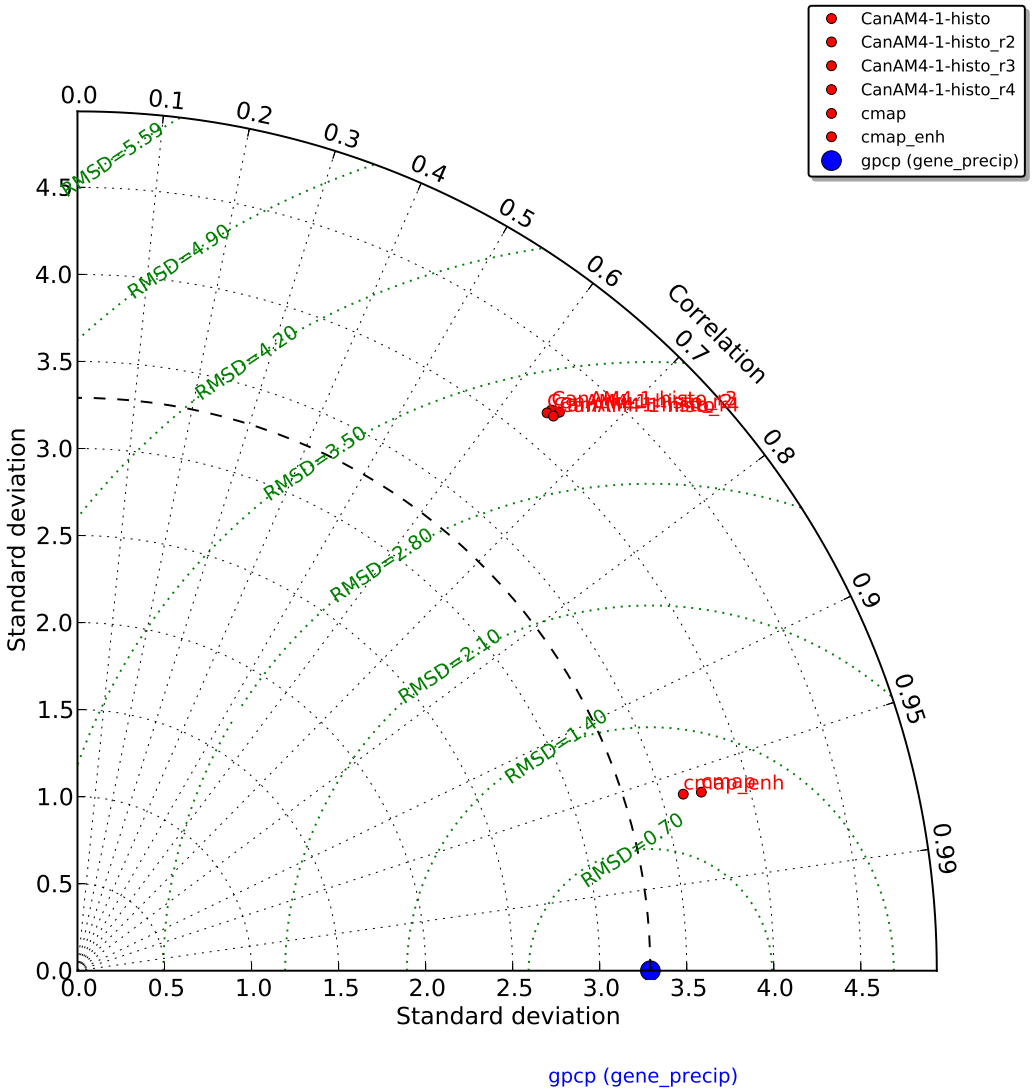

Figure 4.18: Taylor diagram for precipitation rates. (Same as Figure 4.3 but for precipitation). Standard deviations (σ) are given in mm/day. Precipitation rates for the four runs of CanAM-4.1 are very close to each other (top four red dots in figure). Data from CMAP ("cmap" and "cmap_enh") are close to each other (bottom two red dots). Data from GPCP ("gpcp (gene_precip)") is the reference (bottom large blue dot).

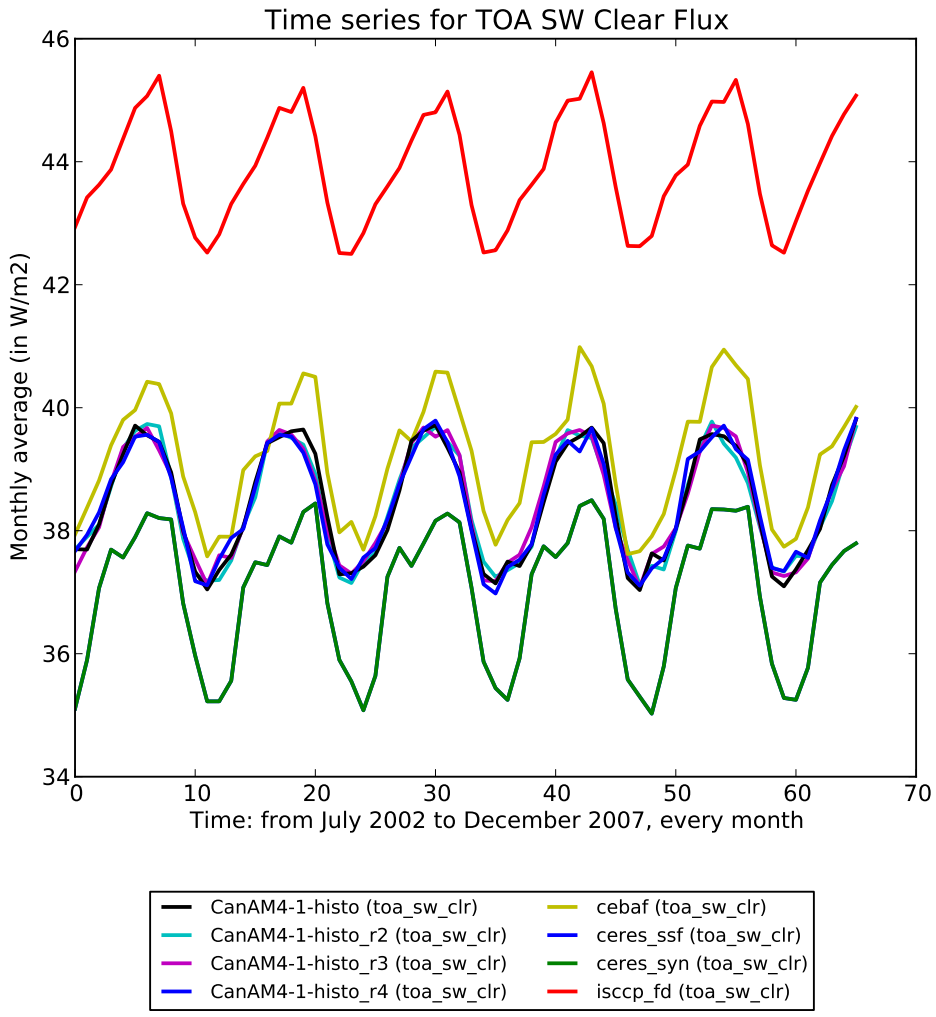

Figure 4.19: TOA SW fluxes (Clear skies) time series by datasets. (Same as Figure 4.1 but for TOA SW fluxes).

4.5 Observation, re-analysis, then simulation

As the figures and tables in this section demonstrate, generally speaking but quite markedly, and with an observational dataset as "reference":

1. other observational datasets are much closer to the reference than re-analysis or model outputs,

2. re-analysis output is still closer than model output to the reference. (precipitation and radiative fluxes are compared with the ECMWF 40 years Re-Analysis (ERA-40) in the next chapter).

Therefore, as clearly shown, only one observational dataset is really necessary when evaluating CanAM-4.1. That is why the actual comparison between CCCma third generation atmospheric GCM (AGCM-3) and CanAM-4.1 can be done (in the next chapter), despite having only one set of observations (for clouds and radiative fluxes). Moreover, only one run of CanAM-4.1's historical run is necessary (making figures easier to read without loosing much information).

For this time period, CanAM-4.1's *ISCCP-simulated* low cloud field ("low_cloud-isccp") is closer to observations than its raw output. On the other hand, it does worsen "high_cloud-isccp". Note that the simulated field seems closer to more conservative approaches ("modis" and "isccp") while the raw output seems closer to more liberal approaches ("modis_mask" and "isccp_IR").

The model tuning for radiative fluxes consistent with the energy balance appears clearly. Thus no particular skill should be inferred or interpreted from the good agreement for TOA net fluxes, all-sky ("toa_net_all").

Although not shown here, results are mostly insensitive to the type of surface (ocean, land, or both). Some differences are: (i) CanAM-4.1 overestimates precipitation rates over land while it underestimates them over ocean; (ii) differences between CanAM-4.1 raw output and its *ISCCP-simulated* field are bigger over land than over ocean; and (iii) ERA-Interim (low) cloud fields are significantly overestimated over land *when outside the tropical domain*.

Although not shown here, results are also mostly insensitive to the geographical extent of the domain (global coverage versus 30°S–30°N "tropical" band). Some differences though, relative to observations, are that the bigger the domain: (i) the better all CanAM-4.1 radiative fluxes; (ii) the worse CanAM-4.1 (low) cloud fractions; and (iii) as already said, the worse ERA-Interim (low) cloud fractions.

Also, ISCCP Flux Data ("isccp_fd") does not seem to agree perfectly with CERES Energy Balanced And Filled (CEBAF) (or "cebaf") or the other Clouds and the Earth's Radiant Energy System (CERES) datasets ("ceres_syn", "ceres_ssf"), which is something to keep in mind in the next section.

Finally, mean values (μ) and standard deviations (σ) are all consistent with the literature, as well as with a preliminary study of these CanAM-4.1 runs. So far, discrepancies in radiative fluxes and precipitation rates seem consistent with clouds simulation difficulties.

Chapter 5

Two generations

Honorable errors do not count as failures in science,
but as seeds for progress in the quintessential activity of correction.

Stephen Jay Gould, "Leonardo's Mountain of Clams and the
Diet of Worms: Essays on Natural History", 1998 (p. 163)

My daughter and the rest of Generation Hot have been given
a life sentence for a crime they didn't commit.

Mark Hertsgaard, "Hot: Living Through
the Next Fifty Years on Earth", 2011

Unless stated otherwise, all figures in this chapter are based on data (i) over the oceans (not over land), (ii) for the 30°S–30°N 'tropical' band, and (iii) from July 1983 to November 2000 (Figure A.1).

Each section compares the Probability Distribution Functions (PDFs), time series, Taylor diagrams, or a statistics table relative to its fields, plus, if necessary, some additional explanation for the comparisons.

5.1 Cloud fractions

5.1.1 Low clouds

According to Figure 5.1, the CCCma updated fourth generation atmospheric GCM (CanAM-4.1) performs better than its predecessor — the CCCma third generation atmospheric GCM (AGCM-3), with no noticeable difference between its raw ("low_cloud") and *ISCCP-simulated* fields ("low_cloud-isccp").

In addition, the ECMWF Interim Re-Analysis (ERA-Interim) can be seen to perform better than ECMWF 40 years Re-Analysis (ERA-40).

In Figure 5.2, ERA-Interim's position (i.e. mean) is closer to the one of the International Satellite Cloud Climatology Project (ISCCP), but it's shape (e.g. standard deviation) does not seem to improve relative to the ERA-40 (which is the closest to "isccp_IR").

CanAM-4.1 raw output is closer to both "isccp" and "isccp_IR" (relative to AGCM-3). The shape of its *ISCCP-simulated* field distribution seems closer to that of ISCCP, but shifted toward the small low fractions (i.e. overestimate small and underestimate medium-to-large low cloud fractions.

Noticing that the change from "isccp_IR" to "isccp" is somewhat similar to the change from CanAM-4.1 raw output to its simulated field, one could (tentatively) infer that the CFMIP Observation Simulator Package (COSP) performs well but starts from a field with too many small and too few large low cloud fractions.

Figure 5.3, Table 5.1, and Figure 5.4 show that, in this case, (i) ERA-40 is not performing better than the models, (ii) CanAM-4.1 does not clearly improve relative to AGCM-3, and (iii) the COSP simulator does provide clear improvements.

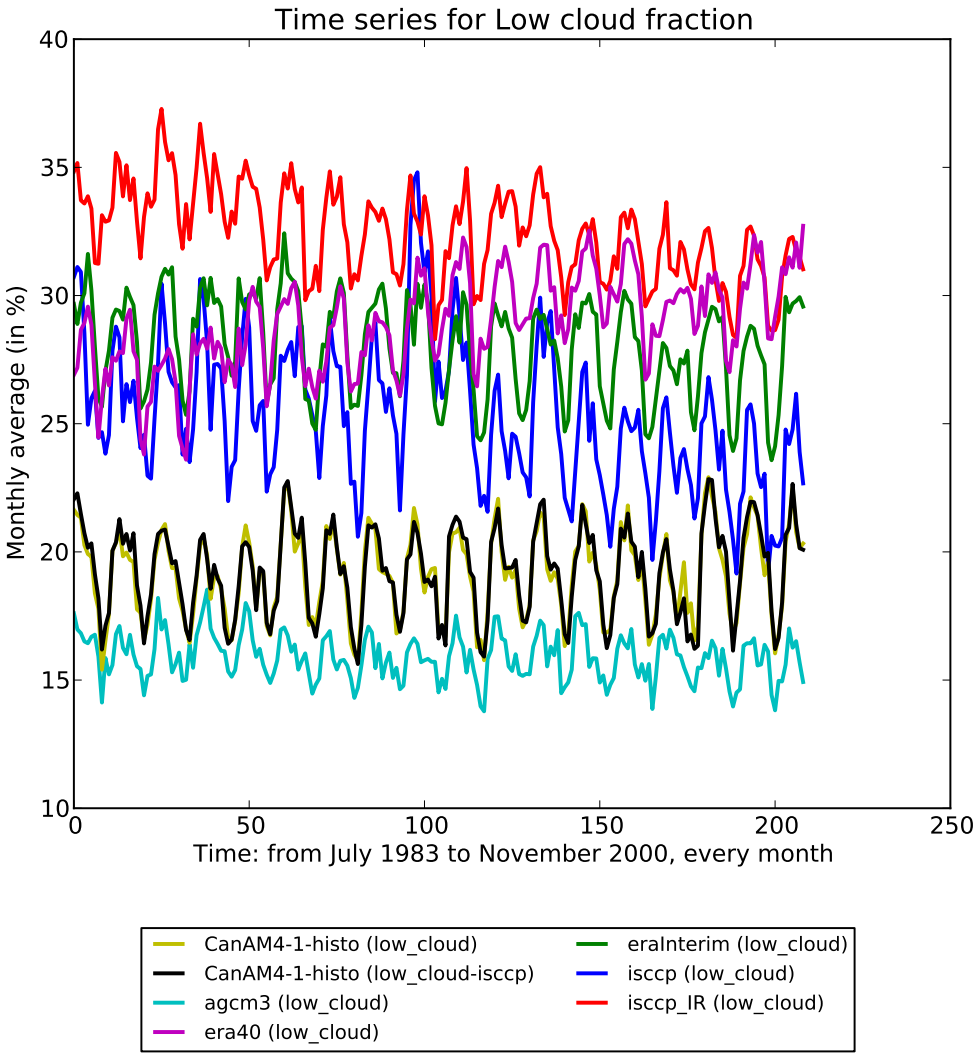

Figure 5.1: Low cloud time series by datasets. From lowest to highest low cloud fractions: AGCM-3, CanAM-4.1 (both raw and simulated), ISCCP, ERA-Interim, ERA-40, "isccp_IR".

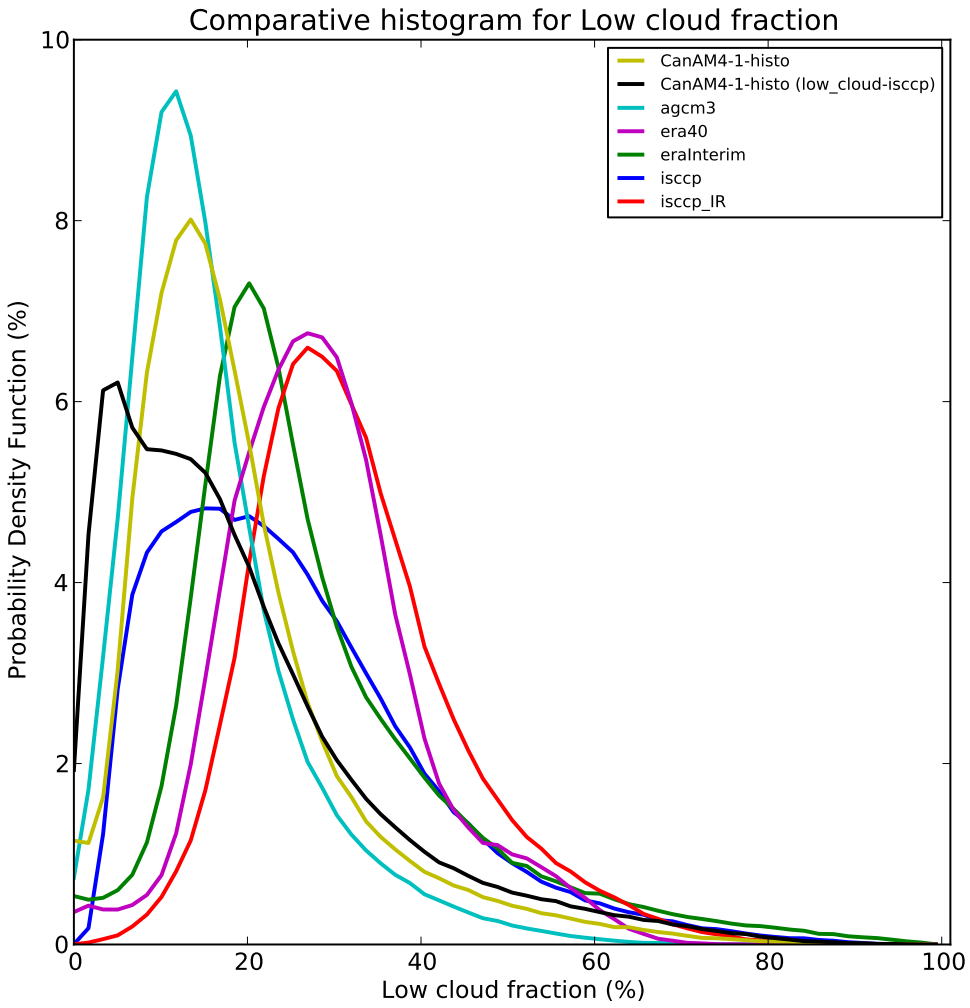

Figure 5.2: Low cloud distributions by datasets.

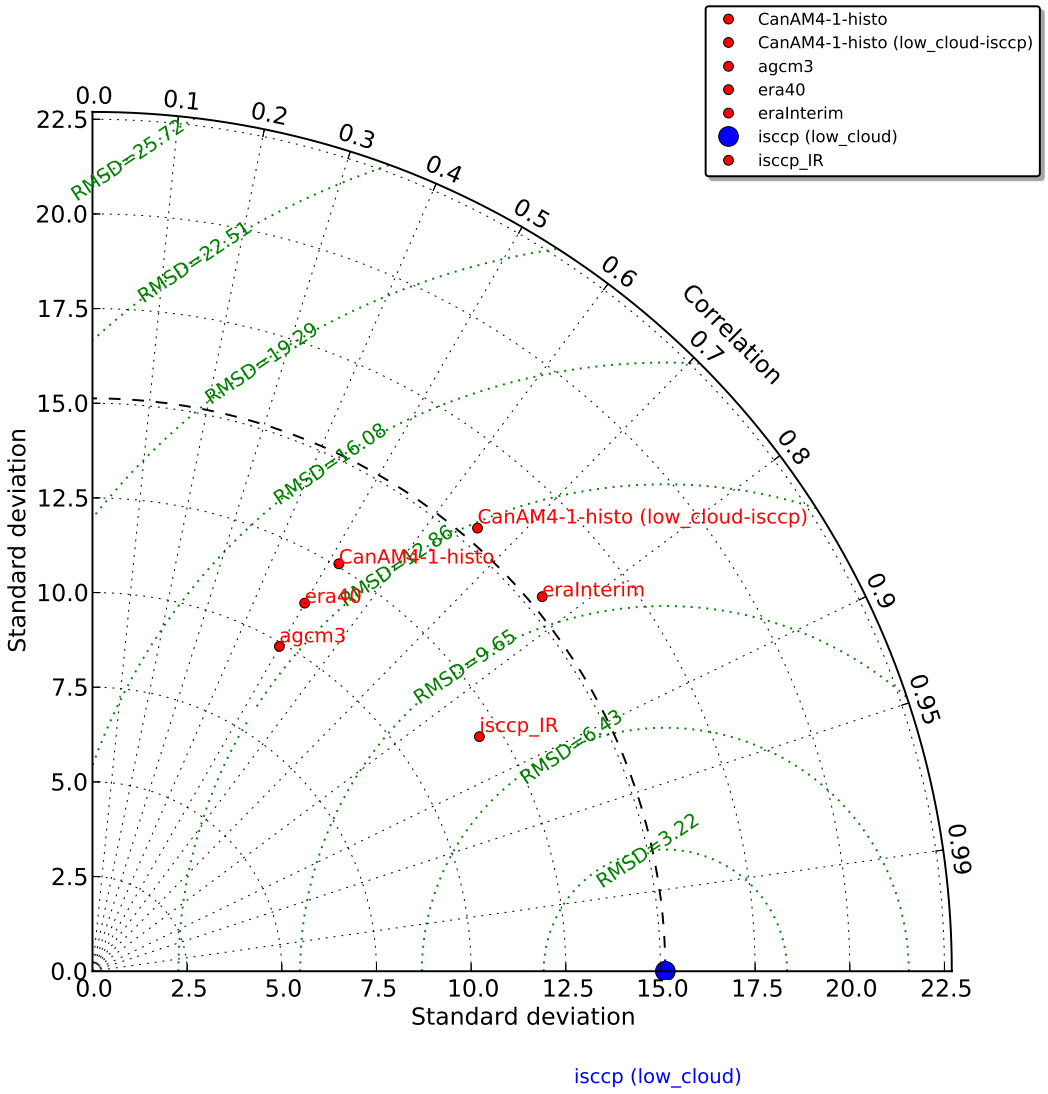

Figure 5.3: Taylor diagram for low clouds. Standard deviations (σ) are given in percent. Correlations are unit-less (dimensionless). All coordinates values are given in Table 5.1: Std (σ), Correlation (Corr), and Root-Mean-Square Difference (RMSD).

Source (Ref. first)	Min	Median	Mean (μ)	Max	Std (σ)	Corr (%)	RMSD	RMSD$/\mu$
isccp	0.0	22.9	25.3	100.0	15.1	100.00	0.00	0.00
CanAM4-1-histo	0.0	16.3	19.1	98.3	12.6	51.74	13.79	0.72
— (low_cloud-isccp)	0.0	15.7	19.3	98.4	15.5	65.59	12.71	0.66
agcm3	0.0	13.9	15.9	83.8	9.9	49.87	13.32	0.84
era40	0.0	28.0	28.9	77.7	11.2	49.95	13.61	0.47
eraInterim	0.0	24.2	28.1	99.4	15.5	76.84	10.42	0.37
isccp_IR	0.6	30.9	32.5	90.4	11.9	85.51	7.91	0.24

Table 5.1: Comparison for low clouds. Minimum (Min), Median, Average (Mean, μ), Maximum (Max), Standard deviation (Std, σ), and Root-Mean-Square Difference (RMSD) are expressed in percent (cloud fraction units). Correlation (Corr) is also expressed in percent. RMSD$/\mu$ is expressed without units. Min, Median, Mean, and Max can be visualized in Figure 5.2. Std, Corr, and RMSD can be visualized in Figure 5.3. Corr, RMSD, and RMSD$/\mu$ are computed relative to the reference (here ISCCP). relative to ISCCP, the ranking from closest to farthest is (almost) identical, whether one looks at correlation or at RMSD (see Figure 5.4).

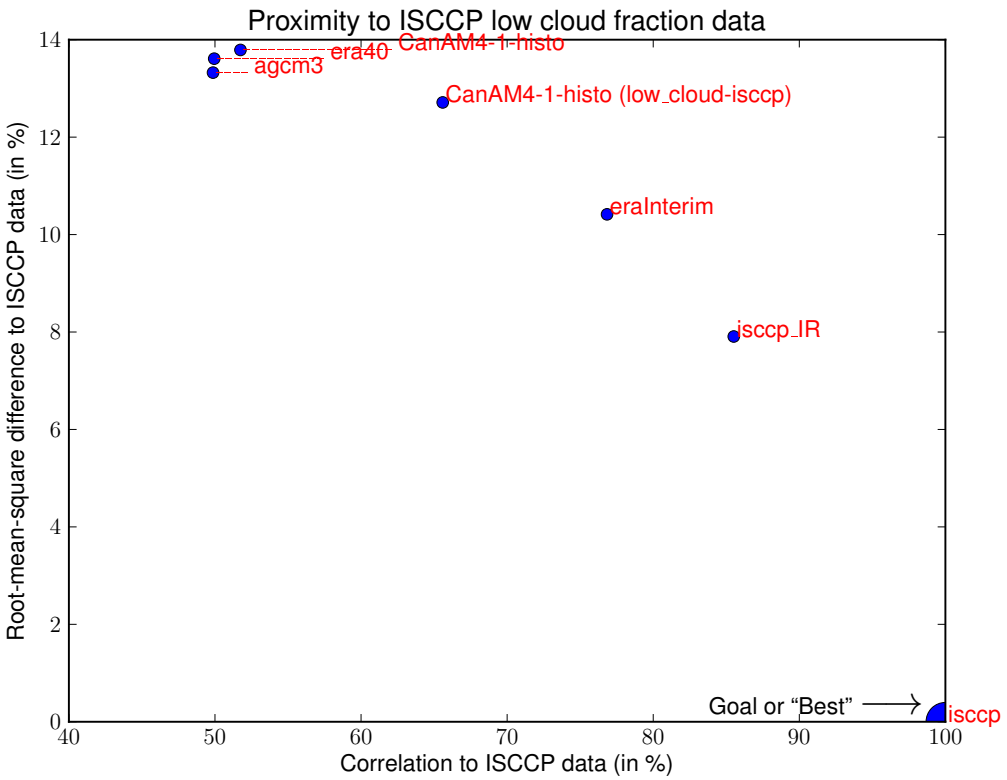

Figure 5.4: Proximity to the low cloud reference (ISCCP) as estimated using two distinct measures: Standard deviation and Correlation. Evolution, although monotonic, is not linear. Like the Taylor diagram, this figure takes into account standard deviations (see relationship in Figure 3.3), but, unlike the Taylor diagram, it does not explicitly display standard deviation differences. The contributions of the COSP simulator may be the most obvious in this figure.

5.1.2 High clouds

As shown in Figure 5.5, "isccp_IR" has the lowest monthly mean averages, while ERA-40 has the highest monthly mean averages. The latter has a clear, although (likely) spurious trend (see section 5.3 for an explanation).

ISCCP data means are mostly in between CanAM-4.1 and its *ISCCP-simulated* fields. AGCM-3 appears to perform particularly well.

Detection patterns for "isccp_IR" in Figure 5.6 are identical to those in Figure 4.6. On the other hand, ERA-40 seems to have the exact opposite patterns (i.e. high detection of small and low detection of large high cloud fractions).

Figure 5.7, Table 5.2, and Figure 5.8 show that, in this case: (i) CanAM-4.1 clearly performs better than AGCM-3, (ii) but CanAM-4.1's *ISCCP-simulated* field ("high_cloud-isccp") does not perform better than the original (raw) output, (iii) both re-analyses are closer to observations (than the models are).

Surprisingly, CanAM-4.1 "high_cloud-isccp" has worse RMSD and standard deviation relative to CanAM-4.1 "high_cloud", when compared to ISCCP, as shown Table 5.2 and Figure 5.8.

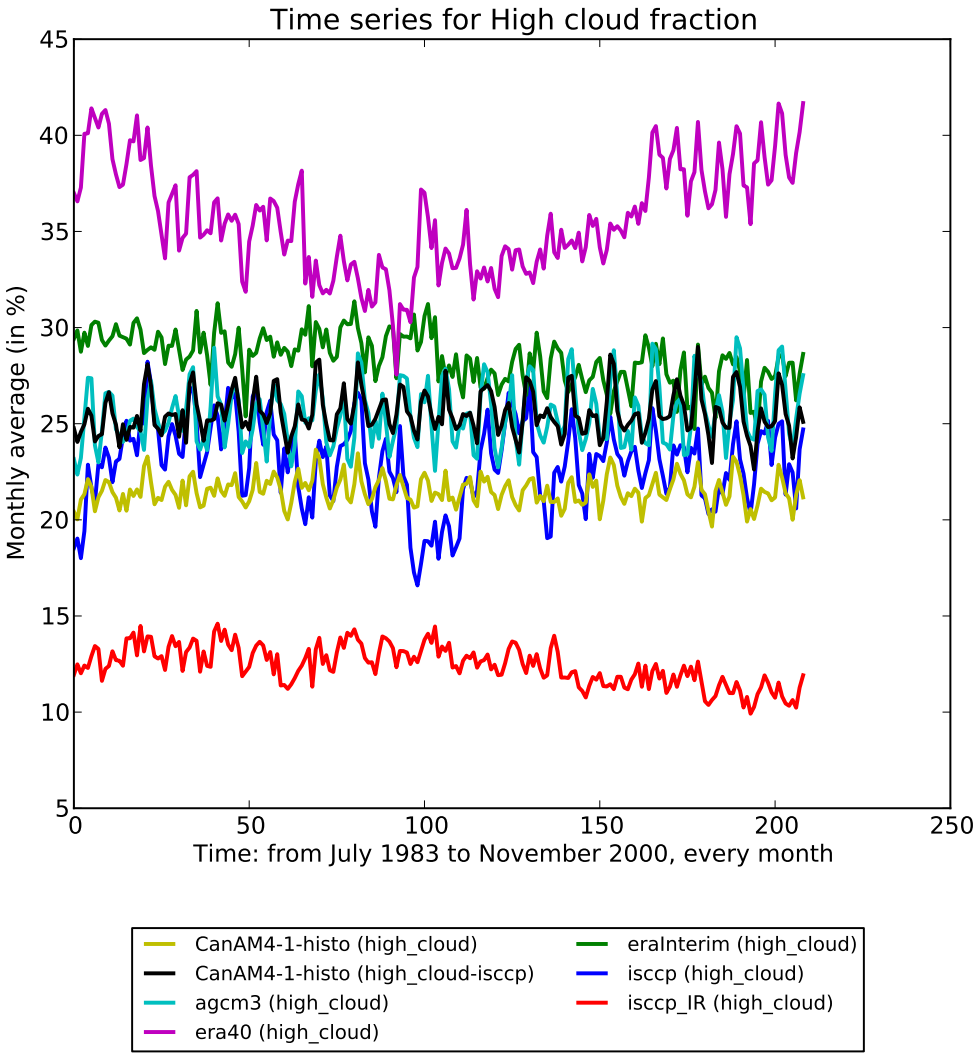

Figure 5.5: High cloud time series by datasets. (Same as Figure 5.1 but for high clouds). From lowest to highest high cloud fractions: "isccp_IR", CanAM-4.1's raw output, ISCCP, AGCM-3, CanAM-4.1's *ISCCP-simulated* field, ERA-Interim, and ERA-40.

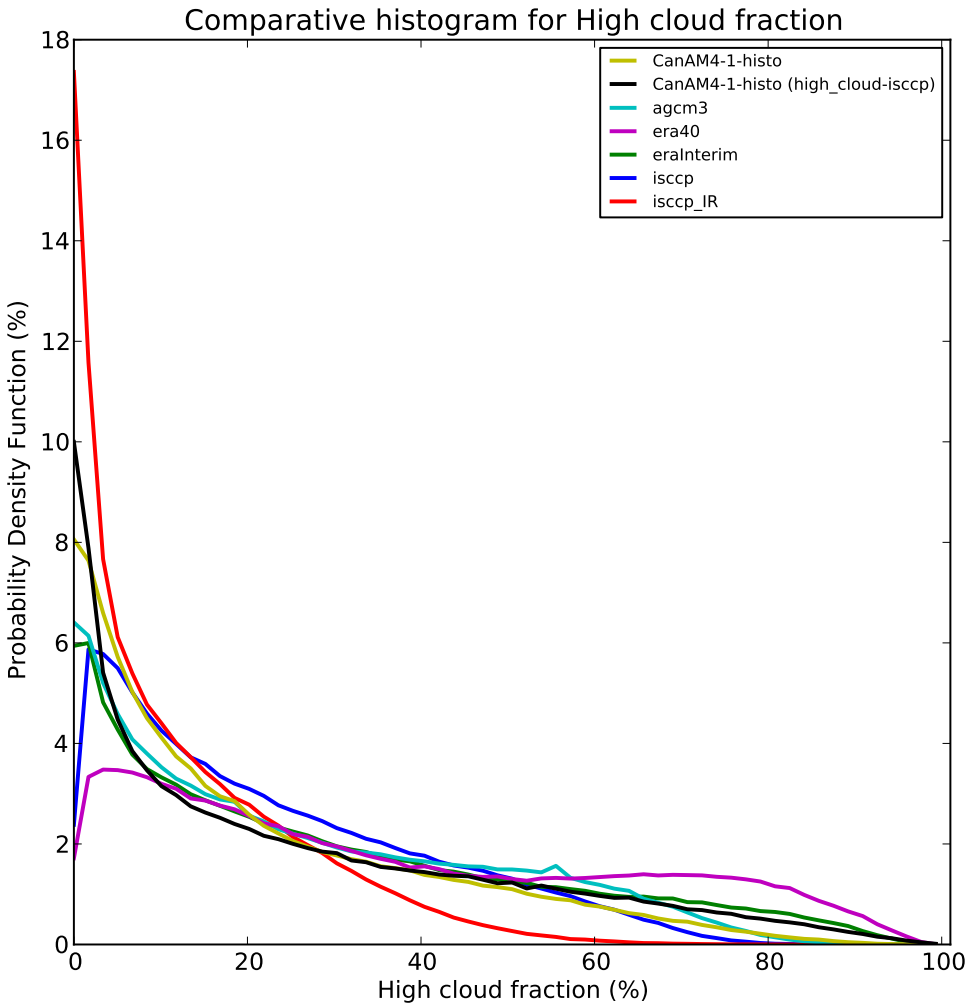

Figure 5.6: High cloud distributions by datasets. (Same as Figure 5.2 but for high clouds).

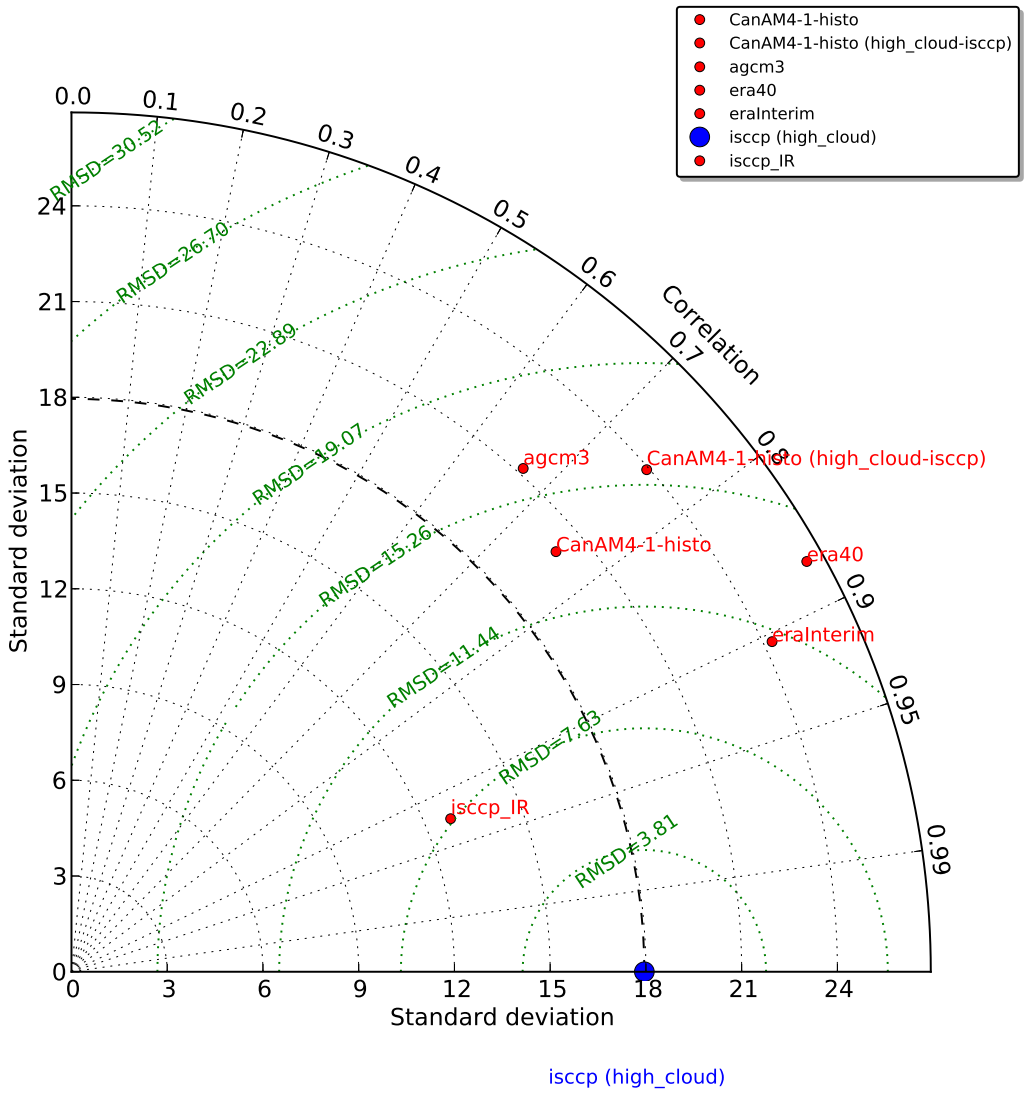

Figure 5.7: Taylor diagram for high clouds. (Same as Figure 5.3 but for high clouds).

Source (Ref. first)	Min	Median	Mean (μ)	Max	Std (σ)	Corr (%)	RMSD	RMSD/μ
isccp	0.0	18.5	23.0	90.2	18.0	100.00	0.00	0.00
CanAM4-1-histo	0.0	14.6	21.5	99.2	20.1	75.55	13.45	0.63
— (high_cloud-isccp)	0.0	18.1	25.5	99.9	23.9	75.34	15.73	0.62
agcm3	0.0	19.8	25.5	96.4	21.2	66.79	16.22	0.64
era40	0.0	28.8	35.7	99.2	26.4	87.33	13.83	0.39
eraInterim	0.0	21.6	28.4	98.6	24.3	90.46	11.09	0.39
isccp_IR	0.0	8.1	12.4	80.7	12.8	92.73	7.74	0.62

Table 5.2: Comparison for high clouds. (Same as Table 5.1).

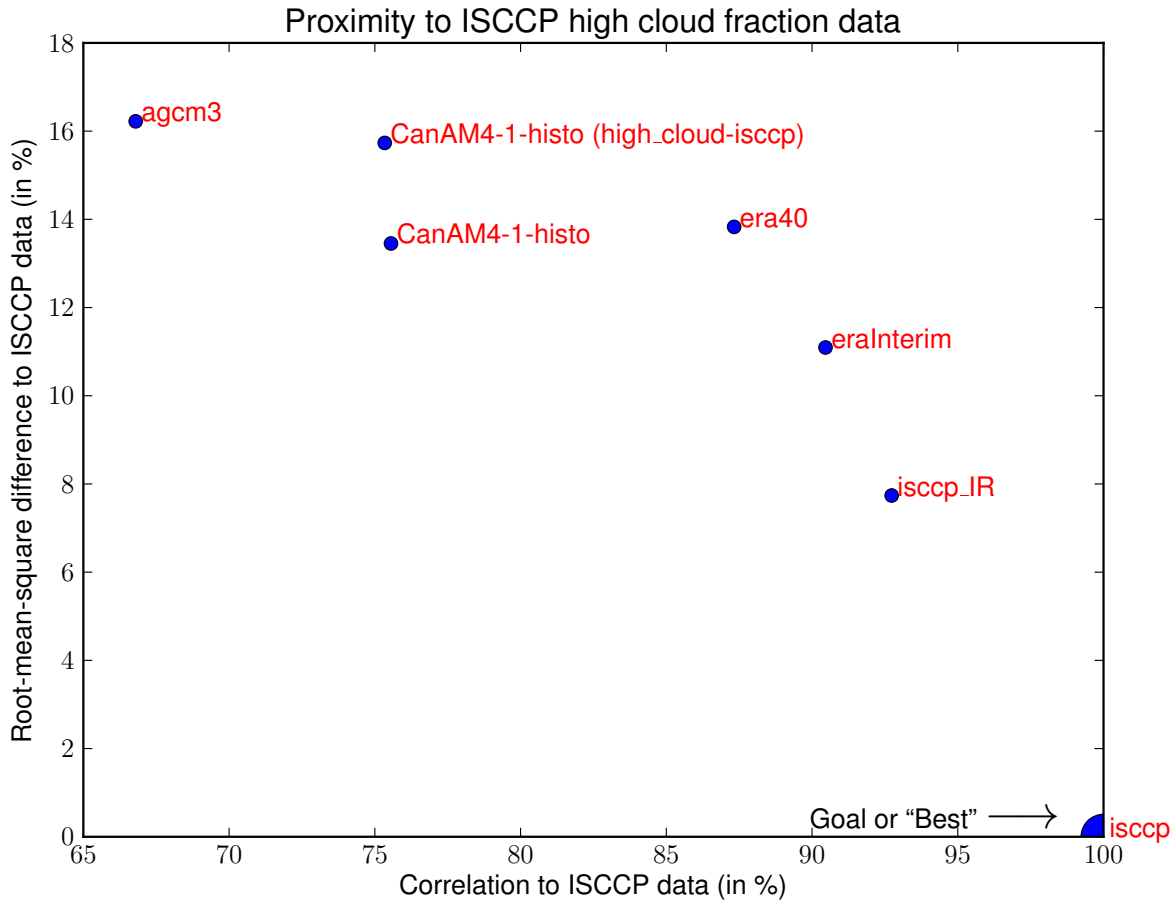

Figure 5.8: Proximity to the high cloud reference (ISCCP) as estimated using two distinct measures: Standard deviation and Correlation. Progression, although monotonic, is not linear.

5.2 Radiation fields

5.2.1 Top of the atmosphere (TOA) shortwave flux (SW), all-sky conditions (ALL)

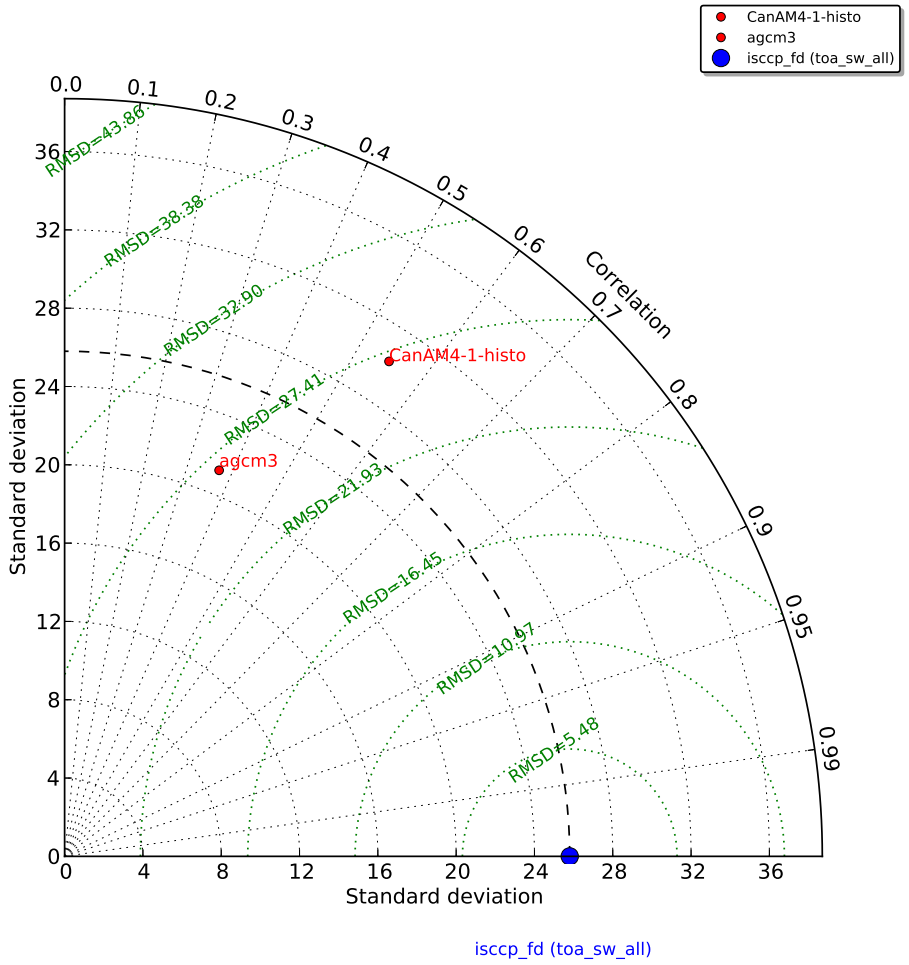

Figure 5.9: Taylor diagram for TOA SW fluxes (All skies). (Same as Figure 5.3 but for TOA SW fluxes (All skies)). Standard deviations (σ) are given in W/m^2. ERA-40 TOA SW fluxes (both All-sky and Clear-sky conditions) were not available.

Source (Ref. first)	Min	Median	Mean (μ)	Max	Std (σ)	Corr (%)	RMSD	RMSD/μ
isccp_fd	36.3	91.6	95.9	237.9	25.8	100.00	0.00	0.00
CanAM4-1-histo	32.0	82.2	88.6	262.6	30.2	54.82	26.91	0.30
agcm3	34.5	90.5	92.3	228.0	21.2	37.16	26.64	0.29

Table 5.3: Comparison for TOA SW fluxes (All skies). (Same as Table 5.1). Minimum (Min), Median, Average (Mean, μ), Maximum (Max), Standard deviation (Std, σ), and RMSD are all expressed in W/m^2 (TOA SW fluxes units). CanAM-4.1 seems to perform somewhat better than AGCM-3.

5.2.2 Top of the atmosphere (TOA) longwave flux (LW), all-sky conditions (ALL)

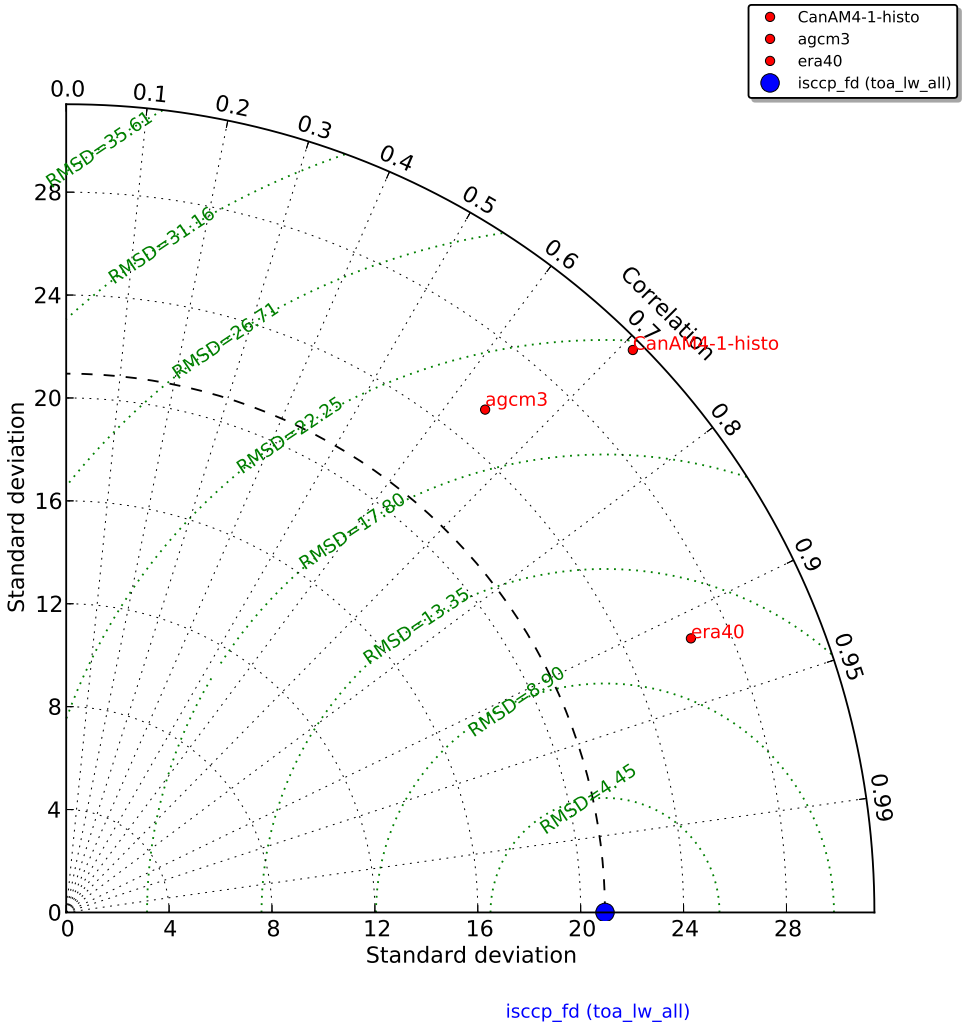

Figure 5.10: Taylor diagram for TOA LW fluxes (All skies). (Same as Figure 5.3 but for TOA LW fluxes (All skies)). Standard deviations (σ) are given in W/m^2. In contrast to SW, ERA-40 TOA LW fluxes (both All-sky and Clear-sky conditions) are (more) consistent with observations.

Source (Ref. first)	Min	Median	Mean (μ)	Max	Std (σ)	Corr (%)	RMSD	RMSD/μ
isccp_fd	167.5	257.0	253.3	313.6	20.9	100.00	0.00	0.00
CanAM4-1-histo	134.7	264.8	257.9	331.7	31.0	70.97	21.89	0.08
agcm3	157.2	262.2	257.5	334.9	25.4	64.01	20.10	0.08
era40	150.0	268.7	263.0	343.2	26.5	91.58	11.17	0.04

Table 5.4: Comparison for TOA LW fluxes (All skies). (Same as Table 5.1). Minimum (Min), Median, Average (Mean, μ), Maximum (Max), Standard deviation (Std, σ), and RMSD are all expressed in W/m^2 (TOA LW fluxes units). CanAM-4.1 has a higher correlation but AGCM-3 has a smaller RMSD.

5.2.3 Top of the atmosphere (TOA) net flux (NET), all-sky conditions (ALL)

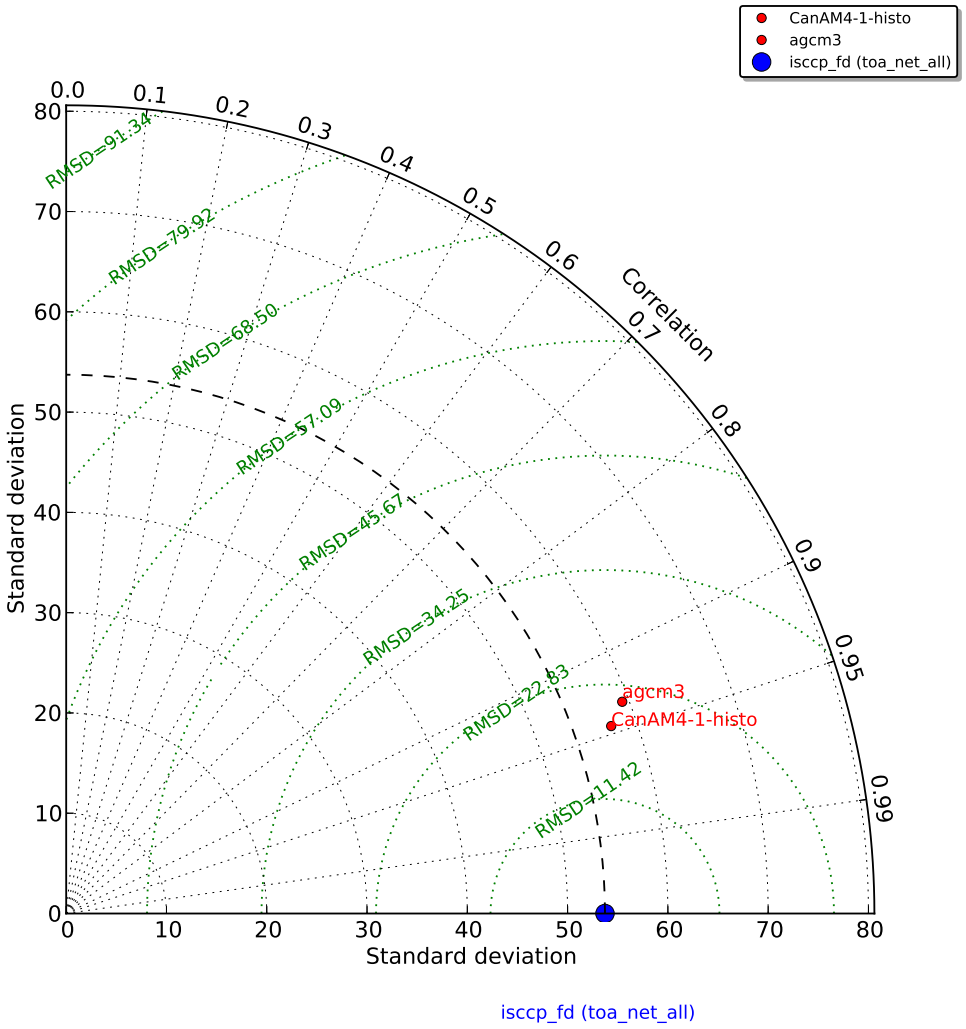

Figure 5.11: Taylor diagram for TOA NET fluxes (All skies). (Same as Figure 5.3 but for TOA NET fluxes (All skies)). Standard deviations (σ) are given in W/m^2. Although close, in this case, CanAM-4.1 seems to be a clearly better than AGCM-3.

Source (Ref. first)	Min	Median	Mean (μ)	Max	Std (σ)	Corr (%)	RMSD	RMSD/μ
isccp_fd	-121.4	66.0	51.8	165.5	53.7	100.00	0.00	0.00
CanAM4-1-histo	-128.2	67.1	54.3	177.8	57.5	94.56	18.72	0.34
agcm3	-132.6	66.1	50.9	171.2	59.3	93.45	21.20	0.42

Table 5.5: Comparison for TOA NET fluxes (All skies). (Same as Table 5.1). Minimum (Min), Median, Average (Mean, μ), Maximum (Max), Standard deviation (Std, σ), and RMSD are all expressed in W/m^2 (TOA NET fluxes units).

5.2.4 Net Cloud Radiative Effect (NCRE)

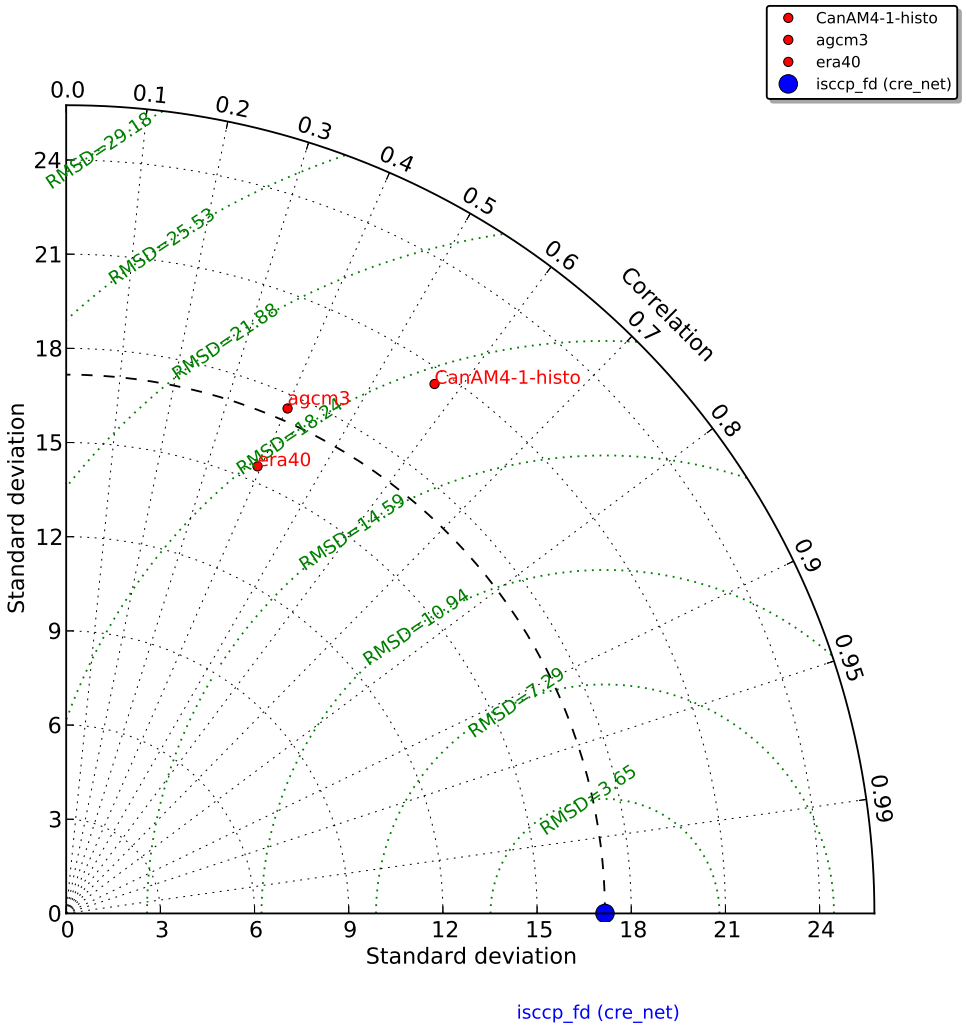

Figure 5.12: Taylor diagram for net CRE. (Same as Figure 5.3 but for net CRE). Standard deviations (σ) are given in W/m^2. Note that considering ERA-40's TOA SW fluxes performances, nothing can be deduced from its Net CRE.

Source (Ref. first)	Min	Median	Mean (μ)	Max	Std (σ)	Corr (%)	RMSD	RMSD/μ
isccp_fd	-146.2	-20.3	-24.1	15.2	17.2	100.00	0.00	0.00
CanAM4-1-histo	-172.2	-17.0	-20.6	41.8	20.5	57.11	17.72	-0.86
agcm3	-134.7	-18.5	-18.9	31.1	17.6	40.15	19.00	-1.01
era40	-128.0	-44.7	-44.7	8.7	15.5	39.35	18.04	-0.40

Table 5.6: Comparison for net CRE. (Same as Table 5.1). Minimum (Min), Median, Average (Mean, μ), Maximum (Max), Standard deviation (Std, σ), and RMSD are all expressed in W/m^2 (TOA NET fluxes units).

5.3 Precipitation rates

The Global Precipitation Climatology Project (GPCP) and the Climate Prediction Center (CPC) Merged Analysis of Precipitation (CMAP) have a consistent average discrepancy (3.0 versus 3.5 mm/day, or 15.4% difference), as shown in Figure 5.13 and Table 5.7)

ERA-40's overestimation of tropical oceanic precipitation and tropical high clouds is a well-known fact in the literature (Uppala et al. 2005). Its (spurious) trend through time, which can be seen in Figures 5.5 or 5.13, is exacerbated in later years by effects of the eruption of Mount Pinatubo in June 1991 (creating bias in satellite radiances, corrupted by the eruption).

ERA-40 seems to overestimate both smaller and larger precipitation rates, while underestimating medium ones (Figure 5.14). Although it is less marked, CanAM-4.1 seems to have the same biases. On the other hand, AGCM-3 does the opposite (significantly underestimate both smaller and larger precipitation rates, while significantly overestimating medium ones).

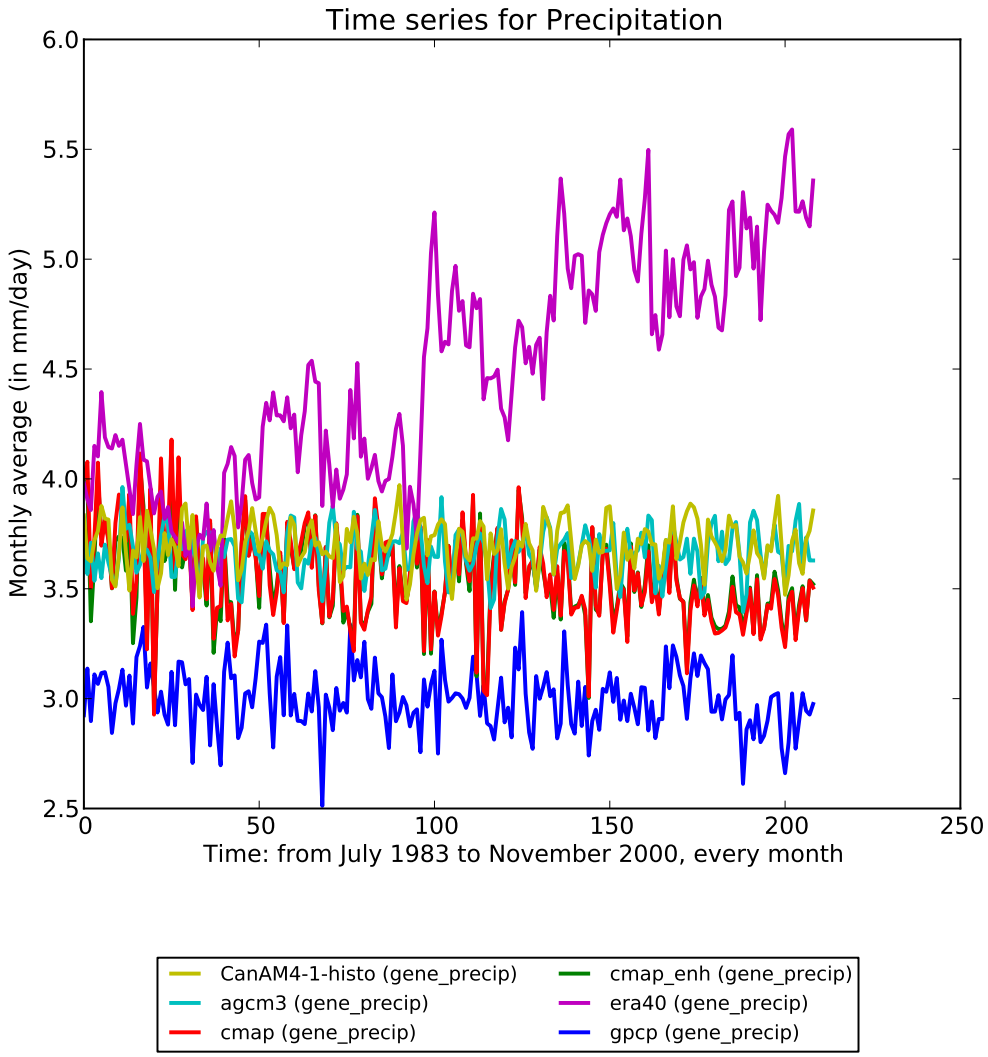

Figure 5.13: Precipitation time series by datasets. (Same as Figure 5.1 but for precipitation rates).

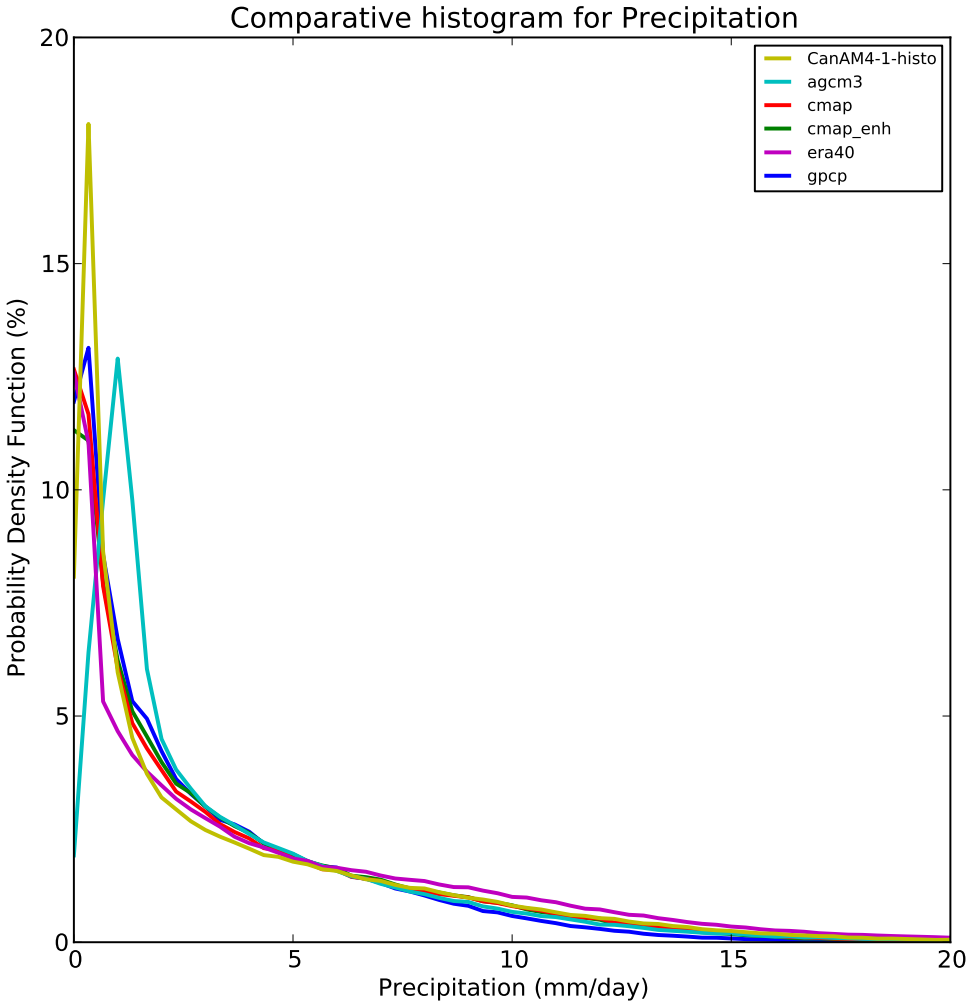

Figure 5.14: Precipitation distributions by datasets. (Same as Figure 5.2 but for precipitation rates).

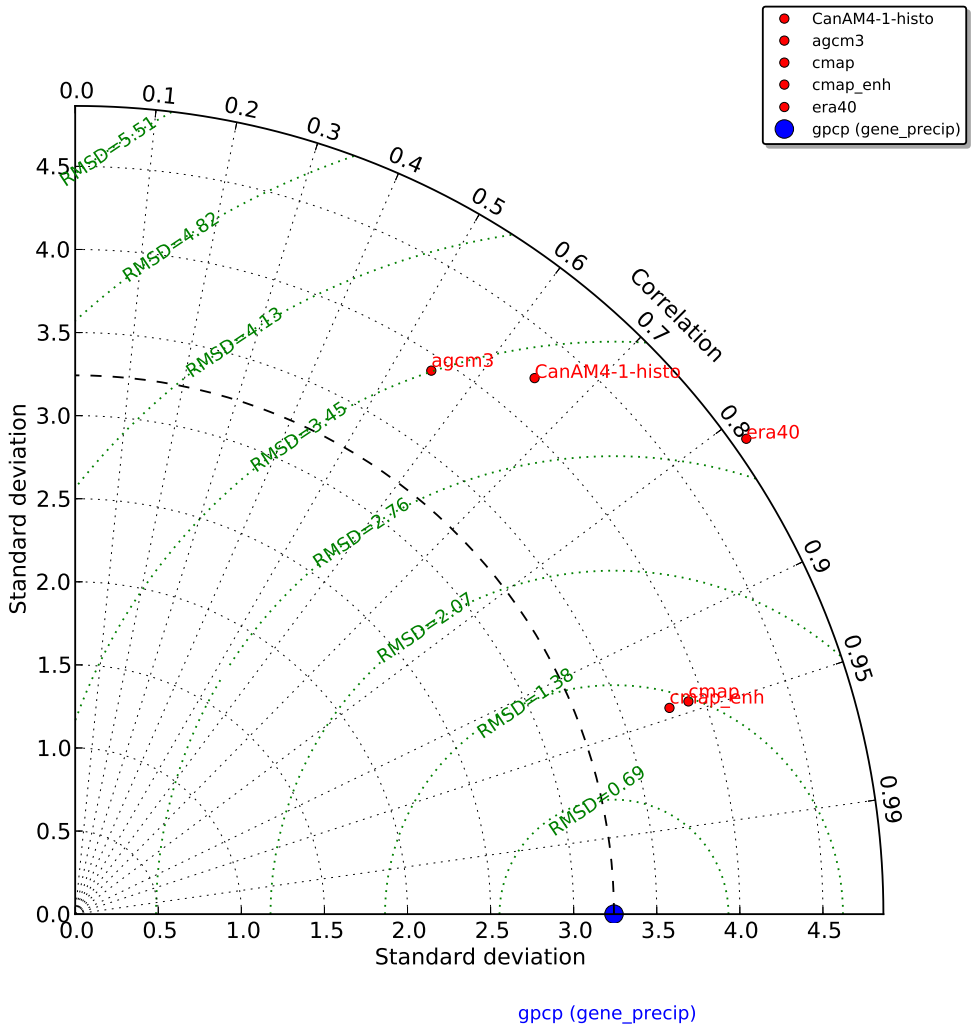

Figure 5.15: Taylor diagram for precipitation rates. (Same as Figure 5.3 but for precipitation). Standard deviations (σ) are given in mm/day. CanAM-4.1 performs better than AGCM-3 (relative to observations).

Source (Ref. first)	Min	Median	Mean (μ)	Max	Std (σ)	Corr (%)	RMSD	RMSD/μ
gpcp	0.0	1.8	3.0	30.1	3.2	100.00	0.00	0.00
CanAM4-1-histo	0.0	1.9	3.7	52.7	4.2	65.07	3.26	0.88
agcm3	0.0	2.1	3.7	58.0	3.9	54.81	3.45	0.94
cmap	0.0	2.0	3.5	38.8	3.9	94.48	1.36	0.38
cmap_enh	0.0	2.1	3.5	38.5	3.8	94.47	1.29	0.36
era40	-0.0	2.7	4.5	72.6	4.9	81.60	2.97	0.66

Table 5.7: Comparison for precipitation rates. (Same as Table 5.1). Minimum (Min), Median, Average (Mean, μ), Maximum (Max), Standard deviation (Std, σ), and RMSD are all expressed in mm/day (precipitation rates units).

5.4 Generations comparison

According to this chapter results, and relative to observations, CanAM-4.1 mostly performs better than AGCM-3 (and ERA-Interim better than ERA-40). This statement is particularly true for both low and high cloud fractions. Most of the time, CanAM-4.1 "wins" by at least two, if not three of the Taylor diagram criteria (standard deviation, correlation, and RMSD).

CanAM-4.1's *ISCCP-simulated* low cloud field ("low_cloud-isccp") is more consistent with observations than CanAM-4.1's raw output. However, this is not true for the high cloud field ("high_cloud-isccp"). This could be interpreted as a symptom of problems related to COSP treatment of high clouds.

Although radiative fluxes results have to be considered carefully — in particular since "isccp_fd" was not the reference in the previous chapter and since ERA-40 radiative fluxes have issues — the following hierarchy seems to be mostly valid:

1. first observations,
2. then re-analyses,
3. finally models

Finally, as in the previous chapter too, mean values (μ) and standard deviations (σ) are all consistent with the literature, as well as with a preliminary study of these CanAM-4.1 runs. So far, discrepancies in radiative fluxes and precipitation rates seem consistent with clouds simulation difficulties.

Chapter 6

Qualitative analysis

Bows and flows of angel hair and ice cream castles in the air
And feather canyons everywhere, I've looked at clouds that way.
But now they only block the sun, they rain and snow on everyone.
So many things i would have done but clouds got in my way.

I've looked at clouds from both sides now,
From up and down, and still somehow
It's clouds' illusions i recall.
I really don't know clouds at all.

"Both Sides, Now", Joni Mitchell, Clouds, 1969.

This chapter looks more closely at (low) cloud behavior dependency on Lower Tropospheric Stability (LTS), Estimated Inversion Strength (EIS), or vertical velocity at the 500 hPa level (ω_{500}).

Conclusions are drawn from visualizations and are in no way quantifiable measures of dependencies (hence "qualitative analysis").

Unless stated otherwise, in this chapter, all figures are based on data (i) over the oceans (not over land), (ii) for the 30°S–30°N 'tropical' band, and (iii) from July 1983 to November 2000.

Conceptually, the steps followed in this chapter, in order to actually compare the CCCma third generation atmospheric GCM (AGCM-3) and the CCCma updated fourth generation atmospheric GCM (CanAM-4.1) (as well as the ECMWF 40 years Re-Analysis (ERA-40) and the ECMWF Interim Re-Analysis (ERA-Interim)), are as follow:

1. section 6.1 tests the consequences of using EIS rather than LTS;

2. section 6.2 tests the consequences of using one particular model or re-analysis to represent observational data;

3. section 6.3 compares observations, AGCM-3, CanAM-4.1 raw output and *ISCCP-simulated* low cloud fields;

4. section 6.4 compares observations, ERA-40 and ERA-Interim low cloud fields;

5. section 6.5 looks at the average (or typical) vertical profile and frequency of occurrence map for three cloud regimes — "Convectiform", "Stratiform", and "Storm track".

6.1 LTS versus EIS

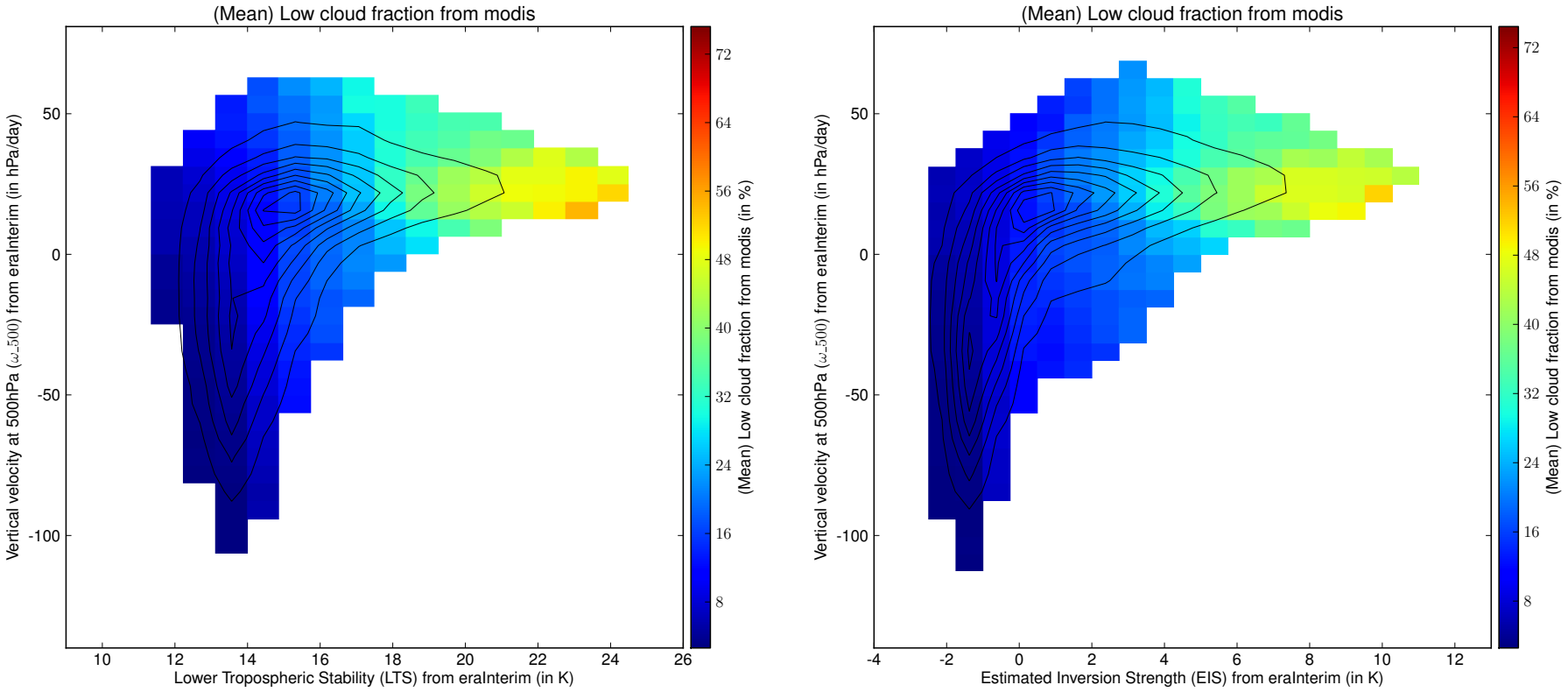

(a) LTS-ω_{500}-MODIS Low cloud

(b) EIS-ω_{500}-MODIS Low cloud

Figure 6.1: 2D-histogram based on LTS versus EIS (from ERA-Interim). Data range from July 2002 to December 2009. Only one 2D-histogram is shown, but all following results are similar whether LTS or EIS is used, with a notable difference in the "Storm track" representation (see subsection 6.5.3, and in particular Figures 6.11a and 6.11b). That is why only LTS is used in the following sections.

6.2 LTS and ω_{500} references

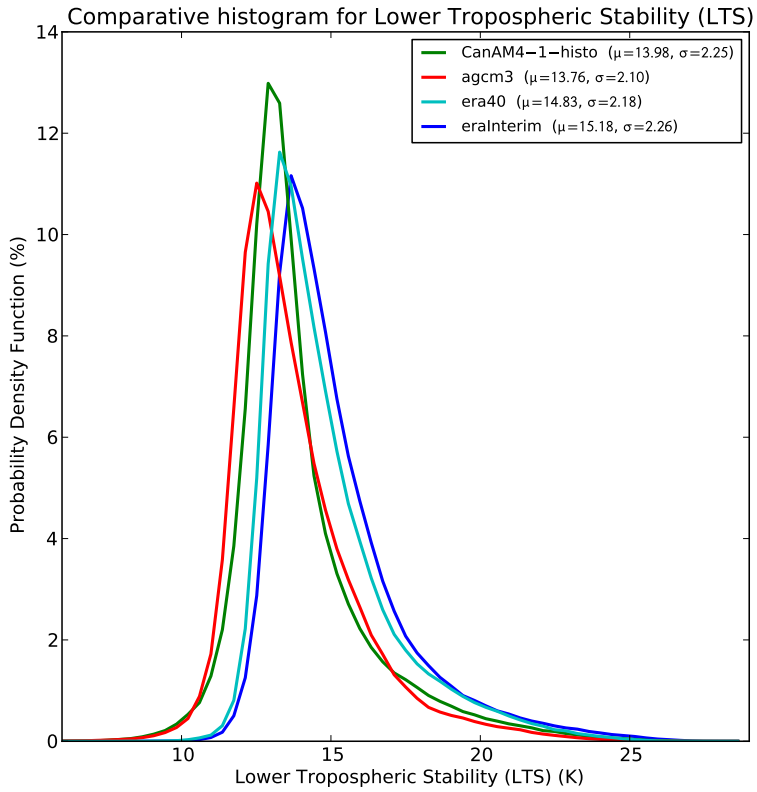

(a) LTS distributions

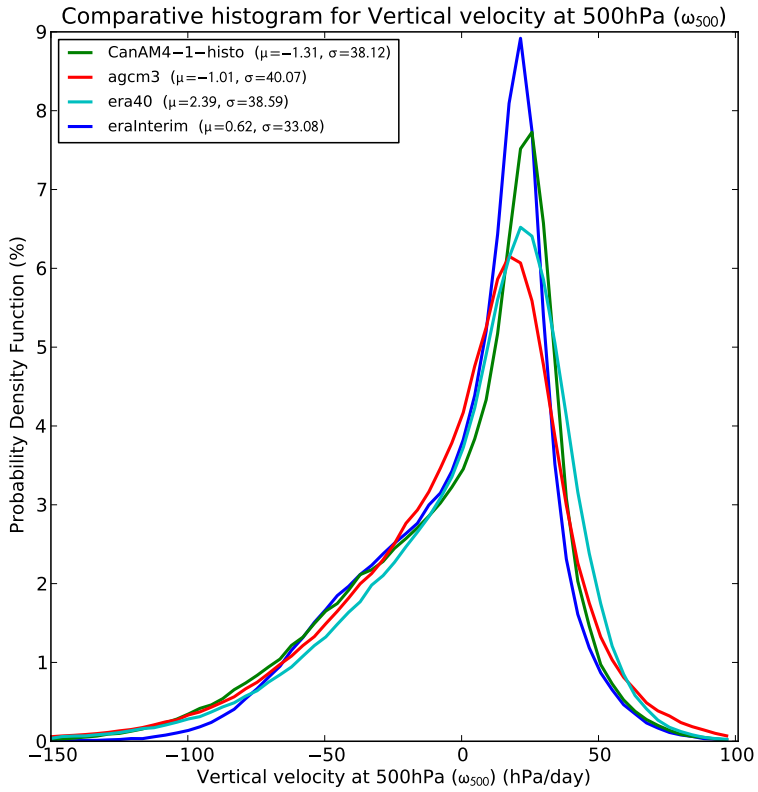

(b) ω_{500} distributions

Figure 6.2: LTS and ω_{500} distributions from ERA-40, ERA-Interim, AGCM-3, and CanAM-4.1. No major differences (in shape or position) distinguishes the two re-analyses and the two simulations. Next figure (6.3) also supports that the choice of the "observational reference for 2D-histograms" does not change the conclusions. To compare (b) with an ω_{500} distribution from the literature, see Figure 2.9 (page 48).

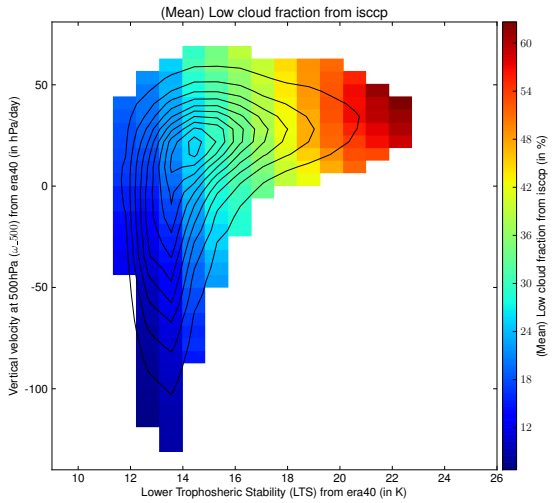

(a) ISCCP data binned based on ERA-40

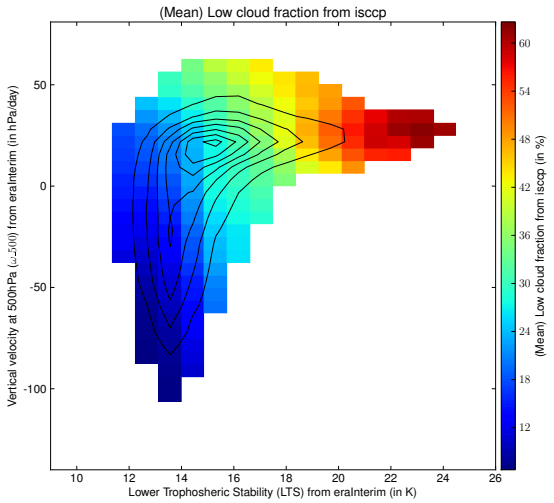

(b) ISCCP data binned based on ERA-Interim

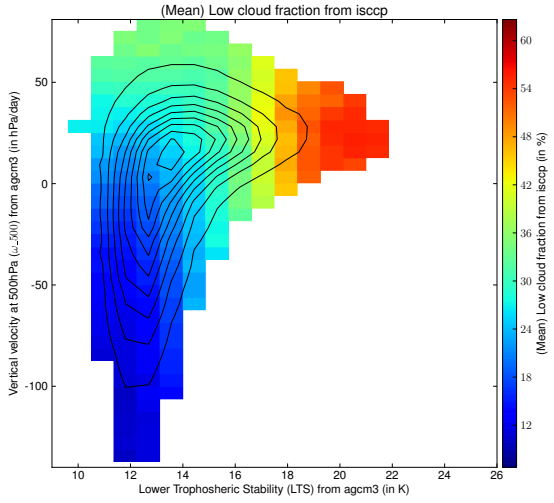

(c) ISCCP data binned based on AGCM-3

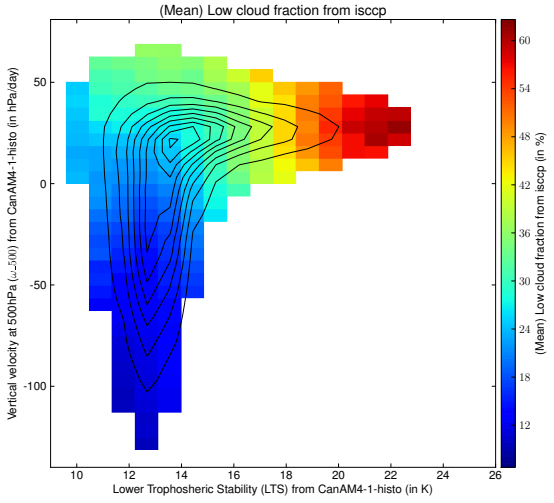

(d) ISCCP data binned based on CanAM-4.1

Figure 6.3: ISCCP Low cloud data binned based with different sources outputs. Note how extremely similar are the four figures, with maybe the exception of (a). Conclusions from representing observations in a 2D-histogram are not sensitive to the choice of the source (for binning). This is even more valid when using EIS (not shown). Considering previous results (see chapter 4 or section 4.5), I thereafter use ERA-Interim outputs when representing an "observational" reference (e.g. in Figure 6.4).

6.3 AGCM-3 versus CanAM-4.1

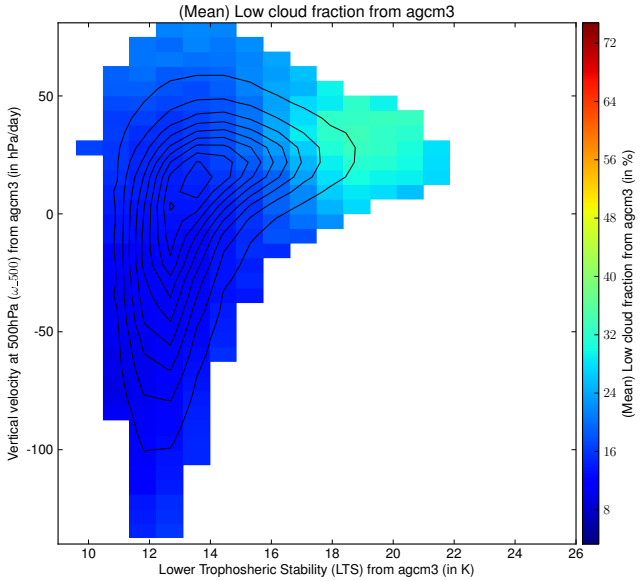

(a) Low cloud from AGCM-3

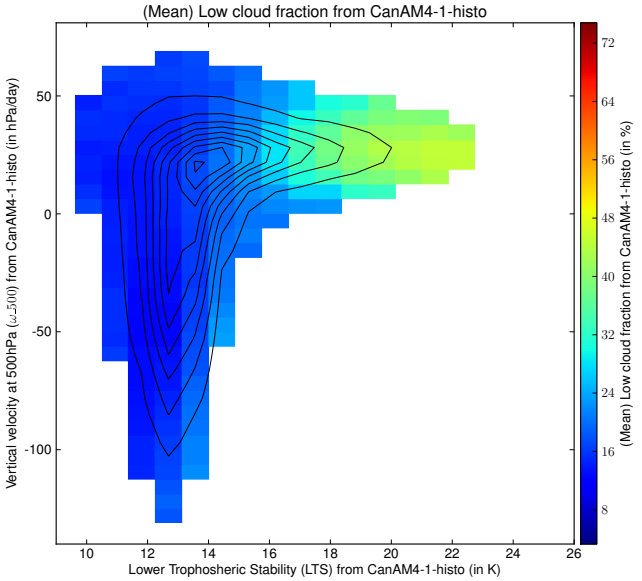

(b) Low cloud from CanAM-4.1

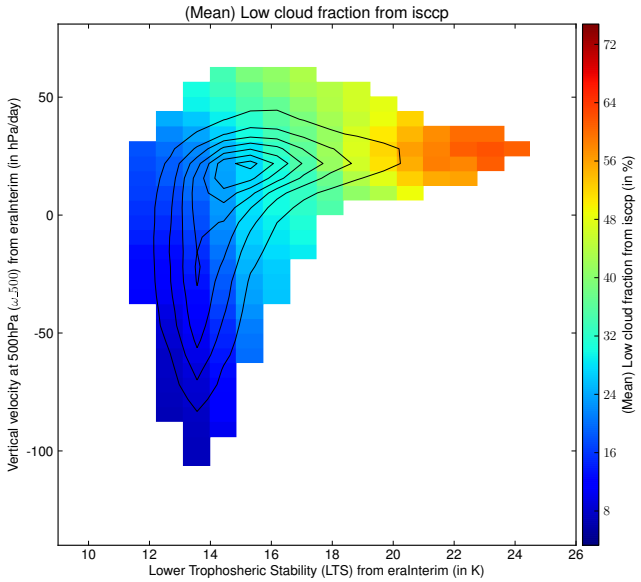

(c) Low cloud from ISCCP

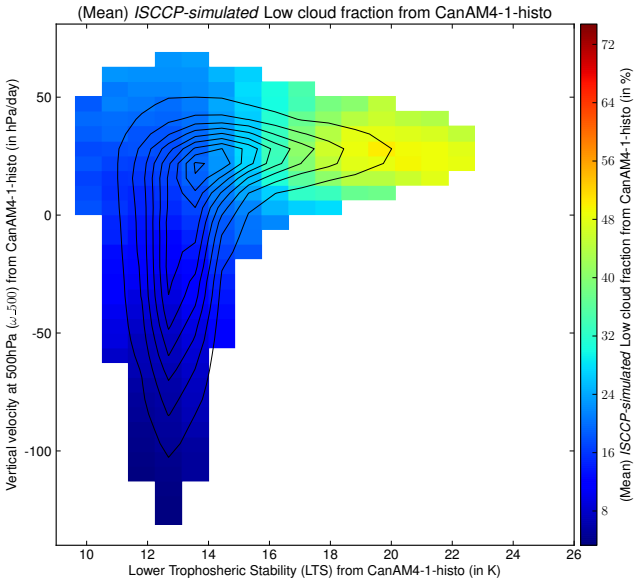

(d) *ISCCP-simulated* low cloud from CanAM-4.1

Figure 6.4: According to these 2D-histograms, CanAM-4.1 seems to perform better than AGCM-3 in simulating low clouds. In particular, both CanAM-4.1's spatial structure (contrasts) and values (means) seem closer to ISCCP observations than AGCM-3's. Then, CanAM-4.1's *ISCCP-simulated* low cloud fractions seem to improve CanAM-4.1's raw output (again, both in structure and values). However, it appears that neither AGCM-3 nor CanAM-4.1 can reproduce the wider range of low clouds seen in the observations.

6.4 ERA-40 versus ERA-Interim

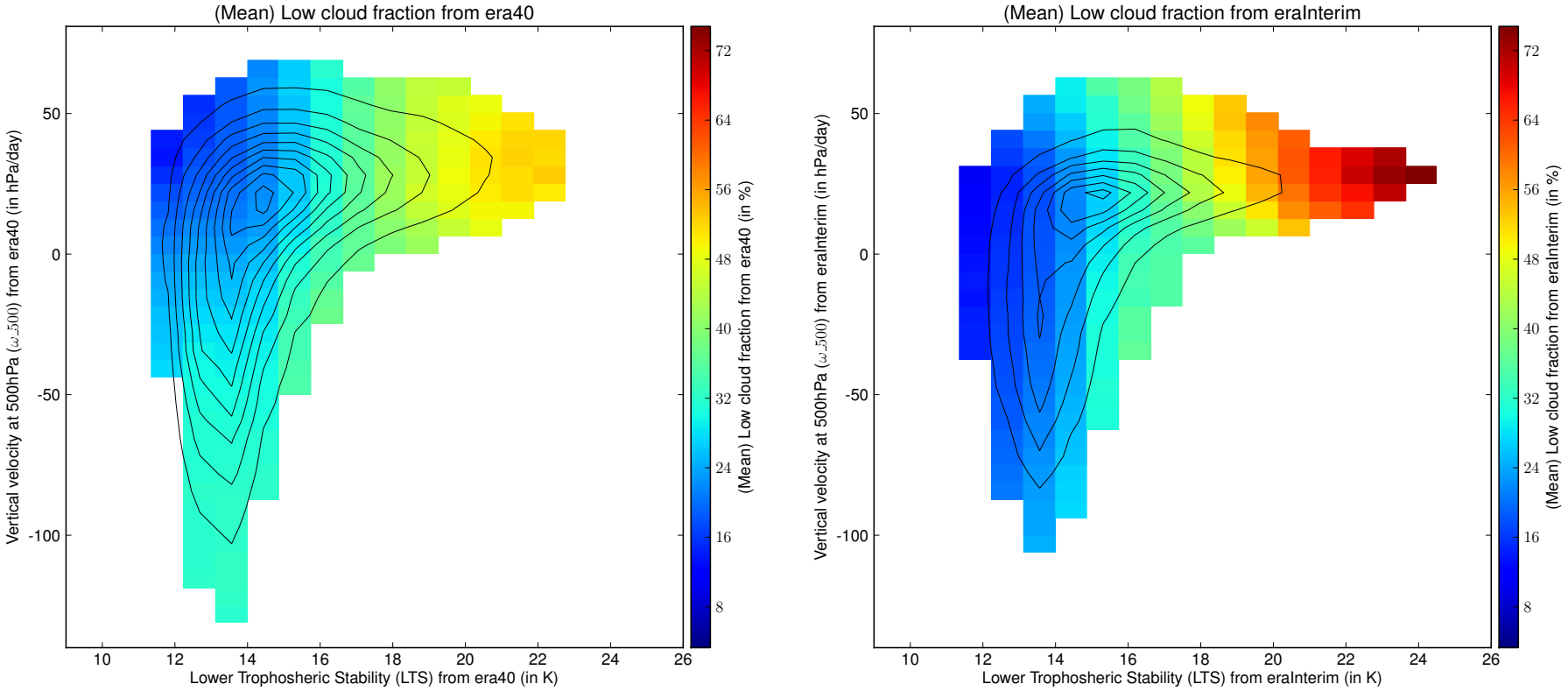

(a) Low cloud from ERA-40

(b) Low cloud from ERA-Interim

Figure 6.5: For the "observational reference", please see Figure 6.4c. According to these 2D-histograms, ERA-Interim clearly performs better than ERA-40 in simulating low clouds. More particularly, both ERA-Interim's spatial structure (contrasts) and values (means) seem closer to observations than ERA-40's. Unlike model simulations (AGCM-3 or CanAM-4.1), re-analyses (ERA-40, but especially ERA-Interim) are able to reproduce the wide range of low clouds seen in the observations.

6.5 Cloud regimes

6.5.1 Convectiform

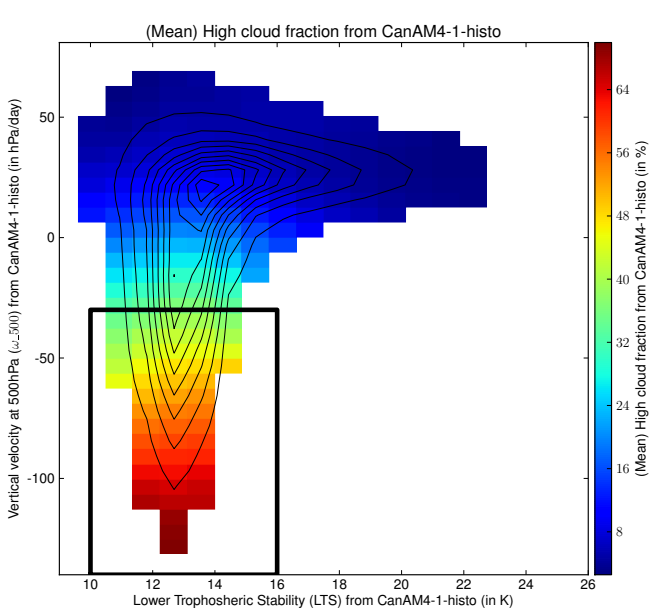

(a) Regime outline (for high clouds)

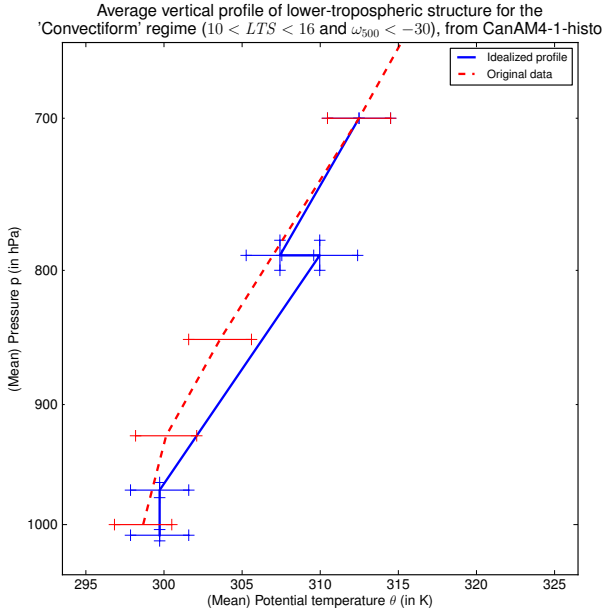

(b) Composite vertical profile

Figure 6.6: The convectiform cloud regime. The vertical profile (b) illustrates how EIS is really defined only when a temperature inversion exists (or, in other words, positive values mean stable, while negative ones "mean" unstable atmosphere). Data span from January 1950 to December 2009.

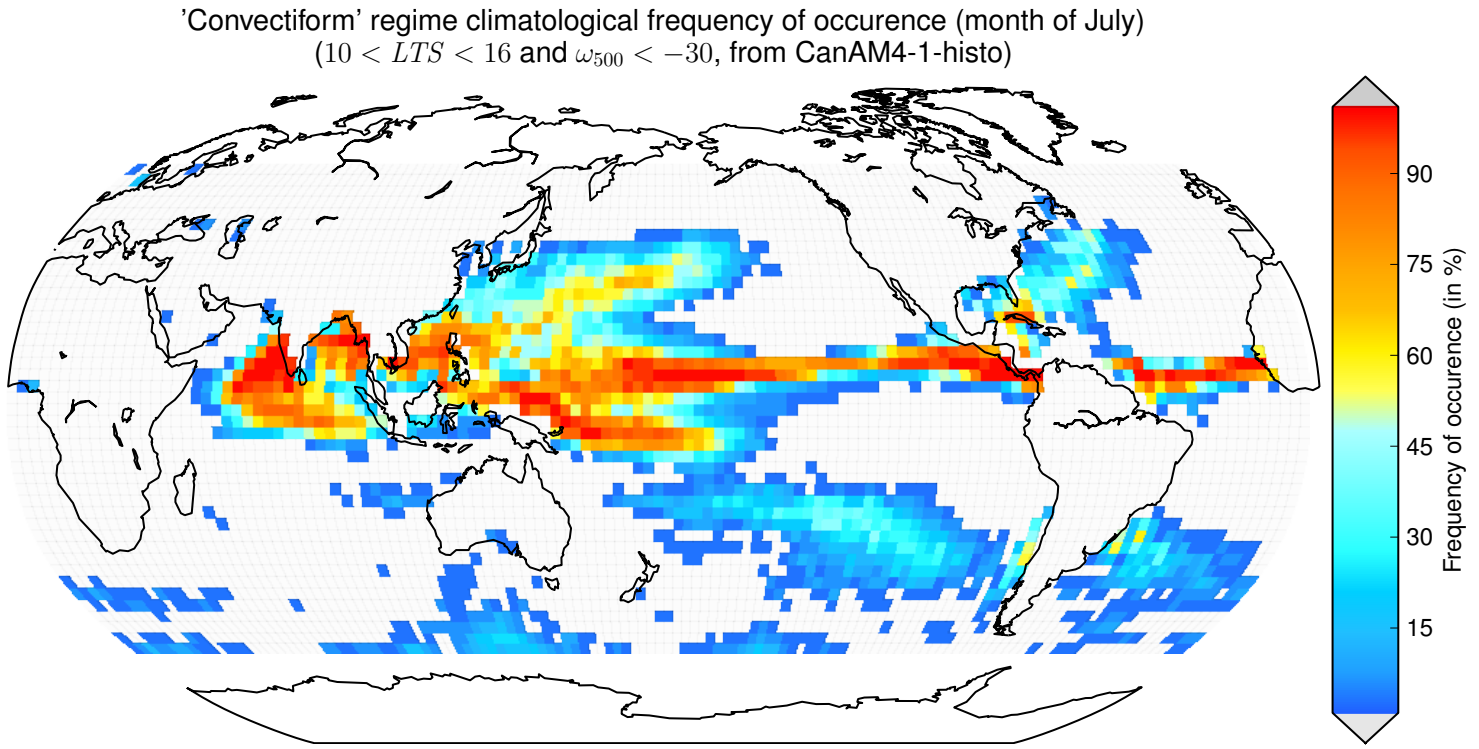

Figure 6.7: Relative occurrence of the convectiform cloud regime (July) As in Figure 6.6, but data span from January 1980 to December 2009. Note that this is the *July* climatological average frequency of occurrence. CanAM-4.1, as well as AGCM-3 (not shown), reproduce well the Inter-Tropical Convergence Zone (ITCZ) (i.e. large amounts of precipitation and high clouds).

6.5.2 Stratiform

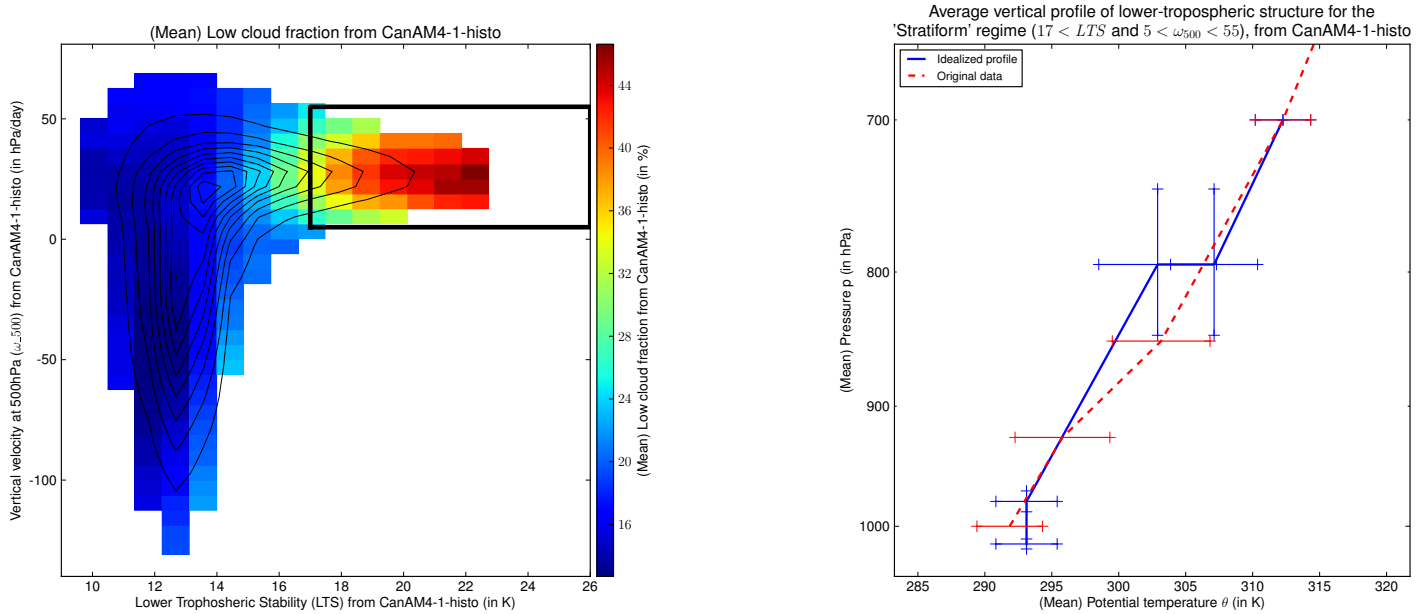

(a) Regime outline

(b) Composite vertical profile

Figure 6.8: The stratiform cloud regime. Figure (b) clearly illustrates both LTS and EIS contributions to the vertical profile (as explained in Figure 2.5); as well as the good match between the data and the idealized profile. Data span from January 1950 to December 2009.

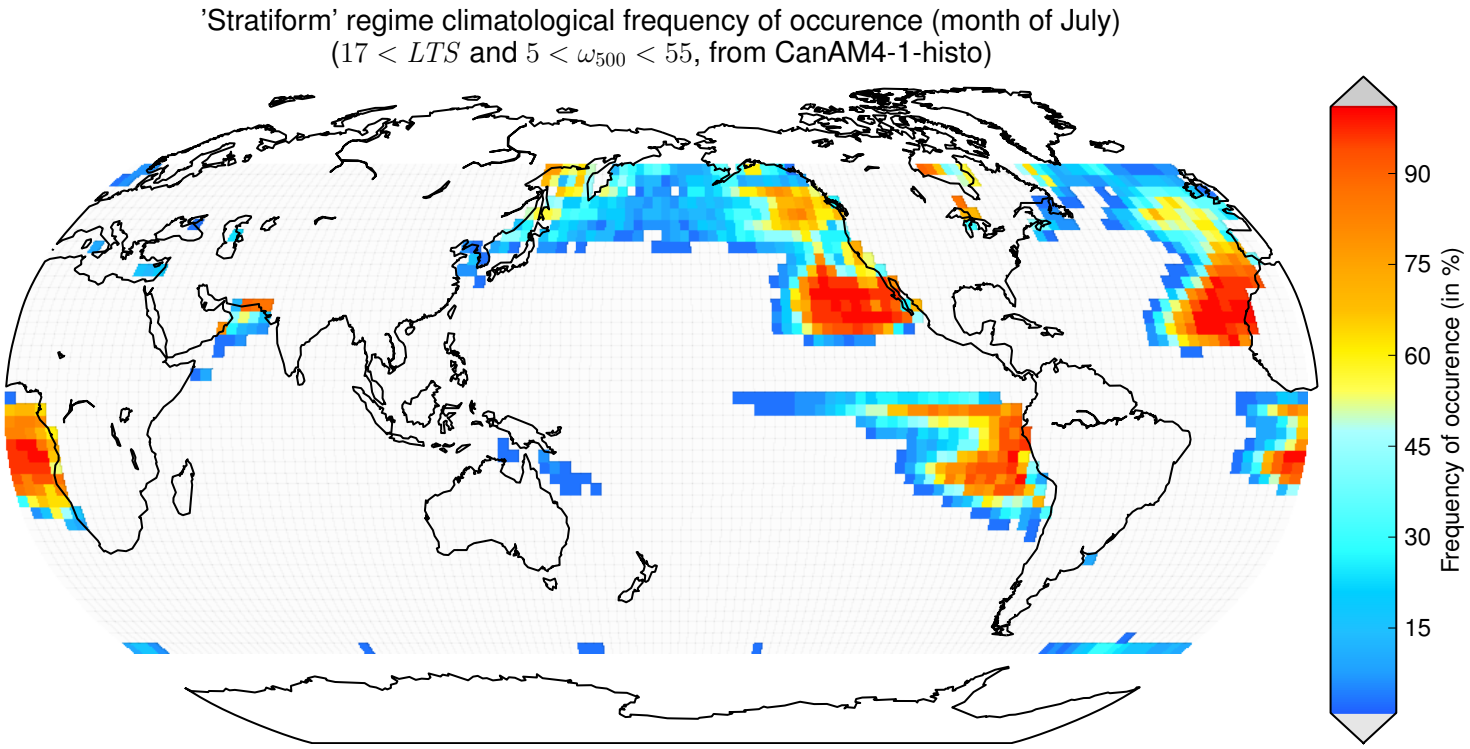

Figure 6.9: Relative occurrence of the stratiform cloud regime (July). As in Figure 6.8, but data span from January 1980 to December 2009. Note that this is the *July* climatological average frequency of occurrence. CanAM-4.1, as well as AGCM-3 (not shown), reproduce well all of the (summer) "10 stratus regions" described in Figure 2.4 (page 38). (The Chinese and Australian regions are missing since this is for July. Arctic and Circumpolar are not plotted.)

6.5.3 Storm track

Figure 6.11a clearly shows two low cloud regimes, i.e. one more than in Figures 6.8a and 6.11b. This distinct regime is called the "Storm track" or "Circumpolar ocean" region as in Figure 2.4 (page 38). CanAM-4.1, as well as AGCM-3 (not shown), reproduce very well this low cloud region (Figure 6.12).

As said in Figure 6.1, as well as shown in Figures 6.11b and 6.10, this is the main (if not only) difference between 2D-histograms based on LTS versus EIS. Figure 6.11b, which is Figure 6.11a using EIS rather than LTS, look much more like Figure 6.8a or 6.3a.

One could speculate on both advantages and drawbacks of using LTS rather than EIS, i.e. having two versus one low cloud regimes. On one hand, two regimes would mean that there is an intrinsic difference (making the description or parametrization richer). On the other hand, one regime would mean a unique treatment of all low clouds (making the description or parametrization easier, and maybe more relevant).

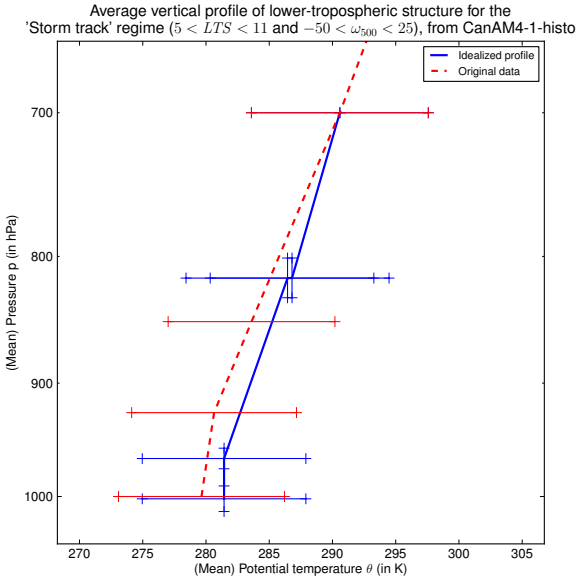

Figure 6.10: Composite vertical profile for the storm track cloud regime. EIS composite average is close to zero, in contrasts with the other low cloud regime (Figure 6.8b). Data span from January 1980 to December 2009 and cover the 60°S–60°N band.

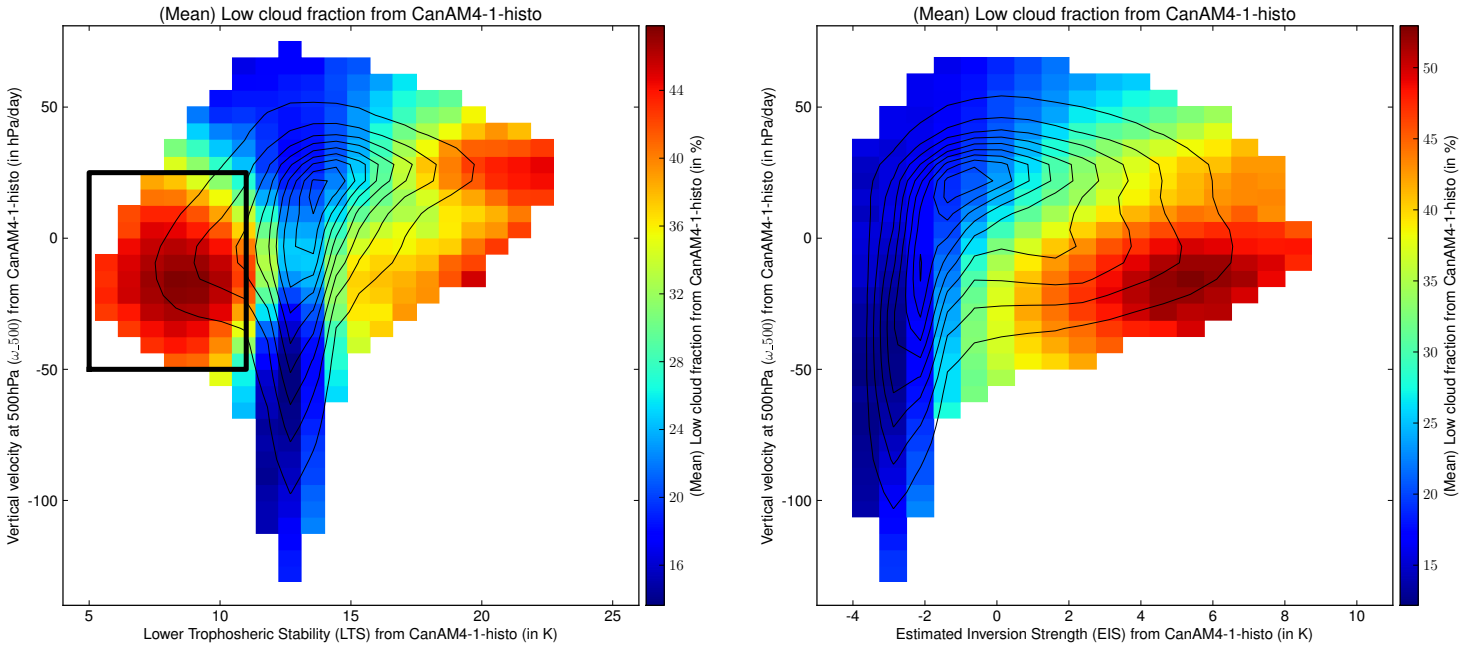

(a) Regime outline (using LTS)

(b) Regime outline (using EIS)

Figure 6.11: The storm track cloud regime: 2D-histograms. As in Figure 6.10.

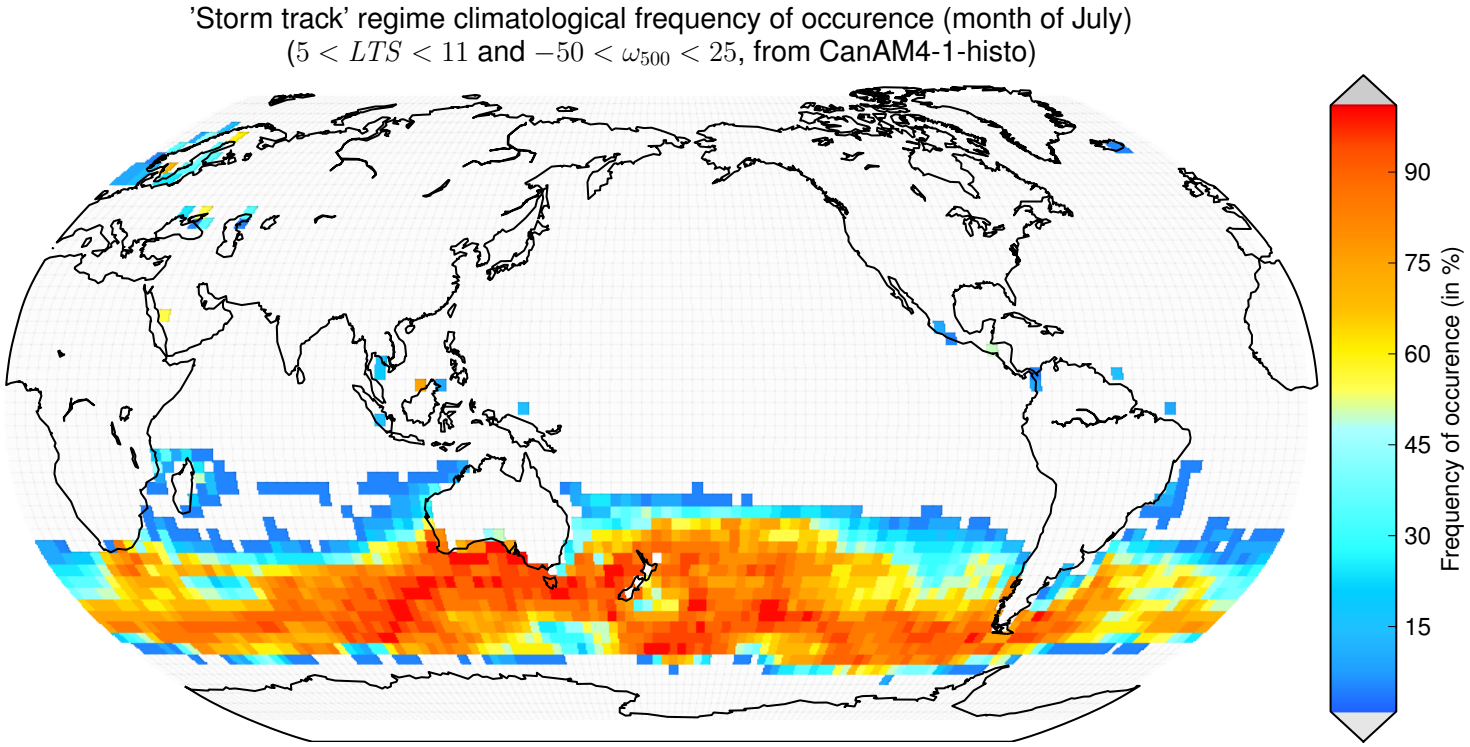

Figure 6.12: Relative occurrence of the storm track cloud regime (July). As in Figure 6.11, but data span from January 1990 to December 2009. Note that this is the *July* climatological average frequency of occurrence.

Conclusions

Research objectives

The role of (low) clouds in our understanding of the climate system and in our capacity to produce reliable and accurate climate projections was reviewed in the first two chapters ("Clouds and climate" and "Stability, dynamics, and clouds"). At the same time, research questions were developed, and then summarized in sections 1.3 and 2.5. Each objective is now answered.

1. How meaningful is a comparison between AGCM-3 and CanAM-4.1, relative to observations (or re-analyses)?

Despite using only one observational dataset when simultaneously comparing CanAM-4.1 and AGCM-3 to observations, this analysis is relevant. Indeed, the variability between observations is systematically (much) smaller than between observations and models (or re-analyses). Correlations are usually larger than 90% or even 95% between observations, whereas model correlations typically range from 50% to 75%. As a result, the validity of an observational "reference", relative to simulations, is demonstrated.

2. How well does CanAM-4.1's simulated (low) cloud field agree with observational data?

Although discrepancy between mean values (or standard deviations) may seem important, CanAM-4.1 simulations still somewhat agrees with observations. The relative difference of means is typically under 20% for cloud fractions or precipitation, and under 5% for radiative

fluxes. Moreover, distributions (i.e. PDF shapes) support this statement. Note that ERA-Interim agrees particularly well with observations, despite significantly overestimating high latitudes low cloud fractions.

3. How well CanAM-4.1 reproduces (low) cloud regimes?

Two low cloud regimes (stratiform and storm track) and one high cloud regime (convectiform) simulations are very realistically simulated by CanAM-4.1. Considering the good but less than perfect agreement between CanAM-4.1 and observations (i.e. ISCCP or MODIS), the reproduction accuracy of these regimes is surprising. Remark: AGCM-3, ERA-40, and ERA-Interim also reproduce well (low) cloud regimes.

4. Does CanAM-4.1 perform better than AGCM-3 when simulating (low) clouds?

CanAM-4.1 is consistently better than (or equivalent to) its predecessor AGCM-3 when compared to observations. The changes implemented between AGCM-3, CanAM-4.0, and CanAM-4.1 make a visible and quantifiable difference. Indeed, improvements in mean, standard deviation, correlation, RMSD, or PDFs shape can range anywhere from 1% to almost 18% (e.g. for low clouds). Note that ERA-Interim is also consistently better than (or equivalent to) its predecessor ERA-40 when compared to observations.

5. How much does CanAM-4.1's *ISCCP-simulated* (low) cloud field improve relative to its raw output?

For low clouds, the post-COSP field (almost) always improves (up to 14.4%), with regards to mean, standard deviation, correlation, or RMSD. It is also clear that the simulator improve the dynamical and thermodynamical consideration of low clouds. Surprisingly, positive effects are less noticeable (if any) when simulating high clouds.

6. How meaningful is a stability and large-scale circulation compositing comparison between observations and simulations (or re-analyses)?

The stability and large-scale circulation compositing comparison is a robust and relevant method that provides new information (relative to a local, geographical, point-by-point comparison). Although variable choices typically do not affect the main conclusions, it is important to understand the underlying reasons for this. Strong relationships (or correlations) exist in all datasets, but more particularly in observations.

7. How predictable are (low) clouds actually with respect to LTS, EIS, and ω_{500} ?

This analysis provides more examples that, on average, stability is a reliable predictor, while large-scale circulation is also a predictor for high clouds and precipitation. The predictability capacity of stability is slightly greater when EIS is used (rather than LTS). Although most of the analysis results do not depend on using LTS rather than EIS, the "Storm track" or "Circumpolar ocean" low cloud regime is a noticeable exception. Here, LTS predicts a regime distinct from the stratiform cloud regime, whereas EIS does not distinguish stratiform and storm track regimes.

8. How well do GCMs (or re-analyses) reproduce the predictability of (low) clouds by LTS, EIS, and ω_{500} ?

GCMs (both AGCM-3 and CanAM-4.1) have the observed stability and large-scale circulation structure, but not its observed range. Indeed models, unlike the best re-analyses, tend to significantly underestimate low cloud fractions. Note that ERA-Interim reproduces this structure particularly well.

Future developments

Challenging assumptions

During this research, assumptions (or choices) were made. Working at freeing the analysis from these limitations could be a direction.

In particular, I would repeat the analysis with a more consistent set of data (regridding, post-processing, etc.). I would also repeat it with *daily data*, in order to uncover if the monthly-averaged stability-circulation-low cloud structure exists at this time scale.

Deepening current results

The LTS/EIS treatments of the storm track regime deserve more work.

The addition of new datasets could only strengthen the analysis. Especially new COSP-simulated fields (e.g. from AGCM-3 or ERA-40, towards MODIS or MISR).

Focusing also on mid-elevation clouds and total cloud fraction would bring a more complete viewpoint (and take more into account mis-attribution of clouds, as well as decorrelation length parametrization).

Quantifying the results yielded by the qualitative analysis, using another skill score (than RMSD) in Taylor diagrams, as well as focusing on anomalies would make inter-study comparisons possible and easier. Finally, evaluating the 2D-histogram identification of cloud regimes with regards to identification schemes or statistics from observations.

Widening the scope

Other predictors or proxies could be tested (e.g. CGLMSE).

The geographical extent of the stability and large-scale circulation structure should be investigated. In particular, testing more extensively differences between: land/ocean, different latitudes, and different "stratus regions".

Also, analysis could be performed with SCM simulations or GCMs high resolution outputs of at specific locations.

Focus could be given to cloud-climate feedback if comparing equilibrium and +4K perturbation runs.

References

Adler, R. F., et al., 2003: The version-2 global precipitation climatology project (GPCP) monthly precipitation analysis (1979-present). *Journal of Hydrometeorology*, **4 (6)**, 1147–1167, doi:{10.1175/1525-7541(2003)004⟨1147:TVGPCP⟩2.0.CO;2}.

Albrecht, B. A., A. K. Betts, W. H. Schubert, and S. K. Cox, 1979: Model of the thermodynamic structure of the trade-wind boundary-layer .1. theoretical formulation and sensitivity tests. *Journal of the Atmospheric Sciences*, **36 (1)**, 73–89.

Albrecht, B. A., C. S. Bretherton, D. H. Johnson, W. H. Scubert, and A. S. Frisch, 1995: The atlantic stratocumulus transition experiment - ASTEX. *Bulletin of the American Meteorological Society*, **76 (6)**, 889–904.

Allan, R. P., M. A. Ringer, J. A. Pamment, and A. Slingo, 2004: Simulation of the Earth's radiation budget by the European Centre for Medium-range Weather Forecasts 40-year reanalysis (era40). *Journal of Geophysical Research-Atmospheres*, **109 (D18)**, doi:{10.1029/2004JD004816}.

Anthes, R. A., 1977: A cumulus parametrization scheme utilizing a one-dimensional cloud model. *Monthly Weather Review*, **105**, 270–286.

Berrisford, P., D. P. Dee, K. Fielding, M. Fuentes, P. W. Kållberg, S. Kobayashi, and S. M. Uppala, 2009: The ERA-Interim Archive. *ECMWF Re-analysis Project Report Series 1*.

Betts, A. K. and W. Ridgway, 1988: Coupling of the radiative, convective, and surface fluxes over the equatorial Pacific. *Journal of the Atmospheric Sciences*, **45 (3)**, 522–536.

Bodas-Salcedo, A., et al., 2011: COSP: satellite simulation software for model assessment. *Bulletin of the American Meteorological Society*, **to appear** (), , doi: {10.1175/2011BAMS2856.1}.

Bony, S. and J.-L. Dufresne, 2005: Marine boundary layer clouds at the heart of tropical cloud feedback uncertainties in climate models. *Geophysical Research Letters*, **32 (20)**, doi:{10.1029/2005GL023851}.

Bony, S., J.-L. Dufresne, H. Le Treut, J. J. Morcrette, and C. A. Senior, 2004: On dynamic and thermodynamic components of cloud changes. *Climate Dynamics*, **22 (2-3)**, 71–86, doi:{10.1007/s00382-003-0369-6}.

Bony, S., K. M. Lau, and Y. C. Sud, 1997: Sea surface temperature and large-scale circulation influences on tropical greenhouse effect and cloud radiative forcing. *Journal of Climate*, **10 (8)**, 2055–2077.

Bretherton, C. S., et al., 2004: The EPIC 2001 stratocumulus study. *Bulletin of the American Meteorological Society*, **85 (7)**, 967+, doi:{10.1175/BAMS-85-7-967}.

Cash, B. A., E. K. Schneider, and L. Bengtsson, 2007: Origin of climate sensitivity differences: Role of selected radiative processes in two GCMs. *Tellus Series A-Dynamic Meteorology And Oceanography*, **59 (2)**, 155–169, doi:{10.1111/j.1600-0870.2006.00224.x}.

Cess, R. D., et al., 1989: Interpretation of cloud-climate feedback as produced by 14 atmospheric general-circulation models. *Science*, **245 (4917)**, 513–516.

Cess, R. D., et al., 1990: Intercomparison and interpretation of climate feedback processes in 19 atmospheric general-circulation models. *Journal of Geophysical Research-Atmospheres*, **95 (D10)**, 16 601–16 615.

Charlock, T. P. and V. Ramanathan, 1985: The albedo field and cloud radiative forcing produced by a general-circulation model with internally generated cloud optics. *Journal of the Atmospheric Sciences*, **42 (13)**, 1408–1429, doi:{}.

Cole, J., H. W. Barker, N. G. Loeb, and K. von Salzen, 2011: Assessing simulated clouds and radiative fluxes using properties of clouds whose tops are exposed to space. *Journal of Climate*, **24 (11)**, 2715–2727, doi:{10.1175/2011JCLI3652.1}.

Cotton, W. R. and R. A. Anthes, 1997: *Storm and cloud dynamics*. 2d ed., Volume 44 of International Geophysics Series, Academic Press, 883 pp.

Covey, C., K. M. AchutaRao, U. Cubasch, P. Jones, S. J. Lambert, M. E. Mann, T. J. P. K. E, and Taylor, 2003: An overview of results from the Coupled Model Intercomparison Project. *Global and Planetary Change*, **37 (1-2)**, 103–133, doi:{10.1016/S0921-8181(02)00193-5}.

Dee, D. P., et al., 2011: The ERA-Interim reanalysis: Configuration and performance of the data assimilation system. *Quarterly Journal of the Royal Meteorological Society*, **137 (656, Part a)**, 553–597, doi:{10.1002/qj.828}.

Fu, R., A. D. del Genio, W. B. Rossow, and W. Liu, 1992: Cirrus-cloud thermostat for tropical sea-surface temperatures tested using satellite data. *Nature*, **358 (6385)**, 394–397, doi:{10.1038/358394a0}.

Gates, W. L., et al., 1999: An overview of the results of the Atmospheric Model Intercomparison Project (AMIP I). *Bulletin of the American Meteorological Society*, **80 (1)**, 29–55, doi:{10.1175/1520-0477(1999)080⟨0029:AOOTRO⟩2.0.CO;2}.

Gibson, J. K., P. W. Kållberg, S. M. Uppala, A. Hernandez, A. Nomura, and E. Serrano, 1997: ERA description. *ECMWF Re-analysis Project Report Series 1*.

Gleckler, P. J., K. E. Taylor, and C. Doutriaux, 2008: Performance metrics for climate models. *Journal of Geophysical Research-Atmospheres*, **113 (D6)**, doi:{10.1029/2007JD008972}.

Gordon, N. D., J. R. Norris, C. P. Weaver, and S. A. Klein, 2005: Cluster analysis of cloud regimes and characteristic dynamics of midlatitude synoptic systems in observations and a model. *Journal of Geophysical Research-Atmospheres*, **110 (D15)**, doi:{10.1029/2004JD005027}.

Graham, N. E. and T. P. Barnett, 1987: Observations of sea surface temperature and convection over tropical oceans. *Science*, **238 (4)**, 657–659, doi:{10.1126/science.238.4827.657}.

Hallberg, R. and A. K. Inamdar, 1993: Observations of seasonal-variations in atmospheric greenhouse trapping and its enhancement at high sea-surface temperature. *Journal of Climate*, **6 (5)**, 920–931.

Hanson, H. P., 1991: Marine Stratocumulus Climatologies. *International Journal of Climatology*, **11 (1)**, 147–164, doi:{}.

Harrison, E. F., P. Minnis, B. R. Barkstrom, V. Ramanathan, R. D. Cess, and G. G. Gibson, 1990: Seasonal-variation of cloud radiative forcing derived from the Earth Radiation Budget experiment. *Journal of Geophysical Research-Atmospheres*, **95 (D11)**, 18 687–18 703.

Hartmann, D. L. and M. L. Michelsen, 1993: Large-scale effects on the regulation of tropical sea-surface temperature. *Journal of Climate*, **6 (11)**, 2049–2062, doi:{10.1175/1520-0442(1993)006⟨2049:LSEOTR⟩2.0.CO;2}.

Hartmann, D. L., M. E. Ockertbell, and M. L. Michelsen, 1992: The effect of cloud type on Earths energy-balance - Global analysis. *Journal of Climate*, **5 (11)**, 1281–1304.

Hawkins, E. and R. Sutton, 2009: The potential to narrow uncertainty in regional climate predictions. *Bulletin of the American Meteorological Society*, **90 (8)**, 1095+, doi:{10.1175/2009BAMS2607.1}.

Houghton, J. T., Y. Ding, D. J. Griggs, M. Noguer, P. van der Linden, X. Dai, K. Maskell, and C. I. Johnson, 2001: *Climate Change 2001: The Scientific Basis. Contribution of Working Group I to the Third Assessment Report of the Intergovernmental Panel on Climate Change*. , Cambridge University Press, Cambridge, United Kingdom and New York, NY, USA, 881 pp.

Houghton, J. T., G. J. Jenkins, J. J. Ephraums, and Intergovernmental Panel on Climate Change, 1990: *Climate change: the IPCC scientific assessment*. Reprint, illustrated ed., Cambridge University Press, 364 pp.

Houghton, J. T., L. G. Meira Filho, B. A. Callander, N. Harris, A. Kattenberg, and K. Maskell, 1996: *Climate Change 1995: The Science of Climate Change, Contribution of Working Group I to the second assessment report of the Intergovernmental Panel on Climate Change*. , Cambridge University Press, New York, 572 pp.

Huffman, G. J., R. F. Adler, M. M. Morrissey, D. T. Bolvin, S. Curtis, R. Joyce, B. Mcgavock, and J. Susskind, 2001: Global precipitation at one-degree daily resolution from multisatellite observations. *Journal of Hydrometeorology*, **2 (1)**, 36–50, doi:{10.1175/1525-7541(2001)002⟨0036:GPAODD⟩2.0.CO;2}.

Huffman, G. J., et al., 1997: The global precipitation climatology project (GPCP) combined precipitation dataset. *Bulletin of the American Meteorological Society*, **78 (1)**, 5–20, doi:{10.1175/1520-0477(1997)078⟨0005:TGPCPG⟩2.0.CO;2}.

Jakob, C. and G. Tselioudis, 2003: Objective identification of cloud regimes in the tropical western Pacific. *Geophysical Research Letters*, **30 (21)**, doi:{10.1029/2003GL018367}.

Kawai, H. and J. Teixeira, 2010: Probability density functions of liquid water path and cloud amount of marine boundary layer clouds: Geographical and seasonal variations and controlling meteorological factors. *Journal of Climate*, **23 (8)**, 2079–2092, doi:{10.1175/2009JCLI3070.1}.

Khairoutdinov, M. F. and D. A. Randall, 2003: Cloud resolving modeling of the ARM summer 1997 IOP: Model formulation, results, uncertainties, and sensitivities. *Journal of the Atmospheric Sciences*, **60 (4)**, 607–625, doi:{10.1175/1520-0469(2003)060⟨0607:CRMOTA⟩2.0.CO;2}.

Khouider, B., J. A. Biello, and A. J. Majda, 2010: A stochastic multicloud model for tropical convection. *Communications in Mathematical Sciences*, **8 (1)**, 187–216.

Klein, S. A., 1997: Synoptic variability of low-cloud properties and meteorological parameters in the subtropical trade wind boundary layer. *Journal of Climate*, **10 (8)**, 2018–2039, doi:{10.1175/1520-0442(1997)010⟨2018:SVOLCP⟩2.0.CO;2}.

Klein, S. A. and D. L. Hartmann, 1993: The seasonal cycle of low stratiform clouds. *Journal of Climate*, **6 (8)**, 1587–1606.

Klein, S. A. and C. Jakob, 1999: Validation and sensitivities of frontal clouds simulated by the ECMWF model. *Monthly Weather Review*, **127 (10)**, 2514–2531.

Kondratyev, K. Y., 1973: *Radiation Characteristics of the Atmosphere and the Earth's Surface (Radiatsionnye Kharaketeristiki Atmosfery i Zemnoi Poverkhnosti)*. Translated from russian ed., TT 71-58003 – NASA TT F-678 – Category 13, Published for NASA and the National Science Foundation, Washington, DC USA, Amerind Publishing Company Pvt. Limited, New Delhi, India, 580 pp.

Larson, K., D. L. Hartmann, and S. A. Klein, 1999: The role of clouds, water vapor, circulation, and boundary layer structure in the sensitivity of the tropical climate. *Journal of Climate*, **12 (8, Part 1)**, 2359–2374.

Lau, K. M., C. H. Sui, M. D. Chou, and W.-K. Tao, 1994: An inquiry into the cirrus-cloud thermostat effect for tropical sea-surface temperature. *Geophysical Research Letters*, **21 (12)**, 1157–1160.

Lilly, D. K., 1968: Models of cloud-topped mixed layers under a strong inversion. *Quarterly Journal of the Royal Meteorological Society*, **94 (401)**, 292–&.

Lindzen, R. S. and S. Nigam, 1987: On the role of sea-surface temperature-gradients in forcing low-level winds and convergence in the tropics. *Journal of the Atmospheric Sciences*, **44 (17)**, 2418–2436.

Loeb, N. G., S. Kato, W. Su, T. Wong, F. G. Rose, and D. R. Doelling, 2011: Advances in understanding top-of-atmosphere radiation variability from satellite observations. *Surveys in Geophysics*, (submitted).

Loeb, N. G., W. Sun, W. F. Miller, K. Loukachine, and R. Davies, 2006: Fusion of CERES, MISR, and MODIS measurements for top-of-atmosphere radiative flux validation. *Journal of Geophysical Research-Atmospheres*, **111 (D18)**, doi:{10.1029/2006JD007146}.

Loeb, N. G., B. A. Wielicki, D. R. Doelling, G. L. Smith, D. F. Keyes, S. Kato, N. Manalo-Smith, and T. Wong, 2009: Toward optimal closure of the Earth's top-of-atmosphere radiation budget. *Journal of Climate*, **22 (3)**, 748–766, doi:{10.1175/2008JCLI2637.1}.

Manabe, S. and R. F. Strickler, 1964: Thermal equilibrium of the atmosphere with a convective adjustment. *Journal of the Atmospheric Sciences*, **21 (4)**, 361–385.

Manabe, S. and R. T. Wetherald, 1967: Thermal equilibrium of atmosphere with a given distribution of relative humidity. *Journal of the Atmospheric Sciences*, **24 (3)**, 241–&.

McAvaney, B. J. and H. Le Treut, 2003: The Cloud Feedback Model Intercomparison Project (CFMIP). *CLIVAR Exchanges – supplementary contributions*.

McFarlane, N. A., J. F. Scinocca, M. Lazare, R. Harvey, D. L. Verseghy, and J. Li, 2005: The CCCma third generation atmospheric general circulation model. *CCCma Internal Report*, 25.

Medeiros, B. and B. Stevens, 2011: Revealing differences in GCM representations of low clouds. *Climate Dynamics*, **36 (1-2)**, 385–399, doi:{10.1007/s00382-009-0694-5}.

Miller, R. L., 1997: Tropical thermostats and low cloud cover. *Journal of Climate*, **10 (3)**, 409–440.

Moeng, C. H., 1986: Large-eddy simulation of a stratus-topped boundary-layer .1. structure and budgets. *Journal of the Atmospheric Sciences*, **43 (23)**, 2886–2900.

Murphy, J. M., D. M. H. Sexton, D. N. Barnett, G. S. Jones, M. J. Webb, and M. Collins, 2004: Quantification of modelling uncertainties in a large ensemble of climate change simulations. *Nature*, **430 (7001)**, 768–772, doi:{10.1038/nature02771}.

Neiburger, M., D. S. Johnson, and C. W. Chien, 1961: *Studies of the structure of the atmosphere over the Eastern Pacific Ocean. I: the inversion over the Eastern North Pacific Ocean*. University of California Publications in Meteorology, University of California Press, 94 pp.

Norris, J. R., 1998: Low cloud type over the ocean from surface observations. Part I: Relationship to surface meteorology and the vertical distribution of temperature and moisture. *Journal of Climate*, **11 (3)**, 369–382, doi:{10.1175/1520-0442(1998)011⟨0369:LCTOTO⟩2.0.CO;2}.

Norris, J. R. and C. B. Leovy, 1994: Interannual variability in stratiform cloudiness and sea-surface temperature. *Journal of Climate*, **7 (12)**, 1915–1925.

Norris, J. R. and C. P. Weaver, 2001: Improved techniques for evaluating GCM cloudiness applied to the NCAR ccm3. *Journal of Climate*, **14 (12)**, 2540–2550.

Oden, J. T. and S. Prudhomme, 2011: Control of modeling error in calibration and validation processes for predictive stochastic models. *International Journal for Numerical Methods in Engineering*, **87 (1-5, SI)**, 262–272, doi:{10.1002/nme.3038}.

Park, S., C. B. Leovy, and M. A. Rozendaal, 2004: A new heuristic lagrangian marine boundary layer cloud model. *Journal of the Atmospheric Sciences*, **61 (24)**, 3002–3024.

Pincus, R., C. P. Batstone, R. J. P. Hofmann, K. E. Taylor, and P. J. Glecker, 2008: Evaluating the present-day simulation of clouds, precipitation, and radiation in climate models. *Journal of Geophysical Research-Atmospheres*, **113 (D14)**, doi:{10.1029/2007JD009334}.

Prabhakara, C., G. Dalu, R. Lo, and N. Nath, 1979: Remote-sensing of seasonal distribution of precipitable water-vapor over the oceans and the inference of boundary-layer structure. *Monthly Weather Review*, **107 (10)**, 1388–1401, doi:{10.1175/1520-0493(1979)107⟨1388:RSOSDO⟩2.0.CO;2}.

Ramanathan, V., 1995: Clouds and climate. *Proceedings of the Koninklijke Nederlandse Akademie van Wetenschappen-Biological Chemical Geological Physical and Medical Sciences*, **98 (4)**, 361–383.

Ramanathan, V., R. D. Cess, E. F. Harrison, P. Minnis, B. R. Barkstrom, E. Ahmad, and D. L. Hartmann, 1989: Cloud-radiative forcing and climate - Results from the Earth Radiation Budget experiment. *Science*, **243 (4887)**, 57–63.

Ramanathan, V. and W. D. Collins, 1991: Thermodynamic regulation of ocean warming by cirrus clouds deduced from observations of the 1987 el-nino. *Nature*, **351 (6321)**, 27–32.

Ramanathan, V., W. D. Collins, and B. Subasilar, 1994: An inquiry into the cirrus-cloud thermostat effect for tropical sea-surface temperature - Comment. *Geophysical Research Letters*, **21 (12)**, 1185–1186.

Randall, D., et al., 2003: Confronting models with data - the gewex cloud systems study. *Bulletin of the American Meteorological Society*, **84 (4)**, 455–469, doi:{10.1175/BAMS-84-4-455}.

Randall, D. A., J. A. Coakley, C. W. Fairall, R. A. Kropfli, and D. H. Lenschow, 1984: Outlook for research on sub-tropical marine stratiform clouds. *Bulletin of the American Meteorological Society*, **65 (12)**, 1290–1301.

Randall, D. A. and B. A. Wielicki, 1997: Measurements, models, and hypotheses in the atmospheric sciences. *Bulletin of the American Meteorological Society*, **78 (3)**, 399–406, doi:{}.

Rasch, P. J. and J. E. Kristjansson, 1998: A comparison of the ccm3 model climate using diagnosed and predicted condensate parameterizations. *Journal of Climate*, **11 (7)**, 1587–1614.

Reichler, T. and J. Kim, 2008: How well do coupled models simulate today's climate? *Bulletin of the American Meteorological Society*, **89 (3)**, 303+, doi:{10.1175/BAMS-89-3-303}.

Riehl, H., T. C. Yeh, J. S. Malkus, and N. E. Laseur, 1951: The north-east trade of the Pacific ocean. *Quarterly Journal of the Royal Meteorological Society*, **77 (334)**, 598–626.

Ringer, M. A. and R. P. Allan, 2004: Evaluating climate model simulations of tropical cloud. *Tellus Series A-Dynamic Meteorology And Oceanography*, **56 (4)**, 308–327.

Ringer, M. A., et al., 2006: Global mean cloud feedbacks in idealized climate change experiments. *Geophysical Research Letters*, **33 (7)**, doi:{10.1029/2005GL025370}.

Roe, G. H., 2009: Feedbacks, timescales, and seeing red. *Annual Review of Earth and Planetary Sciences*, **37**, 93–115, doi:{10.1146/annurev.earth.061008.134734}.

Roe, G. H. and M. B. Baker, 2011: Comment on "another look at climate sensitivity" by zaliapin and ghil (2010). *Nonlinear Processes in Geophyics*, **18 (1)**, 125–127, doi:{10.5194/npg-18-125-2011}.

Rossow, W. B., L. Garder, P. J. Lu, and A. Walker, 1991: *International Satellite Cloud Climatology Project (ISCCP) Documentation of Cloud Data*. WMO/TD-No 266 (rev.), World Climate Research Programme, 76 pp.

Rossow, W. B. and R. A. Schiffer, 1991: ISCCP cloud data products. *Bulletin of the American Meteorological Society*, **72 (1)**, 2–20.

Rossow, W. B. and R. A. Schiffer, 1999: Advances in understanding clouds from ISCCP. *Bulletin of the American Meteorological Society*, **80 (11)**, 2261–2287.

Schiffer, R. A. and W. B. Rossow, 1983: The International-Satellite-Cloud-Climatology-Project (ISCCP) - The 1st project of the world-climate-research-programme. *Bulletin of the American Meteorological Society*, **64 (7)**, 779–784.

Schneider, T. and A. H. Sobel, 2007: *The thermal stratification of the extratropical troposphere in The Global Circulation of the Atmosphere*. in press ed., Princeton University Press, 47–77 pp.

Scinocca, J. F., N. A. McFarlane, M. Lazare, J. Li, and D. Plummer, 2008: Technical note: The CCCma third generation AGCM and its extension into the middle atmosphere. *Atmospheric Chemistry and Physics*, **8 (23)**, 7055–7074.

Senior, C. A., 1999: Comparison of mechanisms of cloud-climate feedbacks in GCMs. *Journal of Climate*, **12 (5, Part 2)**, 1480–1489.

Senior, C. A. and J. F. B. Mitchell, 1993: Carbon-dioxide and climate - The impact of cloud parameterization. *Journal of Climate*, **6 (3)**, 393–418.

Slingo, A., 1990: Sensitivity of the Earth's radiation budget to changes in low clouds. *Nature*, **343 (6253)**, 49–51.

Slingo, J. M., 1987: The development and verification of a cloud prediction scheme for the ECMWF model. *Quarterly Journal of the Royal Meteorological Society*, **113 (477)**, 899–927.

Sobel, A. H., J. Nilsson, and L. Polvani, 2001: The weak temperature gradient approximation and balanced tropical moisture waves. *Journal of the Atmospheric Sciences*, **58 (23)**, 3650–3665, doi:{10.1175/1520-0469(2001)058⟨3650:TWTGAA⟩2.0.CO;2}.

Soden, B. J. and I. M. Held, 2006: An assessment of climate feedbacks in coupled ocean-atmosphere models. *Journal of Climate*, **19 (23)**, 3354–3360.

Solomon, S., D. Qin, M. Manning, Z. Chen, M. Marquis, K. B. Averyt, M. Tignor, and H. L. Miller, 2007: *Climate change 2007: the physical science basis : contribution of Working Group I to the Fourth Assessment Report of the Intergovernmental Panel on Climate Change*. Reprint, illustrated ed., , Cambridge University Press, Cambridge, United Kingdom and New York, NY, USA, 996 pp.

Stephens, G. L., 1990: On the relationship between water-vapor over the oceans and sea-surface temperature. *Journal of Climate*, **3 (6)**, 634–645, doi:{10.1175/1520-0442(1990)003⟨0634:OTRBWV⟩2.0.CO;2}.

Stone, P. H. and J. H. Carlson, 1979: Atmospheric lapse rate regimes and their parameterization. *Journal of the Atmospheric Sciences*, **36 (3)**, 415–423, doi:{10.1175/1520-0469(1979)036⟨0415:ALRRAT⟩2.0.CO;2}.

Stull, R. B., 1988: *An introduction to boundary layer meteorology*. Springer, 670 pp.

Taylor, K. E., 2001: Summarizing multiple aspects of model performance in a single diagram. *Journal of Geophysical Research-Atmospheres*, **106 (D7)**, 7183–7192.

Trenberth, K. E., J. T. Fasullo, and J. T. Kiehl, 2009: Earth's global energy budget. *Bulletin of the American Meteorological Society*, **90 (3)**, 311–323, doi:{10.1175/2008BAMS2634.1}.

Tselioudis, G., Y. Zhang, and W. B. Rossow, 2000: Cloud and radiation variations associated with northern midlatitude low and high sea level pressure regimes. *Journal of Climate*, **13 (2)**, 312–327.

Uppala, S. M., D. P. Dee, S. Kobayashi, and A. J. Simmons, 2008: Evolution of reanalysis at ECMWF. *Proceedings of Third WCRP International Conference on Reanalysis, Tokyo, Japan*.

Uppala, S. M., et al., 2005: The ERA-40 re-analysis. *Quarterly Journal of the Royal Meteorological Society*, **131 (612, Part B)**, 2961–3012, doi:{10.1256/qj.04.176}.

von Ficker, H., 1936a: *Bemerkung uber den Warmeumsatz innerhalb der Passatzirkulation*. Reprint hardcover ed., Sitzungsberichten der preussischen Akademie der Wissenschaften, Phys. Math. Klasse, Vol 11, 102–104, de Gruyter, 14 pp.

von Ficker, H., 1936b: Die Passatinversion. *Veroffentlichungen Meteorologie Institut*, **1 (4)**, 33.

von Salzen, K., M. Lazare, J. Li, N. A. McFarlane, M. C. Reader, J. F. Scinocca, L. Solheim, and D. L. Verseghy, 2007: The climate and its sensitivity in simulations with the Canadian Centre for Climate Modelling and Analysis fourth generation Atmospheric Global Climate Model (CCCma AGCM4). Part I: Model description and climatology. *In preparation for Journal of Climate*.

Waliser, D. E., N. E. Graham, and C. Gautier, 1993: Comparison of the Highly Reflective Cloud and Outgoing Longwave Radiation Datasets for Use in Estimating Tropical Deep Convection. *Journal of Climate*, **6 (2)**, 331–353, doi:{10.1175/1520-0442(1993)006⟨0331:COTHRC⟩2.0.CO;2}.

Wallace, J. M. and P. V. Hobbs, 2006: *Atmospheric science: An introductory survey*. 2d ed., Academic Press, San Diego, 504 pp.

Warren, S. G., C. J. Hahn, J. London, R. M. Chervin, and R. L. Jenne, 1986a: *Global distribution of total cover and cloud type amounts over land*. Volume 273 of NCAR technical note, National Center for Atmospheric Research, Boulder, CO, 29 pp.

Warren, S. G., C. J. Hahn, J. London, R. M. Chervin, and R. L. Jenne, 1986b: *Global distribution of total cover and cloud type amounts over the ocean*. Volume 317 of NCAR technical note, National Center for Atmospheric Research, Boulder, CO, 42 pp.

Weaver, C. P., W. D. Collins, and H. Grassl, 1994: Relationship between clear-sky atmospheric greenhouse-effect and deep convection during the central equatorial Pacific experiment - Model-calculations and satellite-observations. *Journal of Geophysical Research-Atmospheres*, **99 (D12)**, 25 891–25 901.

Weaver, C. P. and V. Ramanathan, 1997: Relationships between large-scale vertical velocity, static stability, and cloud radiative forcing over northern hemisphere extratropical oceans. *Journal of Climate*, **10 (11)**, 2871–2887.

Webb, M. J., C. A. Senior, S. Bony, and J. J. Morcrette, 2001: Combining ERBE and ISCCP data to assess clouds in the Hadley Centre, ECMWF and LMD atmospheric climate models. *Climate Dynamics*, **17 (12)**, 905–922.

Webb, M. J., et al., 2006: On the contribution of local feedback mechanisms to the range of climate sensitivity in two GCM ensembles. *Climate Dynamics*, **27 (1)**, 17–38, doi:{10.1007/s00382-006-0111-2}.

Wielicki, B. A., B. R. Barkstrom, E. F. Harrison, R. B. Lee, G. L. Smith, and J. E. Cooper, 1996: Clouds and the Earth's Radiant Energy System (CERES): An Earth observing system experiment. *Bulletin of the American Meteorological Society*, **77 (5)**, 853–868, doi:{10.1175/1520-0477(1996)077⟨0853:CATERE⟩2.0.CO;2}.

Williams, K. D., M. A. Ringer, and C. A. Senior, 2003: Evaluating the cloud response to climate change and current climate variability. *Climate Dynamics*, **20 (7-8)**, 705–721, doi:{10.1007/s00382-002-0303-3}.

Williams, K. D., C. A. Senior, and J. F. B. Mitchell, 2001: Transient climate change in the Hadley Centre models: The role of physical processes. *Journal of Climate*, **14 (12)**, 2659–2674.

Williams, K. D. and G. Tselioudis, 2007: GCM intercomparison of global cloud regimes: Present-day evaluation and climate change response. *Climate Dynamics*, **29 (2-3)**, 231–250, doi:{10.1007/s00382-007-0232-2}.

Williams, K. D. and M. J. Webb, 2009: A quantitative performance assessment of cloud regimes in climate models. *Climate Dynamics*, **33 (1)**, 141–157, doi:{10.1007/s00382-008-0443-1}.

Williams, K. D., et al., 2006: Evaluation of a component of the cloud response to climate change in an intercomparison of climate models. *Climate Dynamics*, **26 (2-3)**, 145–165, doi:{10.1007/s00382-005-0067-7}.

Wood, R. and C. S. Bretherton, 2004: Boundary layer depth, entrainment, and decoupling in the cloud-capped subtropical and tropical marine boundary layer. *Journal of Climate*, **17 (18)**, 3576–3588, doi:{10.1175/1520-0442(2004)017⟨3576:BLDEAD⟩2.0.CO;2}.

Wood, R. and C. S. Bretherton, 2006: On the relationship between stratiform low cloud cover and lower-tropospheric stability. *Journal of Climate*, **19 (24)**, 6425–6432.

Xie, P. and P. A. Arkin, 1997: Global precipitation: A 17-year monthly analysis based on gauge observations, satellite estimates, and numerical model outputs. *Bulletin of the American Meteorological Society*, **78**, 2539–2558.

Xie, P. P., J. E. Janowiak, P. A. Arkin, R. F. Adler, A. Gruber, R. Ferraro, G. J. Huffman, and S. Curtis, 2003: GPCP Pentad precipitation analyses: An experimental dataset based on gauge observations and satellite estimates. *Journal of Climate*, **16 (13)**, 2197–2214, doi:{10.1175/2769.1}.

Appendices

Appendix A

Datasets time overlaps

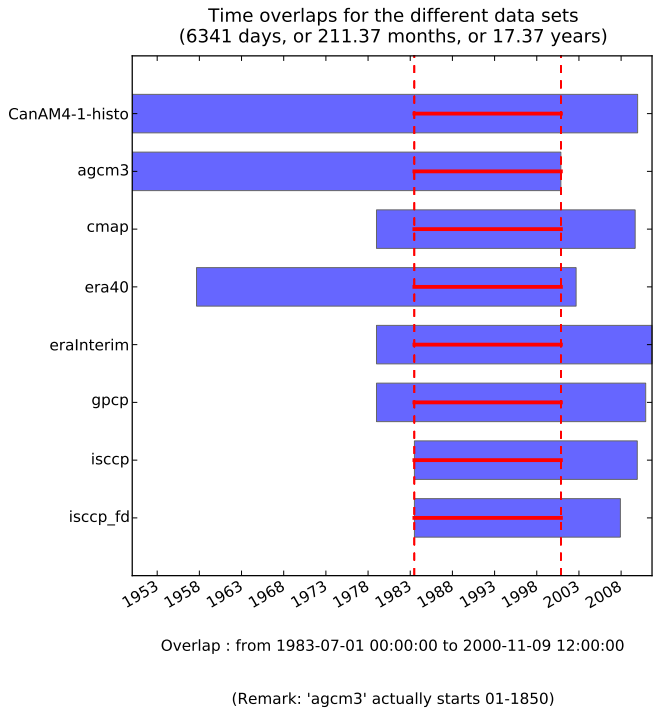

Figure A.1: Time coverages for datasets used in chapter 5. Epochs overlap ranges from July 1983 to November 2000 (or over 17 years) and includes: CanAM-4.1, AGCM-3, ERA-Interim, ERA-40, ISCCP, ISCCP-FD, GPCP, CMAP.

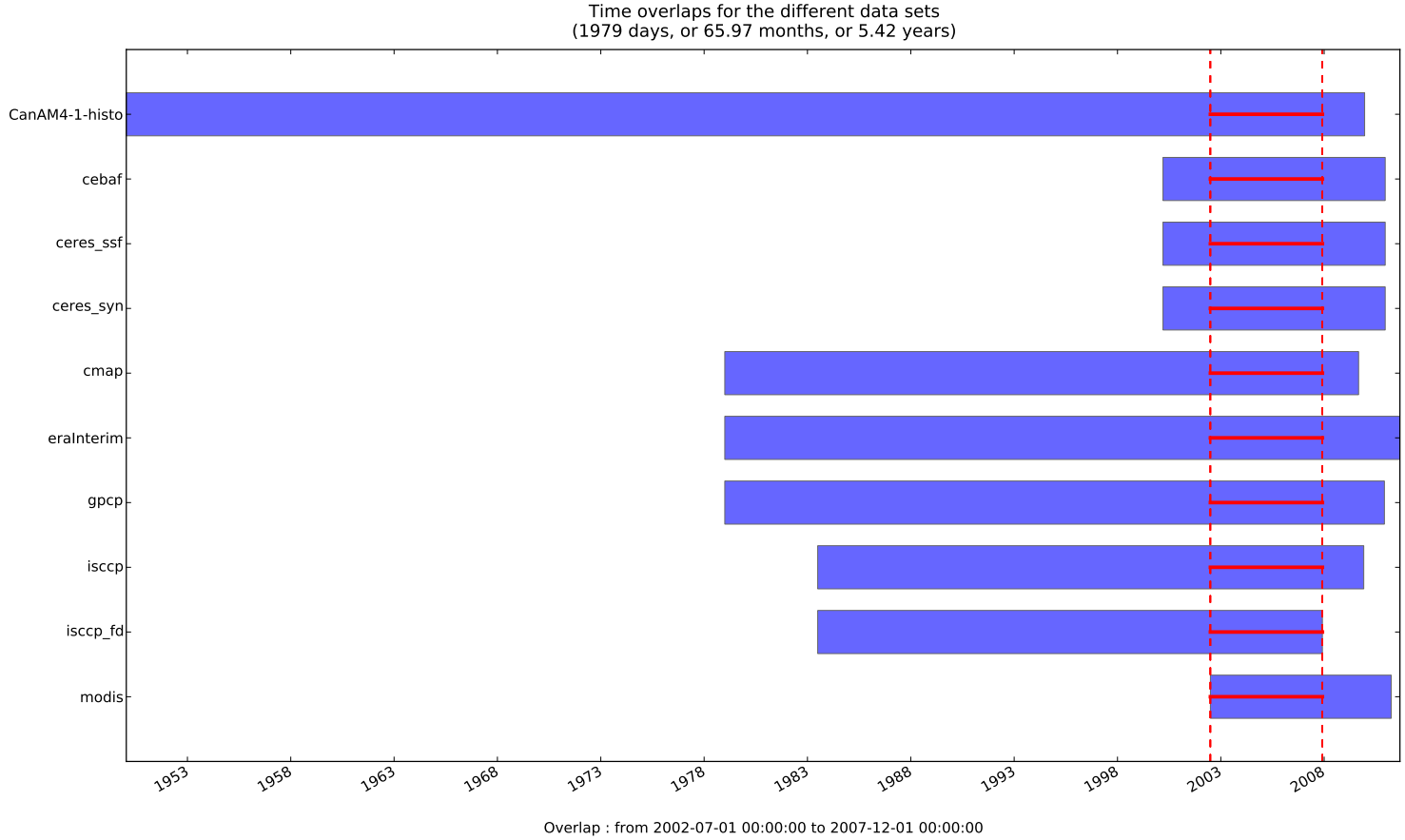

Figure A.2: Time coverages for datasets used in chapter 4. Epochs overlap ranges from July 2002 to December 2007 (or 5.5 years) and includes: CanAM-4.1, ERA-Interim, ISCCP, ISCCP-FD, MODIS, GPCP, CMAP, CERES, CEBAF.

Appendix B

Model-to-satellite approach

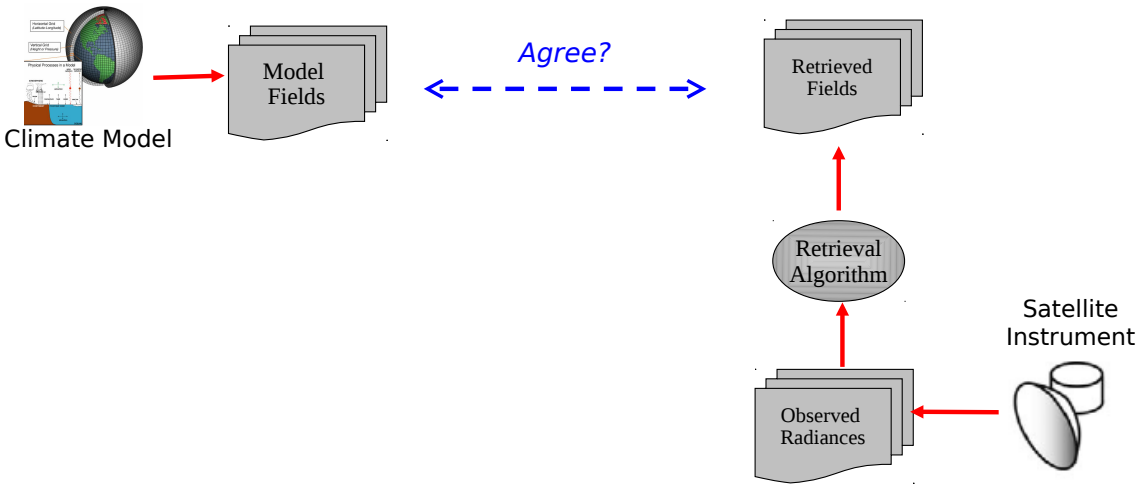

Figure B.1: Model-to-satellite approach, without a simulator. See figure Figure B.2 for the case with a simulator. From Klein S. A., "Using Satellite Simulators to Diagnose Cloud-Processes in CMIP5 Models"; December 9, 2011; American Geophysical Union Fall 2011 Meeting; San Francisco, California; `http://cfmip.metoffice.com/cosp/klein.agu11.talk.pdf`; by permission.

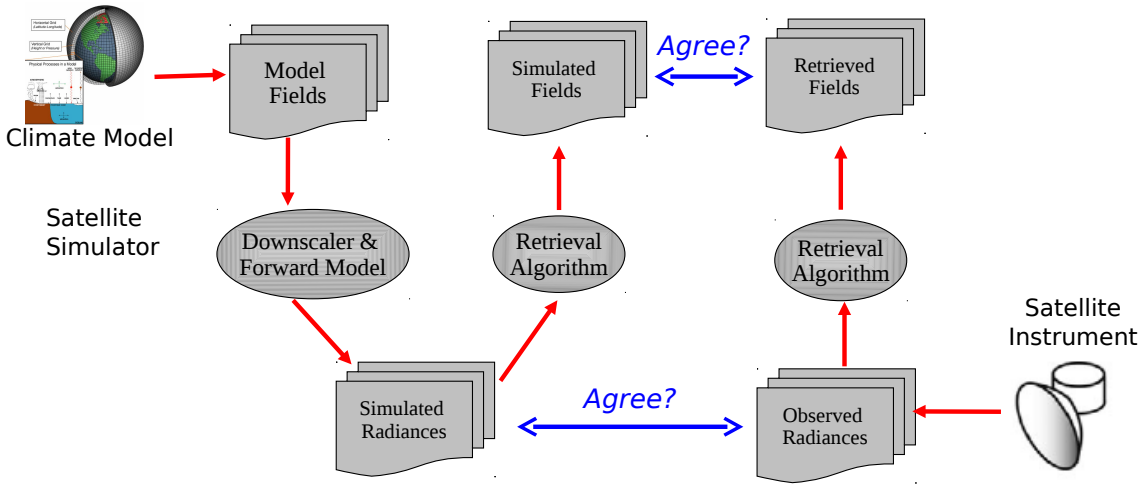

Figure B.2: Model-to-satellite approach, with a simulator. See figure Figure B.1 for the case without a simulator. Adding a (satellite) simulator makes one comparison like in Figure B.1 (blue dashed arrow) more relevant here (top blue arrow). It also makes another comparison (bottom blue arrow) possible. From Klein S. A., "Using Satellite Simulators to Diagnose Cloud-Processes in CMIP5 Models"; December 9, 2011; American Geophysical Union Fall 2011 Meeting; San Francisco, California; `http://cfmip.metoffice.com/cosp/klein.agu11.talk.pdf`; by permission.

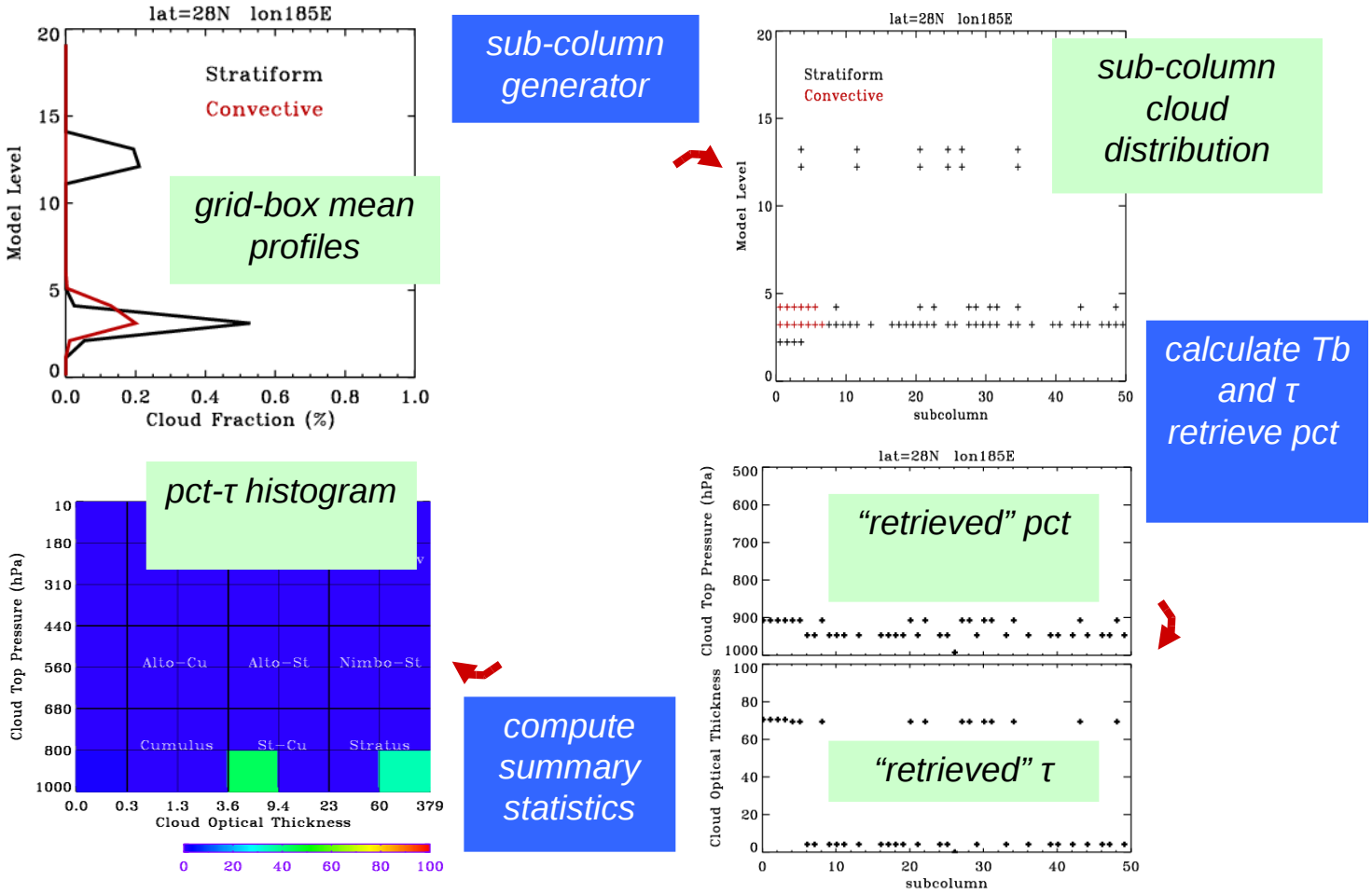

Figure B.3: Model-to-satellite approach, an example from the ISCCP simulator from COSP. From Klein S. A., "Using Satellite Simulators to Diagnose Cloud-Processes in CMIP5 Models"; December 9, 2011; American Geophysical Union Fall 2011 Meeting; San Francisco, California; `http://cfmip.metoffice.com/cosp/klein.agu11.talk.pdf`; by permission.

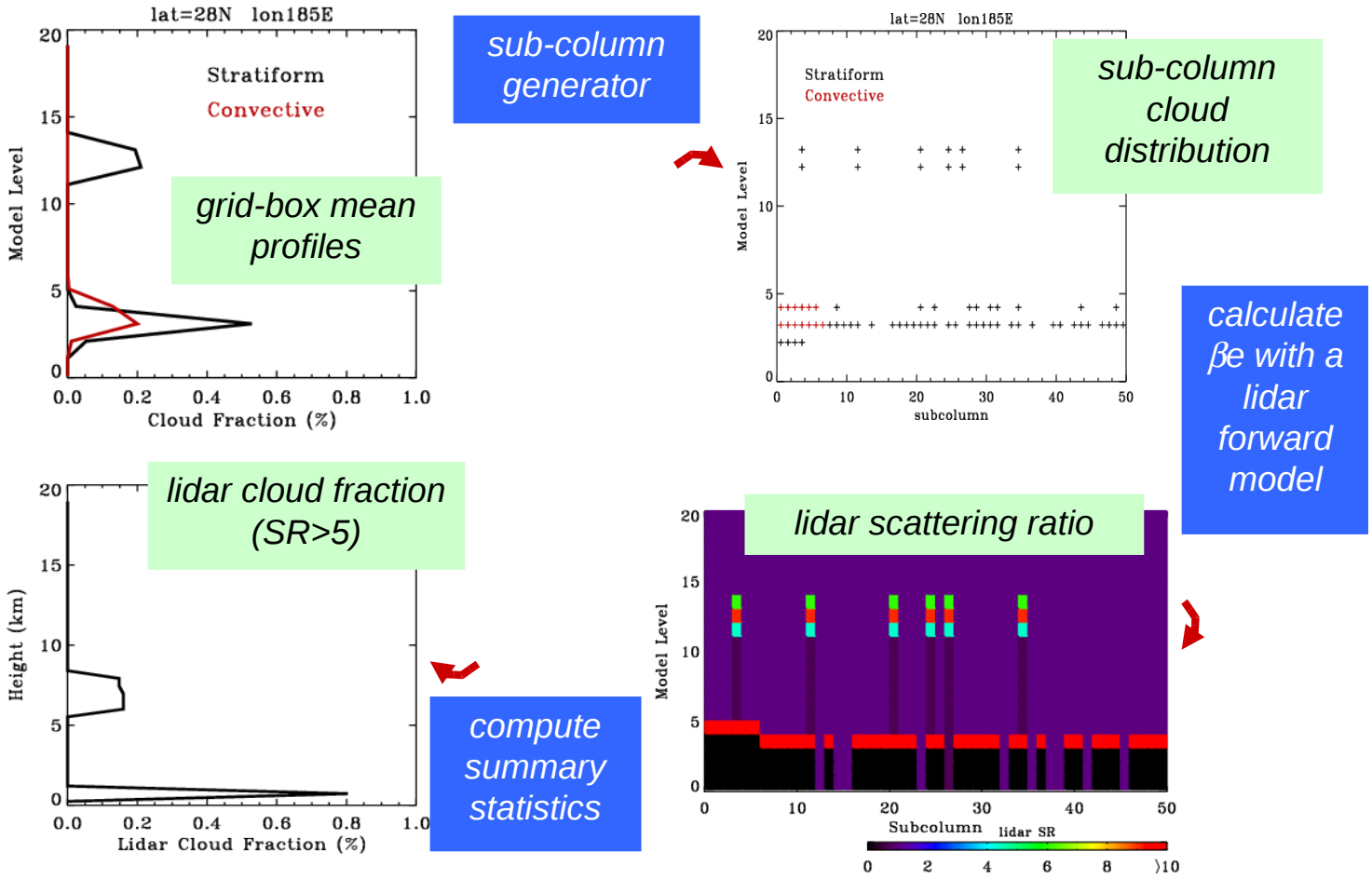

Figure B.4: Model-to-satellite approach, an example from the CALIPSO simulator from COSP. From Klein S. A., "Using Satellite Simulators to Diagnose Cloud-Processes in CMIP5 Models"; December 9, 2011; American Geophysical Union Fall 2011 Meeting; San Francisco, California; `http://cfmip.metoffice.com/cosp/klein.agu11.talk.pdf`; by permission.

Appendix C

Datasets details

Table C.1: All data sets used in this study. Twelve characteristics are detailed for each data set: Full Name, Time coverage (start–stop), Grid type (lon–lat), Interpolation (if any), Overarching project in which it took part, Fields used in this study, Source type, Hardware (model version or satellite type), File conversion (if any), References, and Internet sources.

Acronym	Characteristic	Value or description
ISCCP	Full Name	International Satellite Cloud Climatology Project (ISCCP)
	Time (start–stop)	07-1983 – 12-2009
	Grid (lon–lat)	144×72 (or $2.5^\circ \times 2.5^\circ$) Longitude: 1.25°W-358.75°W – Latitude: 88.75°S-88.75°N
	Interpolation	To the Canadian Centre for Climate Modelling and Analysis (CCCma) grid: simple bilinear interpolation done by me, and mean-preserving interpolation done by CCCma.
	Project	N/A
	Fields	Cloud properties ("ISCCP") and radiative fluxes (ISCCP Flux Data, or "ISCCP-FD")
	Source type	(Satellite) Observations
	Hardware	Most of the time, six satellites (four geostationary and two polar orbiters) were contributing at once to ISCCP; sometimes only four (minimum, three geostationary and one polar orbiter) or up to seven (maximum) satellites. These satellites mostly cover the spectrum from far-infrared to visible with numerous radiometers. See Table C.3 for a list of ISCCP contributing satellites.
	File conversion	N/A (already converted to NETwork Common Data Form (netCDF) format)
	References	Schiffer and Rossow (1983); Rossow et al. (1991); Rossow and Schiffer (1991, 1999)
	Internet sources	`http://isccp.giss.nasa.gov/`

Table C.1 continues on next page.

Table C.1 continued from previous page.

Acronym	Characteristic	Value or description
MODIS	Full Name	MODerate resolution Imaging Spectroradiometer (MODIS) Level 5 cloud product
	Time (start–stop)	07-2002 – 04-2011
	Grid (lon–lat)	360×180 (or $1.0^\circ \times 1.0^\circ$) Longitude: 179.50°E-179.50°W – Latitude: 89.50°S-89.50°N
	Interpolation	To the CCCma grid: simple bilinear interpolation done by me, and mean-preserving interpolation done by CCCma.
	Project	N/A
	Fields	Cloud properties
	Source type	(Satellite) Observations
	Hardware	MODIS is on board the Terra satellite ("Earth Observing System (EOS) AM") since 1999 and on board the Aqua satellite ("EOS PM") since 2002. Data used in this project is the combined products of these two instruments.
	File conversion	N/A (already converted to netCDF format)
	References	N/A
	Internet sources	`http://modis.gsfc.nasa.gov/` or `http://modis-atmos.gsfc.nasa.gov/MOD06_L2/index.html`

Table C.1 continues on next page.

Table C.1 continued from previous page.

Acronym	Characteristic	Value or description
GPCP	Full Name	Global Precipitation Climatology Project (GPCP)
	Time (start–stop)	01-1979 – 12-2010
	Grid (lon–lat)	144×72 (or $2.5° \times 2.5°$) Longitude: 1.25°W-358.75°W – Latitude: 88.75°S-88.75°N
	Interpolation	To the CCCma grid: simple bilinear interpolation done by me, and mean-preserving interpolation done by CCCma.
	Project	N/A
	Fields	Precipitation
	Source type	(Satellite and Station) Observations
	Hardware	Station (rain gauge) data are from over land. Satellite data are collected from several sources: the Defense Meteorological Satellite Program (DMSP) (United States, in sun-synchronous low-Earth orbits), the Television and InfraRed Observation Satellite (TIROS) Operational Vertical Sounder (TOVS), and various geostationary or polar-orbiting satellites operated by the United States, Europe, and Japan.
	File conversion	N/A (already converted to netCDF format)
	References	Huffman et al. (1997, 2001); Adler et al. (2003); Xie et al. (2003)
	Internet sources	`http://www.gewex.org/gpcp.html` or `http://precip.gsfc.nasa.gov/`

Table C.1 continues on next page.

Table C.1 continued from previous page.

Acronym	Characteristic	Value or description
CMAP	Full Name	Climate Prediction Center (CPC) Merged Analysis of Precipitation (CMAP)
	Time (start–stop)	01-1979 – 09-2009
	Grid (lon–lat)	144×72 (or $2.5° \times 2.5°$) Longitude: 1.25°W-358.75°W – Latitude: 88.75°S-88.75°N
	Interpolation	To the CCCma grid: simple bilinear interpolation done by me.
	Project	N/A
	Fields	Precipitation
	Source type	(Satellite) Observations ("CMAP"), plus the NCEP re-analysis ("CMAP Enhanced")
	Hardware	Data are collected from 5 kinds of satellites: GOES Precipitation Index (GPI), Outgoing Longwave Radiation (OLR)-based Precipitation Index (OPI), Special Sensor Microwave/Imager (SSM/I) scattering, SSM/I emission, and Microwave Sounding Unit (MSU). The enhanced file also includes blended National Centers for Environmental Prediction (NCEP) / National Center for Atmospheric Research (NCAR) Re-Analysis (NCEP/NCAR) precipitation values. (The other just includes the satellite estimates.)
	File conversion	N/A (already converted to netCDF format)
	References	Xie and Arkin (1997)
	Internet sources	`www.esrl.noaa.gov/psd/data/gridded/data.cmap.html`

Table C.1 continues on next page.

Table C.1 continued from previous page.

Acronym	Characteristic	Value or description
CERES	Full Name	Clouds and the Earth's Radiant Energy System (CERES)
	Time (start–stop)	03-2000 – 12-2010
	Grid (lon–lat)	360×180 (or $1.0° \times 1.0°$) Longitude: 0.50°W-359.50°W – Latitude: 89.50°S-89.50°N
	Interpolation	To the CCCma grid: simple bilinear interpolation done by me.
	Project	N/A
	Fields	Radiation (fluxes)
	Source type	(Satellite) Observations
	Hardware	The CERES instruments are present on three different EOS satellites: Terra, Aqua, and the Tropical Rainfall Measuring Mission (TRMM). See Table C.2 for a list of CERES contributing satellites. CERES fluxes are then adjusted into: "ceres_ssf", "ceres_syn", "ceres_ebaf" (see subsection 3.1.4).
	File conversion	N/A (already converted to netCDF format)
	References	CERES: Wielicki et al. (1996) CEBAF: Loeb et al. (2006, 2009, 2011)
	Internet sources	`http://ceres.larc.nasa.gov/` or `http://ceres.larc.nasa.gov/products.php?product=EBAF`

Table C.1 continues on next page.

Table C.1 continued from previous page.

Acronym	Characteristic	Value or description
ERA-40	Full Name	ECMWF 40 years Re-Analysis (ERA-40)
	Time (start–stop)	09-1957 – 09-2002
	Grid (lon–lat)	144×73 (or $2.5° \times 2.5°$) Longitude: 0.00°W-357.50°W – Latitude: 90.00°S-90.00°N
	Interpolation	To the CCCma grid: mean-preserving interpolation done by CCCma.
	Project	N/A
	Fields	All (cloud properties, precipitation, temperature, humidity, and radiation)
	Source type	Re-analysis output
	Hardware	Integration: T159L60 version of the Integrated Forecasting System (IFS). Data from: the Vertical Temperature Profile Radiometer (VTPR), the TOVS, the SSM/I, the European Remote-sensing Satellite (ERS) and the Advanced TIROS Operational Vertical Sounder (ATOVS), plus various field experiments such as the GARP Atlantic Tropical Experiment (GATE), First GARP Global Experiment (FGGE), ALPine EXperiment (ALPEX) or Tropical Oceans Global Atmosphere / Coupled Ocean-Atmosphere Response Experiment (TOGA-COARE).
	File conversion	Grib to netCDF format conversion done using the NCAR Command Language (NCL) grib2nc converter ("ncl_convert2nc"). Documentation: `http://www.ncl.ucar.edu/Document/Tools/ncl_convert2nc.shtml`
	References	Gibson et al. (1997); Allan et al. (2004); Uppala et al. (2005)
	Internet sources	`http://www.ecmwf.int/research/era/do/get/era-40`

Table C.1 continues on next page.

Table C.1 continued from previous page.

Acronym	Characteristic	Value or description
ERA-Interim	Full Name	ECMWF Interim Re-Analysis (ERA-Interim)
	Time (start–stop)	01-1979 – 09-2011
	Grid (lon–lat)	240×121 (or $1.5^\circ \times 1.5^\circ$) Longitude: 180.00°E-178.50°W – Latitude: 90.00°S-90.00°N
	Interpolation	To the CCCma grid: mean-preserving interpolation done by CCCma, and interpolation done by the European Centre for Medium-range Weather Forecasts (ECMWF) (at download time).
	Project	N/A
	Fields	All (cloud properties, temperature, humidity) (Precipitation and radiation not readily available)
	Source type	Re-analysis output
	Hardware	Like ERA-40, but with some differences. Integration: T255 horizontal resolution, new humidity analysis, and improved model physics as major changes. Additional data: new ERS altimeter wave-height dataset (European Space Agency (ESA)), reprocessed winds and clear-sky radiances (Meteosat-2, EUropean organisation for the exploitation of METeorological SATellites (EUMETSAT)), reprocessed Global Ozone Monitoring Experiment (GOME) data (ozone profiles, Rutherford Appleton Laboratory), to cite few major additions.
	File conversion	Grib to netCDF format conversion done using the NCL grib2nc converter ("ncl_convert2nc"). Documentation: `http://www.ncl.ucar.edu/Document/Tools/ncl_convert2nc.shtml`
	References	Uppala et al. (2008); Berrisford et al. (2009); Dee et al. (2011)
	Internet sources	`http://www.ecmwf.int/research/era/do/get/era-interim`

Table C.1 continues on next page.

Table C.1 continued from previous page.

Acronym	Characteristic	Value or description
AGCM-3	Full Name	CCCma third generation atmospheric GCM (AGCM-3)
	Time (start–stop)	01-1850 – 11-2000
	Grid (lon–lat)	128×64 (or $\approx 2.79^\circ \times 2.8125^\circ$) Longitude: 0.00°W-357.19°W – Latitude: 87.86°S-87.86°N Remark: the grid cell size slightly changes with latitude (min=2.767°, max=2.791°, mean=2.789°, std=0.004°) because it results from the projection of a spectral grid ("T63"), but is particularly constant in the 60°S-60°N domain (std $< 0.0001^\circ$)
	Interpolation	N/A
	Project	Model output prepared for the IPCC Fourth Assessment climate of the 20th Century experiment (20C3M). This integration started at the same point as the pre-industrial control run, and spans the period 1850 to 2000. GreenHouse Gas (GHG) concentrations are prescribed following observations and match the IPCC Special Report on Emission Scenarios (SRES) concentrations at year 1990.
	Fields	All (cloud properties, precipitation, temperature, humidity, and radiation)
	Source type	Model simulation
	Hardware	"CGCM3.1 (2004): atmosphere: AGCM3 (GCM13d, T63L31); ocean: CCCMA (OGCM3.1,256x192L29)"
	File conversion	N/A (already converted to netCDF format by CCCma)
	References	McFarlane et al. (2005); Scinocca et al. (2008)
	Internet sources	`http://www.cccma.ec.gc.ca/data/cgcm3/cgcm3.shtml` or `http://www.cccma.ec.gc.ca/models`

Table C.1 continues on next page.

Table C.1 continued from previous page.

Acronym	Characteristic	Value or description
CanAM-4.1	Full Name	CCCma updated fourth generation atmospheric GCM (CanAM-4.1)
	Time (start–stop)	01-1950 – 12-2009
	Grid (lon–lat)	128×64 (or $\approx 2.79^\circ \times 2.8125^\circ$) Longitude: 0.00°W-357.19°W – Latitude: 87.86°S-87.86°N Remark: the grid cell size slightly changes with latitude (min=2.767°, max=2.791°, mean=2.789°, std=0.004°) but is very constant in the 60°S-60°N domain (std $< 0.0001^\circ$)
	Interpolation	N/A
	Project	Model output (four runs) prepared for the Atmospheric Model Intercomparison Project (AMIP) and the Climate Model Intercomparison Project (CMIP)- fifth phase
	Fields	All (cloud properties, precipitation, temperature, humidity, and radiation)
	Source type	Model simulation
	Hardware	"CanAM4 2010 atmosphere: CanAM4 (AGCM15i, T63L35) land: CLASS2.7 (Note: Adjusted Land Cover and soil albedo relative to that used in CanESM2 and CanCM4)"
	File conversion	N/A (already converted to netCDF format by CCCma)
	References	von Salzen et al. (2007)
	Internet sources	`http://www.cccma.ec.gc.ca/data/data.shtml` or `http://www.cccma.ec.gc.ca/models` or `http://pcmdi3.llnl.gov/esgcet/home.htm`

Table C.1 finishes here.

Satellite	Launch date	Orbit	Instrument
TRMM	Nov. 27, 1997	350 km altitude, 35° inclination	PFM
EOS Terra	Dec. 18, 1999	Sun-synchronous, near-polar	FM1
			FM2
EOS Aqua	May 4, 2002	Sun-synchronous, near-polar	FM3
			FM4

Table C.2: Clouds and the Earth's Radiant Energy System (CERES) contributing satellites. Orbital details for Aqua and Terra: 705 km altitude, 10:30 a.m. descending node (Terra) and 1:30 p.m. ascending node (Aqua). Aqua and Terra each carry two identical instruments: one operates in a cross-track scan mode and the other in a biaxial scan mode. The cross-track scan essentially continues the measurements of the Earth Radiation Budget Experiment (ERBE). For full names (expanded acronyms) see the glossary page xi.

Series	Description	Satellite/Platform
NOAA	Afternoon (PM)	NOAA-7 NOAA-9 NOAA-11 NOAA-14
	Morning (AM)	NOAA-8 NOAA-10 NOAA-12
GOES	West (W)	GOES-6 GOES-9
	East (E)	GOES-5 GOES-7 GOES-8
METEOSAT	Prime	METEOSAT-2
	Prime + GOES-E	METEOSAT-3
	Prime	METEOSAT-4
	Prime + 63E	METEOSAT-5
GMS		GMS-1 GMS-2 GMS-3 GMS-4 GMS-5

Table C.3: International Satellite Cloud Climatology Project (ISCCP) contributing satellites, from the CLoud Archive User Service (CLAUS) User Guide, accessible here: `http://badc.nerc.ac.uk/data/claus/userguide.pdf`. For full names (expanded acronyms) see the glossary page xi.